(2)

Analytical and Experimental Modeling and Control of Flexible Structures

Final Technical Report
for the period
December 1987 to December 1990
for AFOSR Contract Number
F4962088 C0018

DISCLAIMER NOTICE

THIS DOCUMENT IS BEST QUALITY PRACTICABLE. THE COPY FURNISHED TO DTIC CONTAINED A SIGNIFICANT NUMBER OF PAGES WHICH DO NOT REPRODUCE LEGIBLY.

UA (U)

SECURITY CLASSIFICATION OF THIS PAGE

REPORT DOCUMENTATION PAGE

1a. REPORT SECURITY CLASSIFICATION Unclassified	1b. RESTRICTIVE MARKINGS
2a. SECURITY CLASSIFICATION AUTHORITY	3. DISTRIBUTION/AVAILABILITY OF REPORT Approved for public release, distribution unlimited
2b. DECLASSIFICATION/DOWNGRADING SCHEDULE	
4. PERFORMING ORGANIZATION REPORT NUMBER(S)	5. MONITORING ORGANIZATION REPORT NUMBER(S)
6a. NAME OF PERFORMING ORGANIZATION Research Foundation of the State University of New York 6b. OFFICE SYMBOL (If applicable)	7a. NAME OF MONITORING ORGANIZATION AFOSR/NA
6c. ADDRESS (City, State, and ZIP Code) PO Box 9, Albany, NY	7b. ADDRESS (City, State, and ZIP Code) AFOSR/NA, Bldg. 410 Bolling AFB, DC 20331-6448
8a. NAME OF FUNDING/SPONSORING ORGANIZATION AFOSR 8b. OFFICE SYMBOL (If applicable) NA	9. PROCUREMENT INSTRUMENT IDENTIFICATION NUMBER F49620-88-C-0018
8c. ADDRESS (City, State, and ZIP Code) AFOSR/NA Bldg. 410 AFOSR/NA Bolling AFB DC 20332-6448	10. SOURCE OF FUNDING NUMBERS PROGRAM ELEMENT NO. 61102F; PROJECT NO. 2302; TASK NO. B1; WORK UNIT ACCESSION NO.

11. TITLE (Include Security Classification)
Analytical and Experimental Modeling and Control of Flexible Structures (U)

12. PERSONAL AUTHOR(S)
Daniel J. Inman

13a. TYPE OF REPORT	13b. TIME COVERED	14. DATE OF REPORT (Year, Month, Day)	15. PAGE COUNT
Final Report	FROM 12/87 TO 12/90	January 30, 1991	

16. SUPPLEMENTARY NOTATION

17. COSATI CODES			18. SUBJECT TERMS (Continue on reverse if necessary and identify by block number)
FIELD	GROUP	SUB-GROUP	

19. ABSTRACT (Continue on reverse if necessary and identify by block number)

This report summarizes the research activity supported under contract No. AFOSR F4962088 C0018 for the period of December 1987 to December 1990. Seven major results are reported here. They are: (1) The modeling and experimental verification of closed loop slewing control of flexible structures which has resulted in a substantial improvement in pointing time. (2) The effects of slewing active structures (smart structures) have been modeled, experimentally verified and shown to result in an additional improvement in performance. (3) The nature of control structure interaction has been modeled and experimentally verified for vibration suppression in trusses and for frames using on-board electromagnetic actuators. (4) A Timoshenko model of layered piezoelectric devices has been developed. (5) A significant new model correction method has been developed for adjusting mathematical models based on experimentally obtained data. (6) A robust system identification has been developed and (7) a dynamic analysis and animation of flexible structures has been developed.

20. DISTRIBUTION/AVAILABILITY OF ABSTRACT	21. ABSTRACT SECURITY CLASSIFICATION
☐ UNCLASSIFIED/UNLIMITED ☒ SAME AS RPT. ☑ DTIC USERS	(U)
22a. NAME OF RESPONSIBLE INDIVIDUAL S. Wu/ Lt. Col. G. Haritos/A.K. Amos	22b. TELEPHONE (Include Area Code) 202-767-6962
	22c. OFFICE SYMBOL

DD FORM 1473, 84 MAR 83 APR edition may be used until exhausted. All other editions are obsolete.

SECURITY CLASSIFICATION OF THIS PAGE

(U)

Analytical and Experimental Modeling and Control of Flexible Structures

Final Technical Report
for the period
December 1987 to December 1990
for AFOSR Contract Number
F4962088 C0018

Principal Investigator: Daniel J. Inman
Co-Investigators: Roger W. Mayne, D. Joseph Mook and Neel K. Mani

Mechanical Systems Laboratory
Department of Mechanical and Aerospace Engineering
School of Engineering and Applied Science
State University of New York at Buffalo
Buffalo, NY 14260

Report prepared by D.J. Inman
January 30, 1991

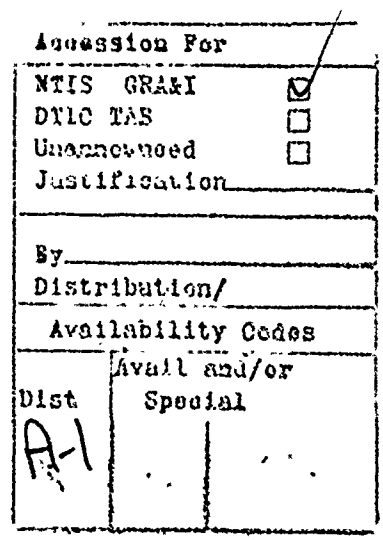

Analytical and Experimental
Modeling and Control of Flexible Structures
Report

Table of Contents

I. Introduction

The global objective of this contract was to construct analytical models of flexible structures controlled by electromagnetic actuators, to perform active control for vibration suppression and to experimentally verify the models and control algorithm by illustrating successful implementation on laboratory structures. Two types of vibration suppression have been examined: slewing control of beam like structures and transient disturbance rejection in frame like structures. Several types of control actuators have been considered as well, mainly piezoelectric strain actuators, reaction mass actuators and electric motors.

In our efforts to bring modeling and control for vibration suppression into the laboratory, we have produced numerous results which can be lumped into 7 categories:

1) The modeling and experimental verification of closed loop slewing control of flexible structures which has resulted in a substantial improvement in pointing time.
2) The effects of slewing active structures (smart structures) have been modeled, experimentally verified and shown to result in an additional improvement in performance.
3) The nature of control structure interaction has been modeled and experimentally verified for vibration suppression in trusses and frames using on-board electromagnetic actuators.
4) A Timoshenko model of layered piezoelectric devices has been developed.
5) A significant new model correction method has been developed for adjusting mathematical models based on experimentally obtained data.
6) A robust system identification algorithm has been developed.
7) A dynamic analysis and animation of flexible structures has been developed.

Each of these results are summarized in section II. Section III list pertinent references. Section IV provides a listing of the personnel, both faculty and students, supported under the 3 years of support provided by this contract. Section V list proceedings papers and journal articles that have been published based on the results generated by this support. Section VI summarizes accomplishments obtained under this contract and discusses research issues illuminated by these results.

II. Summary of Results

II-1. *Modeling of Closed Loop Slewing* The standard approach to modeling a slewing beam is to model the dynamics of the beam as a cantilevered structure with clamped free boundary conditions using a rigid coupling to the drive motor through a gear train. Through observation of a variety of different slewing apparatus, it was observed that some drive motion can be excited by structural vibration in the beam and some cannot. This observation resulted in subtraction modeling and experimental verification of slewing structure (Garcia (1-2)). The outcome of this exercise was that structural vibration in the slewing article can be suppressed much more efficiently by allowing the actuator and structure to interact.

Analytically this amounts to modeling the boundary conditions at the point of connection between the beam and the motor as somewhere "between" clamped and pinned. A parameter depending on the motor parameters, gear ratio and beam stiffness has been derived which characterizes the motor-beam system and is useful for designing an appropriate closed loop system. It was then shown both analytically and experimentally that the proper choice of this parameter can improve the settling time of a slewing maneuver by up to 65%. This result illustrates the significance of control structure interaction in slewing maneuvers. This is reported in Garcia, Inman et al. (3,4,5)

Specifically this extension of previous modeling of the slewing of a flexible structure results from the inclusion of torque and torque slope terms in the boundary condition connecting the flexible beam and the motor. This models the interaction between the actuator and the beam by including modal participation factors in the slewing equation of motion. These modal participation factors indicate the degree to which the structure and actuator interact during slewing. Because of this interaction, large modal damping is obtained through the use of simple (rate) tachometer feedback. Experiments verify both the model and the improved performance and are summarized in figure 1.

II-2. *Effects of Slewing Active Structures* During the third year of the grant the area of investigation known as "smart materials and structures" was applied to the slewing problem. Much work in smart materials and structures had centered around using embedded piezoelectric sensors and actuation (see section II-4). This use of embedded sensors and actuators is referred to here as an "active structure." A large additional increase in pointing performance over the system of section II-1 is gained by slewing an active structure. This has been modeled and predicted analytically as well as experimentally.

The reason why an active structure illustrates such improved performance in slewing maneuvers can be simply explained by appealing to the concept of full state feedback in linear control theory. If full state feedback is available, every state can be completely shaped to have the desired response. For example a pole placement algorithm with full state feedback allows every closed loop eigenvalue to be change to a specified value. However, in most systems, only output feedback is available. This is especially true for distributed parameter systems with an infinite number of modes. An active structure allows the ideal full state feedback law to be approached by providing a large number of actuator locations to be used.

The control law implemented here was to embed several sensor/actuator pairs into our slewing structure to create an active beam. The analytical model of this system was used to calculate an LQR solution assuming full state feedback. This "ideal" solution is then implemented by calculating the output feedback gain matrix associated with the piezoceramic actuators that is closest, in a least squares sense, to the LQR optimal solution. This type of control is only obtained by using an active structure, and results in a substantial increase in performance. The details can be found in Garcia and Inman (6,7,8) and a comparison is illustrated in figure 2.

It is important to note that several control formulations are possible using active structures (on smart materials) that are not possible without this emerging new technology.

II-3. *Vibration Suppression Through Control Structures Interaction* A reaction mass actuator was used to study the effects of control structure interaction on vibration suppression control law design for vibration suppression in flexible space trusses. A strong theoretical result based on including actuator dynamics in control law formulation and structural design is provided which quantifies the nature of control structure interaction. This result, arrived at by employing various definiteness conditions, clearly illustrates the high gain instability experienced by a number of different experimental examples. This result has been applied to the results of other experimental researchers as well. Two different experimental structures were considered. The first was a cantilivered frame in the shape of a "T" and the second was a beam like frame suspended in a "free-free" configuration. Both structures were fitted with NASA/UB proof mass actuators.

A cantilevered seven bay planer truss in the shape of a "T" was controlled using a space realizable proof mass actuator. The reaction mass actuator was attached to the truss at location 8 as indicated in figure 3. The actuator was considered as both a passive and active device. The placement of the actuator was specified by examining the eigenvalues of

the modified model that included the actuator dynamics, and by examining the frequency response function of the modified system. The electronic stiffness of the actuator was specified such that the proof mass actuator system was tuned to the forth structural mode of the truss by using a traditional vibration absorber design. The active vibration suppression law was limited to velocity feedback. The two lower modes of the closed loop structure were placed farther in the left plane (increased damping). The theoretically predicted combined passive and active control law was experimentally verified. The details are given in references (9-10).

Four different feedback control laws were developed to add damping to a 6 bay, 3 meter free-free truss. A proof mass actuator is used as both a point force source and as a link in a mechanism that applies bending moments at two locations on the structure. The first control law uses the actuator as a traditional passive vibration absorber. The second control law consists of direct feedback of both the relative position (i.e., the difference between the proof mass position and the structure position) and the structure's velocity at the point of application. The third control strategy was also direct velocity feedback, but with a compensator for the position of the proof mass. The compensator is designed according to an H_∞ optimization method. The fourth control law uses the actuator as an equivalent viscous damper connected between two locations on the structure.

A theoretical and experimental comparison shows that direct velocity feedback provides better vibration suppression that can be obtained by using passive and/or active vibration absorbers. Furthermore, the tuning criteria is only restricted to maintaining the actuators single frequency below all structural frequencies of interest. It is also observed that H_∞ control design is *not* appropriate for vibration suppression since it produces a compensator that relies on pole zero cancellation (Umland (11-12)).

II.4. *Timoshenko Models of Piezoelectric Devices* A mathematical model of distributed actuator/sensor system for vibration suppression of flexible members using piezoelectric devices has been completed during the reporting period. The development consisted of applying Timoshenko theory to beams with multiple layers of piezoelectric material added. The model is developed using a Hamiltonian approach and includes the external electric circuits as well as a complete set of boundary conditions. This rigorous study indicates that a fully distributed control is not possible, but rather a piece wise distributed control actuator can be constructed using piezoelectric elements. The piezoelectric material is segmented and resistors are added to the layers to provide passive damping. A state space model is developed, discretized (Galerkin Methods) and simulated. This finite dimensional model is then used to perform open loop and closed loop studies. Velocity feedback is used to study closed loop control. The resolution vibration suppression is judged based on a comparison of damping ratios in the open loop system, the passive control system and the closed loop active system. Large increases in damping ratio result as indicated in figure 4. The details of these results are presented in references (13-14).

II.5. *Model Correction Methods* Finite element models (FEM) often fail to exactly agree with experimentally determined model parameters (i.e., frequencies, damping ratios and mode shapes). Hence, it has become standard modeling practice to adjust the analytical model to agree more closely with the test data. The techniques used to adjust the analytical models are called model correction methods and typically have not been very sophisticated (see the review in Inman and Minis 1990 for instance). The result obtained under this contract consists of applying the methods of eigenstructure assignment to the model correction problem to produce a systematic procedure for correcting analytical models with experimentally determined modal data.

The first major use of the model correction technique is to use it to create a non proportional damping matrix for a given finite element model of a structure. Finite element models only yield mass and stiffness matrices Damping is usually included as an ad hoc proportional matrix. Proportionally damped systems yield real valued mode shapes. Yet the majority of tested space structures yield complex valued mode shapes. Hence, the FEM cannot possibly agree with the experimentally determined model parameter. Hence, a technique based on least squares calculation was developed to produce a non proportionally damped real valued symmetric positive definite matrix based on experimentally determined mode shapes, natural frequencies and damping ratios. The results are reported in Minas and Inman (18).

A more general model correction method was developed by recognizing the similarities between the eigenstructure assignment theorem from control theory and the model correction problem from experimental modeling. The eigenstructure assignment algorithm have been modified to yield symmetric positive definite correction matrices. This provides a systematic procedure to apply to experimental and analytical data which results in a model which agrees with experiment. These results are reported in Minas and Inman (10, 17-22).

II.6. *Robust Identification Theory for Flexible Structures* During this reporting period, significant progress was made on our work in robust system identification. This work combines NASA's Eigensystem realization algorithm (ERA) with the investigators Minimum Mode Error (MME) method. Previously, our combined ERA/MME technique had been shown to be considerably more robust than the ERA alone for the realization of the minimum order model, and subsequent identification of the modal frequencies and modal damping. We have now demonstrated considerable improvement in robustness of the identification for the mode shapes. In addition, we are making progress in the direction of the identification of the physical system properties from time-decay data. This

represents a fundamental potential improvement over direct identification of modes since the physical properties can tell us exactly what the control-structure interaction (CSI) is. Knowledge of the physical properties themselves gives us a much better insight into the design/selection of the appropriate actuator in order to accomplish a specific task.

The identification algorithm has been implemented on a laboratory P.C. connected directly to a vibrating beam system. We are currently able to take data and perform the identification in a single session which may be as short as just a few minutes. Subsequent to the identification, a control law can be selected and implemented on a programmable controller, also during the same session (23-29).

II.7. *Dynamic Analysis and Animation of Flexible Structures* Different types of modes such as vibration normal modes and static correction modes have been used to model flexible bodies for dynamic analysis of mechanical systems. Accuracy of using these modes to model a system under different forcing conditions has not been completely investigated. It was shown in this study that the loading on a flexible body consists of applied forces, D'Alembert forces resulting from gross body motion and kinematic joint reactions. Effectiveness of using different modes or their combinations not only depends on the choice of modes but also on the spatial distribution and frequency content of the loading. This work provides a criteria to select the number and types of different modes that must be included in the model. This estimation can be obtained by performing a rigid body analysis of the system.

This work also demonstrates that a set of Ritz vectors that accounts for the dynamic loading on the flexible bodies must also be included in the model in addition to vibration normal modes and static correction modes. The Ritz vectors used in the model are generated from spatial distribution of the loading and are orthogonalized with respect to the vibration

normal modes. These results are reported in Wu and Mani (30-33) and include several numerical examples to demonstrate the need to include different mode shapes in the mode. Guide lines on the selection of mode shapes to model flexible bodies for dynamic analysis are also presented.

III. References

1. Garcia, E., "On the Modeling and Control of Slewing Flexible Structures," Ph.D. dissertation, State University of New York at Buffalo, 1989.

2. Garcia, E. and Inman, D.J., "On the Modeling of the Slewing Control of a Flexible Structure, AIAA Journal of Guidance, Control and Dynamics, to appear.

3. Garcia, E. and Inman, D.J., "Modeling and Tachometer Feedback in the Control of an Experimental Single Link Flexible Manipulator," Proceedings of the 8th International Modal Analysis Conference, to appear February 1990, pp. 735-740.

4. Garcia, E. and Inman, D.J., "Identification of System Parameters in a Slewing Control Experiment," Proceedings of Damping 89, June 1989, pp. CBA-1-CBA-13.

5. Garcia, E., Pokines, B. and Inman, D.J., "Performance Improvement in Slewing Maneuver via CSI," in preparation.

6. Garcia, E. and Inman, D.J., "Advantages of Slewing an Active Structure," Journal of Intelligent Material Systems and Structures, Vol. 1, No. 3, July 1990, pp. 261-272.

7. Garcia, E. and Inman, D.J., "Control Formulations for Vibration Suppression of Active Structures in Slewing Motions," ASME 1990 Winter Annual Meeting. (Invited) *Advances in Dynamic and Control of Flexible Spacecraft and Space Based Manipulators*. Ed. by Joshi, Alberts and Kakad, DSC, Vol. 20, 1990, pp. 1-6.

8. Inman, D.J., Garcia, E. and Pokines, B., "Vibration Suppression and Slewing Control of a Flexible Structure," Proceedings of the 4th NASA Workshop on Computation Control of Flexible Aerospace Systems, July 1990, to appear.

9. Minas, C., Garcia, E. and Inman, "Control of a Flexible Planar Truss Using a Linear Proof Actuator," Proceedings of the 3rd Annual Conference on Aerospace Computational Control, August 1989, pp. 434-445.

10. Minas, C. and Inman, D.J., "Experimental Verification of the Theoretically Estimated Rotational Entries of Mode Shapes," Proceedings of the 8th International Modal Analysis Conference, February 1990, pp. 62-66.

11. Umland, J., "Active Damping in Flexible Structures," Ph.D. dissertation State University of New York at Buffalo, 1990.

12. Umland, J. and Inman, D.J., "Candidate Proof Mass Actuator Control Laws for the Vibration Suppression of a Frame," Proceedings of the 4th NASA Workshop on Computation Control of Flexible Aerospace Systems, July 1990, to appear.

13. Cudney, H.H., Inman, D.J. and Oshman, Y., "Distributed Structural Control Using Multi Layered Piezoelectric Actuators," Proceedings of the AIAA 31st Structures, Dynamics and Materials Conference, 1990, pp. 2257-2265.

14. Cudney, H.H., "Distributed Structural Control Using Multilayered Piezoelectric Actuators," Ph.D. dissertation, State University of New York at Buffalo, July 1989.

15. Cudney, H.H., Inman, D.J. and Oshman, Y., "Distributed Actuators for Structural Control," Proceedings of the American Control Conference, June 1989, pp 1189-1194. (Invited)

16. Cudney, H.H. and Inman, D.J.,"Distributed Structural Control Using Multilayered Piezoelectric Actuators," 7th VPI&SU Symposium on Dynamics and Control of Large Structures, June 1989.

17. Inman, D.J. and Minas, C., "Matching Analytical Models with Experimental Modal Data from Mechanical Systems," Control and Dynamic Systems: Advances in Industrial Systems, Vol. 37, ed. by C.T. Leondes, Academic Press, 1990, pp. 327-363.

18. Minas, C. and Inman, D.J., "Identification of Non-Proportional Damping Matrix from Incomplete Modal Information," ASME Journal of Vibration and Acoustics, to appear.

19. Minas, C. and Inman, D.J., "Matching Finite Element Models to Modal Data," ASME Journal of Vibration and Acoustics, Vol. 112n.1, Jan. 1990, pp. 84-92.

20. Minas, C. and Inman, D.J., "Model Improvement by Using Substructure Modal Testing Results," Proceedings of the 8th International Modal Analysis Conference, February 1990.. pp. 1190-1194.

21. Minas, M.C. and Inman, D.J., "Model Improvement by Pole Placement Methods," Vibration Analysis - Techniques and Applications, ed. T.S. Sankar, ASME, 1989, pp. 179-185.

22. Minas, C. and Inman, D.J., "Correcting Finite Element Models with Measured Modal Results Using Eigenstructure Assignment Methods, " Proceedings of the 6th International Modal Analysis Conference, Vol. 2, February 1988, pp. 583-587.

23. Roemer, M.J., Schlonski, S.T. and Mook, D.J., "Robust Time-Domain Modal Identification on Microcomputers," Experimental Techniques (Society for Experimental Mechanics), Vol. 14, No. 6, pp. 44-46, Nov. - Dec. 1990. Also Proceedings of the International Modal Analysis Conference, Kissimmee, FL, January 1990, pp. 95-101.

24. Mook, D.J. and Lew, J.H., "A Robust Algorithm for System Realization/ Identification," AAS Journal of the Astronautical Sciences, Vol. 38, No. 2, April-June 1990, pp. 229-243.

25. Roemer, M.J. and Mook, D.J., "Enhanced Realization/Identification of Physical Modes," ASCE Journal of Aerospace Engineering, Vol. 3, No. 2, April 1990, pp. 122-136.

26. Roemer, M.J. and Mook, D.J., "Mass, Stiffness and Damping Matrix Identification: An Integrated Approach," in review for the ASME Journal of Vibration and Acoustics.

27. Mook, D.J., "An Optimal Estimation Approach for Enhanced Identification of Large Space Structures," Southeastern Conference on Theoretical and Applied Mechanics, Atlanta, GA, March 1990.

28. Roemer, M.J. and Mook, D.J., "Robust Time Domain Identification of Mass, Stiffness and Damping Matrices," Proceedings of the International Modal Analysis Conference, Kissimmee, FL, January 1990, pp. 1271-1277.

29. Roemer, M.J. and Mook, D.J., "Robust Realization/Identification of Damped Structures," Proceedings of Damping 89, West Palm Beach, FL, February 1989.

30. Wu, H.T., "Dynamic Analysis of Flexible Multibody Systems Using Mode Superposition Method," Ph.D. dissertation, April 1990.

31. Wu, H.T., Mani, N.K. and Ashrafiuon, H., "Modeling of Flexible Bodies for Dynamic Analysis of Mechanical Systems," Mechanism and Machine Theory, under review.

32. Wu, H.T., Mani, N.K. and Ashrafiuon, H., Modeling of Flexible Bodies for Dynamic Analysis of Mechanical Systems, "Proceedings of the First National Applied Mechanisms and Robotics Conference, Nov. 1989, Paper 89AMR-10A-2.

33. Wu, H.T., Mani and N.K., "Modeling of Flexible Bodies for Dynamic Analysis of Mechanical Systems Using Ritz Vectors," under preparation.

IV. Personnel Supported

Four faculty were supported under the contract. Professors R.W. Mayne and D.J. Inman were supported at the full professor level. Two assistant professors D.J. Mook and N. Mani also received substantial support. Professor Mani was only supported the first two years. Professors Mook, Mayne and Inman were supported all 3 years of the award. Two secretaries received partial support form time to time during the three year period: Christine Jerome and Eileen Graber. A total of 11 students received some form of support from this contract. They are (there current position indicated in parenthesis)

John Bellos	(Army, Ph.D. completed 1988)
Donald Leo	(current Ph.D. student)
J.-S. Lew	(NASA, Ph.D. completed 1989)
Constantinos Minas	(GE Corporate Research, Ph.D. completed 1989)

Brett Pokines	(current Ph.D. student)
Ralph Rietz	(current M.S /Ph.D. student)

V. Documentation of Results

This section lists papers, both Journal articles and proceedings papers that were published under support of this grant. The list is organized by principle investigators:

Inman, D.J.

Inman, D.J., "Control Structure Interactions: Effects of Actuator Dynamics," Mechanics and Control of Large Space Structures, Chapter 19, ed. by Junkins, J., AIAA Progress in Aeronautics and Astronautics Series, Vol. 129, 1990, pp. 507-534.

Inman, D.J. and Minas, C., "Matching Analytical Models with Experimental Modal Data from Mechanical Systems," Control and Dynamic Systems: Advances in Industrial Systems, Vol. 37, ed. by C.T. Leondes, Academic Press, 1990, pp. 327-363.

Zimmerman, D.C., Inman, D.J. and Juang, J-N, "Vibration Suppression Using a Constrained Rate-Feedback Threshold Control Strategy," ASME Journal of Vibration and Acoustics, to appear.

Ross, A.D.S. and Inman, D.J., "Design Criteria for Predicting Damping in Underdamped Linear Lumped Parameter Systems," AIAA Journal of Guidance, Control and Dynamics, to appear.

Minas, C. and Inman, D.J., "Identification of Non-Proportional Damping Matrix from Incomplete Modal Information," ASME Journal of Vibration and Acoustics, to appear.

Garcia, E. and Inman, D.J., "On the Modeling of the Slewing Control of a Flexible Structure," AIAA Journal of Guidance, Control and Dynamics, to appear.

Garcia, E. and Inman, D.J., "Advantages of Slewing an Active Structure," Journal of Intelligent Material Systems and Structures, Vol. 1, No. 3, July 1990, pp. 261-272.

Ross, A.D.S. and Inman, D.J., Setting Time of Underdamped Linear Lumped Parameter Systems," Journal of Sound and Vibration, Vol. 140, No. 1, 1990, pp. 117-128.

Bellos, J. and Inman, D.J., "Frequency Response of Non Proportionally Damped Lumped Parameter, Linear Dynamic System," ASME Journal of Vibrations and Acoustics, Vol. 12, No. 2, pp. 194-210, 1990.

Liang, Z. and Inman, D.J., "Rank Decomposition Methods in Modal Analysis," ASME Journal of Vibration and Acoustics, Vol. 112, No. 3, July 1990, pp. 410-413.

Minas, C. and Inman, D.J., "Matching Finite Element Models to Modal Data,"ASME Journal of Vibration and Acoustics, Vol. 112n.1, Jan. 1990, pp. 84-92.

Zimmerman, D.C., and Inman, D.J., "On the Nature of Interactions Between Structures and Actuators," AIAA Journal of Guidance, Control and Dynamics, Vol. 13, No. 1, Jan.-Feb. 1990, pp. 82-88.

DeCaro, S.M. and Inman, D.J., "Stable Eigenvalue Placement by Constrained Optimization," Dynamics and Stability of Systems, Vol. 15, No. 4, 1990.

Bellos, J. and Inman, D.J., "A Survey of Non-Proportional Damping," The Shock and Vibration Digest, Vol. 21, No. 10, 1989, pp. 7-12

Oshman, Y., Inman, D.J. and Laub, A.J., "Square Root State Estimation for Second-Order Large Space Structure Models," AIAA Journal of Guidance, Control and Dynamics, Vol. 12, No. 5, 1989, pp. 698-708.

Bellos, J. and Inman, D.J., "The Nature of Coupling in Nonconservative Lumped Parameter Systems," AIAA Journal of Guidance, Control and Dynamics, Vol. 12, No. 5, 1989, pp. 751-753.

Inman, D.J., "On the Vibration Analysis of Viscoelastic Beams by Separation of Variables and Modal Analysis," Mechanics Research Communications, Vol. 16, No. 3-4, 1989, pp. 213-218.

Ross, A.D.S. and Inman, D.J., "A Design Criterion for Avoiding Resonance in Lumped Mass Normal Mode Systems," ASME Journal of Vibration, Acoustics, Stress and Reliability in Design, Vol. 111, No. 1, January 1989, pp. 48-52.

Cudney, H.H. and Inman, D.J., "Control Formulation for Flexible Structures Using Physical Coordinates," Mechanics of Structures and Machines,Vol. 16, No. 4, 1989, pp. 111-130.

Garcia, E. and Inman, D.J., "Control Formulations for Vibration Suppression of Active Structures in Slewing Motions," ASME 1990 Winter Annual Meeting. (Invited) *Advances in Dynamic and Control of Flexible Spacecraft and Space Based* Manipulators, Ed by Joshi, Alberts & Kakad, DSC Vol. 20, 1990, pp. 1-6.

Cudney, H.H., Inman, D.J. and Oshman, Y., "Distributed Structural Control Using Multi Layered Piezoelectric Actuators," Proceedings of the AIAA 31st Structures, Dynamics and Materials Conference, 1990, pp. 2257-2265.

Umland, J. and Inman, D.J., "Candidate Proof Mass Actuator Control Laws for the Vibration Suppression of a Frame," Proceedings of the 4th NASA Workshop on Computation Control of Flexible Aerospace Systems, July 1990, to appear.

Inman, D.J., Garcia, E. and Pokines, B., "Vibration Suppression and Slewing Control of a Flexible Structure," Proceedings of the 4th NASA Workshop on Computation Control of Flexible Aerospace Systems, July 1990, to appear.

Inman, D.J., "Updating Analytical Models with Experimental Data," Proceedings 2nd USAF/NASA Workshop on System Identification and Health Monitoring of Precision Space Structures, March 1990. (Invited)

Inman, D.J., Garcia, E. and Pokines, B., "Issues in Slewing an Active Structure," Proceedings US/Japan Workshop on Smart/Intelligent Materials and Systems, ed. by Ahmad, Crowson, Rogers and Aizawa, March 1990, pp. 199-210. (Invited)

Minas, C. and Inman, D.J., "Identification of the Damping Matrix from Incomplete Modal Testing Results," AIAA 1990 Dynamics Specialist Conference, April 1990. (Invited)

Inman, D.J., "Control/Structure Interaction: Effects of Actuator Dynamics," AIAA 1990, Dynamics Specialist Conference, April 1990. (Invited)

Inman, D.J., "On the Nature of the Interaction Between Structures and Actuators in Vibration Suppression," Proceedings International Congress on Recent Developments in Air & Structure Borne Sound and Vibration, to appear March 1990. (Invited)

Minas, C. and Inman, D.J., "Experimental Verification of the Theoretically Estimated Rotational Entries of Mode Shapes," Proceedings of the 8th International Modal Analysis Conference, February 1990, pp. 62-66.

Garcia, E. and Inman, D.J., "Modeling and Tachometer Feedback in the Control of an Experimental Single Link Flexible Manipulator," Proceedings of the 8th International Modal Analysis Conference, to appear February 1990, pp. 735-740

Minas, C. and Inman, D.J., "Model Improvement by Using Substructure Modal Testing Results," Proceedings of the 8th International Modal Analysis Conference, February 1990,.pp. 1190-1194.

Inman, D.J. and Umland, J.W., "Controlling Flexible Structures with Second Order Actuator Dynamics," Proceedings of the 3rd Annual Conference on Aerospace Computational Control, August 19, 1989, pp. 879-890. (Invited)

Minas, C., Garcia, E. and Inman, "Control of a Flexible Planar Truss Using a Linear Proof Actuator, " Proceedings of the 3rd Annual Conference on Aerospace Computational Control, August 1989, pp. 434-445.

Minas, M.C. and Inman, D.J., "Model Improvement by Pole Placement Methods," Vibration Analysis - Techniques and Applications, ed. T.S. Sankar, ASME, 1989, pp. 179-185.

Cudney, H.H., Inman, D.J. and Oshman, Y., "Distributed Actuators for Structural Control," Proceedings of the American Control Conference, June 1989, pp 1189-1194. (Invited)

Cudney, H.H. and Inman, D.J.,"Distributed Structural Control Using Multilayered Piezoelectric Actuators," 7th VPI&SU Symposium on Dynamics and Control of Large Structures, June 1989.

Inman, D.J. and Soom, A., "Vibration Control in Spacecraft," Proceedings of Modern Practice in Stress and Vibration, University of Liverpool, Pergamon Press. April 1989, pp. 11-16. (Invited)

Liang, Z. and Inman, D.J., "A Tutorial on Matrix Inversion in Time Domain Modal Analysis," Proceedings of the 7th International Modal Analysis Conference, January 1989, pp. 324-330.

Cudney, H.H. and Inman, D.J., "Experimental Verification of Damping Mechanisms in a Composite Beam," Proceedings of the 7th International Modal Analysis Conference, January 1989, pp. 704-710.

Garcia, E. and Inman, D.J., "Identification of System Parameters in a Slewing Control Experiment," Proceedings of Damping 89, June 1989, pp. CBA-1-CBA-13.

Inman, D.J. and Horner, G.C., "A Survey of Damping in Control of Flexible Structures," Proceedings of Damping 89, June 1989, pp. HBA-1-HBA-5.

Liang, Z and Inman, D.J., "A Modal Parameter Identification Method with Arbitrary Low Sampling Rate," Proceedings of the International Conference on Machine Dynamics and Engineering Applications, August 1988, pp. A1-A5.

Mook, D.J. and Inman, D.J., "A Numerical and Experimental Robustness Investigation of Time-Domain Realization/Identification Techniques," Proceedings of the International Conference on Computational Engineering Science, Vol. 2, April 1988, pp. 64 .iv1-.iv4.

Mayne, R.W. and Inman, D.J., "Prospects of Damping Structures via Actuator Interaction," Proceedings of the International Conference on Computational Engineering Science, Vol. 2, April 1988, pp. 44.vi1-.vi4.

Oshman, Y. and Inman, D.J., "Optimal On-Line Measurement System Configuration Strategies," Proceedings of the 29th Structures, Structural Dynamics and Materials Conference, Vol. 2, April 1988, pp. 1048-1049.

Ross, A.D.S. and Inman, D.J., "On Resonance of Lumped Mass Damped Linear Systems With Normal Modes," Proceedings of the 6th International Modal Analysis Conference, Vol. 1, February 1988, pp. 42-48.

Liang, Z. and Inman, D.J., "On Rank Decomposition Methods for Modal Analysis," Proceedings of the 6th International Modal Analysis Conference, Vol. 2, February 1988, pp. 1176-1179.

Garcia, E., Inman, D.J. and Horner, G.C., "System Identification in the Microcomputer Environment," Proceedings of the 6th International Modal Analysis Conference, Vol. 2, February 1988, pp. 1596-1601.

Minas, C. and Inman, D.J., "Correcting Finite Element Models with Measured Modal Results Using Eigenstructure Assignment Methods," Proceedings of the 6th International Modal Analysis Conference, Vol. 2, February 1988, pp. 583-587.

Bellos, J. and Inman, D.J., "Lumped Systems with Non Proportional Damping," Proceedings of the 6th International Modal Analysis Conference, Vol. 2, February 1988, pp. 876-882.

Zimmerman, D.C., Inman, D.J. and Juang, J-N., "Low Authority-Threshold Control for Large Flexible Structures," Proceedings of the 29th Structures, Structural Dynamics and Materials Conference, Vol. 1, April 1988, pp. 459-469.

Mayne, R.W.

Panza, M.J., Sah, F.J., Mayne, R.W. and Inman, D.J.,"Prospects of Damping Structures via Actuator Interaction," Proceedings of the International Conference on Computational Engineering Science, Atlanta, 1988.

Panza, M.J. and Mayne, R.W., "Mathematical Modeling of Actuator - Flexible Beam Dynamic Systems," Structural Vibrations and Acoustics, ASME Design Conference, Montreal, 1989, pp. 91-98.

Narayanan and Mayne, R.W., "Automating the Parameter Optimization of Dynamic Systems," Computational Structural Mechanics and Multi-Disciplinary Optimization, ASME Winter Annual Meeting, San Francisco, 1989, pp. 51-56.

Sah, J.-J. and Mayne, R.W., "Modeling of a Slewing Motor-Beam System," Computers in Engineering - 1990, ASME Computer in Engineering Conference, Boston, 1990, pp. 481-486.

Panza, M.J.and Mayne, R.W., "Investigation of Hydraulic Actuator-Beam Interaction for a Rotating Flexible Beam," Flexible Mechanism Dynamics and Robot Trajectories, ASME Design Conference, Chicago, 1990, pp. 223-232.

VI. Research Issues and Accomplishments

Important research issues identified during this contract are:

- a need to incorporate smart material and structure principles into the structural control problem.
- formulation of definitions, theories and examples for controlling smart structures.
- how much can be achieved by the use of smart structures and what are the limitations?
- can simple academic formulations be used on complex structures
- can the use of nonlinear control laws and nonlinear dynamics be made practical by using smart structures?

Each of theses issues can be addressed by using successively more complicated experimental structures. One of the difficulties with government laboratory experiments is that they are too complex for research theories to handle. The difficulty with most academic laboratories is that they are too simple to be of significance to "real" space structures. What is needed, is a step by step increased in complexity of ground

experiments unit a complex structure is achieved. At each step research theories can be addressed and understood before the next level of complexity is added. This approach should provide an experimental bridge between research results in structural control and practical space structure vibration problems.

Accomplishments under this grant are summarized as follows:

1) The use of control structure interaction to improve pointing time in slewing maneuvers has been developed both technically and experimentally. Selection rules for the design of a slewing structure have been provided.
2) The preliminary results of slewing an active, or "smart" structure have been established. It has been shown experimentally that these lead to improved performance, via shorter settling times.
3) The nature of control structure interaction for vibration suppression in frames and trusses with onboard electromagnetic actuators has been modeled and experimentally verified.
4) A Timoshenko model of multiple layers of piezoelectric beam has been derived.
5) A significantly new model correction method has been developed for adjusting mathematically finite element models based on experimental modal test data.
6) A robust system identification method has been developed and tested.
   proposed.
7) A dynamic analysis and animation methodology for flexible structure has been proposed.

The attached appendix contains copies of selected papers describing these results.

Selected Papers Content

1. Garcia, E. and Inman, D.J., "Control Formulations for Vibration Suppression of Active Structures in Slewing Motions," ASME 1990 Winter Annual Meeting. (Invited) *Advances in Dynamic and Control of Flexible Spacecraft and Space Based Manipulators*, pp. 1-5..

2. Cudney, H.H., Inman, D.J. and Oshman, Y., "Distributed Structural Control Using Multi Layered Piezoelectric Actuators," Proceedings of the AIAA 31st Structures, Dynamics and Materials Conference, 1990, pp. 2257-2265.

3. Vibration Suppression of a Frame," Proceedings of the 4th NASA Workshop on Computation Control of Flexible Aerospace Systems, July 1990, to appear.

4. Minas, C., Garcia, E. and Inman, D.J., "Control of a Flexible Planer Truss Using Proof Mass Actuator," Proceedings of the 3rd Annual Conference on Aerospace Computational Control," Oxnard, CA, August 1990.

5. Inman, D.J., Garcia, E., and Umland, J., "On the Nature of the Interaction Between Structures and Actuators in Vibration Suppression," Proceedings of the International Congress on Recent Developments in Air and Structure Borne Sound and Vibration, March 1990, pp. 223-227.

6. Garcia, E. and Inman, D.J., "Modeling and Tachometer Feedback in the Control of an Experimental Single Link Flexible Manipulator," Proceedings of the 8th International Modal Analysis Conference, 1990.

7) Cudney, H.H., Inman, D.J. and Oshman, Y., "Distributed Parameter Actuators for Structural Control," Proceedings of the American Control Conference, June1989.

8) Garcia, E. and Inman, D.J., "Advantages of Slewing an Active Structure," Journal of Intelligent Material Systems and Structures, Vol. July 1990, pp. 261-272.

9) Zimmerman, D.C., and Inman, D.J., "On the Nature of Interactions Between Structures and Actuators," AIAA Journal of Guidance, Control and Dynamics, Vol. 13, No. 1, Jan.-Feb. 1990, pp. 82-88.

10) Minas, C. and Inman, D.J., "Matching Finite Element Models to Modal Data," Journal of Vibration and Acoustics, Vol. 112, Jan. 1990, pp. 84-92.

11) Sah, J.-J. and Mayne, R.W., "Modeling of a Slewing Motor-Beam System," Computers in Engineering - 1990, ASME Computer in Engineering Conference, 1990, pp. 481-486.

12) Roemer, M.J. and Mook, D.J., "Enhanced RealizationVIdentification of Physical Modes," ASCE Journal of Aerospace Engineering, Vol. 3, No. 2, 1990, pp. 122-136.

DISTRIBUTED STRUCTURAL CONTROL USING MULTILAYERED PIEZOELECTRIC ACTUATORS

Harley H. Cudney
Department of Mechanical Engineering
Virginia Polytechnic Institute and State University
Blacksburg, Virginia 24061
Member - AIAA
Associate Member - ASME

Daniel J. Inman
Department of Mechanical and Aerospace Engineering
University at Buffalo
Buffalo, New York 14260
Member - AIAA
Member - ASME

Yaakov Oshman
Department of Aerospace Engineering
Technion--Israel Institute of Technology
Haifa 32000, Israel
Member - AIAA

ABSTRACT

One problem that exists with using distributed sensors and actuators is due to the integration of the property to be measured or controlled, which leads to cancellation of the sensor signal or reduction of the actuator effectiveness. A method of segmenting distributed piezoelectric sensors and actuators is proposed here to avoid this problem. This method of segmenting distributed sensors and actuators is demonstrated using a model developed for beam structures to which multiple layers of piezoelectric materials are attached. A numerical study is performed in which active and passive damping of a beam is increased using segmented piezoelectric sensors and actuators over uniform sensors and actuators.

I. INTRODUCTION

For the purposes of this paper, it is necessary to consider two definitions of distributed sensing and control. The first definition of distributed control is represented by Fig. 1, which shows a beam with point forces or moments applied in discrete locations over the surface of the beam. Examples of this type of distributed control include the use of proof-mass actuators to provide point forces for controlling transverse beam vibrations (Zimmerman, et. al., 1988), and the use of small piezoceramic patches to provide point moments also for controlling transverse beam vibrations (Crawley and de Luis, 1987).

The second definition of distributed control describes situations where the control force is distributed over the surface of the structure. This is represented in Fig. 2. An example of this form of distributed control is the experiments performed by Burke and Hubbard (1988) where piezoelectric film is used to control transverse beam vibrations by applying a distributed moment over the surface of the beam.

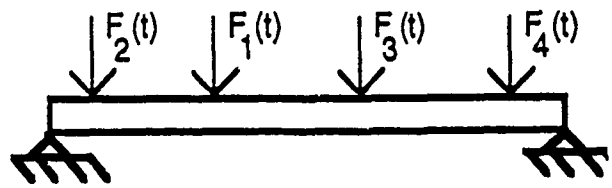

Figure 1. Discrete Force Actuators

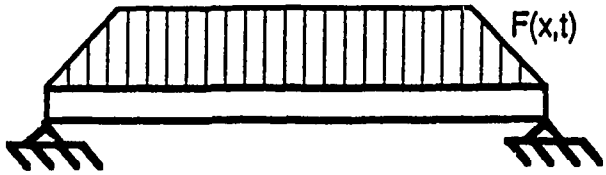

Figure 2. Distributed Force Actuators

A similar difference in definitions of distributed sensing exist. The first definition is represented by discrete sensors distributed over the surface of a structure as shown for strain sensors in Fig. 3. The second definition of distributed sensing describes sensing which is distributed over the surface of the structure. This definition is represented by Fig. 4. An example of this type of sensor is the fiber optic sensor, configured to sense the surface strain of a structure (Blake, et. al., 1987). The resulting sensor signal is influenced by the strain at every point along the surface of the beam to which it is applied.

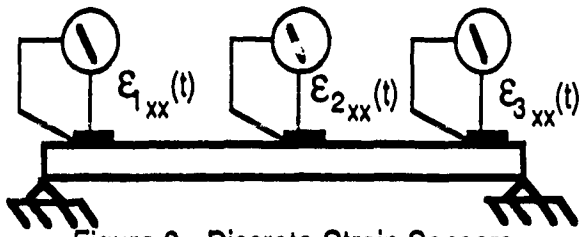

Figure 3. Discrete Strain Sensors

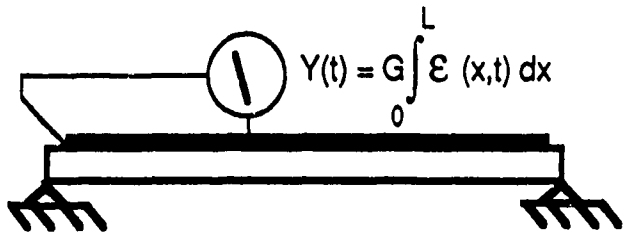

Figure 4. Distributed Strain Sensors

The second definition of distributed control and sensing is examined here. There are several reasons for considering this form of the distributed control system. First, sensors and actuators have recently been developed that allow physical implementation of this form of distributed sensing and control. Examples of these include fiber optic cables used for sensing, shape memory alloys such as Nitinol used for sensing and actuation, and piezoelectric materials such as polyvinylidene film also used for sensing and actuation. The use of each of these materials for distributed sensing and/or distributed control has been demonstrated experimentally.

Another reason for considering this form of distributed control is that the problem of where to place discrete sensors and actuators is avoided. This is especially critical when experimental testing methods are not available to confirm the mathematical models of the structures from which the control law will be designed. The proposed large flexible space structures are an example of this problem: it is increasingly difficult to accurately predict the on-orbit behavior of these structures based on their ground tests.

The most significant reason to consider this form of distributed sensing and actuation is that it allows an essential difference in the solution of control problems. The sensing signal and control signal can be represented by continuous functions rather than discrete functions. Two examples can be cited where this difference is exploited. In the first example, a distributed sensor was formed using piezoelectric film (Lee, et. al., 1989). This sensor was shaped and applied to a beam such that it sensed the strain resulting from only the vibration of the first mode. This is not feasible using only discrete sensors. The second example involves distributed actuation also using piezoelectric film distributed over the surface of a beam (Burke and Hubbard, 1988). A set of guidelines was produced for deciding the spatial variation of the piezoelectric film which would allow all vibrational modes to be controlled, eliminating the problem of spillover. Again, this is not feasible using discrete actuators.

A problem exists with distributed sensors which sense a physical quantity over a distributed area and yield one signal representing the integration of that physical quantity over the area to which the sensor is applied. This problem is illustrated in Figure 5, which shows a generic distributed sensor measuring surface strain in a pinned-pinned beam. The beam is deflecting in its second mode shape. The output of the sensor will be zero in this case. This full or partial cancellation of the sensing signal reduces the usefulness of distributed effect sensors. A similar problem exists with actuators.

Several researchers have proposed solutions to this problem by spatially weighting the sensors and actuators. In the work by Burke and Hubbard, a linear variation in the width of the actuator bonded to the surface of a beam was found to

avoid complete cancellation of the effectiveness of the actuator (1988). However, there will still be some cancellation and the efficiency of the actuator will be reduced. In the work by Lee, et. al., the sensor was shaped precisely to the first mode shape of the cantilever beam, and there was no cancellation of the sensor signal. However, the spatial variation of the sensor is set at the time of fabrication, which does not allow the sensor to be reconfigured in cases where the structure undergoes changes.

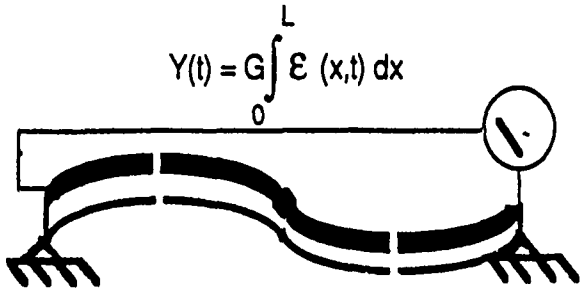

Figure 5. Measuring Strain in Second Mode

Another solution to the problem of cancellation of the distributed sensor and actuator signals is proposed here. Distributed piezoelectric sensors and actuators are attached to a structure. To avoid cancellation, the conducting layers are segmented, and a series of wires, one to a segment, are attached. As a result, each segment of the sensor is less likely to span an area where the physical quantity to be measured has positive and negative components which cancel. Another significant advantage of this approach is that spatial information is available in the sensor signals, and a spatial variation can be implemented in the applied actuator forces. This will be shown to lead to a more effective control system. Note that the sensors and actuators are fully distributed over the surface of the structure, while a series of discrete signals from the distributed sensors, and a series of discrete control inputs to the distributed actuators are available. Using the terminology utilized by Bergman and McFarland, this distributed-discrete system will be termed a "combined system" (1988).

The objective of this research is to use multiple layers of distributed and segmented piezoelectric material to add active damping to transverse beam vibrations. The approach is to develop a model for this configuration and perform a numerical study of simple feedback control to add damping to the structure. The analysis is general to include any piezoelectric material. The model includes structural damping, passive damping created by the external circuits connected to the piezoelectric feedback layers, and uses Timoshenko deformation theory.

Piezoelectric materials such as polyvinylidene flouride film possess some advantages for the control of distributed parameter structures, and partly motivated this research. They are lightweight, have low power consumption, and can easily be applied in a distributed manner. They have no moving parts which increases their reliability when compared to conventional actuators, and they have a wide bandwidth which allows their use on a variety of structures. Several researchers have examined the use of piezoelectric materials to implement distributed control (Hanagud, et. al., 1985a, 1985b, and 1987, Crawley and de Luis, 1987, Tzou and Tseng, 1988, Lee and Moon, 1988, and Bailey and Hubbard, 1985).

Several areas have not been addressed in previous work. First, all the previous models use Euler-Bernoulli deformation theory rather than Timoshenko deformation theory. Timoshenko deformation theory is more accurate for the higher modes of a structure and can be applied to a broader class of structures. Secondly, previous models neglect inherent damping in the structure, which will lead to disagreements between experiment and theory. Thirdly, the external circuits to which the piezoelectric materials are connected are not included in the models, and it will be shown here that these external circuits influence the response of the structure. Finally, although the piezoelectric material is applied in a distributed manner, it will also be shown here that discretizing the conducting surfaces will avoid the the cancellation of the sensor and actuator effectiveness documented earlier.

The configuration to be analyzed is presented in the next section. The model developed for this configuration is presented next. The control law is then described. Several numerical examples are presented to show the effectiveness of segmenting the piezoelectric layers.

II. CONFIGURATION DESCRIPTION

The particular structure to be analyzed is presented in Fig. 6, and consists of a viscoelastic central

layer and four layers of piezoelectric material configured as a multilayered beam. Each layer of piezoelectric material is coated on both sides with a conducting material. The innermost two layers are configured as feedback layers by segmenting the conducting surface adjacent to the central layer and connecting each segment to a series circuit consisting of an inductor and resistor. These external circuits provide both an output voltage which will be proportional to strain rate, as well as to provide a mechanism for dissipating energy. The resistors are used to provide this mechanism, and the inductors are used to give the external circuits tunable dynamics. This is an extension of an experiment performed by Forward (1981) where external circuits were attached to piezoceramic patches bonded to a structure to add electronic damping.

Due to the ability of the external circuits to add passive damping to the structure, the innermost layers can not be termed sensors, because they influence the response of the structure. Therefore, they will be called the feedback layers.

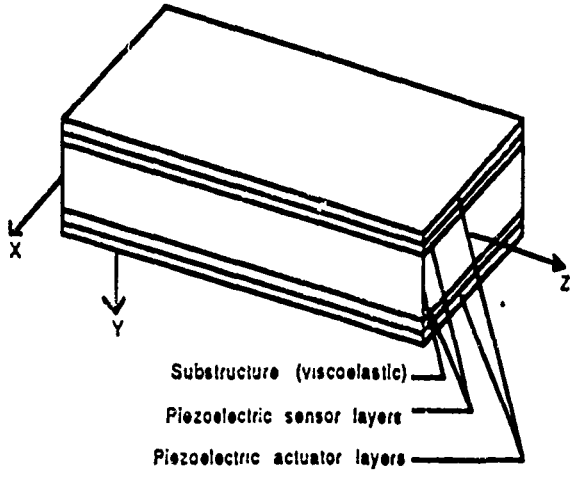

Figure 6. Structure to be analyzed

The outermost two layers of piezoelectric material will provide the actuation. Note that the conducting material common to both the feedback and actuation layers on each side of the beam is connected to ground. This is done to reduce interference between the feedback and actuation layers. Also note that the sensing and control is distributed over the surface, and by segmenting the outer conducting surfaces a series of sensing signals will be produced which contain spatial information. Likewise, a control law can be implemented using spatial information. This configuration is easy to implement since just the conducting surfaces need to be segmented. This also allows a simpler analysis, since the layers which influence the response of the beam are continuous along the beam length.

III. MODELLING RESULTS

To develop the model, Timoshenko deformation theory is used in conjunction with Hamilton's Principle. The contribution to the Lagrangian energy and non-conservative work is found for each layer. Taking a layer-by-layer approach allows the electrical boundary conditions of the different piezoelectric layers to be specified. Summing up the contributions from all the layers as well as the external electric circuits and applying Hamilton's Principle yields a set of partial differential equations and boundary conditions.

There were several assumptions made in developing the model of the structure First, the layers were assumed to be perfectly bonded. The bending strain field was assumed to vary linearly through the cross section of the multilayered structure. The internal energy dissipation in the structure was assumed to be accurately represented by the Kelvin-Voigt model, and that energy was also dissipated by air acting on the surface of the beam, modelled as viscous damping Note that the model was kept general, for any piezoelectric elastic material used for the feedback and actuation layers, and for any boundary conditions.

The development of this model is thoroughly documented in Cudney (1989), and Cudney, et. al. (1989a, 1989b). The equations of motion derived for this structure are given as

$$-\frac{\partial}{\partial t}\rho A\dot{w} + \frac{\partial}{\partial x}\kappa_2 GA\,(w' - \psi) + \frac{\partial}{\partial x}\kappa_2 C_s A(\dot{w}' - \dot{\psi}) - C_1\,\dot{w} + Q = 0 \quad (1)$$

$$-\frac{\partial}{\partial t}\kappa_1 \rho I\dot{\psi} + \frac{\partial}{\partial x}\kappa_1 EI\,\psi' + \kappa_2 GA\,(w' - \psi) + \frac{\partial}{\partial x}\kappa_1 C_n I\dot{\psi}' + \kappa_2 C_s A(\dot{w}' - \dot{\psi})$$

$$\boxed{+\frac{\partial}{\partial x}\left(2\kappa_s M_s h_s \sigma_s\right)}$$

$$\boxed{-\frac{\partial}{\partial x}\left(\frac{(2\kappa_a M_a h_a)^2}{\beta_a A_a}\psi'\right)}$$

$$= \boxed{-\frac{\partial}{\partial x}\left(\frac{4\kappa_a b_{sc} M_a h_a}{\beta_a A_a}\right)} \boxed{\bullet \sum_{i=1}^{m} \phi_{ai}(t)\, H(x-x_{i-1})\, H(x_i-x)} \qquad (2)$$

$$\boxed{-2\kappa_s M_s h_s \psi' - \beta_s A_s \sigma_s}$$

$$\boxed{-\sum_{i=1}^{n} 2L_i b_{cs}^2 \left[\int_0^L \ddot{\sigma}_s\, H(x-x_{i-1})\, H(x_i-x)dx\right]}$$

$$\boxed{\bullet H(x-x_{i-1})\, H(x_i-x)}$$

$$\boxed{-\sum_{i=1}^{n} 2R_i b_{cs}^2 \left[\int_0^L \dot{\sigma}_s H(x-x_{i-1})H(x_i-x)dx\right]}$$

$$\boxed{\bullet H(x-x_{i-1})H(x_i-x) = 0} \qquad (3)$$

where w is the transverse displacement of the beam and ψ is the beam bending angle. The terms ρA, ρI, GA, and EI are composite terms for the density, total cross sectional area, total moment of inertia, shear modulus of elasticity, and Youngs' modulus of elasticity for the structure. C_s, C_n, and C_l are the shear and normal strain and air damping coefficients, respectively. κ_1, κ_2, κ_s, and κ_a are terms used to account for the nonlinear deformation of the cross section of the structure.

M_a and M_s are the first moment of area of the lower actuator and sensor layers about the neutral axis, respectively. The piezoelectric stress-charge coefficients for the sensor and actuator layers are given by h_s and h_a, while β_s and β_a are the dielectric impermeabilities of the two layers. The b_c term is the width of the con ..cting surface, and A_a is the cross sectional area of the actuator layer. L is the length of the structure, and x_{i-1} and x_i are the beginning and endpoints of the i^{th} conducting segment. H represents the Heaviside step function, σ_s is the charge density of the sensor layer, and $\phi_{ai}(t)$ is the voltage applied to the i^{th} actuator segment. There are n conductor segments for the sensor layers, and m conductor segments for the actuator layers. L_i and R_i are the i^{th} inductor and resistor values. The overdots represent differentiation with respect to time, and Q represents the mechanical loading and disturbance forces.

The terms set off in boxes are the terms resulting from the piezoelectric action of both the sensor and actuator layers. Note that the forces applied by the piezoelectric actuator layers are represented by the term on the right hand side of Eq. 2. Also note that these equations are of a combined system, that is, the system is composed of both distributed and discrete elements. Applying Hamilton's Principle also yields a complete set of boundary conditions given by,

$$\int_{t_0}^{t_1}\Big[-\kappa_2 GA(w'-\psi) - \kappa_2 C_s A(\dot{w}'-\dot{\psi})\Big] \bullet \delta w \Big|_0^L dt = 0 \qquad (4)$$

$$\int_{t_0}^{t_1}\Big[-\kappa_1 EI\,\psi' - \kappa_1 C_n I\dot{\psi}' - \boxed{2\kappa_{s3} M_s h_s \sigma_s} + \boxed{\frac{(2\kappa_a M_a h_a)^2}{\beta_a A_a}\psi'} + \boxed{\frac{4\kappa_a b_s M_a h_a}{\beta_a A_a}} \sum_{i=1}^{m} \phi_{ai}(t) H(x-x_{i-1})H(x_i-x)\Big] \bullet \delta\psi \Big|_0^L dt = 0 \qquad (5)$$

where the terms in boxes result from the piezoelectric action of the outer layers.

IV. CONTROL LAW DESCRIPTION

The equations are discretized using the Ritz-Galerkin procedure, and the resulting ordinary differential equations are cast in state space form. A control law is formulated using the voltage outputs of the individual sensor segments measured at the resistor terminals, multiplied by a gain, as inputs to the corresponding actuator segments. The voltage will be proportional to the current through the resistor, such that the control law will be the electrical analogue of velocity feedback. A schematic of the control law is presented in Fig. 7.

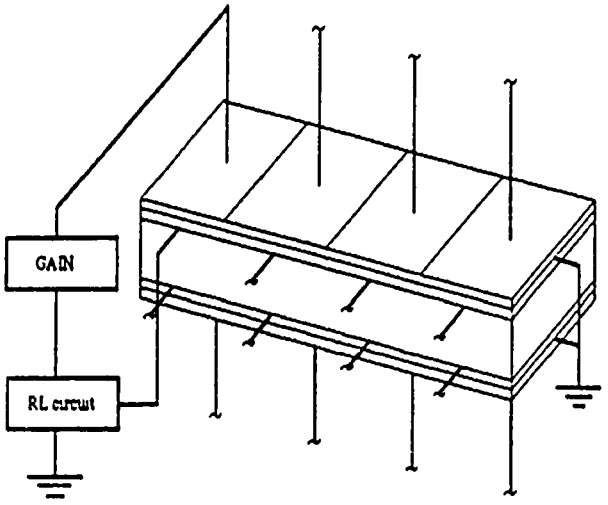

Figure 7. Schematic of the control law.

The damping mechanisms will be enhanced in the structure both by the passive energy dissipation through the resistor and by active feedback of the strain rate to the piezoelectric actuators. Two control laws are considered. In the first case, called the local control case, the sensors and actuators are collocated. The input to each actuator is only from the feedback layer segment adjacent to it. The gains are calculated by finding the maximum gain that does not cause instability in the electronic circuit. For the assumed case that the number of actuators equals the number of sensors, the feedback gain matrix is then a diagonal, square n by n matrix, where n is the number of actuators and sensors.

In the second case, called global control, each actuator segment receives information from all the feedback segments. Note that the structure is assumed to be symmetric, so that the size of the gain matrix is m by n, where n is the number of sensor segments, and m is the number of actuator segments. The gains are calculated after the model is discretized, using the LQR algorithm, where the Q and R matrices are adjusted to allow the electronic degrees of freedom to remain stable.

V. EXAMPLES AND RESULTS

A numerical demonstration of the control law is performed. The substructure properties are those of a pultruded quasi-isotropic composite viscoelastic material shown to have a high strength to weight ratio, and which has been investigated for use in manufacturing large space structures (Wilson and Miserentino, 1986). The dimensions of the substructure are .25 x .1 x .005 meters. The impact response of the first four modes of the state space model for this single layer structure is simulated. The simulation is for the structure with pinned-pinned boundary conditions, and the impact is placed at .1L, and the response is measured at .9L. The uncontrolled response of the structure is shown in Fig. 8. The sampling frequency was 8192 Hz., and the simulation was performed for .1 sec., using the MATLAB software package.

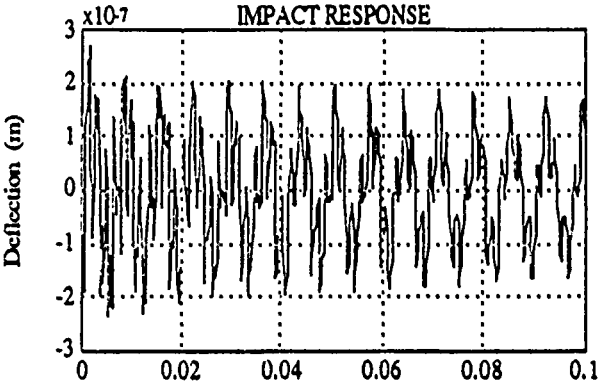

Figure 8. Uncontrolled response (Time - sec).

The structure is then modified by adding four layers of polyvinylidene flouride film to form the structure represented by Fig. 1. Each layer has a thickness of 220 x 10^{-6} m, and the resistor and inductance values are 10 kΩ and 1.0 H, respectively. The conductors are segmented into four sections, and the gains between the sensor and actuator layers represented in Fig. 2 are chosen to give a stable response. A simulation of this controlled structure to the same input that was applied to the uncontrolled structure is presented in Fig. 4.

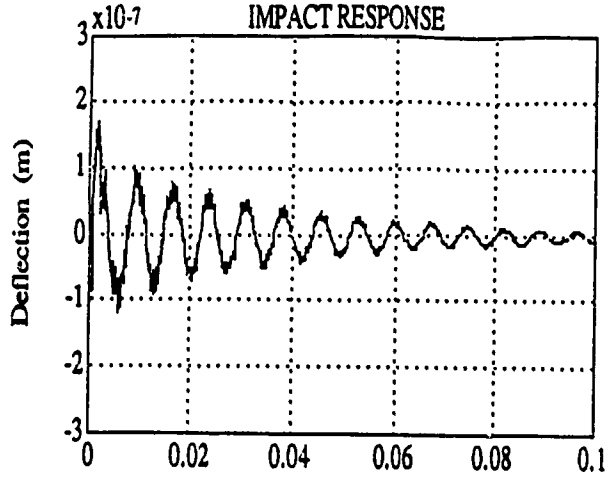

Figure 9. Case 1:Controlled response (Time - sec).

The uncontrolled and controlled damping ratios are presented in Table 1 for the local control case. Compiling the results of several simulations, it was observed the control law increases the damping ratios of all the modes simulated, with the greatest increases found in the higher modes. Using segmented the conducting surfaces yields higher damping ratios when compared to previous work using non-segmented conducting surfaces (Bailey and Hubbard, 1985).

	Uncontrolled		Controlled	
Mode	Freq.	Damping	Freq.	Damping
	(Hz.)	(% Critical)	(Hz.)	(% Critical)
1	143.52	0.15	137.89	1.65
2	572.96	0.17	552.66	5.45
3	1285.03	0.32	1251.02	10.15
4	2274.35	0.55	2169.03	38.19

The simulation was repeated for the global control case, where the signal to each actuator is composed of feedback from each of the feedback segments. It was found that a higher penalty needed to be assigned to the lower modes in the Q matrix during the calculation of the control law gains. The simulation results are shown in Fig. 10, and the calculated controlled frequencies and damping ratios are shown in Table 2.

Note that the amount of passive damping using the polyvinylidene flouride film was negligible, even when the inductors were sized such that the external circuits were tuned to a natural frequency of the structure. However, when the piezoelectric layers were given the properties of piezoceramic materials, the passive damping was significant.

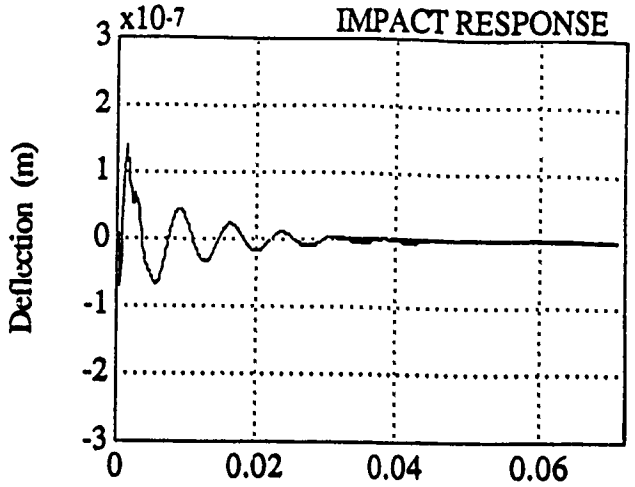

Figure 10. Global Control Using PVDF (sec).

Mode	Frequency (Hz)	Damping Ratio (% Critical)
1	138.60	10.80
2	568.97	18.71
3	1368.70	34.14
4	2315.86	65.90

Table 2. Natural Frequencies and Damping Ratios for the Global Control Case.

Note that the amount of passive damping using the polyvinylidene flouride film was negligible, even when the inductors were sized such that the external circuits were tuned to a natural frequency of the structure. However, when the piezoelectric layers were given the properties of piezoceramic materials, the passive damping was significant.

VI. CONCLUSIONS

Using a model developed for beams with multiple layers of segmented piezoelectric materials attached, a numerical study of passive and active control of the beam to increase the damping was performed. The results showed that by segmenting the conducting surfaces of the distributed piezoelectric layers, a number of modes equal to the number of segments can be controlled. This avoids the problem of not being able to control certain modes due to cancellation of the distributed sensing signal or the distributed actuator effort. In particular, control of the second mode of a pinned-pinned beam was demonstrated numerically, which would not have been possible with-

out segmenting the uniform feedback and actuation layers.

ACKNOWLEDGEMENTS

This research was supported in part by a NASA Headquarters grant from the Office of University Affairs (NGT-331-83-802), under the Graduate Students Researchers Program, administered by Dr. F. C. Owens, with Dr. G. C. Horner of the Spacecraft Dynamics Branch and Controls/Structures Interaction Office at the NASA Langley Research Center serving as technical contact and monitor. This research was also supported by an AFOSR contract (AFOSR-F49620-86-C-0111), with Lt. Col. J. Crowley serving as the contract monitor.

VII. REFERENCES

Bailey, T., and J. E. Hubbard, 1985. "Distributed Piezoelectric Polymer Active Vibration Control of a Cantilever Beam," J. Guidance, Control and Dynamics, Vol. 8 (5), pp. 605-611.

Burke, S. E., and J. E. Hubbard, Jr., 1988. "Distributed Actuator Control Design for Flexible Beams," Automatica, Vol. 24(5), pp. 619-627.

Burke, S. E., and J. E. Hubbard, 1987. "Active Vibration Control of a Simply Supported Beam Using a Spatially Distributed Actuator," IEEE Controls Systems Magazine, pp. 25-30.

Crawley, E. F., and J. de Luis, 1987. "Use of Piezoelectric Actuators as Elements of Intelligent Structures," AIAA Journal, Vol. 25, No. 10, pp. 2000 - 2010.

Cudney, H. H., 1989. "Distributed Structural Control Using Multilayered Piezoelectric Actuators," Ph.D. Dissertation, State University of New York at Buffalo, September.

Cudney, H. H., Inman, D. J., and Oshman, Y., 1989. "Distributed Parameter Actuators for Structural Control," Proceedings of the 1989 American Control Conference, June 21-23, Pittsburgh, PA, pp. 1189 - 1194 (Invited).

Cudney, H. H., Inman, D. J., and Oshman, Y., 1989. "Distributed Structural Control Using Multilayered Piezoelectric Actuators," Proceedings of the 7th VPI & SU/AIAA Symposium on Dynamics and Control of Large Structures, May 8 - 10.

Forward, R. L., 1981. "Electronic Damping of Orthogonal Bending Modes in a Cylindrical Mast Experiment," AIAA J. of Spacecraft, V. 18(1), pp. 11-17.

Hanagud, S. and M. W. Obal, 1985a. "Identification of Dynamic Coupling Coefficients in a Structure with Piezoceramic Sensors and Actuators," Proc. of the 29th AIAA/ASME/ASCE/AHS/ASC Structures, Structural Dynamics, and Materials Conference, Williamsburg, Va., pp. 1611-1620.

Hanagud, S. M. W. Obal, and M. Meyyappa, 1985b. "Electronic Damping Techniques and Active Vibration Control," Proc. of the 26th AIAA/ASME/ASCE/AHS/ASC Structures, Structural Dynamics, and Materials Conference, pp. 443-453.

Hanagud, S., M. W. Obal, and A. J. Calise, 1987. "Optimal Vibration Control by the Use of Piezoceramic Sensors and Actuators," Proc. of the 28th AIAA/ASME/ASCE/AHS/ASC Structures, Structural Dynamics, and Materials Conference, pp. 987-997.

Lee, C.-K, and F. C. Moon, 1988. "Modal Sensors/Actuators," IBM Research Report RJ 6306, submitted to the ASME J. of Applied Mechanics.

Lee, C.-K., W.-W. Chiang, and T. C. O'Sullivan, 1989. "Piezoelectric Modal Sensors and Actuators Achieving Critical Active damping on a Cantilever Plate," Proceedings of the AIAA/ASME/AHS/ASC 30th Structures, Structural Dynamics, and Materials Conference, April 3-5, Mobile, AL, pp. 2018-2026.

Tzou, H.-S., and C. I. Tseng, 1988. "Development of a Thin Piezoelectric Finite Element Applied to Distributed Sensing and Vibration Controls," Proceedings of the ASME Winter Annual Meeting, Chicago, Il., Nov. 27 - Dec. 2.

Wilson, M. L., and R. Miserentino, 1986. "Pultrusion Process Development for Long Space Boom Models," Proceedings of the 41st Annual Conference of the Reinforced Plastics/Composites Institute, Society of the Plastics Industry, paper #6-D.

Candidate Proof Mass Actuator Control Laws for the Vibration Suppression of a Frame

Jeffrey W. Umland†

Daniel J. Inman††

Dept. of Mechanical and Aerospace Engineering
University at Buffalo
Buffalo, NY 14260

Abstract

The vibration of an experimental flexible space truss is controlled with internal control forces produced by several proof mass actuators. Four candidate control law strategies are evaluated in terms of performance and robustness. These control laws are experimentally implemented on a quasi free-free planar truss. Sensor and actuator dynamics are included in the model such that the final closed loop system is self-equilibrated. The first two control laws considered are based on direct output feedback and consist of tuning the actuator feedback gains to the lowest mode intended to receive damping. The first method feeds back only the proof mass's position and velocity relative to the structure, this results in a traditional vibration absorber. The second method includes the same feedback paths as the first plus feedback of the local structural velocity. The third control law is designed with robust H_∞ control theory. The fourth control strategy is an active implementation of a viscous damper, where the actuator is configured to provide a bending moment at two points on the structure.

The vibration control system is then evaluated in terms of how it would benefit the space structure's position control system. This assessment is necessary since the additional actuator dynamics in the model effectively adds two state variables to the system which could lead to instabilities in the position control system.

1 Introduction

Proof mass actuators (PMA's) have been considered for use in large space structure vibration control systems[1]. These control systems are usually configured such that the PMA's provide a closed loop control force based on the output from a combination of both colocated and noncolocated sensors[2,3]. The colocated sensor provides measurements of the position of the proof mass relative to the structure. A benefit of colocated control is that stable control laws can be designed that provide vibration attenuation at the point of actuator attachment. Several experimental implementations of colocated PMA control have resulted in control laws that are based on the traditional vibration absorber[4,5]. In an effort to gain increased vibration attenuation, noncolocated sensors provide actual structural vibration measurements at the point where performance is desired. The problem of designing a noncolocated control is constrained by the requirement that the control law must provide stable vibration suppression at sensor locations on a flexible structure that is not necessarily well modeled.

This paper addresses the issue of the effective use of the proof mass actuator's control effort towards the robust vibration suppression of a flexible unconstrained planar frame. An

---

† Graduate Research Assistant
†† Professor

unconstrained or free-free structure is used, rather than a constrained or cantilevered structure. It is observed that in some cases an entire vehicle will vibrate indicating that a constrained analysis is not appropriate[7,8]. The approach taken is to compare several control law and actuator-sensor combinations when the actuator provides a point force on the structure. As a counterpoint, the actuator is also mounted to the structure such that the actuator's control effort provides both an axial force and a bending moment applied at two points on the structure. A control structure interaction approach is undertaken in the sense that the actuator, sensor, and controller dynamics are included or accounted for in the structural control design.

The paper outline is as follows: Section 1 gives an introduction to the control structure interaction problem undertaken here. The flexible structure control testbed is described in Section 2. The PMA control law designs to be compared are detailed in Section 3. The results of experimental implementation of these control laws are provided in Section 4. The research is summarized in the final section.

2 Hardware Description

The experimental flexible structure is constructed such that it exhibits the characteristics commonly associated with large flexible space structures. The structure is light weight, with most of its mass concentrated at the joints. There are both colocated and noncolocated sensors and actuators. The structure displays numerous modes of vibration that have a low natural frequency, are lightly damped, and are closely spaced relative to each other. A soft cable suspension system is used to simulate the free boundary conditions of space, and to minimize the effects of attaching the structure to ground.

2.1 Flexible Structure

Figure 1 illustrates the 6-bay, 3 m long plane frame. The width of the structure is 0.5 m, and the diagonal dimension is 0.707 m. The frame is constructed from aluminum truss links and joints manufactured by the Mero Corporation. A truss link consists of an aluminum tube, with nominal cross section dimensions of 22 mm O. D. and 20 mm I. D., terminated in bolt assemblies which attach to the truss nodes. The truss node is Mero's standard M12 aluminum node. The links are attached to the nodes and tightened with a torque wrench to 25 in-lb. The total weight of the structure is 61 N.

The frame is suspended from the ceiling by two soft bungee cables 2 m in length. It was found necessary to double up the cables to support the total weight of the structure and actuators. The cables are attached at nodes 2 and 6. These joints were chosen for the suspension points since they were nearly coincident with the nodes of the first structural mode of vibration, therefore minimizing the interaction of the structure and its suspension. The electrical cables are suspended from the ceiling such that they do not carry the weight of the structure, and the mass loading of the structure by these cables is minimized.

The dynamic characteristics of this structure are evident in figure 2, which shows an experimental transfer function of node 1's linear acceleration in the x direction given an impact at node 1 in the x direction. The modal properties of the first 8 structural modes of vibration are given in table 1. The vibration of the frame is characterized by flexural deflection rather than axial deflection that would occur in a true truss structure. The structure is sufficiently long such that the low structural vibration modes are not coupled to local member bending modes.

Not all of the dynamic characteristics displayed in figure 2 can be attributed to the structure, rather the suspension provides a significant portion of the response shown in this test. Three pendulous modes at approximately 1/3 Hz replaced the three rigid body modes in the x-y plane. A double pendulum mode at 1.2 Hz replaced the rigid body rotation about the y -axis. Translation in the z direction and rotation about the x axis are replaced by two translational vibration modes at 1/2 Hz which are due to stretching of the suspension cables. The cables also have transverse vibration modes that occur at 12 Hz, 37 Hz, and 55 Hz.

2.1.1 Structural Model

A finite element model of the structure was constructed for use in control design. The frame links were modeled as uniform aluminum tubes whose dimensions are the same as the manufacturer's nominal specifications. The frame joints were modeled as rigid. The combined mass of the joints and the link bolt assemblies were modeled as a point mass, with zero rotational inertia, located at each finite element node. Table 2 gives the structural parameters used in the finite element analysis. In order to simplify the model, Guyan reduction was used to eliminate translation in both the z and y directions, and rotations about the x axis. Only motion out of the y-z plane is modeled.

The transverse vibration of the suspension cables was also modeled, since these vibration modes appear in the control bandwidth. Modeling the suspension gave better agreement between the pole-zero pairs as shown in figure 2.

2.2 Proof Mass Actuators

The proof mass actuators used are illustrated in figure 3. These actuators were originally developed at the NASA Langley Research Center[1]. The intent of this design is that a magnetic field is produced by the permanent magnets and the iron in the proof mass that is normal to the current flowing through conductors in the coil. This electromagnetic coupling is then described by Eq. 1.

$$\mathbf{F} = nl\mathbf{I} \times \mathbf{B} \tag{1}$$

I represents the current carried in the conductor, n the number of conductors in the gap, **B** the magnetic field across the gap, l the length of the conductor. An average conductor length is found from the average circumference around the coil. A useful control force oriented along the axis of the coil results from this coupling. This force is then applied to the conductors in the coil, and subsequently the structure. The reaction of this force is applied to the proof mass and causes it to translate upon a linear bearing. Hence, the PMA can be modeled as providing an ideal point force at the place of attachment on the structure and a reaction force on the proof mass. This force is taken to be proportional to the current supplied to the coil. The power amplifier for the actuator is configured as a current amplifier, which provides a means by which the actuator can be controlled by a voltage signal. The proof mass actuator characteristics are given in table 3.

A complete model of the PMA should also include the dead mass and rotational inertia associated with the actuator. The motivation behind this is that for lightweight structures the actuator's dead mass will constitute a significant percentage of the total mass of the structure. The addition of a relatively large discrete mass to a structure has the tendency to attract the nodes of the higher modes of vibration of the structure to the point of attachment. This effect minimizes the ability of a point force to provide a useful control force to higher modes of vibration. The rotational inertia of the actuator used here cannot be considered negligible compared to the structure. The high actuator inertia is in part due to the overall length of actuator measured from the base.

2.2.1 Actuator Nonlinearities

There are several nonlinearities associated with the actuator, several of these are better described as saturation limits. The total stroke length of the proof mass is ±0.0127 m. The actuator produces a useful control force only when the proof mass is free to translate. Therefore, feedback of the proof mass position relative to the structure is used to maintain the proof mass in

the center of its stroke. The finite stroke length is the limiting factor for low frequency, large amplitude motions.

The power amplifier used is operated as a voltage controlled current amplifier On the amplifier there is a current limiter that provides for a saturation limit on the output. The maximum output current of the amplifier determines the maximum force output of the actuator. An important design tradeoff here is to determine how much control effort should be used towards the proof mass centering force and how much should be available for a control force based on a noncolocated sensor.

The damping in the actuator is primarily due to friction in the linear bearing and steel shaft interface. This friction has been described by a typical Coulomb friction relation. The normal load that generates the friction force is a combination of the weight of the proof mass and a magnetic force between the permanent magnets and the steel shaft and ball bearings. These frictional effects further limit the effectiveness of the actuator at low frequencies. Secondly, the source of the damping is important in the sense that previously implemented PMA control laws have relied upon available actuator damping to obtain closed loop stability. The problem is that a large portion of this damping would not be available in a zero-g environment.

The electromagnetic coupling between the coil and the proof mass is described by Eq. 1 for only a portion of the total stroke. This is illustrated in figure 4. This plot shows the static force produced by the actuator for a constant input current. Ideally the actuator should output a constant force for a constant input current independent of the stroke position. During bench testing of the actuator, this led to closed loop instability.

2.2.2 Attachment to Structure

The structural equations of motion must be modified to include the actuator dynamics. The structure is originally described by m degrees of freedom **x**, and if n actuators are used then n degrees of freedom represented by the relative displacements η are appended to the equations of motion. Note that the coupling appears in the mass matrix rather than the stiffness matrix.

$$M_{ol}\,\ddot{\mathbf{x}} + K_{ol}\,\mathbf{x} = B\,\mathbf{f_g} \tag{2a}$$

$$\mathbf{x} = \left\{ x_{fem} \quad \eta_{act} \right\}^T \tag{2b}$$

$$K_{ol} = \begin{bmatrix} K_{fem} & 0_{mxn} \\ 0_{nxm} & 0_{nxn} \end{bmatrix} \tag{2c}$$

$$M_{ol} = \begin{bmatrix} M_{fem} & 0_{mxn} \\ 0_{nxm} & 0_{nxn} \end{bmatrix} + \begin{bmatrix} M_d + J_d + M_{p1} & M_{p2} \\ M_{p2}^T & m_p I_{nxn} \end{bmatrix} \tag{2d}$$

$$M_d = m_d\ \mathrm{diag}(0,\ldots,\ 0,1,0,0,\ldots,0) \tag{2e}$$

$$J_d = j_d\ \mathrm{diag}(0,\ldots,\ 0,0,1,0,\ldots,0) \tag{2f}$$

$$M_{p1} = m_p\ \mathrm{diag}(0,\ldots,\ 0,1,0,0,\ldots,0) \tag{2g}$$

$$M_{p2j} = m_p(0,\ldots,\ 0,1,0,0,\ldots,0)^T,\ j = 1{:}n \tag{2h}$$

$$B = \begin{bmatrix} 0_{mxn} \\ g_{act} I_{nxn} \end{bmatrix} \tag{2i}$$

2.3 Linear Variable Differential Transformer

A linear variable differential transformer (LVDT) is mounted on each PMA to provide a measurement of the proof mass position relative to the structure. The LVDT used is a Schaevitz Eng. No. 500. The input voltage is selected such that a displacement of ±0.375 inch produces ±5 Volts. The sensor bandwidth is 0 - 500 Hz. These sensors produce a measurement that is colocated with the control force.

2.4 Accelerometers

The structural sensors are Kistler Piezobeam accelerometers. The calibration is 10 mv/g, and have a frequency range of 0.5 to 5000 Hz. An approximate integrator is then used to integrate the acceleration signal to provide a measurement of the structural velocity[2]. The approximate integrator is given by the following input/output description

$$\frac{O}{I}(s) = \frac{\omega_c^2 s}{s^2 + \omega_c s + \omega_c^2} \tag{3}$$

This approximate integrator is the combination of a critically damped unity gain second order low pass filter, and a pure differentiator. The low pass filter provides the integrating action, while the differentiator removes the DC portion of the input signal. The transfer function is strictly proper, giving a state space realization for either analog or digital implementation. This type of integrator is used in order to avoid the integration of any DC bias produced by the accelerometer and associated signal conditioning.

2.5 Digital Controller

The digital controller used is a Systolic Systems Optima 3. The input and output voltage range is ±5 Volts The input channels are anti-alias filtered and the output channels are smooth filtered. The digital to analog converters on this system present a practical design issue, since they do not saturate. Rather, when the control law produces an output that exceeds the output range of the converter the conversion process wraps the desired signal value around the available output range. In other words, if the control law produces a desired signal of 6 Volt, the D/A converters will produce a -4 Volt signal. The solution to this problem used is to place the static controller gain on the power amplifiers. This is fine for static compensators or direct output feedback of sensor signals of known and bounded signal strength, such as the LVDT output. For dynamic compensators this is not necessarily a robust solution. A second solution would be to place logic statements in the control software that would provide saturation levels. Such logic statements would lower the achievable sampling rate.

3 Control Design

The application of a proof mass actuator to the control of a simple flexible structure is considered in this section. The structure consists of one rigid body mode, and one flexible mode of vibration. This problem is illustrated in figure 5. This problem has been proposed as a benchmark robust control problem[14]. The difference here is that the control force is produced by an actuator whose dynamics cannot be ignored. The open loop equations for this system are given by

$$\begin{bmatrix} M_S & 0 & 0 \\ 0 & M_S+m_p+m_d & m_p \\ 0 & m_p & m_p \end{bmatrix}\begin{Bmatrix} \ddot{x}1 \\ \ddot{x}2 \\ \ddot{\eta} \end{Bmatrix} + \begin{bmatrix} K_S & -K_S & 0 \\ -K_S & K_S & 0 \\ 0 & 0 & 0 \end{bmatrix}\begin{Bmatrix} x1 \\ x2 \\ \eta \end{Bmatrix} = g_{act}\begin{Bmatrix} 0 \\ 0 \\ 1 \end{Bmatrix} f_g(t) + \begin{Bmatrix} -1 \\ 1 \\ 0 \end{Bmatrix} d(t) \qquad (4)$$

The measurement equations are for the relative position, η,

$$y_p = K_{LVDT}\eta = [0\ 0\ K_{LVDT}]\ x \qquad (5)$$

The following values are used for all calculations in this section.

$M_s = 1$
$0.5 < K_s < 2$, nominally $K_s = 1$
$m_p = 0.2$
$m_d = 0$
$g_{act} = 1$
$K_{LVDT} = 1$

In the following subsections several vibration control strategies are considered. The effectiveness of each system is then evaluated by giving the system an impact disturbance across masses 1 and 2, and the response of x_2 is measured. This type of disturbance does not excite the system's rigid body mode.

3.1 Controllability

The controllability of this system is then computed with standard techniques[9]

$$\text{rank}\left[B\ AB\ A^2B\ \ldots\ A^5B\right] = 4 \neq 6 \qquad (6)$$

Indicating that the system is not completely controllable. The control force produced by the actuator should be considered as a force internal to the system, and as such cannot change the location and motion of the system's center of mass. The lack of complete controllability is because the actuator cannot control the rigid body mode of the system. A further explanation of this is the actuator configured as a point force cannot produce a force at zero frequency. Therefore, a statement of the obvious is that the actuator should be only used for vibration control. In other words the actuator should be used to give the structure damping. It is also evident that a rigid body control system must be designed for this system. A design goal for the vibration control system is that it should enhance the rigid body controller.

3.2 Observability

The observability of the system is computed from

$$\text{rank}\left[C\ CA\ CA^2\ \ldots\ CA^5\right]^T = 4 \neq 6 \qquad (7)$$

Indicating that the system is also not completely observable. Similar to the previous section the rigid body modes of the system are not observable.

3.3 Vibration Absorber

The first control law considered is direct feedback of the relative proof mass position, η, and velocity, $\dot{\eta}$. This is considered a colocated design, since the resulting closed loop stiffness and damping matrices are symmetric. Although the LVDT measures the position η only, it is assumed that $\dot{\eta}$ is available from a lead network or digital derivative. This type of feedback compensation is a proportional plus derivative control. Equivalently, this type of control may also be thought of as designing an actuator spring stiffness, k_a, and viscous damper, c_a. One criterion for the choice of the feedback gains, k_a and c_a, is that used to design a passive vibration absorber[10,11,4]. The actuator spring stiffness is found from

$$\omega_a^2 = \frac{k_a}{m_p} = \frac{\omega_i^2}{(1+\mu_a)^2} \tag{8}$$

$$c_a^2 = m_p \mu_a \omega_i^2 \frac{1}{(1+\mu_a)^3} \tag{9}$$

$\mu_a = m_p(\phi_{ij})^2$
$k_a = g_{act}K_{pos}K_{LVDT}$
$c_a = g_{act}K_{vel}K_{LVDT}$
ω_i - frequency of interest, ith mode
ϕ_{ij} - jth degree of freedom, eigenvector of the ith mode, normalized with respect to the mass matrix

The resulting closed loop equations of motion are then

$$\begin{bmatrix} M_S & 0 & 0 \\ 0 & M_S+m_p+m_d & m_p \\ 0 & m_p & m_p \end{bmatrix}\begin{Bmatrix} \ddot{x}1 \\ \ddot{x}2 \\ \ddot{\eta} \end{Bmatrix} + \begin{bmatrix} 0 & 0 & 0 \\ 0 & 0 & 0 \\ 0 & 0 & c_a \end{bmatrix}\begin{Bmatrix} \dot{x}1 \\ \dot{x}2 \\ \dot{\eta} \end{Bmatrix} + \begin{bmatrix} K_S & -K_S & 0 \\ -K_S & K_S & 0 \\ 0 & 0 & k_a \end{bmatrix}\begin{Bmatrix} x1 \\ x2 \\ \eta \end{Bmatrix} = \begin{Bmatrix} -1 \\ 1 \\ 0 \end{Bmatrix} d(t) \tag{10}$$

Alternatively, the feedback gains can be calculated from the following quadratic cost function[11]

$$J = E\left[\int_0^\infty q_{ei}^2 \, dt\right] = E\left[\int_0^\infty z^T Q z \, dt\right] \tag{11}$$

This system is stable provided that the feedback gains, k_a and c_a, are positive. The constant gain feedback of sensor signals that are colocated with an actuator does not destabilize the system. The colocation of sensors and actuators is evidenced by the symmetric closed loop stiffness and damping matrices.

The spring stiffness and damping coefficient for this example are calculated to be

$k_a = 0.331$
~~$c_a = 0.173$~~
$c_a = 0.0680$

The response of x_2 for the given disturbance is shown in figure 7. The responses shown are calculated for the minimum, maximum and nominal value for the structural spring stiffness, K_S. The vibration control system's performance when K_S is increased to its maximum value is comparable to its performance for the nominal value of K_S. On the other hand, when K_S is allowed to decrease to its minimum the performance of the system is diminished.

The performance of this type of control is explained in a control system sense as a pole-zero cancellation. The second order dynamics of the PMA add a pole and a zero to the system, which will be less that the structure's pole and zero. The zero associated with the structure will appear in between the actuator pole and the structural pole. These poles are closely spaced, since the mass ratio, μ_a, is usually small. Hence, the structural zero will tend to cancel either the actuator or the structural pole, depending on sensor and actuator placement. Because this type of control relies upon pole zero cancellation its effectiveness for more than one mode of vibration is limited.

3.4 Direct Velocity Feedback

The second control strategy considered consists of direct structural velocity feedback[13]. The idea being that the actuator will provide a force at a given point on the structure that is directly proportional and opposite in direction to the structure's velocity at that point. It is pointed that the control force is determined on the basis of both a colocated and a noncolocated sensor. Therefore, the stability of the closed loop system must be considered. The difficulty here is the design of the feedback compensator to provide the proof mass centering force. The control force is given as

$$f_g(t) = c\,\dot{x}_2 - f(\eta) \tag{12}$$

where $f(\eta)$ represents the output of the feedback compensator.

In the following subsections the velocity feedback gain, c, is held constant and two feedback compensators for η are designed. The value used for the feedback gain c is

$$c = 0.5$$

3.4.1 Direct Output Feedback

In this section a proportional plus derivative compensator is designed for the feedback of the proof mass relative position, η. Again, this type of control may be thought of as determining an equivalent actuator spring stiffness, k_a, and viscous damper, c_a. The control force is

$$f_g(t) = c\,\dot{x}_2 - k_a\eta - c_a\dot{\eta} \tag{13}$$

The closed loop equations of motion for this system are then

$$\begin{bmatrix} M_S & 0 & 0 \\ 0 & M_S+m_p & m_p \\ 0 & m_p & m_p \end{bmatrix}\begin{Bmatrix} \ddot{x}_1 \\ \ddot{x}_2 \\ \ddot{\eta} \end{Bmatrix} + \begin{bmatrix} 0 & 0 & 0 \\ 0 & 0 & 0 \\ 0 & -c & c_a \end{bmatrix}\begin{Bmatrix} \dot{x}_1 \\ \dot{x}_2 \\ \dot{\eta} \end{Bmatrix} + \begin{bmatrix} K_S & -K_S & 0 \\ -K_S & K_S & 0 \\ 0 & 0 & k_a \end{bmatrix}\begin{Bmatrix} x_1 \\ x_2 \\ \eta \end{Bmatrix} = \begin{Bmatrix} -1 \\ 1 \\ 0 \end{Bmatrix} d(t) \tag{14}$$

This is a noncolocated control system, and as such its stability is in question. The characteristic equation for this system is evaluated to be

$$s^2\left[s^4 + \left(\frac{c_a+c}{M_s} + \frac{c_a}{m_p}\right)s^3 + \left(\frac{2K_s+k_p}{M_s} + \frac{k_p}{m_p}\right)s^2 + \left(\frac{(c_a+c)K_s}{M_s^2} + \frac{2c_aK_s}{M_sm_p}\right)s + \left(\frac{K_sk_p}{M_s^2m_p}(2M_s + m_p)\right)\right] = 0 \qquad (15)$$

Applying the Routh-Hurwitz test to portion of the characteristic equation inside the brackets the following stability relation is obtained, assuming that each individual parameter is positive

$$\left(c_a^2 + 2c_ac + c^2\right)K_s^2m_p^2 + \left[2\left(c_a^2 + c_ac\right)K_s^2 + \left(-c_ac - c^2\right)K_sk_a\right]M_sm_p - c_acK_sk_aM_s^2 > 0 \qquad (16)$$

When the actuator damping is held at zero, i. e. $c_a = 0$, Eq.13 reduces to

$$\frac{K_s}{M_s} > \frac{k_a}{m_p} \qquad (17)$$

In other words, the actuator natural frequency should be less than the structure's natural frequency of vibration. Also, note that the velocity feedback gain, c, is not present in Eq. 14. Figure 6 illustrates the stability boundary of k_a for a range of both c_a and c, for the nominal spring stiffness K_s. Actuator spring stiffnesses below this boundary result in a stable system. The smallest stable k_a in figure 6 occurs for $c_a = 0$, independent of c. Also, the surface is relatively flat over most of the range of c_a and c, indicating that in this case stability is insensitive to actuator damping. In order to ensure stability robustness against the permissible variations in the structural spring stiffness, K_s, the minimum permitted value should be used as the nominal of design value.

The feedback gains, k_a and c_a, are determined by following the same optimization strategy that was outlined in the previous section[12]. For this example k_a and c_a are found to be

$k_a = 0.105$
$c_a = -0.0027$

The performance of this system is illustrated in figure 8. The system's settling time for both the nominal and maximum spring stiffnesses is less than that of the vibration absorber design. Although it is not apparent in this figure, when K_s is varied to its minimum value the system becomes unstable.

Following this strategy the actuator spring stiffness is found to be less than the vibration absorber spring stiffness. Performance is improved with an increased feedback gain c. In comparison to the vibration absorber system the proof mass here exhibits more relative motion and does more work on the structure.

3.4.2 Robust Control Design

An attempt to design a compensator for the feedback of the relative position, η, using an H_∞ robust control design technique was unsuccessful. The system rigid body modes were first removed from the state space equations of motion by model reduction. The rigid body mode associated with the proof mass was retained in the system equations, since it is this output that the compensator is being designed to control. The H_∞ design procedure failed because there was a plant pole on the $j\omega$-axis which then produces a closed loop pole also on the $j\omega$-axis.

3.5 Passive Damper

As a counterpoint to the above control designs the actuator is also configured to act as a passive linear damper which applies a bending moment at two locations on the structure, as shown in figure 10. Only feedback of the proof mass relative velocity, $\dot{\eta}$ is used here. In other words this is direct velocity feedback. A proof mass centering force is not required since this is provided for by the structure and fixturing. The actuator can be attached at nonadjacent joint locations to better distribute the control effort to low frequency modes.

4 Experimental Implementation

The experimental implementation of the control laws considered above is addressed in this section. An impact is given to the structure at node 1 in the x direction and the structure's acceleration is measured at node 4 also in the x direction. Each response is filtered with a 25 Hz low pass filter to give a cleaner picture of the actuator's effect. The resulting settling time for each test is used as a measure of control law performance. The actuator location is chosen in order to provide the greatest effect on the first vibration mode. The control laws are implemented digitally, with the sampling rate for each set at 4000Hz. As a basis for comparison the response of the uncontrolled structure is shown in figure 10. The settling time for this test is greater than 3.5 seconds. It is also evident that the structure must be considered more complicated than a single degree of freedom.

The vibration absorber was designed to provide damping to the first mode whose frequency is shifted to 5.8 Hz when the actuator dead mass and inertia are added. The actuator is placed at node 4. The result of this implementation is illustrated in figure 11. It is seen here that the settling time is reduced in comparison to the uncontrolled structure, but is greater than 2.5 seconds. When the actuator was tuned to the second mode at approximately 12 Hz the actuator was made unstable. This is a result of the nonlinear electromagnetic coupling of the coil and permanent magnets.

The effect of adding structural velocity feedback is shown in figure 12. The acceleration of node 4 is integrated by the approximate integrator given in Eq. 3. The cutoff frequency for the integrator is 1 Hz. Following the stability guideline for this case the actuator spring stiffness is kept low such that the actuator frequency is below that of the first mode of vibration. The settling time for this case is an improvement from the vibration absorber. Figure 12 displays a signal of approximately 1 Hz, which is the double pendulum mode of the structure suspension system. Closed loop instability for this set of feedback paths resulted when the magnitude of the disturbance impact caused the proof mass to hit the end of its stroke. These resulting impacts caused the accelerometer to overload which subsequently made the control computer overflow which induced the more proof mass impacts.

Figure 13 illustrates that the viscous damper implementation has an effect comparable to that of using structural velocity feedback. Although, there is more second mode behavior for this case. The actuator was attached at nodes 3 and 5. In comparison to the point force application of the actuator where the proof mass uses the entire stroke length, the travel of the proof mass here is at most 0.25 in.

5 Conclusions

Several structural vibration control laws have been considered analytically and implemented experimentally. Two of these control strategies are essentially active implementations of passive control concepts, namely the viscous damper and the vibration absorber. The feedback of the local structural velocity is an active control idea. A control structure interaction approach was taken in the sense that the actuator dynamics were included in the control design, and that there are several nonlinearities in the closed loop system that can lead to instability.

6 References

[1]Zimmerman, D. C., G. C. Horner, and D. J. Inman, 1988. "Microprocessor Controlled Force Actuator," *AIAA J. of Guidance, Control, and Dynamics*, Vol. 11, No. 3, pp. 230-236.

[2]Hallauer, W. and S. Lamberson, 1989. "Experimental Active Vibration Damping of a Plane Truss Using Hybrid Actuation," AIAA Paper No. 89-1169, *Proc. of the 30th AIAA/ASME/ASME/ASCE/AHS/ASC Structures, Structural Dynamics, and Materials Conference*, Mobile, AL, pp. 80-90.

[3]Balas, G. J., and J. C. Doyle, 1990. "Collocated versus Non-collocated Multivariable Control for Flexible Structure," *Proc. of the 1990 American Control Conference*, San Diego, CA, pp. 1923-1928.

[4]Minas, C., E. G. Garcia, D. J. Inman, 1989. "Control of a Flexible Planar Truss Using Proof Mass Actuators," *Proc. of the 3rd Annual Conference on Aerospace Computational Control*, Oxnard, CA, pp. 434-445.

[5]Miller, D. W. and E. F. Crawley, 1988. "Theoretical and Experimental Investigation of Space-Realizable Inertial Actuation for Passive and Active Structural Control," *AIAA J. of Guidance, Control, and Dynamics*, Vol. 11, No. 5, pp. 449-458.

[6]Balas, M. J., 1982, "Trends in Large Space Structure Control Theory: Fondest Hopes, Wildest Dreams," *IEEE Trans. on Automatic Control*, Vol. AC-27, No. 3, pp. 522-535.

[7]Hablani, H. B., 1982. "Constrained and Unconstrained Modes: Some Modeling Aspects of Flexible Spacecraft," *AIAA J. of Guidance, Control, and Dynamics*, Vol. 5, No. 2, pp. 164-173.

[8]Hughes, P. C., 1974. "Dynamics of Flexible Space Vehicles with Active Attitude Control," *Celestial Mechanics*, Vol. 9, pp 21-39.

[9]Inman, D. J., 1989. *Vibration with Control, Measurement, and Stability*, Prentice Hall, Englewood Cliffs, NJ.

[10]Den Hartog, J. P., 1956. *Mechanical Vibrations*, 4th ed., McGraw-Hill Book Co., New York, NY.

[11]Juang, J., 1984. "Optimal Design of a Passive Vibration Absorber for a Truss Beam," *AIAA J. of Guidance, Control, and Dynamics*, Vol. 7, No. 6, pp. 733-739.

12 Umland, J. W., 1989. "Proof Mass Actuators and Vibration Absorption," Mechanical Systems Laboratory Report No. 89-10, State University of New York at Buffalo, Buffalo, NY.

[13]Balas, M. J., 1979. "Direct Velocity Feedback Control of Large Space Structures," *AIAA J. Of Guidance and Control*, Vol. 2, No. 3, pp. 252-253.

[14]Wie, B., and D. S. Bernstein, 1990. "A Benchmark Problem for Robust Control Design," *Proc. of the 1990 American Control Conference*, San Diego, CA, pp. 961-962.

Mode #	Experimental Natural Frequency (Hz)	Damping Ratio (%)	MSC/PAL Natural Frequency (Hz)	Mode Type
1	6.4	0.021	6.5	1st bending
2	15.1	0.026	15.6	1st torsional
3	17.7	0.010	17.7	2nd bending
4	29.6	0.018	29.9	2nd torsional
5	35.4	0.025	35.2	3rd bending
6	45.6	0.014	45.2	3rd torsional
7	58.0	0.026	55.6	4th bending
8	63.3	0.022	60.8	4th torsional

Table 1: Modal Properties of Flexible Structure

Link O. D.	d_o	22 mm
Link I. D.	d_i	20 mm
Density	ρ	2.45×10^3 kg/m^3
Elastic modulus	E	70 GPa
Shear modulus	G	26 GPa
Joint mass	m_j	0.0759 kg
Bolt mass	m_b	0.0578 kg

Table 2: Structure link and joint characteristics

Proof mass	m_p	0.225 kg
Dead mass	m_d	0.730 kg
Dead inertia	j_d	0.008 kg-m^2
Force constant	g_{act}	2.75 N/A
Friction coefficient	μ	0.01

Table 3: Linear Proof Mass Actuator Properties

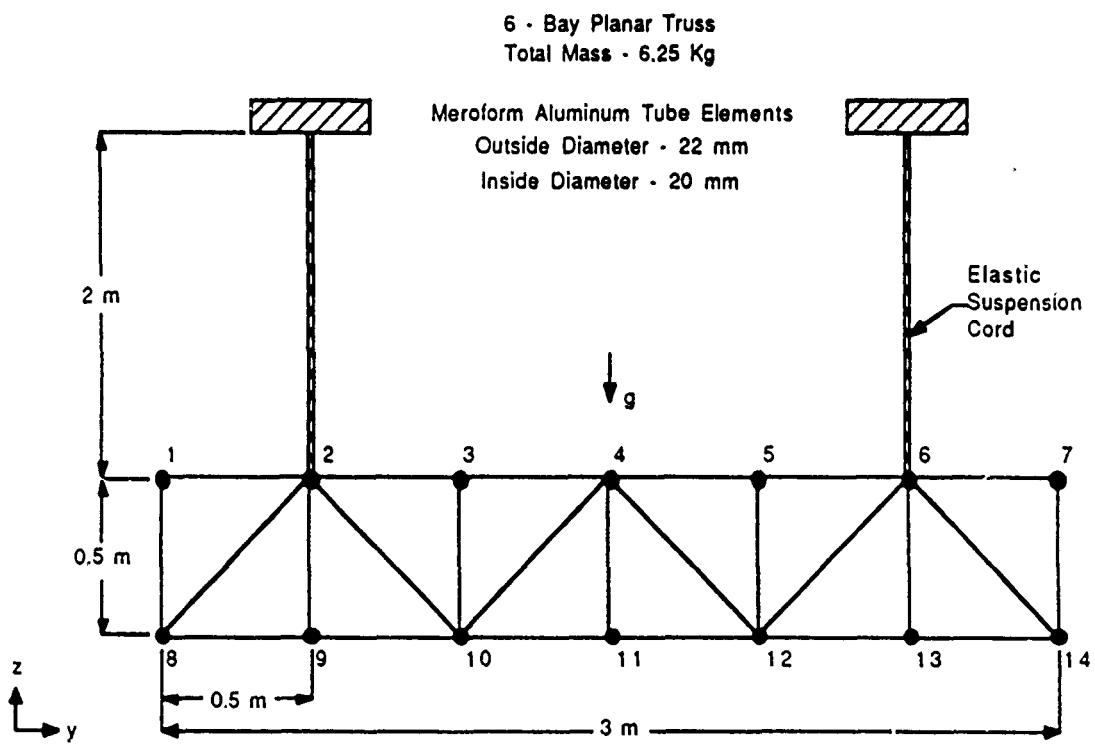

Figure 1: Experimental Flexible Structure

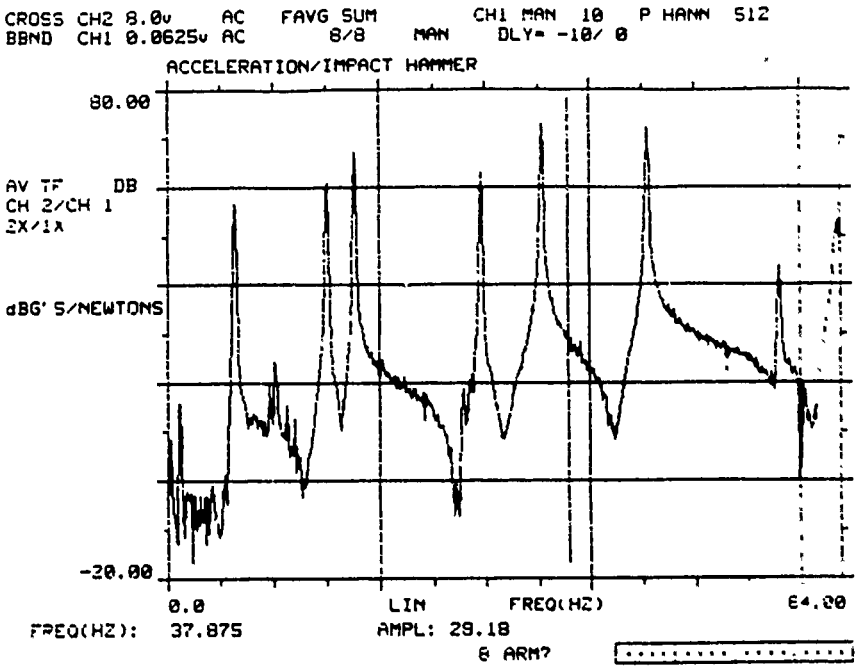

Figure 2a: Experimental Frequency Response

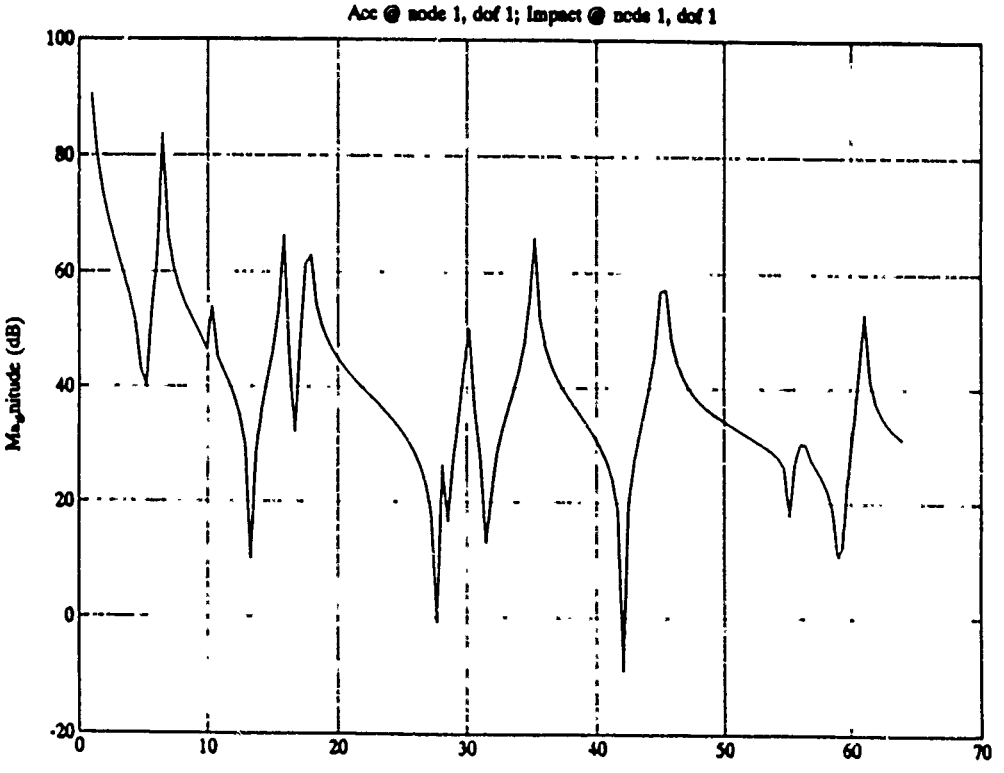

Figure 2b: Analytical Frequency Response

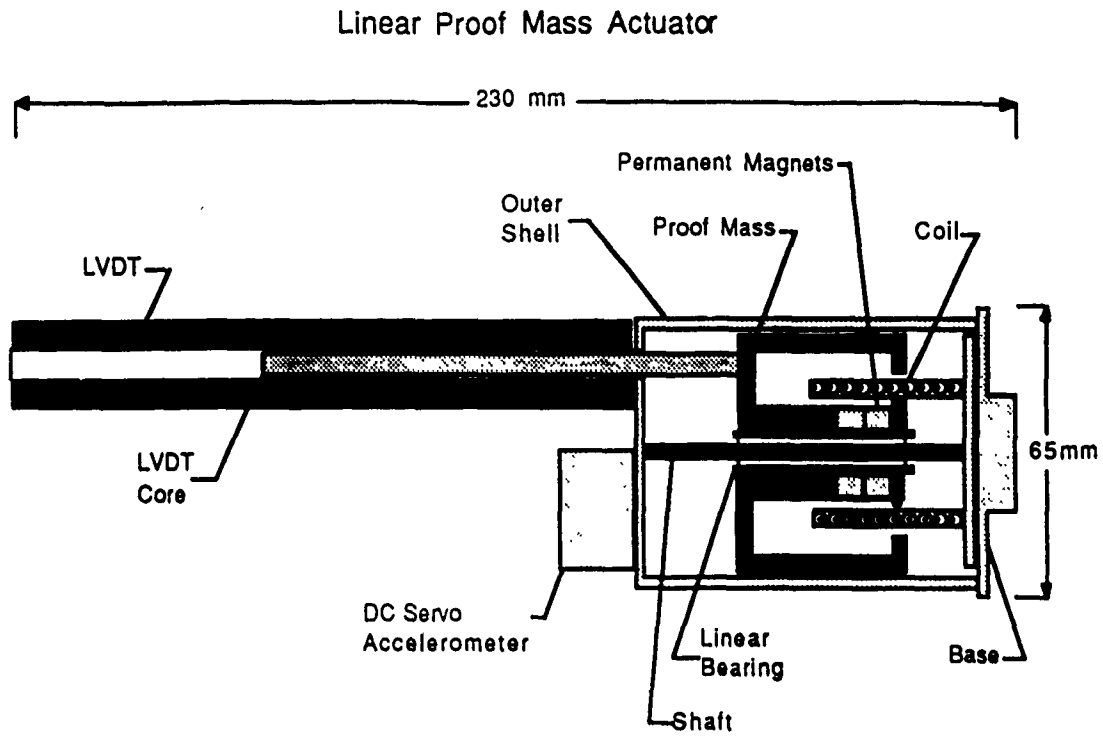

Figure 3: Linear Proof Mass Actuator

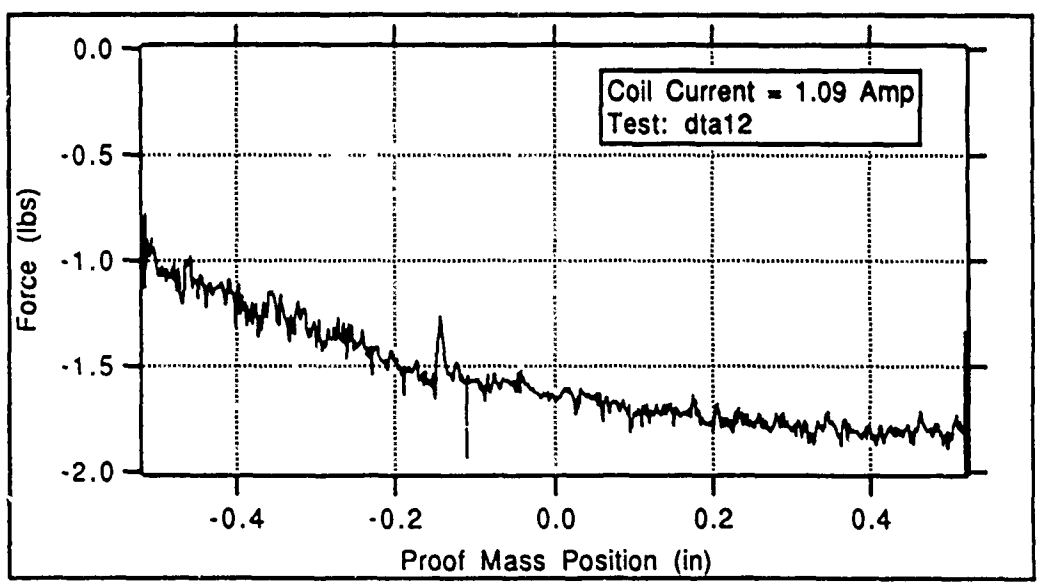

Figure 4: Static force versus proof mass position, coil current constant

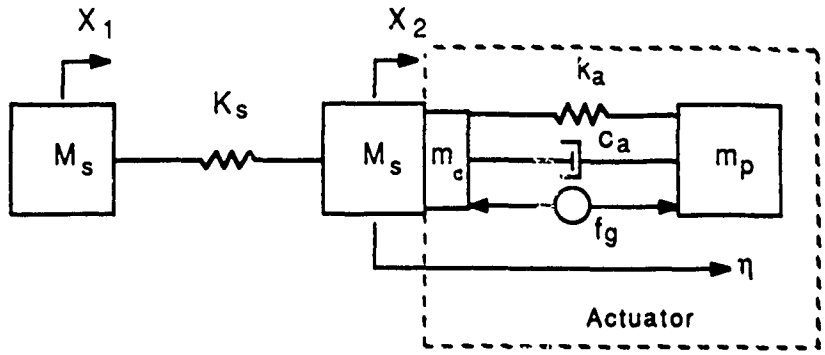

Figure 5: Free single mode structure with proof mass actuator

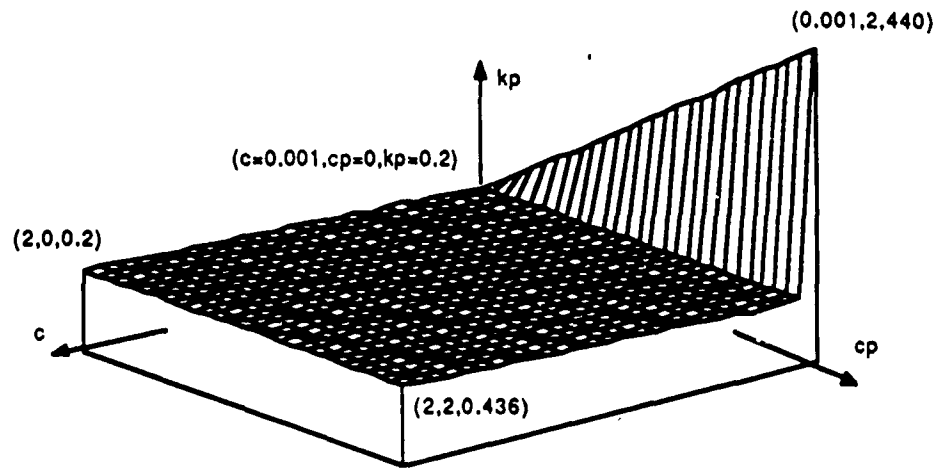

Figure 6: Constant feedback gain stability map

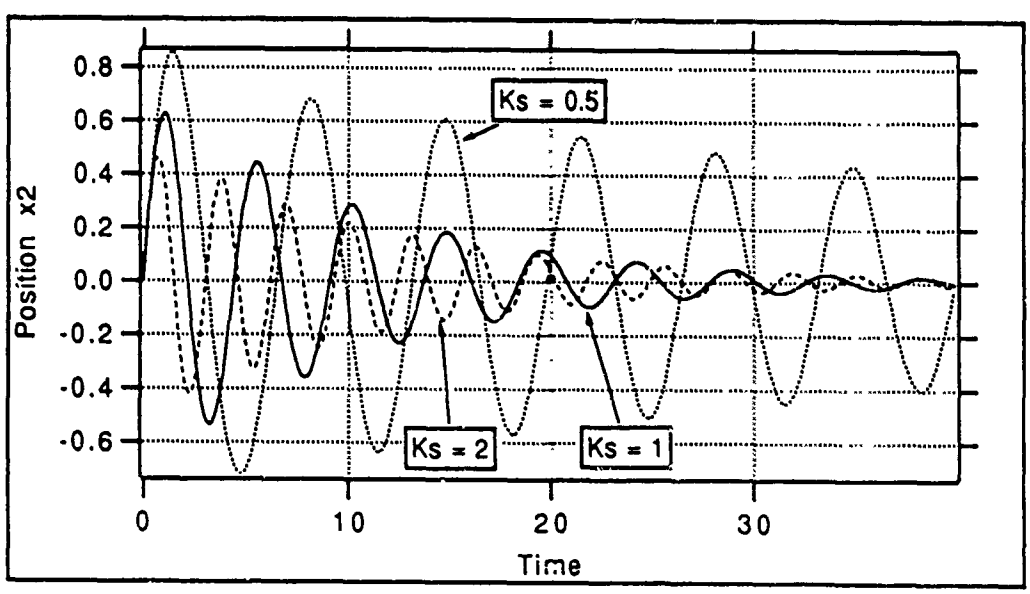

Figure 7: X_2 response to disturbance for minimum, maximum, and nominal K_s, vibration absorber design.

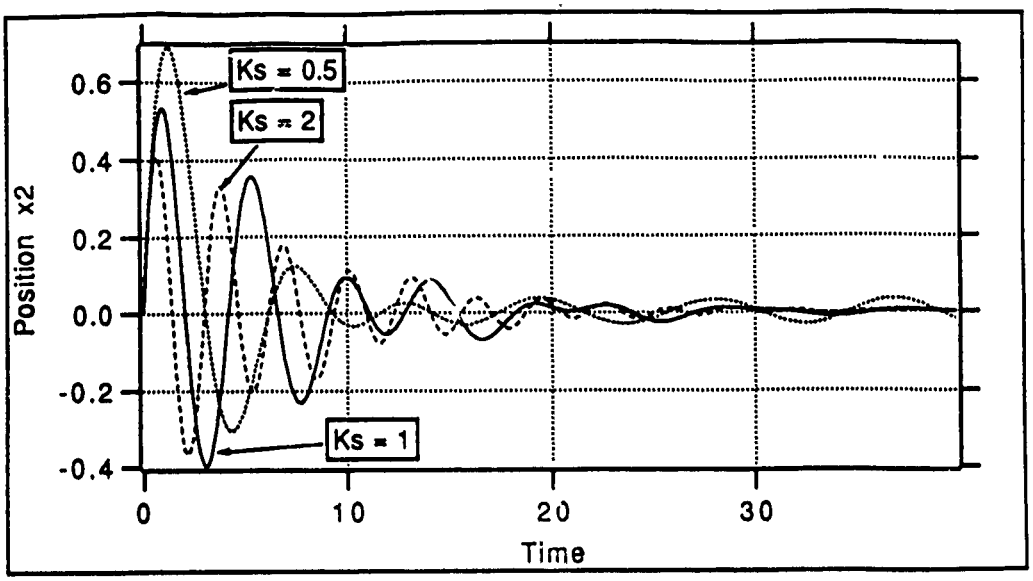

Figure 8:X2 response to disturbance for minimum, maximum, and nominal Ks, with structural velocity feedback.

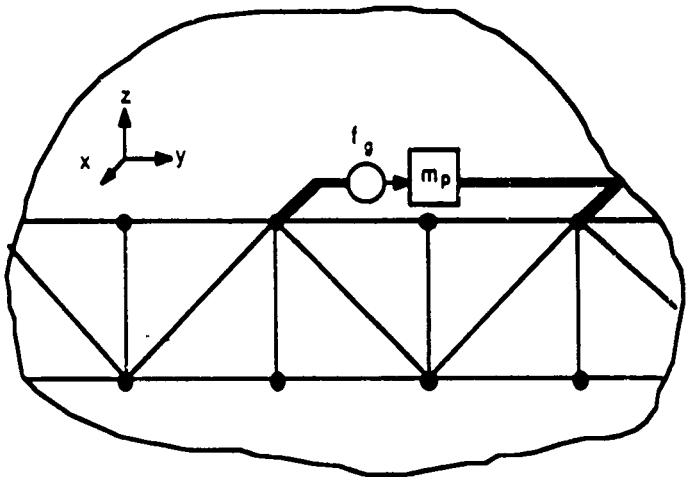

Figure 9: Viscous damper configuration

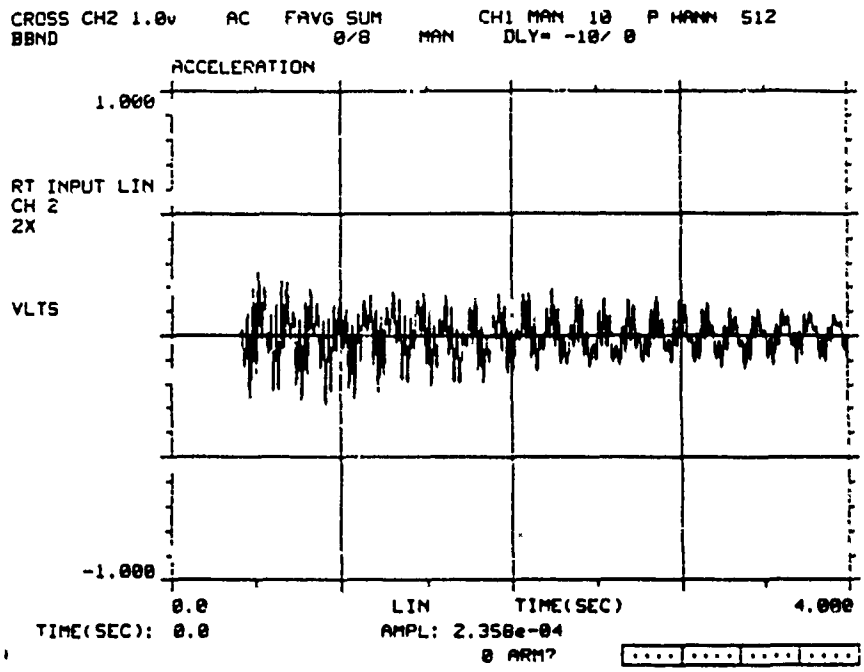

Figure 10: Response of uncontrolled structure.

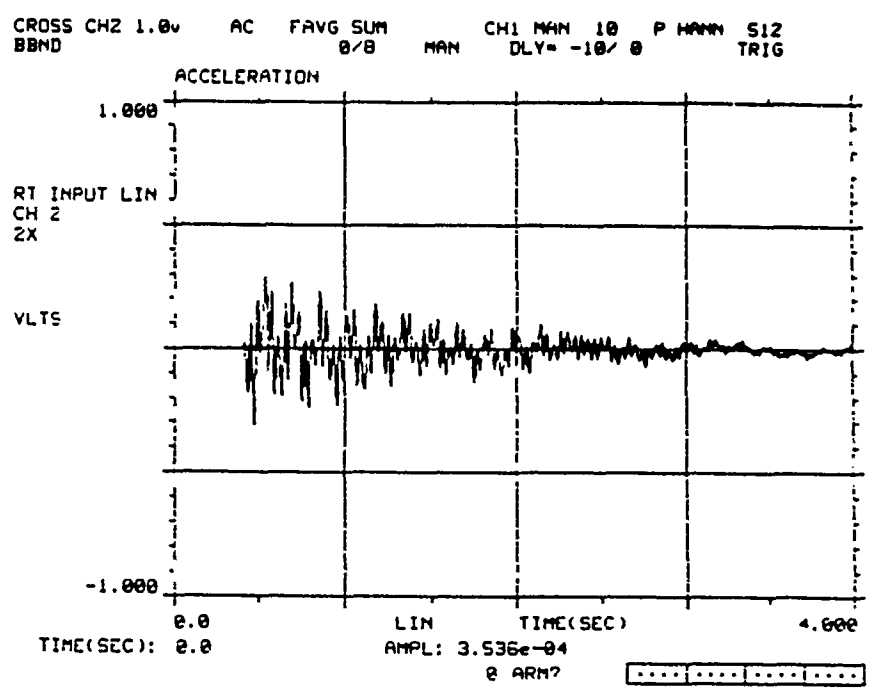

Figure 11: Response of structure, vibration absorber design.

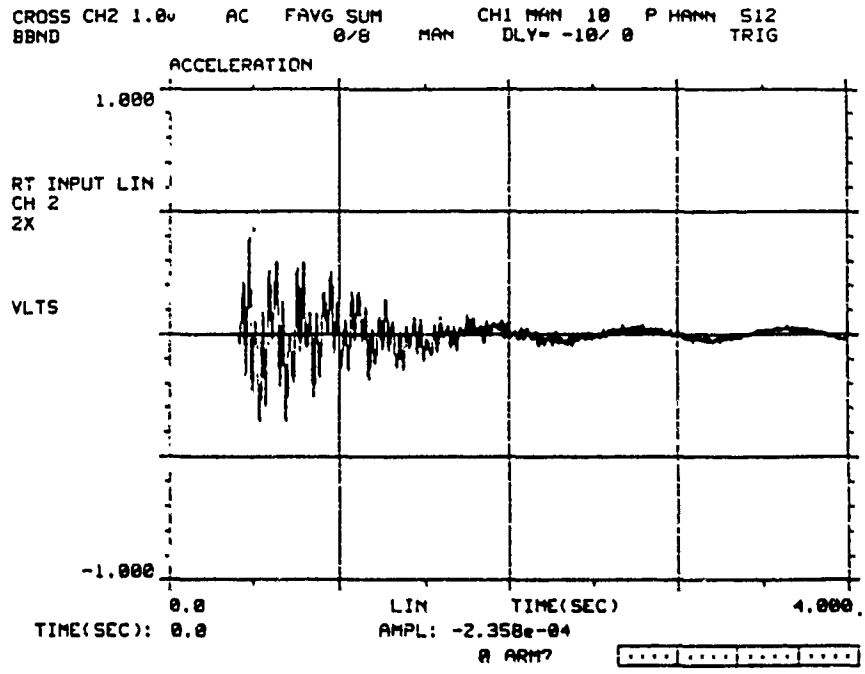

Figure 12: Response of structure, direct velocity feedback.

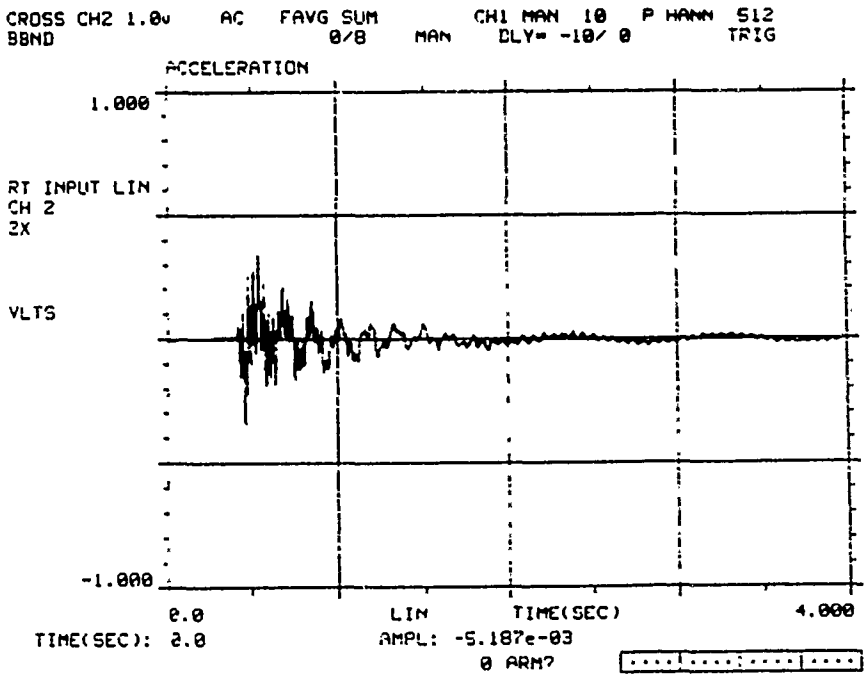

Figure 13: Response of structure, viscous damper.

3rd. Int. Conf. on Recent Oxford

CONTROL OF A FLEXIBLE PLANAR TRUSS USING PROOF MASS ACTUATORS

Constantinos Minas*
Ephrahim Garcia
Daniel J. Inman
Department of Mechanical and Aerospace Engineering
State University of New York at Buffalo
Buffalo, N.Y. 14260

Abstract

A flexible structure was modelled and actively controlled by using a single space realizable linear proof mass actuator. The NASA/UVA/UB actuator was attached to a flexible planar truss structure at an "optimal" location and it was considered as both passive and active device. The placement of the actuator was specified by examining the eigenvalues of the modified model that included the actuator dynamics, and the frequency response functions of the modified system. The electronic stiffness of the actuator was specified, such that the proof mass actuator system was tuned to the fourth structural mode of the truss by using traditional vibration absorber design. The active control law was limited to velocity feedback by integrating of the signals of two accelerometers attached to the structure. The two lower modes of the closed-loop structure were placed further in the LHS of the complex plane. The theoretically predicted passive and active control law was experimentally verified.

1. Introduction

Large continuous structures, like space structures tend to have tight restrictions on the actual response of the structure. A passive or active control design is often necessary for the structure to satisfy the desired response restrictions. The success of the passive and active control design is based on the accuracy of the model that describes the dynamic characteristics of the structure. Flexible distributed parameter systems can be successfully modelled by finite element analysis [1]. This category of structures is lightly damped and tends to have most of its mass concentrated at the joints [2]. Their natural frequencies are low and appear in closely spaced groups. The finite element model of the structure that consists of a mass and a stiffness matrix, can be reduced by traditional model reduction techniques by eliminating the insignificant displacements at the nodal points [3]. The dissipation energy of the system can be modelled by constructing a system damping matrix, by assuming a normal mode system [4], and by using the damping ratios obtained experimentally from modal parameter estimation methods [5, 6, 7]. In the case where the discrepancy between the analytical model and the experimentally obtained modal model is significant, the reduced order analytical damped model can be further modified [8], such that it is in agreement with the experimental natural frequencies, damping ratios and mode shapes [8,9,10,11,12,13]. It is important to realize that the design of the "optimal" control is based on the modified reduced order model, but it is actually applied to the real structure. Therefore, the model improvement mentioned above, becomes very important and its accuracy is vital in the success of the design of the control law.

The structure used here, is a planar truss constructed with space realizable links and joints in the configuration presented in fig.1. The truss is lightly damped and has the behavior of a large

---

*Currently with G.E. Corporate Research and Development Center, Advanced Projects Laboratory, Schenectady, N.Y. 12301.

space structure, with most of its mass concentrated at the joints [2]. It possesses low resonant frequencies that appear in closely spaced groups and has both translational and rotational modes of vibration.

The structure is passively and actively controlled by a single actuator. The actuator used in this experiment is the NASA/UVA/UB proof mass actuator system. The actuator dynamics are taken into consideration and a global model is constructed which includes both the structure and the actuator dynamics [14,15]. The location of the actuator is specified [16,17] by examining the eigenvalues of the uncontrolled global model and the frequency response functions of the global system. The actuator is considered as both a passive and an active device with two design variables, its electronic stiffness and the generated force. The electronic stiffness is specified such that the actuator proof-mass-electronic-spring system is tuned to one of the structural modes of the truss by using traditional vibration absorber design [18,19,20]. The generated force of the actuator is specified by using output feedback techniques. Here, the active control law was limited to velocity feedback by integrating the signals of two accelerometers attached to the structure. The objective is to move the two lower modes of the closed-loop structure further in the LHS of the complex plane and at the same time maintain stability of the closed-loop system [21,22]. The theoretically predicted passive and active control law are experimentally implemented and the results are evaluated.

2. Modeling

2.1 Construction of the Finite Element Model

The finite element model of the structure was constructed by using the commercially available MSC/PAL package for dynamic modeling. The structure weighed 7.335 Kg and was constructed with links and joints, mainly made of aluminum alloy. The density of the material was measured experimentally by using standard techniques. The Young's modulus of aluminum alloy was used, since the links and joints are mainly constructed with this material. The nodal points of the finite element model coincide with the location of the joints of the structure. Every nodal point was allowed to have three degrees of freedom, that is translation in the z-axis and rotations about the x and y-axis resulting in a 48-degree-of-freedom model (see Fig.1). The boundary conditions were assumed to be clamped for nodes 15 and 16 and free for the rest of the nodes, since the structure was supported as illustrated in fig.1. After the boundary conditions were applied the final model was a 42-degree-of-freedom model.

2.2 Mass Distribution

The mass distribution of a non-uniform structure is a problem, that should by no means be ignored. Here, two approaches were used. The first approach was to calculate an equivalent internal diameter of the hollow links, such that the links had the measured mass. The links were treated as uniform hollow tubes constructed with aluminum alloy with an equivalent length of 0.5m. The joints were modelled as a concentrated mass at the particular location and are treated as rigid. The natural frequencies of this model were calculated and are presented in table 1. The results were considered unsatisfactory and one of the links was disassembled for more insight to the mass distribution of the link. In the second approach, the real internal diameter of the links was used and the excessive mass was distributed to the nodes accordingly. The resulting natural frequencies of the model are compared to the experimental results in table 1. The finite element model was constructed using a finer grid which include more nodal points, specifically an additional nodal point at the mid-point of each link. The resulting model after the boundary conditions were applied was a 126-degree-of-freedom model.

It can be concluded that the 45-node(126-dof) model is not significantly better than the 16-node(42-dof) model in predicting the first fourteen natural frequencies. Therefore, it was found unnecessary to use the 45-node(126-dof) model in the determination of the control design of the structure, since the 16-node(42-dof) model was as accurate.

Table 1 : Comparison of the theoretical and experimental natural frequencies of the structure.

	FEM				TEST I (rot accel)
	Uniform mass distribution	Corrected mass distribution			
	42dof	42dof	126dof	14dof	SDOF analysis
Frequency in Hz					
1	1.38	1.045	1.048	1.039	1.07
2	4.56	3.467	3.468	3.469	3.54
3	10.88	8.050	8.050	8.051	7.94
4	26.98	19.894	19.894	19.902	-
5	29.68	21.746	21.748	21.750	-
6	30.94	22.077	22.074	22.087	22.54
7	42.63	30.468	30.472	30.477	32.61
8	53.79	39.268	39.252	39.326	40.35
9	68.46	48.524	48.521	48.552	-
10	72.61	51.746	51.704	51.842	52.51
11	82.93	58.645	58.629	58.718	61.41
12	101.93	71.169	71.116	71.275	65.62
13	102.88	72.090	72.039	72.285	78.24
14	116.52	80.741	80.610	80.920	91.74
15	236.64	219.856	183.903	-	187.13

2.3 Model Reduction

Most of the control algorithms are designed for first order systems. Transforming the 16-node(42-dof) model in the state space results in a 84-dof state space matrix. This matrix is quite large, and it was found that it is difficult to manipulate in vibration prediction, and control algorithms. Therefore, it was necessary to reduce the order of the model before performing control analysis and designing a control law. From the configuration of the model the rotational degrees of freedom can be considered as less significant than the translational ones, and can be eliminated from the model by using the Guyan reduction method [3]. The resulting reduced order model is a 14-dof model. Eigenvalue analysis of this model showed that this model maintained the first fourteen natural frequencies of the larger model quite accurately. The damping ratios determined from the modal test were used in the construction of the system's damping matrix, by assuming that the system exhibited normal mode behavior. The damping matrix is calculated by the following equation:

$$D = MU_F \text{diag}(2\zeta_i\omega_i)U_F^{-1} \qquad (1)$$

where U_F is the eigenvector matrix of $M^{-1}K$, and ζ_i are the experimentally obtained damping ratios. The final reduced order model is described by the following equation:

$$M\ddot{q}(t) + D\dot{q}(t) + Kq(t) = 0 \qquad (2)$$

This equation describes only the dynamic characteristics of the structure. The actuator dynamics were considered important and they were included in the dynamic model.

2.4 Actuator Dynamics

The actuator that was used in this experiment was the NASA/UVA/UB proof mass actuator, presented in fig.2. The actuator system is comprised of a movable proof mass (m_{prf} = 0.225Kg), a fixed coil that applies an electromagnetic force on the proof mass, an analog interface board, a power amplifier and a linear variable differential transformer (LVDT) sensor. The LVDT transducer is an electromechanical transducer that measures the relative position of the proof mass with respect to the actuator housing. The actuator can be modelled as single degree of freedom mass-spring system, with a variable electronic stiffness and the ability to apply a force on the

structure at the attachment point. An equal and opposite force is applied on the proof mass of the actuator. The actuator is space-realizable in the sense that it does not have to be attached to the ground. The equations of motion are written by taking into account the actuator dynamics[15]. Let's assume that the actuator is attached to the structure at the ith nodal point. The global system that includes both the structure and the actuator dynamics, is of higher order, equal to the order of the original system plus the order of the actuator dynamics, and it is described by:

$$\begin{bmatrix} M_1 & 0 \\ 0 & m_{prf} \end{bmatrix}\begin{bmatrix} \ddot{q} \\ \ddot{q}_{prf} \end{bmatrix} + \begin{bmatrix} D_1 & 0 \\ & -c_{act} \\ & 0 \\ 0 \; -c_{act} & 0 \; c_{act} \end{bmatrix}\begin{bmatrix} \dot{q} \\ \dot{q}_{prf} \end{bmatrix} + \begin{bmatrix} K_1 & 0 \\ & -k_{act} \\ & 0 \\ 0 \; -k_{act} & 0 \; k_{act} \end{bmatrix}\begin{bmatrix} q \\ q_{prf} \end{bmatrix} = \begin{bmatrix} 0 \\ 1 \\ 0 \\ -1 \end{bmatrix} f_g \quad (3a)$$

where q_{prf} is the displacement of the proof mass (m_{prf}), the scalars k_{act} and c_{act} are the stiffness and damping of the electronic spring of the actuator, m_{par} is the parasitic mass of the actuator, f_g is force generated by the actuator, and the matrices M_1 ,D_1 and K_1 are the following matrices:

$$M_1 = M + m_{par}\text{diag}[0,...,0,1,0,...,0] \quad (3b)$$

$$K_1 = K + k_{act}\text{diag}[0,...,0,1,0,...,0] \quad (3c)$$

$$D_1 = D + c_{act}\text{diag}[0,...,0,1,0,...,0] \quad (3d)$$

This is referred to as the open-loop system and the mass, damping and stiffness matrices are denoted by subscript ($_{OL}$) for convenience. Note that the non-zero elements correspond to the ith row or/and column of the particular matrix or vector of the previous set of equations. The force f_g is the actuator-generated force applied on the structure. The electronic stiffness of the actuator can be selected in a variety of ways for various design approaches.

3. Passive Control Design

3.1 Structural Modification Design

The parasitic mass of the actuator housing has the same effect as adding a dead parasitic mass at the point of attachment. Increasing the mass of the structure is a structural modification, with the direct effect of reducing the lower natural frequencies of the system. The natural frequencies of the new model with the dead mass were examined both theoretically and experimentally, and the results are tabulated in table 2. The experimental results are presented in the form of point and transfer inertance (transfer function) plots. The transfer function of nodes 1 and 8, of both the original structure and the modified structure are presented in fig.3 and fig.4 respectively. The effect of attaching the PMA (inactive) was also examined. This configuration is equivalent of having a dead mass equal to the parasitic mass of the actuator housing plus the proof mass. However, when the actuator's electronic stiffness is activated, the proof mass becomes an additional degree of freedom, and it is not part of the parasitic mass any longer.

The results indicate that the modified structure has lower natural frequencies than the original structure. This is true for the first five structural modes as indicated in the table above. The experimental frequency response plots show that the level of the vibration response was reduced considerably, especially in the lower frequency region.

If the design methodology was limited to structural modification, it will be considered necessary to examine the effect of adding the dead mass at different nodal points. The results are presented in table 3. The design criterion that was used to place the actuator was to reduce the overall vibration level at node 1, because a sensitive device will be attached at that point. The actuator cannot be placed at node 1 because there is no room. Note that different design criterion results in different locations of the actuator. Placing the actuator at node 10 doesn't reduce the vibration at node 1 at all. Nodes 2, 3, and 4 have the same effect in reducing the vibration level of node 1. But the first structural mode is shifted at 0.92 Hz. This was considered undesirable because it is hard to control the low frequencies by active control. Placing the actuator at nodes 6,7 and 8 has the same effect in reducing the vibration level of node 1 and the first structural mode is not shifted considerably. Therefore, any of nodes 6,7, and 8 can be used as an "optimal" location of the actuator. The results that follow are for placing the actuator at node 8.

Table 2 : Comparison of the theoretical and experimental natural frequencies of the structure with and without the parasitic mass.

	FEM		TEST I		
	w/o	w	w/o	w dead mass	w PMA inactive
	Frequency in Hz				
1	1.04	0.97	1.07	1.01	1.02
2	3.47	2.94	3.54	3.09	2.96
3	8.05	8.00	7.94	7.69	7.88
4	19.90	16.42	-	17.01	16.03
5	21.75	21.44	-		22.39
6	22.09	22.06	22.54	22.02	23.50
7	30.48	28.53	32.61	30.08	29.50
8	39.33	39.12	40.35	39.78	39.33
9	48.55	46.40	-	-	-
10	51.84	51.45	52.51	49.31	50.68
11	58.72	58.52	61.41	54.57	57.36
12	71.27	70.71	65.62	65.02	66.29
13	72.28	72.28	78.24	77.73	78.41
14	80.92	80.74	91.74	84.8	-

Table 3 : Comparison of the theoretical natural frequencies of the structure with the parasitic mass at various nodal points.

	FEM								
	w/o	8	2	3	4	5	6	7	10
	Frequency in Hz								
1	1.04	0.97	0.93	0.93	0.92	0.98	0.98	0.98	1.01
2	3.47	2.94	3.39	3.40	2.94	2.96	3.41	3.40	3.42
3	8.05	8.00	7.71	7.66	7.65	7.95	7.93	7.95	7.28
4	19.90	16.42	18.25	18.41	17.47	15.54	19.84	19.88	19.52
5	21.75	21.44	21.74	21.45	20.17	21.75	20.52	20.24	20.52
6	22.09	22.06	21.98	22.07	21.77	21.96	21.94	21.75	22.00
7	30.48	28.53	30.09	30.02	29.60	27.79	30.07	30.43	29.83
8	39.33	39.12	39.17	38.15	37.87	36.87	39.30	38.92	37.06
9	48.55	46.40	45.12	46.65	48.35	48.35	43.27	45.40	43.03
10	51.84	51.45	51.67	49.02	49.76	50.89	49.56	51.40	51.83
11	58.72	58.52	54.15	57.71	58.47	58.54	58.60	56.68	56.07
12	71.27	70.71	68.85	68.34	70.27	70.62	67.91	68.31	68.53
13	72.28	72.28	71.87	72.26	72.26	72.09	71.67	72.23	71.34
14	80.92	80.74	80.44	80.13	80.69	80.67	79.27	79.27	77.81

3.2 Vibration absorber design

There are several criteria for tuning the absorber to a MDOF structure. The simplest criterion is to tune the natural frequency of the absorber to exactly one of the natural frequencies of the structure[18], that is:

$$\omega_a = \omega_i \qquad (4a)$$

The design of the damped absorber results in an optimal tuned frequency given by[18]:

$$\omega_a = \frac{\omega_i}{1+\mu_i} \qquad (4b)$$

where μ_i is the ratio of the mass of the absorber (here, the proof mass) over the mass of the SDOF structure (here, the modal mass at mode ω). The ratio μ_i or the modal mass can be calculated in a trial and error procedure. The difficulty of applying the second method is the fact that it is difficult to determine the optimai value for μ for the higher modes [22].

An optimal tuning criterion for MDOF systems was presented in reference [19]. The absorber frequency (ω_a) and damping coefficient (c_a) are given by:

$$\omega_a^2 = \omega_i^2 \frac{1+\mu_t}{(1+\mu_t+\mu_a)^2} \quad (5a)$$

$$c_a^2 = m_a^2 \omega_i^2 \mu_a \frac{1+\mu_t}{(1+\mu_t+\mu_a)^3} \quad (5b)$$

where,

$$\mu_t = m_t \phi_{i_j}^2 \text{ and } \mu_a = m_a \phi_{i_j}^2 \quad (5c)$$

The scalars m_t and m_a are the parasitic mass and the mass of the absorber, respectively, and the scalar ϕ_{i_j} is the jth entry of the associated eigenvector of the ith mode, where j is the degree of freedom corresponding to the location of the absorber. Note that the eigenvectors derived form the finite element model, are normalized with respect to the mass matrix.

3.2.2 Experimental implementation of the passive control design

The stiffness of the PMA can be electronically varied, such that the actuator system can be tuned to different frequencies. The PMA was attached to ground, and the LVDT signal was examined for random signal input that generates an electromagnetic force on the proof mass. The LVDT signal gives the relative position of the proof mass with respect to the housing of the actuator. As it can be clearly seen in the experimental bode plot in fig.5, the PMA system is well modelled by a SDOF system, with a natural frequency depending on the gain that determines the electronic stiffness. The stiffness is a function of the external gain (α), and other electromagnetic constants of the coil and the amplifier (included in the factor K) . The natural frequency of the system is given by:

$$\omega_a = 1/2\pi \sqrt{\alpha K/m_{prf}} \quad (6)$$

The damping in the actuator was identified as Coulomb damping due to the friction in the bearings. An equivalent viscous coefficient was calculated from the frequency response functions of the LVDT signal at particular tuning frequencies. It was found that the lower the tuning frequency becomes, the higher the equivalent damping becomes. This is actually due to the fact that at low frequencies the proof mass of the actuator cannot overcome the friction. As a consequence, the natural frequency of the SDOF model of the actuator dynamics cannot go lower than a certain frequency, since the stiffness is electronically determined and it depends on the relative motion of the proof mass with respect to the housing of the actuator. It was found that the actuator system behaves like an overdamped system when tuned to frequencies below 8 Hz. Therefore, it was practically impossible to tune the actuator to frequencies lower than 8 Hz. Note that, this range includes the three lower natural frequencies of the modified structure. Therefore, the PMA is tuned to the fourth mode, by using the criteria described above. The results from only the second criterion are presented here in the top part of fig.6, due to the fact that the plots from the simple criterion (equation 4a) and the optimal tuning criterion (equation 5) were very similar. It can be clearly seen that the vibration response is clearly reduced.

4. Active Control design

The active control law is implemented, by using one actuator and two sensors. The force generator signal of the actuator was then given by:

$$f_g = FCy(t) \tag{7}$$

where F the feedback gain matrix and C the output matrix. The sensors were placed at node 1 and node 4 as indicated in fig.1. Node 1 was chosen because this is the possible point of attachment of a sensitive device, where the vibration level is required to be reduced. Node 4 was chosen, because it moves in the opposite direction of node 1, when the structure is excited at one of its rotational modes. Here, accelerometers were used and their signals were integrated once by an analog computer, to give the corresponding velocity signals. The output position matrix was therefore zero, and the velocity output matrix was of the form:

$$C_1 = \begin{bmatrix} 1 & 0_{1\times 14} \\ 0_{1\times 3} & 1\ 0_{1\times 11} \end{bmatrix} \tag{8}$$

The gain matrix is therefore given by:

$$F = [g_1 : g_2] \tag{9}$$

where g_1 and g_2 are the two gains to be determined. Substituting into the previous equation results in:

$$f_g = F\begin{bmatrix} 1 & 0_{1\times 14} \\ 0_{1\times 3} & 1\ 0_{1\times 11} \end{bmatrix}\dot{q}(t) \tag{10}$$

The closed-loop system written in physical coordinate system, is given by the following equation:

$$M_{OL}\ddot{q}(t) + D_{OL}\dot{q}(t) + K_{OL}q(t) = B_{OL}FC_1\dot{q}(t) \tag{11}$$

The objective here is to calculate the gain matrix F such that the system has poles at the desired locations. The right hand side of the previous equation is expanded as:

$$B_{OL}FC_1 = \begin{bmatrix} 0 \\ 1 \\ 0 \\ -1 \end{bmatrix}[g_1 : g_2]\begin{bmatrix} 1 & 0_{1\times 14} \\ 0_{1\times 3} & 1\ 0_{1\times 11} \end{bmatrix} = \begin{bmatrix} 0_{7\times 15} \\ g_1\ 0\ 0\ g_2\ 0_{1\times 11} \\ 0_{6\times 15} \\ -g_1\ 0\ 0\ -g_2\ 0_{1\times 11} \end{bmatrix} \tag{12}$$

Note that this is a square sparse asymmetric matrix with only four non-zero elements. This results in a closed-loop system damping matrix of the form:

$$D_{CL} = \begin{bmatrix} D_1 & 0 \\ & -c_{act} \\ & 0 \\ 0\ -c_{act}\ 0 & c_{act} \end{bmatrix} + \begin{bmatrix} 0_{7\times 15} \\ g_1\ 0\ 0\ g_2\ 0_{1\times 11} \\ 0_{6\times 15} \\ -g_1\ 0\ 0\ -g_2\ 0_{1\times 11} \end{bmatrix} \tag{13}$$

where c_{act}, corresponds to the equivalent viscous damping coefficient of the actuator system.

The objective here, was to decrease the amplitude of the vibration response at the low modes that have high participation factors. Note that, direct pole placement design could not be applied since with one actuator and two sensors, only one closed-loop pole can be placed. The gains were determined in an ad hoc design, from an algorithm that covered a broad region of values, with the main objective to move the lower two poles further in the LHS complex plane. The results are presented in table 6. It can be clearly seen that the closed-loop system is stable when the two gains g_1 and g_2, are in the region -10 to 10 and 0 to 15 respectively. A finer grid that covered the part of the stable region, where the damping of the first two modes was increased (g_1 from 0 to 10 and g_2 from 10 to 20) was also examined [22].

It was discovered that the "optimal " gain of F= [5 : 15] increases the damping on modes 1, 2, 4, 5, 6 and decreases the damping at mode 3. Note that, further increase of the gains towards the "optimal" direction, resulted in an unstable closed-loop system. The experimentally obtained transfer functions of nodes 1 and 8, are presented in fig.6, and they are compared directly with the open-loop system, tuned to the fourth structural mode. The results show clearly, a decrease in the response at modes 1 and 2. The decrease of the vibration response is not very large as desired, because of the following reasons:

(i) By using only one actuator and two sensors, we can only affect 4 elements of the 15x15 closed-loop damping matrix.

(ii) Further increase in the gains towards the "optimal " direction drives the third mode unstable.

(iii) We are trying to control a flexible structure with many significant modes that cannot be ignored.
(iv) We are only using velocity feedback

It was also illustrated experimentally that by increasing the gains at higher values drove the proof mass system unstable.

Table 6 : Determination of the feedback gain matrix

g_2 \ g_1	-20	-15	-10	-5	0	5	10	15	20	25	30
-20	U	U	U	U	U	U	U	U	U	U	U
-15	U	U	U	U	U	U	U	U	U	U	U
-10	U	U	U	U	U	U	U	U	U	U	U
-5	U	U	U	U	U	U	U	U	U	U	U
0	U	U	U	S	S	U	U	U	U	U	U
5	U	U	S	S	S	S	U	U	U	U	U
10	U	U	U	S	S	S	S	U	U	U	U
15	U	U	U	U	S	S	U	U	U	U	U
20	U	U	U	U	U	U	U	U	U	U	U

U = unstable, S = stable.

5. Closing Remarks

An experimental flexible planar truss structure was modelled and successfully controlled in a passive and active way by using a space realizable linear proof mass actuator system. The PMA was attached to the truss at a desired location, and tuned as traditional vibration absorber to one of the structural modes of the truss by using several criteria. The actuator dynamics were successfully modelled and taken into consideration in the design of the passive and active control law. The active control design was adopted in the form of output velocity feedback by integrating the signals of two accelerometers, attached to the structure. The limitations of this method were indicated and difficulties of applying output feedback on large flexible structures with several significant modes are identified and pointed out.

6. Acknowledgements

This work was supported in part by AFOSR grants no F49620-88-00018 and F49620-86-6-0111. Much of the equipment used was funded through instrumatation grants numbers AFOSR-85-0119 and AFOSR-88-450-0390.

7. References

(1) Shames, I.H. and Dym, C.L., 1985, Energy and Finite Element Methods in Structural Mechanics, Hemisphere Publishing Corp., Chapter 16, pp.643-657.
(2) Balas, M. J., 1982, "Trends in Large Space Structure Control Theory: Fondest hopes, Wildest Dreams," IEEE Transactions on Automatic Control, Vol. AC-27, No. 3, June, pp. 522-535.
(3) Guyan, R.J., 1965, "Reduction of Stiffness and Mass Matrices," AIAA Journal, Vol. 14, pp.1627-1628.
(4) Caughey, T.K. and O'Kelly, M.E., 1965, "Classical Normal Modes in Damped Linear Dynamic Systems," ASME Journal of Applied Mechanics, Vo. 32, pp.583-588.
(5) Ewins, D.J., 1986, Modal Testing: Theory and Practice, Research Studies Press Ltd., England.
(6) Ibrahim, S.R. and Mikulcik, E.C., 1976, "The Experimental Determination of Vibration Parameters from Time Responses," Shock and Vibration Bulletin, No. 46, pt.5, pp.187-196.
(7) Juang, J.N. and Pappa, R.S., 1985, "An Eigensystem Realization Algorithm (ERA) for Modal Parameter Identification and Model Reduction," AIAA Journal of Guidance, Control and Dynamics, vol.8, 5, Sept-Oct, pp.620-627.

(8) Kammer, D.C., 1987, "An Optimum Approximation for Residual Stiffness in Linear System Identification," Proceedings of the 28th SDM Conference, Monterey, California, pp.277-287.
(9) Berman, A., 1984, "System Identification of Structural Dynamic Models-Theoretical and Practical Bounds," Proceedings of the 25th SDM Conference, Palm Springs, California, May, pp.123-129.
(10) Berman, A. and Nagy, E.Y., 1983, "Improvement of a Large Analytical Model Using Test Data," AIAA Journal, Vol.21, Aug., pp.1168-1173.
(11) Minas, C. and Inman, D.J., 1988, "Correcting Finite Element Models with Measured Modal Results using Eigenstructure Assignment Methods," Proceedings of the 6th International Modal Analysis Conference, Orlando, Florida, February, pp.583-587.
(12) Minas, C. and Inman, D.J., 1989, "Matching Finite Element Models to Modal Data," ASME Journal of Vibration, Acoustics, Stress, and Reliability in Design, (accepted for publication, paper No. 88-487).
(13) Minas, C. and Inman, D.J., 1989, "Model Improvement by using Pole Placement Methods," Proceedings of the 12th Biennial ASME Conference in Vibration and Noise, Sept., Montreal, Canada.
(14) Zimmerman, D. C., Horner, G. C., and Inman, D. J., 1988, "Microprocessor Controlled Force Actuator," AIAA Journal of Guidance, Control, and Dynamics, Vol. 11, No. 3, May-June, pp.230-236.
(15) Harokopos, E. G. and Mayne, R. W., 1986, "Motor Characteristics in the Control of a Compliant Load," AIAA Journal of Guidance, Control, and Dynamics, Vol. 9, No. 1, Jan.-Feb., pp. 113-118.
(16) Chiang,H.D., Thorp, J.S., Wang, J.C., and Lu, J., 1989, "Optimal Controller Placements in Large Scale Linear Systems," Proceedings of the American Control Conference, pp.1615-1620.
(17) Min, I.J., Chang, and Soong,T.T., 1980, "Optimal Controller Placement in Modal Control of Complex Systems," Journal of Mathematical Analysis and Applications, Vol.75, pp.340-358.
(18) Den Hartog, 1956, Mechanical Vibrations, 4th edition, McGraw-Hill, New York.
(19) Juang, J.N., 1984, Optimal Design of a Passive Vibration Absorber for a Truss Beam," AIAA Journal of Guidance, Control and Dynamics, vol.7, 6, Nov.-Dec., pp.733-739.
(20) Miller, D.W. and Crawley, E.F., 1988, "Theoretical and Experimental Investigation of Space-Realizable Inertial Actuation for Passive and Active Structural Control," AIAA Journal of Guidance, Control and Dynamics, vol.11, 5, Sept-Oct, pp.449-458.
(21) Andry, A.N., Shapiro, E.Y., and Chung, J.C., 1983, "Eigenstructure Assignment for Linear Systems, "IEEE Transactions on Aerospace and Electronic Systems, " Vol. AES-19, no.5, September, pp.711-729.
(22) Minas, C., 1989, "Modeling and Active Control of Large Flexible Structures," Ph.d. dissertation, State University of New York at Buffalo .

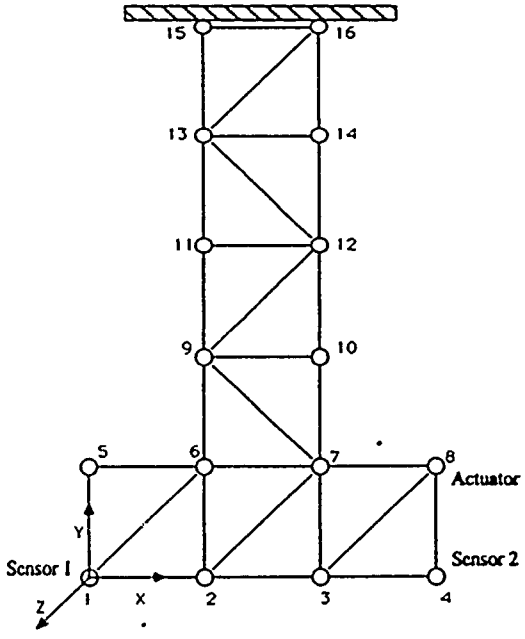

Fig.1 : Structure configuration with locations of sensors and actuator

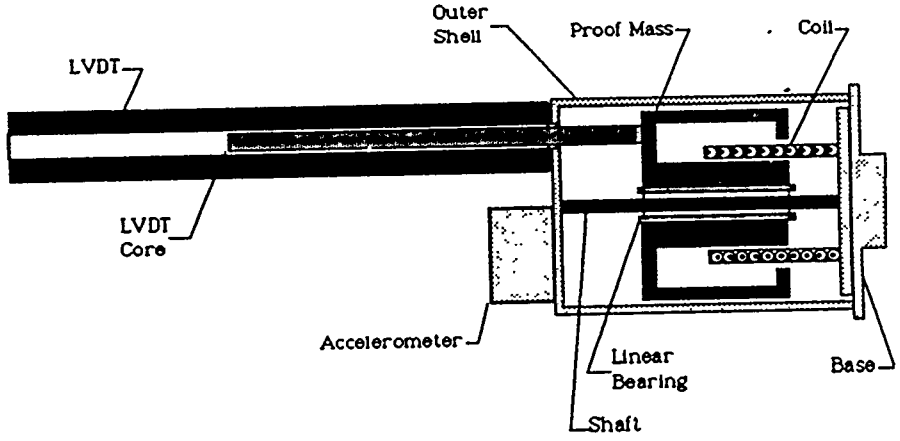

Fig 2 : Configuration of the proof mass actuator system

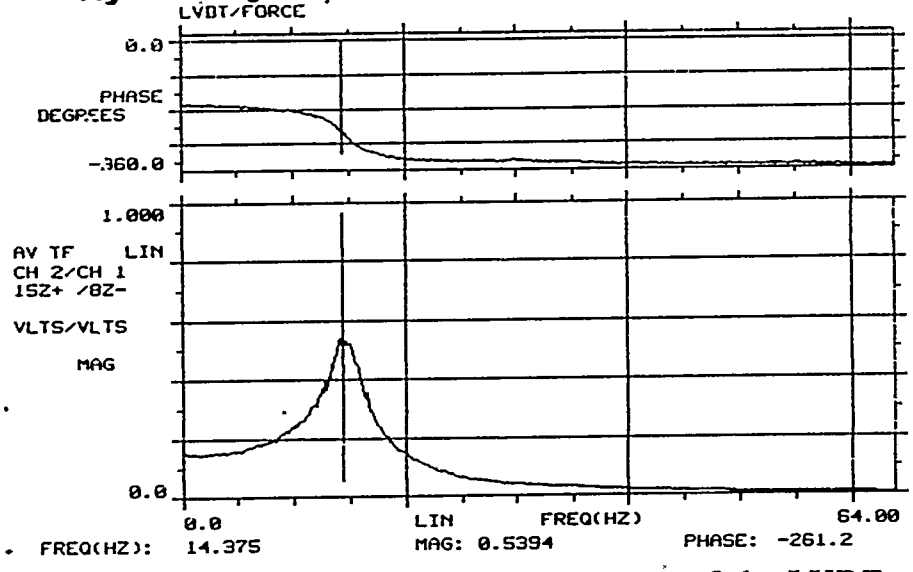

Fig.5 : Frequency Response function of the LVDT signal of the Proof-mass-actuator tuned to 14.4 Hz

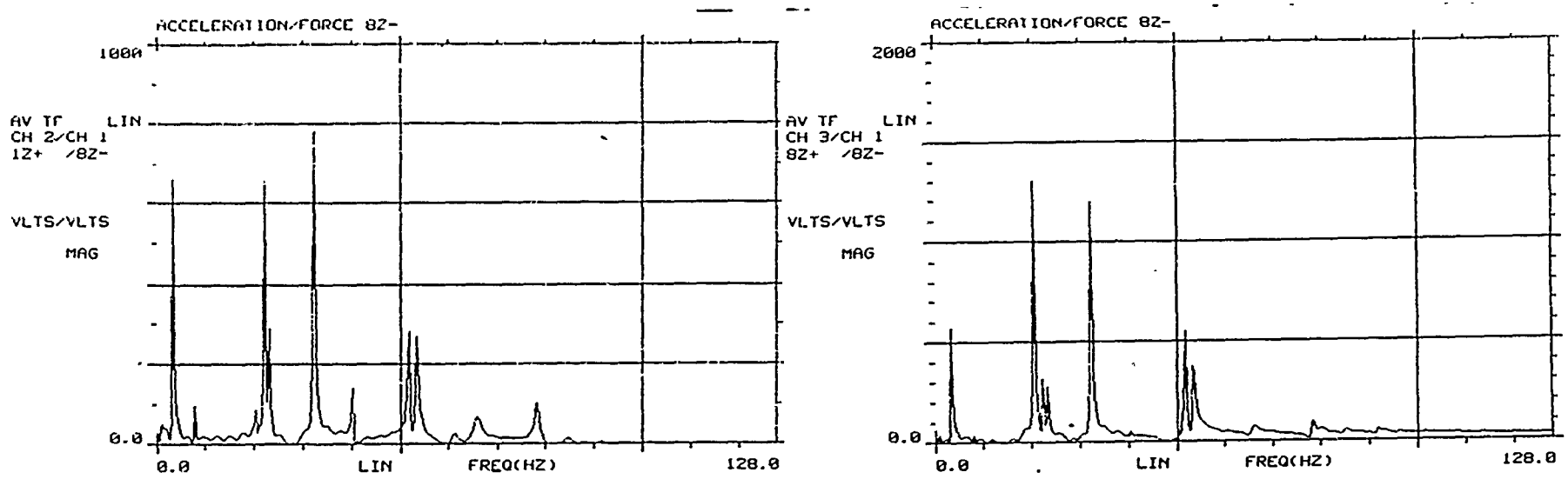

Fig.3 : Transfer function of the uncontrolled structure

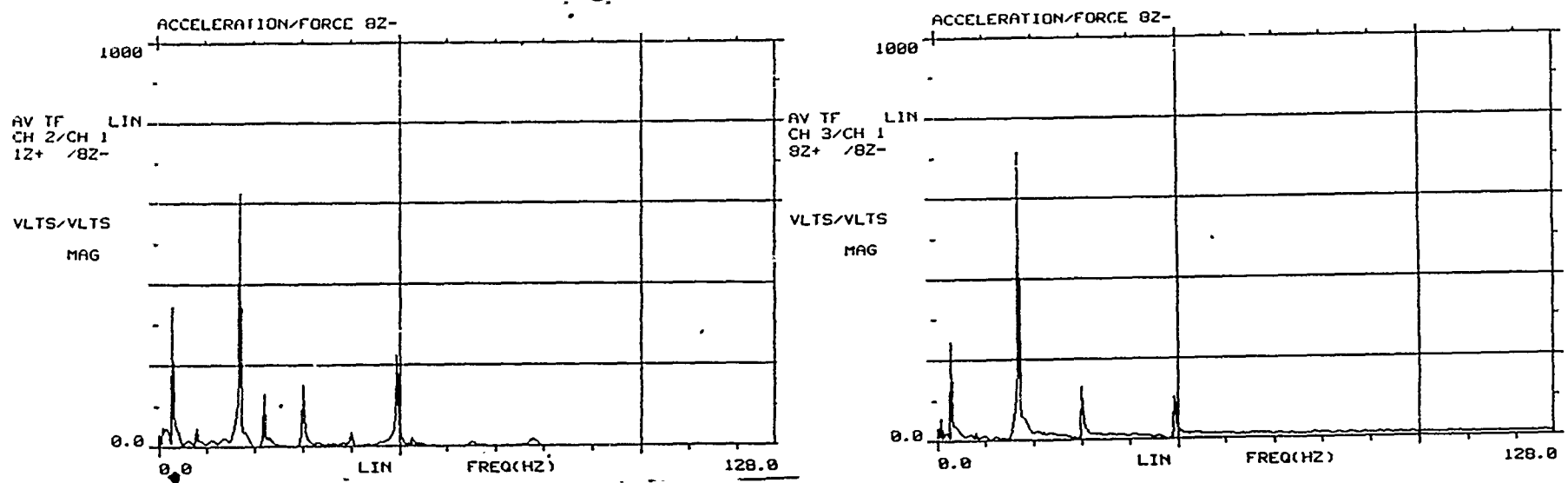

Fig.4 : Transfer function of the uncontrolled structure with parasitic mass

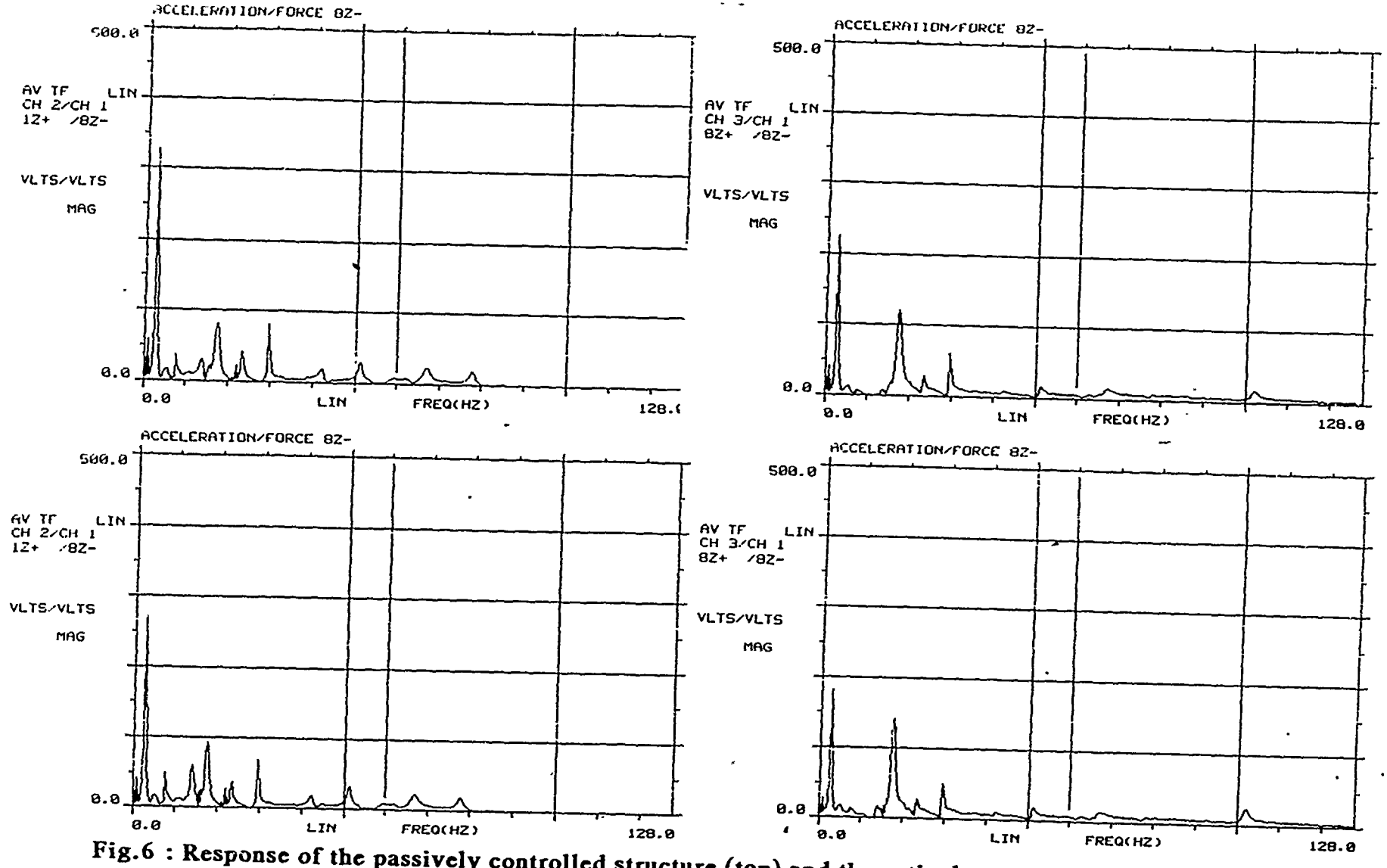

Fig.6 : Response of the passively controlled structure (top) and the actively controlled structure (bottom)

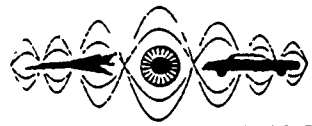

II.ITERNATIONAL CONGRESS ON
RECENT DEVELOPMENTS IN AIR- AND
STRUCTURE-BORNE SOUND AND VIBRATION
MARCH 6-8, 1990 AUBURN UNIVERSITY, USA

ON THE NATURE OF THE INTERACTION BETWEEN STRUCTURES AND ACTUATORS IN VIBRATION SUPPRESSION

Daniel J. Inman
Ephrahim Garcia
Jeff Urnland
Department of Mechanical and Aerospace Engineering
State University of New York at Buffalo
Buffalo, New York 14260
U.S.A.

ABSTRACT

This lecture presents a summary of work on the analysis of the interaction between a structure, an actuator used to suppress the vibration of the structure, and the control law implemented by the actuator. Two control applications are considered. First, a proof-mass actuator with experimentally verified dynamics, capable of being used in a space structure configuration is examined. This is connected to a cantilevered beam modeled as a single degree of freedom system. Secondly, an electric motor, again with experimentally verified dynamics, is used to slew a beam modeled by a partial differential equation. Both the experimental and numerical configuration predict the presence of potential instabilities in system performance if proper consideration is not given to interactions between the control law, the structure and the actuator. In addition, an understanding of the interaction is shown to greatly effect performance. In particular it is shown that a judicious choice of actuator parameters greatly improves closed loop performance.

INTRODUCTION

The purpose of this paper is to summarize several results expressing the nature of control structure interaction. These results point to the importance of modeling actuator dynamics in designing vibration suppression systems for flexible structures. It is common practice for designers of servo control system to incorporate the dynamics of the servo motor into the closed loop design of the system under consideration. Yet a majority of the literature on the control of flexible structures ignores the actuator dynamics in developing control methods [1]. This paper illustrates two types of active vibration suppression systems and points out the effects of considering the dynamics of the actuators in the closed loop design.

The two systems considered are a linear electromechanical actuator, consisting of a proof-mass actuator [2], and an electric motor, both used to control the transverse vibrations of an Euler Bernoulli beam. The proof-mass actuator is used to control the transverse vibration of a cantilevered beam. The electric motor is used to control the transverse vibration of a beam during a slewing maneuver. Slewing refers to the rotation of the beam about the motor axis similar to the motion of a door rotating on a hinge.

It is illustrated here that the interaction between the actuator dynamics, the choice of control law and the nature of the structural dynamics is critical in both cases. In particular

- the choice of feedback paths through the actuator is critical
- instabilities result if one ignores the interaction, or coupling between the actuators and structure dynamics
- performance of the closed loop system is significantly enhanced if the nature of the interaction is considered in the choice of the actuator dynamics

These points are illustrated and verified in the remainder of this paper.

PROOF-MASS ACTUATOR/BEAM MODEL

Proof-mass actuator systems have been considered by several authors [2-10]. The actuator used here to demonstrate the nature of control/structure interaction is a linear actuator, composed of a solenoid-like arrangement of a mass moving in an electric field. This proof-mass actuator (PMA) is a reaction type force actuator, which creates a force by reacting against an inertial mass. Such actuators are also called Reaction-Mass Actuators (RMA). This actuator has been extensively tested [2] and is capable of generating an arbitrary (but bounded) control force. The actuator consists of a movable "proof-mass," a fixed coil, two collocated sensors, a digital microcontroller and a power amplifier as described in detail in Ref. 2. All of the actuator components are mounted on a single compact fixture. Power lines are are the only external connection required to operate the actuator unless uncollocated control is used. In the uncollocated case, the actuator accepts signals from sensors at other locations on the structure. In addition, an optional analog or digital input can be used as the control law for design purposes.

As illustrated in Ref. 6, the PMA's transfer function clearly dictates a second order model of the form of a single degree of freedom oscillator. Laboratory bench tests and tests with the actuator mounted on a variety of structures indicate that the model of Figure 1 provides an accurate description of the actuator dynamics. In the Figure, m_a represents. the internal moving mass, or proof-mass, of the actuator, and x_a is the time dependent

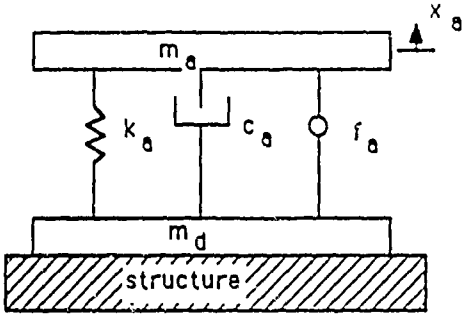

Figure 1. Dynamics of a proof-mass actuator.

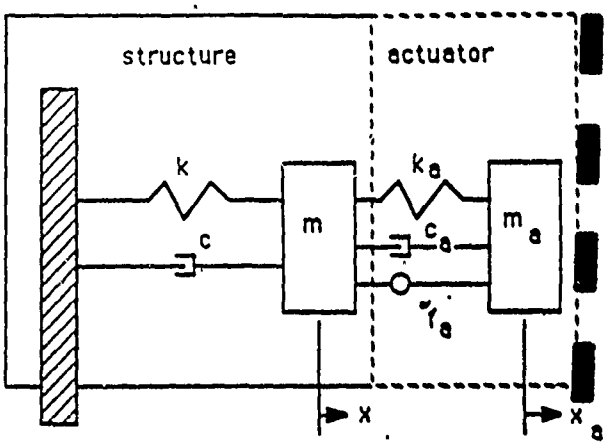

Figure 2. A single degree of freedom system with control actuator attached.

position of the actuator relative to the base. The quantity m_d is the dead, or non-moving, mass of the actuator (i.e., the housing, transducers, magnets, control electronics, etc. fixed to the structure). The damping coefficient, c_a, is determined experimentally and represents an equivalent viscous damping coefficient for the internal friction of the actuator. The quantity k_a, also determined experimentally, is the electronic stiffness force required to keep the proof-mass centered in its housing. This force, as well as the internal damping force, is required for stability of the actuator. The control force is generated between the proof-mass and the structure and is denoted as f_a. Reference 6 reports the dynamic modeling in detail.

The basic phenomena of interest here can be illustrated by treating the beam as a single degree of freedom system. The extension to larger order models is contained in Ref. 11. To illustrate the basic instability problems consider the simple case of velocity feedback which performs vibration suppression by adding damping to the system. Without actuator dynamics, the single degree of freedom model of the beam with velocity feedback is:

$$m\ddot{x} + c\dot{x} + kx = -g\dot{x} \qquad (1)$$

Here $x = x(t)$ is the nominal transverse displacement of the beam, m is the mass of the beam, c is the approximate internal damping and k is the beam stiffness. The quality g is the electronic gain which is to be adjusted to produce the desired vibration suppression.

In the case of the ignoring actuator dynamics one would rearrange Eq. (1) and note that the velocity coefficient becomes c + g. Hence the desired vibration suppression control law would be to make the gain, g, as large as possible. Next consider applying this control law, developed without regard for the actuator dynamics, to a model which includes actuator dynamics. The equations of motion become (see Figure 2).

$$\begin{bmatrix} m & 0 \\ 0 & m_a \end{bmatrix} \begin{bmatrix} \ddot{x} \\ \ddot{x}_a \end{bmatrix} + \begin{bmatrix} c+c_a & -c_a \\ -c_a & c_a \end{bmatrix} \begin{bmatrix} \dot{x} \\ \dot{x}_a \end{bmatrix} + \begin{bmatrix} k+k_a & -k_a \\ -k_a & k_a \end{bmatrix} \begin{bmatrix} x \\ x_a \end{bmatrix} = \begin{bmatrix} -f_a \\ f_a \end{bmatrix} \tag{2}$$

Using the same simple velocity feedback control of the form $f_a = g\dot{x}$, this becomes

$$\begin{bmatrix} m & 0 \\ 0 & m_a \end{bmatrix} \begin{bmatrix} \ddot{x} \\ \ddot{x}_a \end{bmatrix} + \begin{bmatrix} c+c_a+g & -c_a \\ -g-c_a & c_a \end{bmatrix} \begin{bmatrix} \dot{x} \\ \dot{x}_a \end{bmatrix} + \begin{bmatrix} k+k_a & -k_a \\ -k_a & k_a \end{bmatrix} \begin{bmatrix} x \\ x_a \end{bmatrix} = \begin{bmatrix} 0 \\ 0 \end{bmatrix} \tag{3}$$

Note that the matrix coefficient of the velocity vector in Eq. (2) is asymmetric. Every matrix can be written as the sum of a symmetric matrix and skew symmetry matrix. In this case the symmetric part of the closed loop damping matrix becomes

$$\begin{bmatrix} \cdot & \cdot \\ \cdot & c_a \end{bmatrix} \tag{4}$$

If this matrix becomes indefinite or negative definite, it is well known that instability results [12]. This matrix clearly becomes indefinite as the gain g is increased as suggested by the control law calculated by omitting the actuator dynamics.

The high gain instability effect is also obvious from applying the Routh-Hurwitz test to the characteristic equation associated with Eq. (3). However, the matrix approach is applicable to larger order models with a greater number of actuators. This is presented in Ref. 11.

It should be noted that several researchers [7,8,10] involved in using reaction mass actuators for vibration suppression in flexible structures have avoided this instability problem by using relative velocity feedback of the form

$$f_g = g(\dot{x}_a - \dot{x}) \tag{5}$$

The use of this feedback path causes the matrix coefficient of the velocity vector to be symmetric and positive definite for any value of the gain g. However, relative velocity feedback as given in equation (5) and used in Refs. 7,8, and 10, reduces the control problem to one of parameter optimization similar in performance to a passive vibration absorber. This point is made in more detail in Ref. 9 which compares the response of closed loop systems with the two different feedback paths.

Comparing the use of [illegible] feedback paths for fixed beam parameters and actuator dynamics yields that a shorter settling [illegible] overshot is obtainable by using the potentially destabilizing control law of Eq. (3) then is obtain[illegible]ative velocity feedback of the form of Eq. (5). This is illustrated in Figures 3 and 4. There are several [illegible]s that can be learned from controlling a single degree of freedom structure with a PMA that can be applied to the vibration control of both multiple degree of freedom and distributed parameter structures. Control laws that ignore actuator dynamics may result in closed loop instability. The use of only safe or nondestabilizing feedback paths may not yield the best performance. Furthermore, using only relative position and velocity feedback results in a control law that is no different than that of a traditional vibration absorber. This type of design tends to require low feedback gains, such that the motion of the proof mass is unimpeded. Finally, better performance is achieved with structural velocity feedback combined with relative velocity feedback. In fact, a high structural feedback gain can only be tolerated in the presence of a high relative velocity feedback gain.

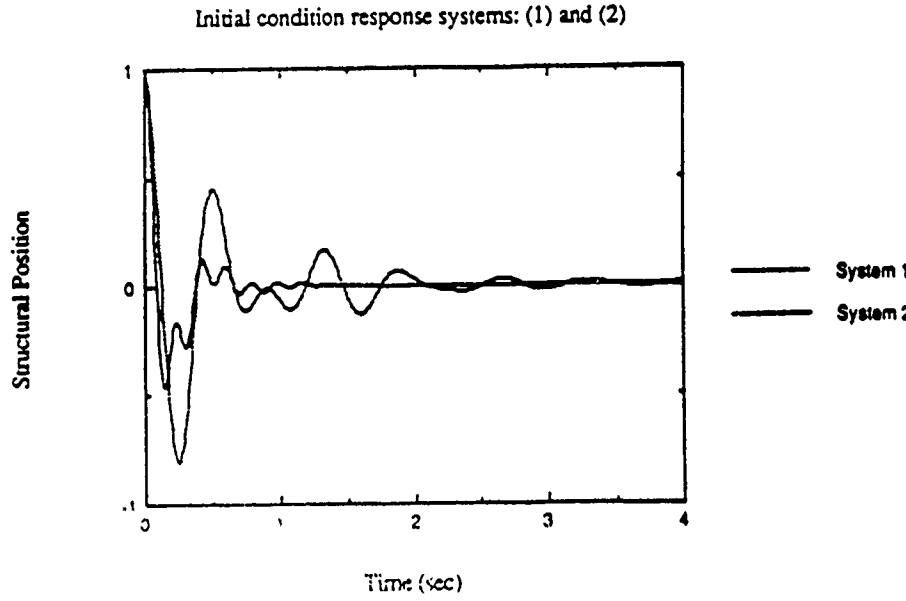

Figure 3. Structural response: system (1) vibration absorber
system (2) active control with velocity feedback.

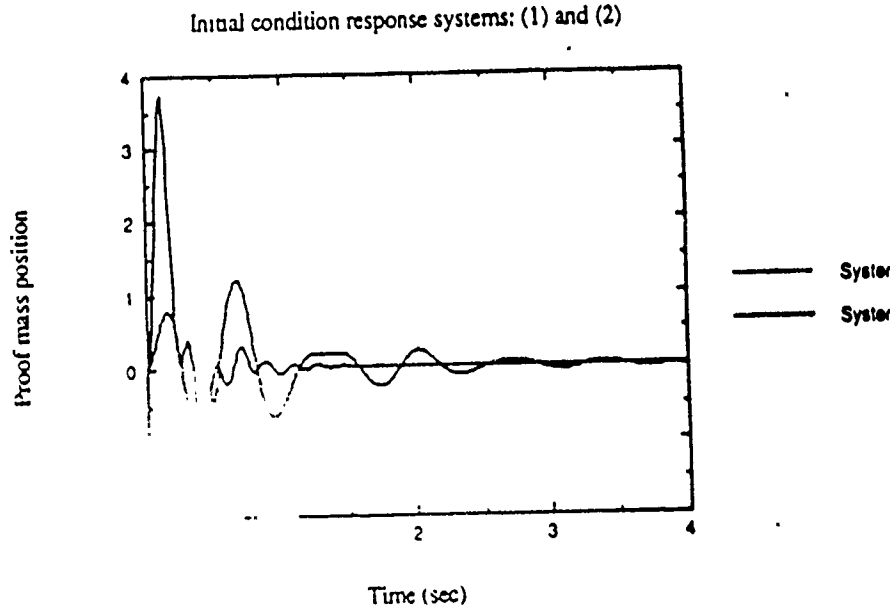

Figure 4. Actuator mass response: system (1) vibration absorber
system (2) active control with velocity feedback.

SUPPRESSION DURING SLEWING

In this section, vibration suppression during slewing of a beam by a simple, armature controlled, DC electric motor is presented. The electric motor model is standard and can be found in Ref. 13. By applying Hamilton's principle to an Euler Bernoulli beam moving in a horizontal plane driven by the DC motor yields the equation of motion of the structure/actuator system. While the control structure interaction problem has been considered previously [14 the effects of a flexible load (beam) have not been generally addressed in the previous literature. In particular, the modeling approach suggested here focuses on the effective boundary condition of the beam at the point of attachment to the motor.

A majority of the previous work in slewing assumes that this arrangement defines a clamp-free beam. However, the approach taken here is that the point of attachment does not define a clamped end, but rather the boundary condition for the beam at the point of attachment rotates and depends directly on the motor dynamics.

As derived in Ref. 15, the equations of motion for the open loop beam actuator system are:

$$EI\frac{\partial^4 y(x,t)}{\partial x^4} + \rho\frac{\partial^2 y(x,t)}{\partial t^2} + \rho x\ddot{\theta}(t) = \tau\,\delta'(0,t) \tag{6}$$

with boundary conditions

$$y(0,t) = 0 \quad , EI\frac{\partial^2 y(0,t)}{\partial x^2} = -I_m N_g^2\frac{\partial^3 y(0,t)}{\partial x \partial t^2}$$

at the point of attachment to the motor and

$$EI\frac{\partial^2 y(l,t)}{\partial x^2} = 0 \quad , \quad \frac{\partial}{\partial x}EI\frac{\partial^2 y(l,t)}{\partial x^2} = 0$$

at the free end, coupled with motor equation:

$$\tau = \frac{N_g K_t}{R_a}e_a - I_m N_g^2\ddot{\theta} - \left(C_v + \frac{K_b k_t}{R_a}\right)\dot{\theta} \tag{7}$$

where θ is the total angular displacement which includes rigid body rotation and the angular displacement due to flexure. Here E, I and ρ are the beam elastic modulus, moment of inertia and density per unit length respectively. The motor constants K_t, K_b, R_a, I_m and C_v denote the motor torque constant, back emf constant, armature resistance, motor inertia and equivalent bearing friction respectively. The gear ratio is denoted by N_g and l denotes the length of the beam. The term of the right hand side of equation (6) represents the direct transmission of torque into flexural deflection, y(x,t). The point moment delta operator is denoted by $\delta'(0,t)$, $\theta(t)$ denotes the angular position of the underflected beam and e_a denotes the applied armature voltage. This formulation considers the interaction between the beam flexural dynamics and the motor dynamics.

The coupling between the beam and actuator dynamics highlighted in this model allows the motor parameter, beam parameters and control law to be chosen to more efficiently control the higher modes of flexural vibration. This is illustrated in the following experimental verification of a servo control implemented based on Eqs. (6)-(7). The actuator structure system consists of a DC armature controlled electric motor connected to a .85 meter aluminum beam in a direct drive configuration. The direct drive configuration allows significant coupling between the motor and beam dynamics. This allows more of the beam vibrational energy to be dissipated through the actuator that drives the system.

The experiment consisted of 30° step slew of the aluminum beam. A comparison was made between two simple servo control laws. First, a standard servo control was implemented (PD control of θ). This control law does not capitalize on the interaction between the structure and actuator as suggested by Eqs. (6)-(7). The second control implemented was again a PD control, however the tachometer feedback gain was increased to take advantage of the actuators ability to dissipate the energy by of the transverse vibration of the beam. The model presented in Eqs. (6)-(7) predicts this energy dissipation and subsequent improved vibration suppression. The results of these experiments as illustrated in fig.5 which consists of the time histories of the top acceleration for each control law. In addition, a third course indicates the theoretically predicted response use a finite approximation of Eqs. (6)-(7). Note that the PD controller with increase tach feedback yields approximately 70% decrease in the settling (or pointing) time of the maneuver as well as a 40% reduction in maximum vibration amplitude.

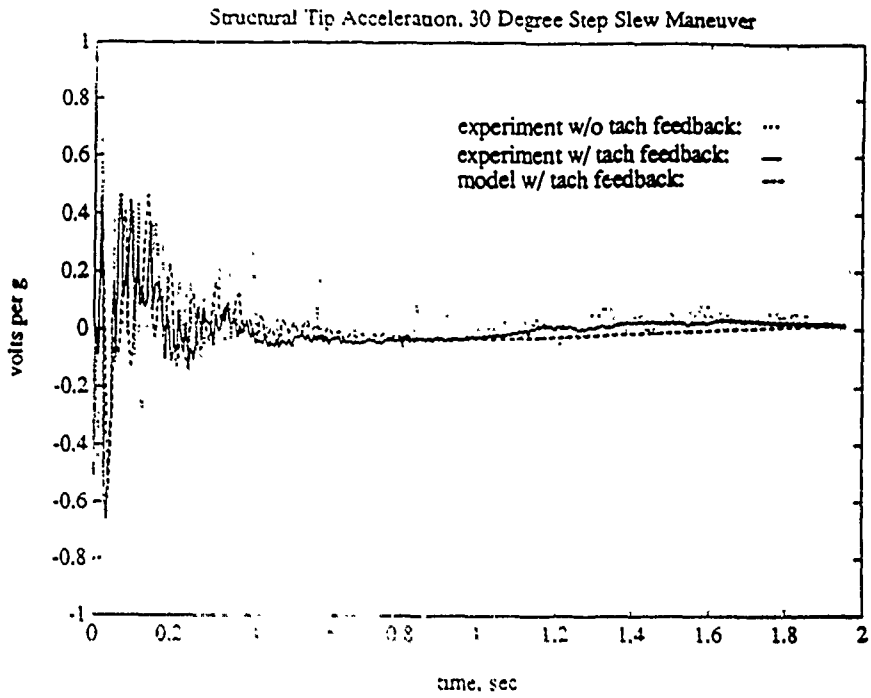

Figure 5. Tip accelerations for a step command to the system.

ACKNOWLEDGMENTS

The authors gratefully acknowledge the support of AFOSR grant number F49620-88-C-0018 monitored by Lt. Col. G. Haritos and NASA grants number NAG-1-178 and NGT-33183804 monitored by Dr. G.C. Horner of the Langley Research Center.

REFERENCES

[1] Balas, M.J., "Trends in Large Space Structure Control Theory: Fondest Hopes, Wildest Dreams," *IEEE Transactions on Automatic Control*, Vol AC-27, No. 3, June 1982, pp. 522-535.

[2] Zimmerman, D.C., Horner, G.C. and Inman, D.J., "Microprocessor Controlled Force Actuator," AIAA *Journal of Guidance, Control and Dynamics*, Vol. 11, No. 3, May-June 1985, pp. 230-236.

[3] Zimmerman, D.C., Dynamic Characterization and Microprocessor Control of the NASA/UVA Proof-Mass Actuator, M.S. Thesis, Department of Mechanical & Aerospace Engineering, State University of New York at Buffalo, June 1984.

[4] Haviland, J.K., Lim, T.M., Pilkey, W.D. and Politansky, H., "The Control of Linear Dampers for Large Space Structures," *Proceedings of the 1987 AIAA Guidance and Control Conference*, Monterey, CA August, 1987, pp. 106-116.

[5] Pilkey, W.D. and Haviland, J.K., "Large Space Structure Damping Design, Final Report," University of Virginia, VA 1983.

[6] Zimmerman, D.C. and Inman, D.J., "On the Nature of the Interaction Between Structures and Proof-Mass Actuators," *AIAA Journal of Guidance Control and Dynamics*, to appear.

[7] Hallauer, W.L. and Lamberson, S.E., "Experimental Active Vibration Damping of a Plane Truss Using Hybrid Actuation," AIAA paper #89-1169, Proceedings of the [illegible]th Structure, Structural Dynamics and Materials Conference, April 1989, pp. 80-90.

[8] Juang, J., "Optimal Design of a Passive Vibration Absorber for a Truss Beam," *AIAA Journal of Guidance, Control and Dynamics*, Vol. 7, No. 6, Nov.-Dec. 1984, pp. 733-739.

[9] Inman, D.J., Umland, J.W. and Andrews, J., "Controlling Flexible Structures with Second Order Actuator Dynamics," 3rd Annual Conference on Aerospace Computational Control," August 1989.

[10] Miller, D.W. and Crawley, E.F., "Theoretical and Experimental Investigation of Space-Realizable Inertial Actuation for Passive and Active Structural Control," *AIAA Journal of Guidance, Control and Dynamics*, Vol. 11, No. 5, Sept.-Oct. 1988, pp. 449-458.

[11] Inman, D.J., "Control/Structure Interaction: Effects of Actuator Dynamics, Proceedings of the AIAA Dynamic Specialist Conference, April 1990, to appear.

[12] Inman, D.J., *Vibration with Control Measurement and Stability*, Prentice Hall, 1989.

[13] Kuo, B.C., *Automatic Control Systems*, 5th Edition, Prentice Hall, 1988.

[14] Harokopos, E.G and Mayne, R.W., "Motor Characteristics in the Control of a Compliant Load," AIAA Journal of Guidance Control and Dynamics, Vol. 9, No. 1, 1986, pp 113-118.

1990 IMAC

Modeling and Tachometer Feedback in the Control of an Experimental Single Link Flexible Structure

Ephrahim Garcia
Research Assistant Professor

Daniel J. Inman
Professor

Department of Mechanical and Aerospace Engineering
State University of New York at Buffalo
Buffalo, New York 14260

Abstract

In this work a formulation for the modeling of a single link flexible structure will be introduced that includes the effects of dynamic interaction between the actuator and structure. These effects are the rotational modal participation factors for the structure's vibratory motion that occurs at the slewing axis. It will be shown, both theoretically and experimentally, that this dynamic interaction can be advantageous for vibration suppression of the flexible modes of the system during slewing positioning maneuvers.

Introduction

Research in the control of flexible structures has been carried out in the fields of robotics[1-6] and spacecraft with flexible appendages[7-9]. Although a continuous beam is a simplification of more complicated structures actually used in these fields[19, 20], studying simple beams often yields insite into the underlying physics that governs the overall system behavior. In the area of robotics, light-weight (flexible) manipulators are seen as a way to reduce energy consumption and therefore operating cost in industrial robots. In space, reducing structural mass of space-bound robots and satellite appendages allows for lighter, and hence, more cost effective payloads for orbital delivery.

The modeling presented here in an extension of the modeling done by other researchers[1-3]. This modeling includes the effects of actuator-structure interaction via the modal participation factors of the flexible modes of the system[11].

Finally, the dynamics of a experimental flexible beam slewing in the horizontal plane are investigated. Servo positioning is often the goal of many control applications, such as robotic arm positioning for assembly line applications or the attitude orientation of a spacecraft. The response of the beam with a servo positioning control law will also be investigated to determine the validity of the proposed model.

Modeling

The dynamics of the system will be derived in two parts. First, the structural dynamics will be formulated from Hamilton's principle. The equations of motion for the actuator will then be derived and combined with the equations of motion for the structure. Finally, the angular position and velocity matrices for a servo feedback control using the driving motor will be derived.

Structural Dynamics

The problem under consideration is the slewing of a flexible beam in the horizontal plane and is schematically represented in figure 1.

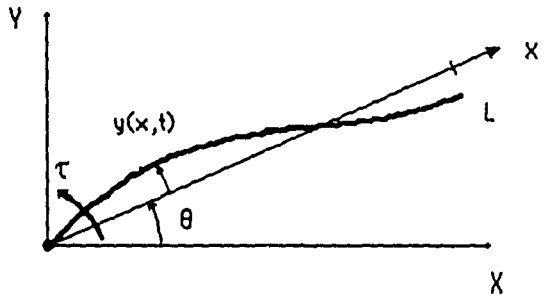

figure 1. Slewing flexible beam - top view.

In figure 1, XY is an inertial reference frame, and xy is a rotating reference frame. This rotating reference frame represents the position of the undeflected beam. It is assumed that the beam is moving in the horizontal plane and that flexural vibrations occur only in this plane. It is assumed that gravity has a uniform effect on the system that is out of plane and therefore can be ignored. The beam is pinned at the slewing axis, and the torque is applied at this axis.

A modal summation procedure is applied for the motion of the structure, e.g.,

$$y(x,t)=\sum_{i=1}^{n}\phi_i(x)\,q_i(t) \tag{1}$$

The eigenfunctions or mode shapes are defined by $\phi_i(x)$, and the time dependent modal displacements are defined by $q_i(t)$. Hamilton's principle for dynamic system's is stated as follows[14,15].

$$\delta^{(1)}\int_0^L [\,L_g + W_{nc}]\,dt = 0 \tag{2}$$

where, $\delta^{(1)}$ denotes the first variation and L_g denotes the system's Lagrangian. The term, W_{nc}, is the nonconservative work done by the applied, τ, in figure 1. The nonconservative work done by the applied torque becomes,

$$W_{nc} = \tau\,\theta + \tau\,\frac{\partial y(0,t)}{\partial x} \tag{3}$$

Accounting for the rotation of the flexible structure, y'(0,t), in the nonconservative work term leads to the inclusion of the modal participation factors in the structure's equations of motion[11]. Generally modes should be chosen within a practical bandwidth or frequency range of interest[17]. This modal summation procedure is also known as the Rayleigh-Ritz method or the expansion theorem[12]. The following Lagrangian for this system was found using an assumed-mode method application of Hamilton's principle[13].

$$L_g = \frac{1}{2} I_b \dot{\theta}^2 + \int_0^L \rho x \dot{\theta} \sum_{i=1}^{n} \phi_i \dot{q}_i \, dx + \frac{1}{2} \int_0^L \sum_{i,j}^{n} \dot{q}_i \dot{q}_j \phi_i \phi_j - \frac{1}{2} \int_0^L EI \sum_{i,j}^{n} q_i q_j \phi_i'' \phi_j'' \qquad (4)$$

where, for convenience, $\phi = \phi_i(x)$, and $\theta_i = \theta_i(t)$. Substituting this into the Euler-Lagrange equation, an expression for the rigid body position, θ, is found to be,

$$I_b \ddot{\theta} + \sum_{i=1}^{n} \int_0^L \rho x \phi_i \, dx \, \ddot{q}_i = \tau \qquad (5)$$

The equation for the ith flexible modes of the structure, q_i, is as follows.

$$\int_0^L \rho x \phi_i \, dx \ddot{\theta} + \sum_{j=1}^{n} \int_0^L \rho \phi_i \phi_j \, dx \, \ddot{q}_i + \sum_{i,j}^{n} \int_0^L EI \, \phi_i'' \phi_j'' \, dx \, q_i = \phi_i'(0) \, \tau \qquad (6)$$

The term, $\phi_i'(0)\,\tau$, is reflective of the direct transmission of torque into the modal deflections of the structure.

Actuator Dynamics

The torque applied to the beam is considered here to be generated by an armature controlled DC electric motor, whose behavior is represented by the following schematic.

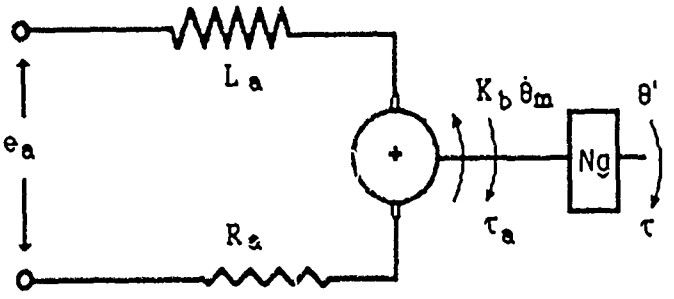

figure 2. Motor armature circuit and gear box schematic.

Here, e_a is the voltage applied across the armature, i_a is the current in the motor circuit, L_a is the motor inductance, R_a is the armature resistance, N_g is the gear ratio and K_b is the motor back-emf. Applying Kirchoff's law and summing the torques about the motor armature, the following expression for the torque is found as a function voltage across the motor armature,

$$\tau = \frac{N_g K_t}{R_a} e_a - I_m N_g^2 \left(\ddot{\theta} + \sum_{i=1}^{n} \phi_i'(0) \, \ddot{q}_i \right) - \left(c_v + \frac{K_b K_t}{R_a} \right) N_g^2 \left(\dot{\theta} + \sum_{i=1}^{n} \phi_i'(0) \, \dot{q}_i \right) \qquad (7)$$

where c_v is the viscous damping in the motor and K_t is armature torque constant. Since the electrical time constant of the motor is much smaller than the mechanical time constant of the system, the inductance is considered negligible so that it does not appear in the expression for torque. Before combining the structure equations of motion with the actuator dynamics we will consider the eigenanalysis of the structure taking into account the physical constraints of a motor actuated beam.

Eigenanalysis

It can be said a motor-actuated beam has an eigensolution that satisfies the boundary conditions imposed by the motor acting hinge. These boundary conditions for the structure are pinned with a rotatory inertia at the pinned axis and free at the other end(or simply, inertia-free). The inertia acting at the beam axis is usually referred to as a constraint[1]. Thus, the inertia-free eigenfunctions are considered to be the constrained modes of the beam, and the pin-free modes are the unconstrained modes of vibration for the structure. The first mode of a pin-free beam with various degrees of constraining inertia is plotted in figure 3 (see also reference[1]). These modes are plotted for a generic robot meter structure with varying beam to servo inertia ratios - I_b/I_s = (0.1, 1.0, 10.0).

The strongly constrained, or clamp-free, eigenfunctions were used successfully for modeling experimental slewing apparatus[2,3]. However, no verification of a model with significant actuator structure interaction (i.e., unconstrained or lightly constrained modes of vibration) has been found in the literature.

The condition for a flexible beam with a rotatory inertia due to the motor acting at the slewing axis is,

$$M_i \delta_{ij} = I_s \phi_i'(0) \phi_j'(0) + \int_0^L \rho \phi_i \phi_j dx \qquad (8)$$

where, δ_{ij} is the Kronecker delta operator. Since the structure operator is self-adjoint, and positive semi-definite the off diagonal terms of the structure's mass and stiffness submatrices decouple[11,12].

Combined Motor/Beam Equations

The eigenfunctions of the previous section can now be applied to the beam's slewing equations of motion, Eqs. (5) and (6), and the actuator's dynamics, Eq. (7), to represent the system's equations of motion in matrix notation. For *n* modes of vibration, we can represent the system as,

$$M\ddot{x} + D\dot{x} + Kx = B_f e_a \qquad (9)$$

where

$$M = \begin{bmatrix} I_b + I_s & I_1 + I_s\Gamma_1(0) & \cdots & I_n + I_s\Gamma_n(0) \\ I_1 + I_s\Gamma_1(0) & M_1 & \cdots & 0 \\ \vdots & \vdots & & \vdots \\ I_n + I_s\Gamma_n(0) & 0 & \cdots & M_n \end{bmatrix}$$

$$D = \begin{bmatrix} b_v & b_v\Gamma_1(0) & \cdots & b_v\Gamma_n(0) \\ b_v\Gamma_1(0) & b_v\Gamma_1(0)^2 & \cdots & b_v\Gamma_1(0)\Gamma_n(0) \\ \vdots & \vdots & & \vdots \\ b_v\Gamma_n(0) & b_v\Gamma_n(0)\Gamma_1(0) & \cdots & b_v\Gamma_n(0)^2 \end{bmatrix}$$

$$K = \begin{bmatrix} 0 & 0_{1xn} \\ & M_1\omega_1^2 \quad \dots \quad 0 \\ 0_{nx1} & \vdots \qquad\qquad \vdots \\ & 0 \qquad \dots \quad M_n\omega_n^2 \end{bmatrix}$$

$$B_f{}^T = \frac{N_g K_t}{R_a} [1.0, \Gamma_1(0), ..., \Gamma_n(0)]$$

$$\Gamma_i(0) = \phi_i'(0), \quad I_i = \int_0^L \rho x \phi_i(x)\, dx$$

and

$$x^T = [\theta, q_1, ..., q_n]$$

where, $I_s = I_m N_g^2$, is the effective servo inertia, and $b_v = (c_v + \frac{K_b K_t}{R_a}) N_g^2$, is equivalent viscous friction due to the the viscous bearing friction of the system, c_v, and the back emf constant of the motor. The $(^T)$ denotes the transpose of a matrix or vector, and M_i is a constant of normalization for the eigenfunction, ϕ_i.

The modal coordinates, q_i, are not coupled to one another in either the mass or stiffness structural submatrices, except of course through the viscous dissipation in the actuator as one would expect.

Closed Loop System

To arrive at a closed loop response for the system, the motor armature is set equal to various states of the model, e.g.,

$$e_a = - G_p x - G_v \dot{x} \tag{10}$$

The matrices G_p and G_v are the position and velocity feedback row vectors, respectively. Since precise position, or servo control, is usually the goal of a controlled flexible beam, the effects of a servo controller will be considered on the open loop equations of motion. For the closed loop response, the armature voltage is set proportional to the error signal generated by the difference between a reference signal, θ_{ref}, and the measured beam position, i.e.,

$$e_a = K_g(\theta_{ref} - (\theta + \frac{\partial y(0,t)}{\partial x})) \tag{11}$$

Tachometer feedback is usually obtained by adding the negative tachometer signal to Eq. (11) in order to obtain a control based on the angular velocity as well as the angular position of the system, such that,

$$e_a = K_g(\theta_{ref} - (\theta + \sum_{i=1}^{n} \Gamma_i(0)\, q_i)) - K_v(\dot{\theta} + \sum_{i=1}^{n} \Gamma_i(0)\, \dot{q}_i) \tag{12}$$

where, $K_v = \frac{K_{tach} K_t N_g^2}{R_a}$ is the tachometer signal measured at the motor and K_{tach} is the tachometer gain. The tachometer feedback, K_v, has the effect of changing the level of viscous damping in the motor, and hence, the slewing axis

Combining the position and velocity feedback , Eq. (12) with the open loop system, Eq. (9), the closed loop system of equations are found to be,

$$\tilde{M}\ddot{x} + \tilde{D}\dot{x} + \tilde{K}x = B_f \theta_{ref} \tag{13}$$

The closed loop system matrices of Eq (13) are defined as,

$$\tilde{M} = M$$

$$\tilde{D} = D$$

$$\tilde{K} = K + K_p K_{fb}$$

$$B_f{}^T = [K_p, K_p\Gamma_1(0), ... , K_p\Gamma_n(0)]$$

and

$$K_{fb} = \begin{bmatrix} K_p & K_p\Gamma_1(0) & \dots & K_p\Gamma_n(0) \\ K_p\Gamma_1(0) & K_p\Gamma_1(0)^2 & \dots & K_p\Gamma_1(0)\Gamma_n(0) \\ \vdots & \vdots & & \vdots \\ K_p\Gamma_n(0) & K_p\Gamma_n(0)\Gamma_1(0) & \dots & K_p\Gamma_n(0)^2 \end{bmatrix}$$

The servo stiffness is defined as,

$$K_p = \frac{N_g K_t K_g}{R_a} \tag{14}$$

where, K_g is the amplification gain. Since the equivalent viscous damping of the system, b_v, now includes the damping due to the tachometer feedback, it is redefined as,

$$b_v = (c_v + \frac{K_t(K_b + K_{tach})}{R_a}) N_g^2 \tag{15}$$

The inclusion of the modal participation factors cause the position and velocity feedback matrices to becomes fully populated, as opposed to the single element feedback terms.

Experimental Apparatus

This experiment consists of a a 0.0825 cm (1/32") thick by 7.62 cm (3") wide aluminum beam fixed to a 1/4 inch stock shaft - the slewing axis. The beam is fixed to the slewing axis via a rigid clamp. The structure used in this had an effective length of .848 m, measured from the slewing axis to the beam's free end. The motor was directly linked to the flexible structure through the slewing axis as indicated in the schematic of figure 4. The beam's slewing axis is bearing mounted in a rigid aluminum base which is fixed to ground. A 1/16" square key way (channel) is cut in the shaft, the rigid clamp, and the motor/beam coupler.

The motor used in the experiment was an armature controlled DC electric motor manufactured by the Electro-Craft corporation, model# 586-MGHP, with the following specifications.

- I_m - 5.5×10^{-3} oz in s^2
- L_a - 2.3×10^{-3} H
- R_a - 1.1 Ω
- K_b - 5.8 V/kRPM
- K_t - 7.8 oz in/A

An EAI2000 analog computer was used to condition the sensor signals, as well as to close the servo loop. The amplified servo signals were fed to a Copley Servo Controller, model# 215, in the power amplifier mode of operation. This closed loop system can be represented by the block diagram of figure 5. The constants from figure 5 have the following definitions.

- K_g - analog computer gain
- K_{amp} - power amplification gain
- K_{pot} - position feedback
- K_{tach} - tachometer feedback

A potentiometer was used to generate a position signal for the motor beam system, and the angular velocity was measured via a "built in" tachometer in the motor housing. In addition to these sensors an accelerometer was used to measure the acceleration

at the beam tip. The mass of the accelerometer was approximately 5 grams and its effects were not considered in the modeling of the system.

The physical properties of the beam were found to be,

$E = 69 \times 10^9$ Pa

$I = \frac{1}{12} bh^3$

b = 3" (7.62 cm) h ≅ 1/32" (.8 mm)

$\rho = .1698$ kg/m

$EI = .2631$ Nm^2

The rigid body inertia of the beam about the slew axis is calculated to be,

$$I_b = .1698\frac{(.848)^3}{3} = 3.45 \times 10^{-2} \text{ kgm}^2$$

The effective inertia acting at the root of the beam is, $I_s = 1.94 \times 10^{-4}$ kgm^2, which accounts for the servo motor inertia as well as the system's rigid clamp.

The experimental modes of vibration were found using the open loop transfer function of the system. The experimental and theoretical natural frequencies of the motor/beam system are given in Table 2. The agreement between theory and experiment diverges for the higher modes of vibration. This is most likely due to the rigid clamp between the beam and the axis. This clamp extends from the axis of rotation 7.4% of the beam length in the *x* direction from the slewing axis.

System Responses

To verify the proposed model, a closed loop servo controller was added to the experimental slewing beam as depicted in the block diagram of figure 5.

Frequency response functions(FRFs) were measured between the system output signals and a disturbance reference signal for the closed loop system. Figure 6 shows both the measured tachometer/disturbance FRF and the acceleration/disturbance FRF. This model was used to generate the tachometer/disturbance FRF for the system, figure 7. The first low frequency peak corresponds to the rigid body position of the structure while the higher modes of vibration corresponds to the flexible modes of the structure. The predicted tach/disturbance FRF agrees reasonably well for the first up to the third natural frequency of the system.

The time domain response were also measured. A a large angle slewing manuever was performed for a 30° step command signal. Figure 8 contains the experimental response with and without added tachometer feedback. In both cases the system was expected to have roughly the same performance, i.e., a settling time of approximately 4 seconds, and a time to maximum overshoot of 1 second. The predicted response of the model is plotted in figure 9. Because of the interaction between the beam and the actuator, tachometer feedback was added to the system, the flexural vibrations of the structure were damped out for the slewing maneuver. The effects of the added tachometer on the structural dynamics can clearly seen in figure 10; this plot contains the experimental tip acceleration with and without added tachometer feedback as well as the model's response with added feedback. The proposed model predicted the effects of this added damping on the modes of vibration because of the inclusion of the modal participation factors in our model.

Closing Remarks

The model presented in this paper generalizes other models in the literature. Here the effects of the motor on the dynamics of the structure are accounted for through the boundary condition. The interaction of the beam and the motor are then coupled by consideration of the rotation due to the modal deflections of the structure. The experimental result indicates that this modeling approach describes the physical system behavior fairly accurately.

The significance here is that the interaction between structure and actuator can be advantageous for vibration suppression without needing any structural sensors. The interaction allows for the servo angular position and velocity sensors to measure structure vibrations directly. When the modal participation factors of the system are nonzero, feeding back the tachometer signal generates damping for not only the rigid body position of the system but also damps the flexible modes of the structure.

Acknowledgment

The authors gratefully acknowledge support from the Air Force Office of Scientific Research, grant number AFOSR-F49620-86-C-0011. Additional support was provided by the National Aeronautics and Space Administration, NASA Headquarters Graduate Student Researchers' Program, grant number NGT 33183-804.

References

1) Barbieri, E., and Ozguner, U., 1988, "Unconstrained and Constrained Mode Expansion for a Flexible Slewing Link," Trans. ASME, J. of Dynamic Systems, Measurement and Control, Vol. III, pp. 416-421.

2) Juang, J.N., Horta, L.G. and Robershaw, H., 1986, "A Slewing Control Experiment for Flexible Structures," AIAA J. of Guidance, Control and Dynamics, Vol. 9, No. 5, pp. 599-607.

3) Hastings, G.G. and Book, W.J., 1987, "A Linear Dynamic Model for Flexible Robotic Manipulators," IEEE Control Systems Magazine, pp. 61-64.

4) Cannon, H.C., Jr. and Schmitz, E., 1984, "Initial Experiments on the End-Point Control of a Flexible One-Link Robot," International Journal of Robotics Research, Vol. 3, No. 3, pp. 62-75.

5) Book, W.J., Maizza-Neto, O., and Whitney, D.L., 1975, "Feedback Control of Two Beams, Two Joint Systems with Distributed Flexibility," ASME J. of Dynamic System, Measurement and Control, pp. 429-431.

6) Fukuda, T., 1985, "Flexibility Control of Elastic Robotic Arms," Journal of Robotic Systems, 2(1), pp. 73-83.

8) Hughes, P C., 1974, "Dynamics of Flexible Space Vehicles with Active Attitude Control," Celestial Mechanics, vol. 9, pp. 21-39

9) Meirovitch, L. and Juang, J.N., 1976, "Natural Modes of Oscillation of Rotating Flexible Structures about Nontrivial Equilibrium," AIAA J of Spacecraft and Rockets, Vol. 13, No. 1, pp. 37-44.

10) Breakwell, J.A., 1981, "Optimal Feedback Slewing of Flexible Spacecraft," AIAA J. Guidance and Control, Vol. No. 5, pp. 472-479.

11) Garcia, E., 1989, "On the Modeling and Control of Slewing Flexible Structures," Ph.D. Thesis, Department of Mechanical and Aerospace Engineering, State University of New York at Buffalo, Buffalo, New York.

12) Inman, D.J., 1989, *Vibration with Control, Measurement, and Stability*, Prentice-Hall, Englewood Cliffs, New Jersey.

13) Meirovitch, L., 1980, *Computational Methods in Structural Dynamics*, Sijthoff and Noordhoff International Publishers, Rockville, Maryland.

14) Reismann, H., 1988, *Elastic Plates: Theory and Applications*, John Wiley and Sons, New York, New York.

15) Shames, I.H., and Dym, C.L., 1987, "Energy and Finite Element Methods in Structural Mechanics," Hemisphere Publishing Corp., New York, New York.

16) Goldstein, H., 1981, *Classical Mechanics*, Second Edition, Addison-Wesley Publishing Co., Reading, Ma.

17) Hughes, P.C., 1987, "Space Structure Vibration Modes: How many Exist? Which ones are Important?," IEEE Control System Magazine, February, pp. 22-28.

18) Kuo, B.C., 1982, *Automatic Control Systems*, 4th edition, Prentice-Hall, Englewood Cliffs, New Jersey.

19) Sunada, W.H. and Dubowsky, S., 1983, "On the Dynamic Analysis and Behavior of Industrial Robotic Manipulators with Elastic Members," ASME J. of Mechanisms, Transmissions and Automation in Design, Vol. 105, pp. 43-51.

20) Pappa, R.S. and Juang, J.-N.,1985,"Galileo Spacecraft Modal Identification Using an Eigensystem Realization Algorithm," Journal of Astronautical Sciences, vol. 33, Jan.-March, pp.15-33.

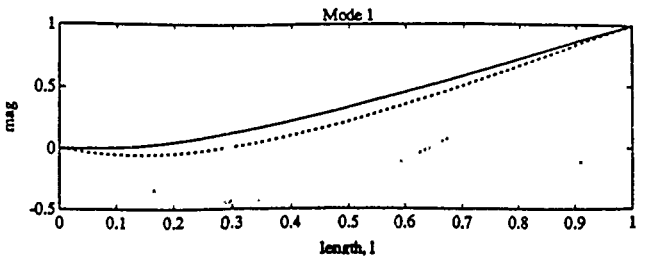

figure 3. Mode 1 with varying inertia constraints, I_b/I_s=(.01, 1.0, 10).

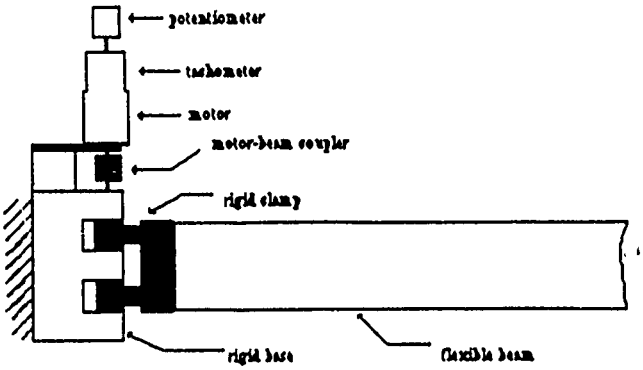

figure 4. Schematic of the motor/beam assembly.

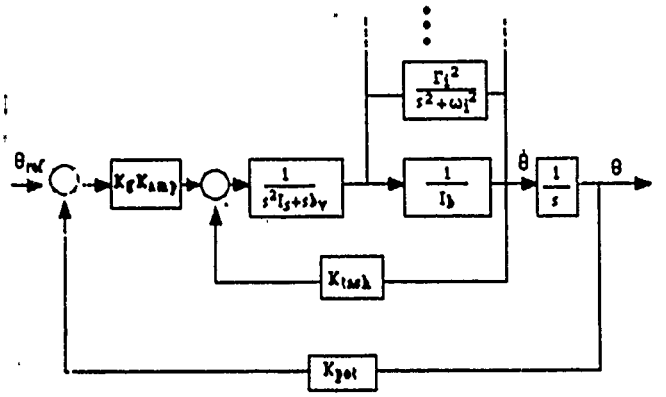

figure 5. Block diagram of the slewing control of a flexible structure.

I_b/I_s	0.0	0.01	0.1	1.0	10.0	pin-free ∞
a_1L	1.8751	1.8796	1.9189	2.2135	3.1677	3.9256
a_2L	4.6941	4.6944	4.6970	4.7234	5.0011	7.0682
a_3L	7.8548	7.8548	7.8554	7.8610	7.9190	10.2078
a_4L	10.9955	10.9956	10.9958	10.9978	11.0185	13.3492

Table 1. Eigenvalues of an inertia-free beam for various I_b/I_s.

mode	1	2	3	4	5	
Theory	4.130	12.345	22.579	36.384	56.763	(Hz)
Experiment	4.0	11.625	22.813	39.625	63.125	(Hz)

Table 2. Theoretical and experimental natural frequencies.

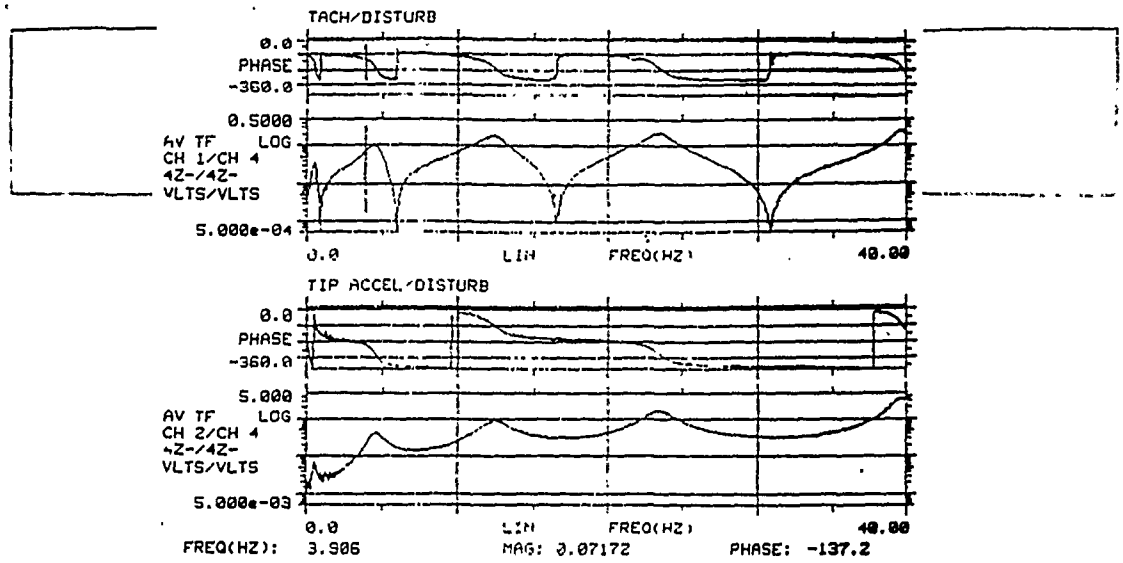

figure 6. Measured transfer functions of the closed loop system.

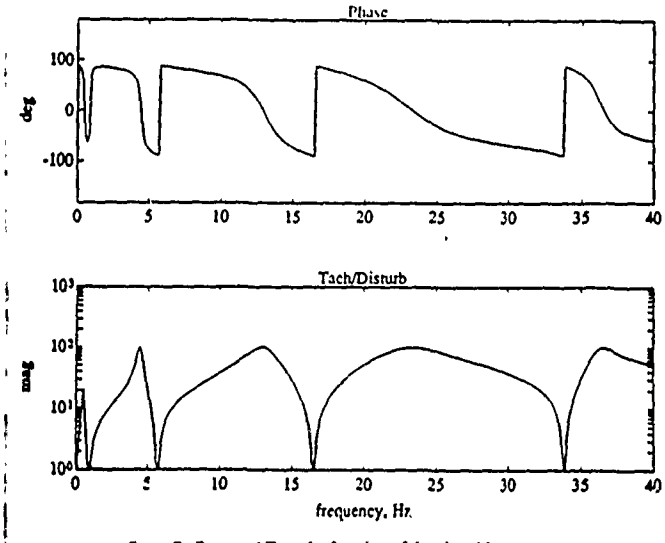

figure 7. Predicted Transfer function of the closed loop system.

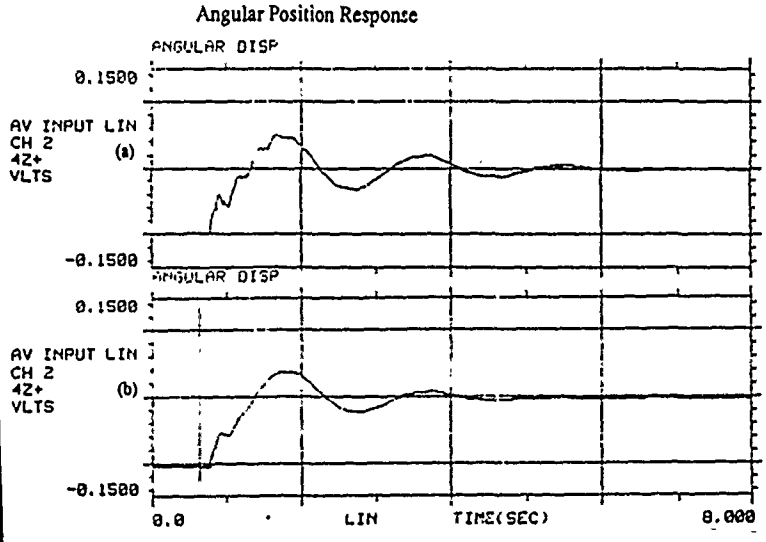

figure 8. Experimentally measured angular step response:
(a) no added feedback (b) with added tach feedback.

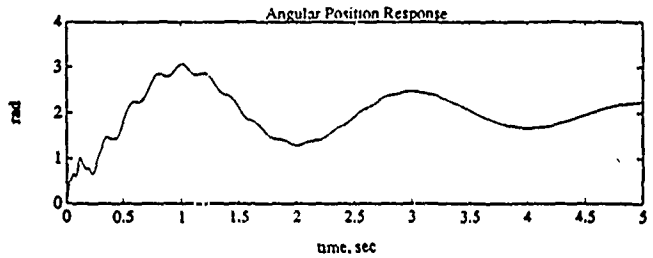

figure 9. Predicted system response to a step command without added feedback.

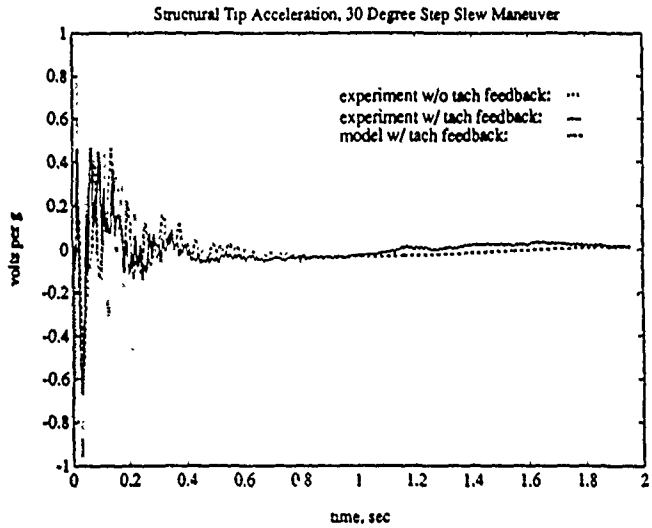

figure 10. Tip accelerations for a step command to the system.

Distributed Parameter Actuators for Structural Control

H. H. Cudney
D. J. Inman
Department of Mechanical and Aerospace Engineering
University at Buffalo, Buffalo NY 14260

Y. Oshman
Department of Aeronautical Engineering
Technion, Haifa Israel 32000

Abstract

Timoshenko beam theory is applied to beams with multiple layers of piezoelectric material attached. The model is developed using a Hamiltonian approach, and includes the external electrical circuit as well as a com plete set of boundary conditions. Resistors are added to the sensor layers for passive damp - ing. The resulting model is then formulated in state space.

Nomenclature

Subscripts a,,s , c	actuator, sensor, beam
A	Cross sectional area
b_c	width of the conducting surface
C_{ij}	element of lastic matrix
E	Youngs modulus
G	shear modulus
h_a, h_a	z-coordinate of actuator, sensor
h	outer z-coordinate
H_i	Heaviside step function.
I	Second moment of inertia
n	number of segments
P	Ext. applied normal forces
P_s, P_a	exposed normal force dist.
R_i	ith discrete resistor.
u_i	displacement field
E, D (3x1)	electric and displacement fields
e (3x6)	piezoelectric strain-charge coeff.
h (3x6)	piezoelec. strain-voltage coeff.
σ, ε (6x1)	stress and strain fields
ε_e(3x3)	dielectric permittivity coeff.
β_e(3x3)	dielectric impermeability coeff.
$\beta(x,z,t)$	shear bending angle
ε_{xx} , ε_{xz}	normal strain, shear strain
η^*	accounts for non-linear cross-section deformation
$\phi(x,t)$	voltage
σ_e	electric charge
ρ	density
$\psi(x,t)$	beam bending angle

1. Introduction

The problem of controlling the dynamic re - sponse of large space structures has been the subject of much research for the last several years. Several types of control systems have been investigated. They can be broadly classified as discrete and distributed control systems. Examples of discrete control systems include proof mass actuators [1], torque wheels [2], thrusters [3], and discrete piezoelectric ele ments [4]. Distributed control systems can be broadly classified as passive and active. The most common example of passive control is constrained layer damping treatments, which are compared in [5]. An example of dis tributed active control are layers of piezoelec tric materials.

There are several advantages to implementing a distributed control scheme. First, as the current designs for space structures grow in - creasingly flexible, the difference between ground tests of these structures in a strong gravity field and their actual on-orbit behavior increases, and determining discrete actuator and sensor placement becomes more difficult. This can be avoided using distributed actuators and sensors. Distributed control schemes are less sensitive to individual actuator and sensor failure. Some distributed control schemes can control all modes for certain boundary conditions, and thereby avoid modal truncation and the ac companying

problems of control and observation spillover [6].

In terms of resulting loss factors, piezoelectric control can achieve higher damping ratios than equivalent passive damping treatments [5,7,8]. Primarily for this reason, several researchers have been examining different aspects of the problem of controlling vibrations with piezoelectric materials. Hubbard, et. al., have developed a model of a beam with has both a layer of piezoelectric sensor material and a layer of piezoelectric actuator material, using Euler-Bernoulli beam theory [6,7,9]. Similar models were developed by Obal and Hanagud [10]. Tzou developed a model of distributed piezoelectric materials using Euler-Bernoulli beam theory [11], while Lee and Moon developed a model for a plate using Euler-Bernoulli bending deformation assumptions [12].

The objective of this research is to develop an electromechanical equations of motion for a beam with multiple layers of attached piezo - electric materials. The motivation for using multiple layers is to provide greater control authority to the structure to be controlled. The approach taken is to use Timoshenko beam theory in conjunction with a Hamiltonian energy method for each individual layer of the beam. Since one control objective is to add damping to a structure, a resistor network is added to the sensor layers to provide both the sensor output voltage in an explicit form as well as a mechanism for dissipating energy.

2. Theory

The structure of interest is shown in Fig. 1, and is considered to have 5 layers: an original substructure, a top and bottom layer adjacent to the substructure which will be considered the sensors, and outer layers on the top and bottom which are considered to be the actuators, where the sensors and actuators are piezoelectrically active material. The procedure this analysis follows is to analyze each layer separately as shown in Fig. 2, which exposes the electrical boundaries as well as the interlaminar stress distribution. Hamilton's principle will then be applied to each layer and electrical network. The layers can be linked through the exposed interlaminar stress distribution.

Several assumptions are made about the configuration to be analyzed. First, the piezoelectric material is taken to be polyvinylflouride film (PVDF). While it does not exhibit the forces that piezoelectric ceramic materials generate, it is very pliable and not brittle like the crystals are. Additionally, it can easily be manufactured in sheets, and applied in a distributed manner.

The layers are assumed to be perfectly bonded. This configuration was also chosen such that the structure is symmetric about the centroidal axis, hence the neutral axis is coincident with the centroidal axis, which allows a clearer analysis of the piezoelectric effects on the equations of motion. The mechanical effects of the conducting surfaces sputtered on the piezoelectric materials can be neglected since their thickness is on the order of microns. The mechanical effects of the bonding layers will also be neglected, at the appropriate time they can be included in the model by increasing the number of layers to be analyzed. As a final assumption, none of the layers are considered to deform in the thickness direction.

The assumption about deformation of the beam follows Timoshenko beam theory, and is given as,

$$\begin{aligned} u_1 &= -z\,\eta^*\,\psi(x,t) \\ u_2 &= 0 \\ u_3 &= w(x,t) \end{aligned} \qquad (1)$$

where displacement directions u_1, u_2, and u_3 correspond to the x, y, and z directions, respectively, shown in Fig. 1.

The strain displacement relations are given as,

$$\begin{aligned} \varepsilon_{xx} &= -z\,\eta^*\,\frac{\partial\psi(x,t)}{\partial x} \\ \varepsilon_{xz} &= \frac{1}{2}\beta(x,z,t) \end{aligned} \qquad (2)$$

and all other strains are considered zero.

There are two mechanisms by which energy is considered to be dissipated. Viscous (air) damping occurs because the structure is usually vibrating in a fluid, and is represented by the coefficient C_1. The structural damping is modelled as Kelvin-Voight damping, and is proportional to strain rate, therefore there is a coefficient for the normal strain, C_d, and the shear strain, C_s.

The constitutive laws for piezoelectric materials relate the electrical and mechanical effects. Two versions of the constitutive laws are presented here, and they can be related to one another by simple transformations [13]. If the piezoelectric layer is configured as a sensor, that is, if the voltage output is of interest, then the appropriate constitutive law to use is

$$\sigma = c^E \varepsilon + e^t E$$

$$D = e\,\varepsilon + \varepsilon_e E \qquad (3)$$

where superscript t represents the transpose. If the layer to be modelled is configured as an actuator, then the voltage field is applied, and is an independent variable, so the appropriate form of the constitutive law is,

$$\sigma = c^D \varepsilon - h^t E \qquad (4)$$
$$E = -h\varepsilon + \beta_e D$$

Analysis of the Sensor Layer

The Hamiltonian for the sensor layer is given as,

$$\delta^{(1)}\mathcal{H}_s = \int_{t_0}^{t_1}\left[\int_v \delta^{(1)}(T - H)\,dv + \int_v \delta^{(1)}W_{nc} + \int_s \delta^{(1)}W_{ext}\right]dt \qquad (5)$$

where T is the kinetic energy, W_{nc} represents the energy dissipation due to damping mechanisms, and W_{ext} represents the work crossing the boundary of the system. This term accounts for mechanical work in the form of the applied forces to the beam and the exposed interlaminar stress distribution, and electrical energy crossing the boundary. The integrals are with respect to time, or over the volume, v, or the surface area, s.

H represents the electric enthalpy, which is the appropriate term to use for the sensors, since the sensor voltage distribution, which can be related to the electric field within the piezoelectric layer,

$$E_3 = \frac{\partial \phi(x,t)}{\partial x} \qquad (6)$$

is the variable of interest [14]. This term can be derived from the internal energy through a Legendre transformation, H = U - ED. The unknowns are the sensor voltage distribution, interlaminar stress distribution, and beam displacements.

Developing a Hamiltonian formulation of the external electric circuit yields,

$$\delta^{(1)}\mathcal{H}_{ext} = \int_{t_0}^{t_1}\left[\delta^{(1)}W_{nc} + \int_s \delta^{(1)}W_{ext}\right]dt \qquad (7)$$

where W_{nc} represents the energy dissipated by the resistor, and W_{ext} represents the energy crossing the boundary from the surface of the piezoelectric material conductor surface.

Taking the first variation and setting the result equal to zero yields the resulting equations of motion. Since the variation of each of the unknowns is arbitrary, to set the complete Hamiltonian to zero requires that the terms modifying each unknown must equal zero. Thus, each unknown will yield an equation. For the first variation of the transverse displacement of the beam, $\delta w(x,t)$, the resulting equation is,

$$-\rho_s A_s \frac{\partial^2 w(x,t)}{\partial t^2} + \frac{\partial}{\partial x}[\kappa_{ss}^2 C_{55s} A_s (\frac{\partial w(x,t)}{\partial x} - \psi(x,t))] + \frac{\partial}{\partial x}\{\kappa_{ds}^2 C_{ss} A_s \frac{\partial}{\partial t}[\frac{\partial w(x,t)}{\partial x} - \psi(x,t)]\} + P_a(x,t) - P_s(x,t) = 0 \qquad (9)$$

where the first three terms are the same as for a Timoshenko beam, $P_a(x,t)$ represents the normal component of the exposed force distribution between the actuator and sensor layer, and $P_s(x,t)$ represents the normal component of the exposed force distribution between the sensor layer and the sub-structure.

For the first variation of the bending angle of the beam, $\delta\psi(x,t)$, the resulting equation is,

$$-\rho_{ss} I \frac{\partial^2 \psi(x,t)}{\partial t^2} + \frac{\partial}{\partial x}(C_{11ss} I \frac{\partial \psi(x,t)}{\partial x}) + [\kappa_{Ss}^2 C_{55s} A_s (\frac{\partial w(x,t)}{\partial x} - \psi(x,t))] + \frac{\partial}{\partial x}[C_{nss} I \frac{\partial}{\partial t}(\frac{\partial \psi(x,t)}{\partial x})] + [\kappa_{ds}^2 C_{ss} A_s \frac{\partial}{\partial t}(\frac{\partial w(x,t)}{\partial x} - \psi)] + \frac{\partial}{\partial x}[b_c e_{31} \frac{h_s + h_a}{2} \phi_s(x,t)] + v_s(x,t)h_s - v_a(x,t)h_a = 0 \qquad (10)$$

The first five terms would result from a standard Timoshenko beam with damping. The shear force distribution from the actuator layer and sub-structure are represented by $v_a(x,t)h_a$ and $v_s(x,t)h_s$, respectively. The term of interest in this equation is

$$\frac{\partial}{\partial x}[b_c e_{31} \frac{h_s + h_a}{2} \phi_s(x,t)] \qquad (11)$$

where $\phi_s(x,t)$ is the resulting voltage distribution. It is through this term that the mechanical deformation of the beam is directly influenced by the piezoelectric properties of the sensor layer. Note that if none of the quantities in this term vary spatially, then when the derivative term is applied the result will be zero, and the most direct electro-mechanical coupling mechanism will be lost. Note that although $\phi_s(x,t)$ is represented as being spatially dependent, the conducting surface causes the voltage to be constant along the surface of the beam.
This has been recognized by other researchers. To keep this term active, Hubbard, et. al. varied the width of the conducting surface with respect to the length of the beam [6]. Lee and Moon used that technique in addition to varying the piezoelectric property represented by e_{31} with respect to space by varying the polarization field during manufacture of the film [12].

We propose to vary the voltage $\phi_s(x,t)$ by segmenting the conducting surface in a manner analogous to finite element analysis of beams, and can be easily accomplished by etching the conducting surface. This is represented in Fig. 3, and for n segments results in n sensor output voltages. Given this structure, we will still consider $\phi_s(x,t)$ as a distributed quantity, and the first variation yields the equation,

$$b_c e_{31} \frac{h_s + h_a}{2} \left(\frac{\partial \psi(x,t)}{\partial x}\right) + \frac{b_c \varepsilon_{33}}{t} \phi_s(x,t) + b_c \sigma_{se}(x,t) = 0 \qquad (12)$$

where σ_{se} is the charge distribution, which can vary spatially. Note that this is also a coupled electro-mechanical equation. A complete set of boundary conditions result when the first variation is applied, and these are given as

$$\int_{t_1}^{t_2} \left[-C_{11s} I_s \frac{\partial \psi(x,t)}{\partial x} - C_{ns} I_s \frac{\partial}{\partial t}\left(\frac{\partial \psi(x,t)}{\partial x}\right) + b_c e_{31} \frac{h_s + h_a}{2} \phi_s(x,t) \right] \delta\psi \Big|_0^L dt = 0 \qquad (13)$$

and

$$\int_{t_1}^{t_2} \left[-\kappa_{ss}^2 C_{55s} A_s \left(\frac{\partial w(x,t)}{\partial x} - \psi(x,t)\right) + \kappa_{ds}^2 C_{ss} A_s \frac{\partial}{\partial t}\left(\frac{\partial w(x,t)}{\partial x} - \psi(x,t)\right) \right] \delta w \Big|_0^L dt = 0 \qquad (14)$$

The only term different than the usual boundary conditions for the Timoshenko beam is the last term in Eq. (13). If none of the quantities vary spatially, this is the only term through which electro-mechanical coupling can be implemented, and leads to a boundary control problem [6].
The equation describing the external circuit results from the variation of the current in Eq. (7), and is given as

$$\int_{x_i}^{x_{i+1}} R_i b_c \frac{\partial \sigma_{se}(x,t)}{\partial t} dt = \phi_{si}(t) \quad \text{for } i = 1,\ldots,n-1 \qquad (15)$$

Note that energy dissipation is represented by the first time derivative of the charge distribution. Using Heaviside unit step functions, the discrete sensor output voltages can be related to the distributed sensor voltages, and will allow us to view the structure as a combined distributed and discrete system. This relation is given as,

$$\phi_s(x,t) = \sum_{i=1}^{n} [\phi_{si}(t) H_{i1}(x - x_i) H_{i2}(x_{i+1} - x)] \qquad (16)$$

Analysis of the Actuator Layer

The analysis of the outer actuator layer proceeds in a similar fashion as the sensor layer, with two important differences. First, since the electric field is applied, the dependent variable is the actuator charge distribution. Therefore, the proper energy term to use in Eq. (5) is U, the internal energy, not the electric enthalpy. The most convenient form of the constitutive law to use is given by Eq. (4). Secondly, there is no significant external electric circuit to consider, the applied voltage $\phi_a(x,t)$ is taken to be an ideal voltage source. The unknowns are the interlaminar stress distribution, beam displacements, and the actuator charge distribution.

3. State Space Formulation

A set of equations is obtained for each layer. They can be combined through the interlaminar stress distribution terms, which will be equal and opposite for adjacent layers. The resulting combined equations are then cast in a state space model, given as

$$\dot{\mathbf{x}} = \mathbf{A}\mathbf{x} + \mathbf{b}\mathbf{u}$$
$$\mathbf{y} = \mathbf{c}\mathbf{x} \qquad (17)$$

where the state variables are given as $\mathbf{x} = [w, \psi, \dot{w}, \dot{\psi}, \dot{\sigma}]^t$, $\mathbf{y}$ is the output vector of discrete sensor voltages given as $[\phi_{s1}(t), \phi_{s2}(t), \ldots, \phi_{sn}(t)]^t$. The inputs to the multilayered beam are the external forces and the applied voltage distribution, so that $\mathbf{u} = [P(x,t), \phi_a(x,t)]^t$, and $\mathbf{b}$ is given as

$$\mathbf{b}^t = \begin{bmatrix} 1 & 0 & 0 & 0 & 0 \\ 0 & 0 & 0 & 0 & 1 \end{bmatrix} \qquad (18)$$

The distributed state space model, A, is given in operator notation as,

$$\begin{bmatrix} 0 & 0 & 1 & 0 & 0 \\ 0 & 0 & 0 & 1 & 0 \\ L_1 & -L_2 & L_3 - L_4 & -L_5 & 0 \\ L_6 & L_{10} - L_9 & L_{11} & L_{12} - L_{13} & -L_{14} \\ 0 & -L_{15} & 0 & 0 & -L_{16} \end{bmatrix} \qquad (19)$$

where the operators are presented in Table 1. The output matrix, c, is given as

$$\begin{bmatrix} & & & & \\ 0 & 0 & 0 & 0 & \frac{d}{dt}\int_{x_0}^{x_1} R_1 b_1(\bullet)dt \\ & & & & \\ \cdot & \cdot & \cdot & \cdot & \cdot \\ \cdot & \cdot & \cdot & \cdot & \cdot \\ \cdot & \cdot & \cdot & \cdot & \cdot \\ & & & & \\ 0 & 0 & 0 & 0 & \frac{d}{dt}\int_{x_{n-1}}^{x_n} R_n b_n(\bullet)dt \\ & & & & \end{bmatrix} \qquad (20)$$

Using the sensor voltages as the control inputs to the actuators, multiplied by a gain. This is represented as

$$[\phi_{a1}(t), \phi_{a2}(t), \ldots, \phi_{an}(t)]^t =$$
$$-[G]_{nxn}[\phi_{s1}(t), \phi_{s2}(t), \ldots, \phi_{sn}(t)]^t \qquad (21)$$

where specifying collocated sensors and actuators will yield a diagonal gain matrix. The discrete actuator voltages, $\phi_{a1}(t)$ can be mapped into the distributed actuator voltage $\phi_a(x,t)$ using the technique presented in Eq. 16. The energy dissipation taking place in the external resistors connected to the sensor segments can then be enhanced by feedback to the actuator layer.

5. Summary

A Hamiltonian approach has been used to develop the equations of motion for a beam consisting of a substructure with multiple layers of piezoelectric material attached. There are several significant aspects to this model. First, the individual layers of the beam are separated to help obtain the proper electrical and mechanical boundary conditions, and Timoshenko bending deformation assumptions are utilized. Secondly, the conductors of the sensor and actuator layers are considered segmented to allow for a spatially varying voltage distribution. Resistors are added to the sensor layer to allow for passive damping. Finally, it is shown that different energy functions are appropriate to use in the Hamiltonian formulation of each layer, depending on whether that particular layer is configured as a sensor or as an actuator.

A state space model is then proposed which will implement the control objective of adding damping to the beam. Future research will focus on discretizing this model, and simulating and evaluating the disturbance attenuation of the system.

Acknowledgements

This research was supported by a NASA Headquarters grant from the Office of University Affairs (NGT-331-83-802), and by an AFOSR grant (AFOSR-F49620-86-C-0111)

References

[1] D. C. Zimmerman, G. C. Horner, and D. J. Inman, "Microprocessor controlled force actuator," *Proc. of the 27th AIAA/ASME /ASCE/AHS Struct., Struct. Dyn., and Materials Conf.*, San Antonio, TX, pp. 573-577, 1986.

[2] J. P. Williams and R. C. Montgomery, "Simulation and testing of digital control on a flexible beam", *Proc. of the AIAA Guid. and Cont. Conf.*, pp. 403-409, 1982.

[3] W. L. Hallauer and S. E. Lamberson, "Experimental active vibration damping of a plane truss using hybrid actuation," *Proc. of*

the 30th AIAA/ASME/ASCE/AHS/ASC Struct., Struct. Dyn., and Materials Conf., Mobile, AL, pp. 80-90, 1989.

[4] E. F. Crawley and J. de Luis, "Use of piezoelectric actuators as elements of intelligent structures," *AIAA Journal*, Vol. 25, No. 10, pp. 1373-1385, 1987.

[5] L. C. Rogers and K. E. Richards, "PACOSS program overview and status," *First NASA/DoD Cont. Struct. Interaction Conf.*, NASA CP 2447, Part 1, 1986.

[6] S. E. Burke and J. E. Hubbard, "Active vibration control of a simply supported beam using a spatially distributed actuator," *IEEE Cont. Sys. Magazine*, pp. 25-30, 1987.

[7] T. Bailey and J. E. Hubbard, "Distributed piezoelectric polymer active vibration control of a cantilever beam," *J. Guid., Cont. and Dynamics*, Vol 8, No. 5, pp. 605-611, 1985.

[8] A. D. Nashif, D. I. G. Jones, and J. P. Henderson, Vibration damping, Wiley, NY, NY, 1985.

[9] S. E. Burke and J. E. Hubbard, "Distributed Parameter control design for vibrating beams using generalized functions," IFAC Symp. on Cont. of Dist. Param. Sys., 1986

[10] M. W. Obal and S. Hanagud, "Identification of dynamic coupling coefficients in a structure with piezoceramic sensors and actuators," *Proc. of the 29th AIAA/ASME/ASCE/AHS/ASC Struct., Struct. Dyn., and Materials Conf.*, Williamsburg, VA, pp. 1611-1620, 1988.

[11] H.-S.Tzou, "Active vibration control of flexible structures via converse piezoelectricity," *Devel. in Mechanics*, Vol. 14, pp. 1201-1206, 1987

[12] C.-K. Lee and F. C. Moon, "Piezoelectric laminates for torsional and bending modal control: theory and experiment," Ph. D. dissertation, Cornell, 1987

[13] R. Holland and E. P. EerNisse, Design of resonant piezoelectric devices, MIT Press, Cambridge, MA, 1969.

[14] H. F. Tierston, Linear Piezoelectric Plate Vibrations, Plenum Press, NY, NY, 1969.

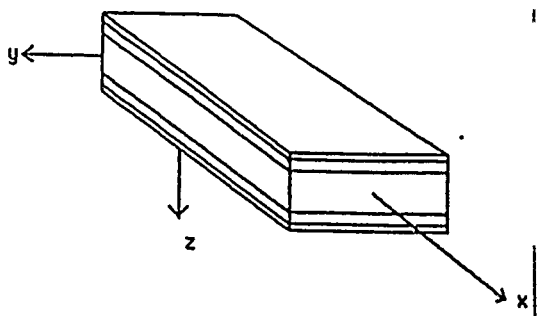

Figure 1: Typical Multilayered Beam

Table 1. Operator Definitions

op.	definition	op.	definition
1	$\frac{1}{\rho A}\kappa^2 GA\frac{\partial^2}{\partial x^2}$	8	$\frac{\kappa^2 GA}{\rho I}$
2	$\frac{1}{\rho A}\kappa^2 GA\frac{\partial}{\partial x}$	9	$\frac{\partial}{\partial x}\left[\frac{H^2}{\beta}\frac{\partial}{\partial x}\right]$
3	$\frac{\partial}{\partial x}\left[\frac{\kappa_d^2}{\rho A}C_s A\right]\frac{\partial}{\partial x}$	10	$\frac{\partial}{\partial x}\frac{B^2}{\varepsilon}$
4	$\frac{C_1}{\rho A}$	11	$\frac{\kappa_d^2 C_s A}{\rho I}\frac{\partial}{\partial x}$
5	$\frac{\partial}{\partial x}\left[\frac{\kappa_d^2}{\rho A}C_s A\right]$	12	$\frac{\partial}{\partial x}\left[\frac{C_n}{\rho}\frac{\partial}{\partial x}\right]$
6	$\frac{\kappa^2 GA}{\rho I}\frac{\partial}{\partial x}$	13	$\frac{K_d^2 C_s A}{\rho I}$
7	$\frac{E}{\rho}\frac{\partial^2}{\partial x^2}$	14	$\frac{\partial}{\partial x}\frac{b_c}{\varepsilon}$
15	$\frac{\partial}{\partial x}\frac{B}{\varepsilon}\sum_{i=1}^{n}\int_{x_i}^{x_{i+1}} R_i b_c H_{i1}(x-x_i)H_{i2}(x_{i+1}-x)(\bullet)$		
16	$\frac{B}{\varepsilon}\sum_{i=1}^{n}\int_{x_i}^{x_{i+1}} R_i b_c H_{i1}(x-x_i)H_{i2}(x_{i+1}-x)(\bullet)$		

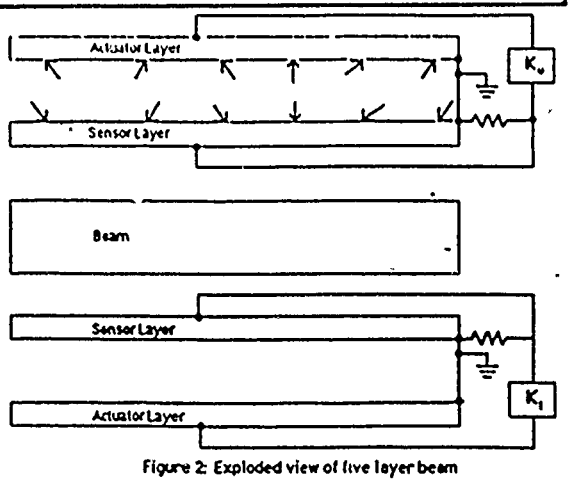

Figure 2: Exploded view of five layer beam

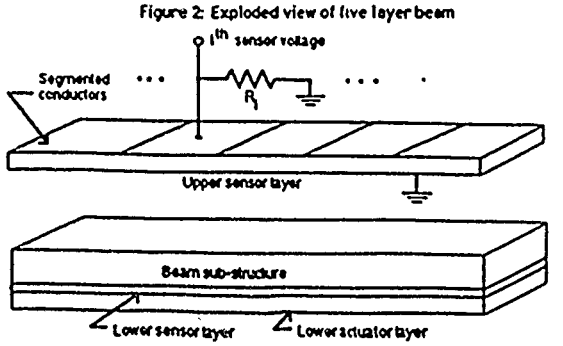

Figure 3: Discretised sensor

Advantages of Slewing an Active Structure

EPHRAHIM GARCIA AND DANIEL J. INMAN
Mechanical Systems Laboratory
Department of Mechanical and Aerospace Engineering
State University of New York at Buffalo
Buffalo, New York 14260

ABSTRACT: The slewing control of an active flexible structure is considered by examining the equations of motion of an integrated actuator/structure system containing both the actuator and structure dynamics. These equations are derived using a Hamiltonian approach. The system under consideration is a slewing flexible structure, a thin aluminum beam, torque driven by an armature controlled DC electric motor and actuated by a piecewise distributed piezoceramic actuator. An improvement in performance is gained by 1) including the effects of motor actuator and beam dynamic interaction and 2) using a piezoelectric device, layered on the structure, for direct vibration suppression of the structural dynamics. A comparison is made using simulations, to point out the advantages of slewing an active structure versus slewing a passive structure. This presents a multi input slewing control problem which is implemented using a standard linear quadratic regulator control design.

INTRODUCTION

A SLEWING MOTION consists of the rotation of a structure, in this case an Euler Bernoulli beam, about a point. In the case considered here, a DC electric motor is used to move a beam about the axis of the motor in order to orient the length of the beam in a new direction (see Figure 1). In the past slewing maneuvers have been carried out on passive structures, i.e., structures which have no internal control or sensing mechanisms. Here, the effects of slewing an active structure are considered. An active or smart structure is defined as a structure with sensors and actuators integrated within the structure (Wada, 1989). A passive structure does not contain any integrated control hardware. The slewing of a passive beam has been considered by several researchers. Garcia (1989) and Garcia and Inman (1990) examine the dynamic interaction between the structure and actuator in slewing a passive beam. Juang et al. (1986), Yurkovich and Tzes (1990), Cannon and Schmitz (1984) and Hastings and Book (1987) have all considered the effects of slewing passive beams. Park et al. (1989) considered slewing a passive beam with a secondary voice coil actuator attached to improve vibration suppression. Their results motivated the work presented here which considers the effects of slewing an active beam. This presents a multiple input

1045-389X/90/03 0261–12 $4.50/0

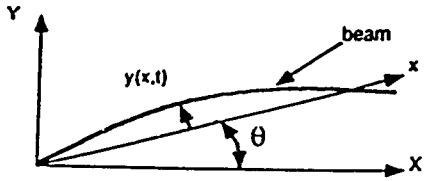

Figure 1. Slewing flexible beam schematic illustrating the coordinate system used in the analysis.

control problem. The active beam consists of a flexible aluminum beam with embedded piezoelectric actuators and sensors.

The analysis proceeds by forming a Hamiltonian consisting of the elastic and kinetic energy in the Euler-Bernoulli beam, plus the nonconservative work done on the beam by the DC motor and piezoceramic actuator. Garcia (1989) illustrated that the dynamic interaction between the slewing actuator (a DC motor) and the flexible structure can lead to improved vibration suppression. Traditionally, the slewing control of a flexible single link structure has been a single actuator problem. Park et al. (1989) proposed the use of a "voice-coil" actuator in addition to the slewing motor; this actuator was rigidly attached to the slewing hub and actuated the beam near the clamped end. This approach achieved improved structural dynamic performance and reduced peak motor voltages. However, these performance gains were at the cost of adding the mass of the coil actuator and its supporting mechanical fixture to the slewing payload.

We propose that direct structural actuation be achieved in the slewing maneuver by use of a piezoceramic actuator. This active beam will contain a layered piece-wise distributed, or segmented, piezoceramic crystal. The active beam being considered here is similar to those considered earlier in a damped configuration by Fanson and Caughey (1987) and Burke and Hubbard (1987). Fanson and Caughey considered a cantilevered flexible beam controlled by a collocated pair of piezoelectric actuators and strain sensors coupled with a positive position feedback control law. In the case modeled here piezoceramics are used for actuators and sensing is simulated by full state feedback.

A theoretical optimal control study is performed using a linear quadratic regulator (LQR) control formulation on a system with parameters obtained from experiments. A comparison of control laws is made where the penalty function is varied to change the degree of control effort afforded by the active beam. The goal here is to illustrate through simulation that increased vibration suppression may occur in slewing maneuvers by taking advantage of control structure interaction and to investigate the vibration suppression effects of slewing an active structure.

SYSTEM DYNAMICS

The dynamics of the slewing beam system are developed from Hamilton's principle. First, the dynamics of a slewing piezo-actuated structure are considered

with the effects of a piece-wise distributed piezo actuator. The actuator dynamics, that is, the interaction of motor and beam, are also modeled. The moment generated by the piece-wise distributed, piezo actuator is calculated. Finally, the equations of motion for this active slewing structure are assembled in a lumped mass model representation.

Figure 1 illustrates the coordinates used in defining the equations of motion of a flexible structure undergoing a slewing motion through an angle $\theta(t)$. The deflection of the beam $y(x,t)$ is defined relative to the rigid motions θ. The torque causing the motion is denoted by τ and acts at the beam's hinged end. The beam, of length L, deforms and rotates in the X-Y plane. Only small displacements relative to x are considered.

STRUCTURAL EQUATIONS

Using the coordinates of Figure 1, the Lagrangian, denoted by L_s, of a slewing flexible beam of length L can be stated as.

$$L_s = \frac{1}{2}\int_0^L \varrho(x\dot{\theta} + \dot{y})^2 dx - \frac{1}{2}\int_0^L EI\left(\frac{\partial^2 y}{\partial x^2}\right)^2 dx \tag{1}$$

Here ϱ, E and I are the usual beam parameters (mass per unit length, elastic modulus and moment of inertia, respectively), and then standard derivative notation is used ($\cdot$ for temporal derivatives, $\partial/\partial x$ for partial spatial derivatives, and $d(\cdot)$ for the total derivative).

Thus the first term represents the structure's kinetic energy and the second represents the structure's total potential, or elastic strain energy, for the system. Hamilton's principle for dynamic systems states that the first variation must vanish, or

$$\delta^{(1)}\int_{t_1}^{t_2}[L_s + W_{nc}]dt = 0 \tag{2}$$

where $\delta^{(1)}$ denotes the first variation of the integral and the term W_{nc} represents the nonconservative work done by the actuators on the slewing beam system. The nonconservative work is modeled here as,

$$W_{nc} = \tau\left(\theta + \frac{\partial y(0,t)}{\partial x}\right) + \int_0^L M(x,t)\Lambda(x)\frac{\partial^2 y}{\partial x^2}dx \tag{3}$$

where the first term is the work provided by the applied torque (from the DC motor) acting through the total angular deflection which consists of the rigid body rotation, θ, plus the slope due to flexure in the beam. The second term models the nonconservative work provided by the piezoceramic actuator which results

from a piece-wise distributed moment, $M(x,t)$ acting between points L_1 and L_2. The function, $\Lambda(x)$, is a distribution function which defines the location of the segmented piezo actuator as suggested by Fanson and Caughey (1987) and is defined by the step function $h(x - x_0)$ as,

$$\Lambda(x) = h(x - L_1) - h(x - L_2) \tag{4}$$

where, $L_1 < L_2$. The length of the piezoceramic is $L_2 - L_1$. The form of this moment is introduced .n a later section.

We now substitute a set of assumed modes for the dynamics of the flexible structure, that is,

$$y(x,t) = \sum_{i=1}^{n} \phi_i(x) q_i(t) \tag{5}$$

where, $\phi_i(x)$ is the ith eigenfunction for the beam and $q_i(t)$ is its corresponding modal amplitude, into Equations (1) and (3) along with Equation (4). Following the assumed mode method (see Meirovitch, 1980), the expanded Equations (1) and (3) are then substituted into Equation (2) applying the Euler-Lagrange equation for the system to determine the equations of motion.

From the Euler-Lagrange equation the following expression describes the motion for the rigid body coordinate,

$$I_b \ddot{\theta} + \sum_{i=1}^{n} \left[\int_o^L \varrho x \phi_i dx \right] \ddot{q}_i = \tau \tag{6}$$

where I_b is rigid body inertia of the beam with respect to the slewing axis. Likewise the equation for the ith flexible mode of the tructure, q_i, follows as

$$\left[\int_0^L \varrho x \phi_i dx \right] \theta + \left[\sum_{j=1}^{n} \int_0^L \varrho \phi_i \phi_j dx \right] \ddot{q}_i + \left[\sum_{ij=1}^{n} \int_0^L EI \phi_i'' \phi_j'' dx \right] q_i$$

$$= \phi_i'(0)\tau + \int_0^L \frac{\partial^2}{\partial x^2} (M(x,t)\Lambda(x))\phi_i(x) dx \tag{7}$$

Here $\phi_i'(0)$ denotes the slope of the ith eigenfunction evaluated at the point of attachment to the motor system. The distributed moment term on the right hand side of Equation (7) can be rewritten as,

$$\int_0^L \frac{\partial^2}{\partial x^2} (M(x,t)\Lambda(x))\phi_i(x) dx = \mu V_p(t)[\phi_i'(L_1) - \phi_i'(L_2)] \tag{8}$$

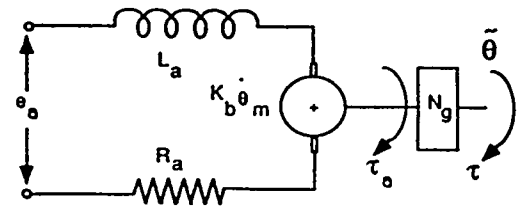

Figure 2. *Motor armature circuit and gear box schematic.*

where, $M(x,t) = \mu V_p(t)$. The constant, μ, is due to the geometry and properties of the piezoceramic and will be examined in the next section. The quantity $V_p(t)$ is the voltage applied across the piezo actuator. Note that the second derivative of a step function yields a point moment delta operator (see Garcia, 1989).

MOTOR AND PIEZO ACTUATOR FORCES

The torque applied to the beam at the slewing axis is considered here to be generated by an armature controlled DC electric motor, whose behavior is represented by the schematic in Figure 2.

Here, e_a is the voltage applied across the armature, L_a is the motor inductance, R_a is the armature resistance and K_b is the motor back-emf. Applying Kirchoff's law for the potential drop across the circuit, we obtain,

$$e_a = i_a R_a + L_a \frac{di_a}{dt} + K_b \dot{\theta}_m \tag{9}$$

The sum of the torques about the motor armature yields,

$$I_m \ddot{\theta}_m + c_v \dot{\theta}_m + \tau_a = K_t i_a \tag{10}$$

where τ_a is the torque applied to the gearbox, θ_m is the angular position of the motor, I_m is the motor inertia, K_t is the motor constant, i_a is the current and the constant c_v models the motor friction. The motion of the motor and the torque applied to the gearbox relate to the beam motion and the torque applied to the beam by

$$\tau = N_g \tau_a \tag{11}$$

and

$$\theta_m = N_g \tilde{\theta} \tag{12}$$

where N_g denotes the gear ratio and the total angular displacement is $\tilde{\theta}$. Equations (9) and (10) are now combined by substituting with the relationships in Equations

(11) and (12). The expression for the applied torque is found in terms of the voltage applied to the armature circuit, and is,

$$\tau = \frac{N_g K_t}{R_a} e_a - I_m N_g^2 \ddot{\theta} - \left(c_v + \frac{K_b K_t}{R_a} \right) N_g^2 \dot{\theta} \tag{13}$$

Here, the motor inductance is assumed negligible since the electric time constant is much smaller than the mechanical time constant of the system.

The effects of the segmented piezo actuator can be approximated by the following analysis. Fanson and Caughey (1987) and Burke and Hubbard (1987) have shown that the force generated by layered piezoceramic material is a distributed moment. Referring to Figure 3, intergrating the stress of the piezoceramic about the mid-plane of the beam for a unit cross section we obtain.

$$M(x,t) = b_a \int_0^L \sigma_{yy} z dz = b_a E_a d_{31} (t_a + t_b) V_p(t) \tag{14}$$

where, b_a is the width of the segmented actuator, E_a is the elastic modulus of the piezo material, d_{31} is the charge coefficient of the piezo material, t_a is the actuator thickness, t_b is the beam thickness, and $V_p(t)$ is the control voltage applied across the piezoelectric crystal. Since the segmented structure has constant properties over its distributed domain, the distributed movement can be written as $M(x,t) = \mu V_p(t)$, where the constant μ, of Equation (8) becomes

$$\mu = b_a E_a d_{31} (t_a + t_b) \tag{15}$$

This formulation was used successfully by Fanson and Caughey (1987) for controlling the vibration of a cantilevered beam, and is adapted to the slewing beam here.

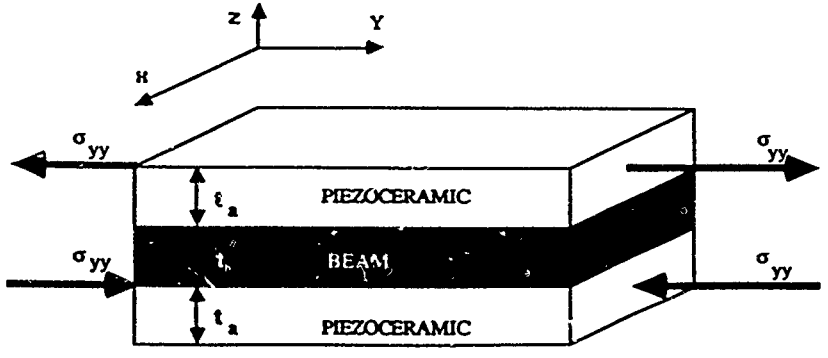

Figure 3. An infinitesimal element of the piezoceramic actuator sandwiched on the beam illustrating the stress relation for an applied voltage.

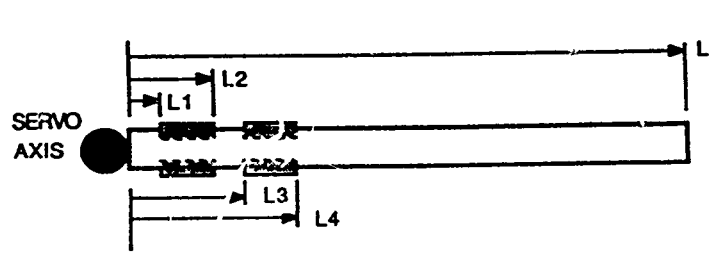

Figure 4. Schematic of the slewing beam showing the location of embedded piezoceramic actuators.

PIEZOELECTRIC PRINCIPLES

Additional vibration attenuation is provided during slewing by a piezoelectric actuator system described here. This consists of embedded piezoceramic providing force actuators. Piezoelectrics produce an electrical potential when deformed. Conversely, an applied charge produces a dimension alteration. Variation in the charge densities due to volume changes of the material results in an electric potential formation. This property is the result of lattice asymmetry as discussed by Randall and O'Neil (1981). Expansion of the material occurs when an electric potential is placed across the material surface which has the same polarity as the substructure. A more complete discussion of piezoceramic actuators can be found in Crawley and Anderson (1990).

Piezoceramics can be efficiently used to actuate a thin beam as illustrated by Fanson and Caughey (1987). The strain produced by attaching piezoceramics in a tension/compression laminate is depicted in Figure 3. The effect of this actuator results in a moment described by Equation (8) and used in Equations (3) and (7). For the system under consideration the moment equation becomes

$$M(x,t) = 4.345 \times 10^{-5} V_p \text{Nm/volt} \tag{16}$$

This value comes from Equations (8) and (14) with values taken from an inch square lead zirconate piezoceramic (Piezo Electric Products, Inc. Model No. G-1195). With two actuator segments as indicated in Figure 4 the moment expression for these segments becomes

$$\int_0^L M(x,t) \Lambda(x) dx = \mu [\phi_i'(L_1) - \phi_i'(L_2) + \phi_i'(L_3) - \phi_i'(L_4)] \tag{17}$$

Here the same voltage applies to each actuator pair. It should be noted that this equation does not include error produced by imperfections in the bonding of the piezoceramics to the beam as discussed in the paper by Crawley and Anderson (1990), but is consistent with the experimental results reported by Fanson and Caughey (1987).

CONTROL DESIGN

A linear quadratic regulator control law was designed to illuminate the effects of slewing an active structure versus slewing a passive structure. The results are based on a beam/motor system designed to take maximum advantage of the interaction between the structural modes and the motor torque. Both the voltages to the electric motor and to the embedded piezoceramic were used as control inputs.

To perform the control analysis, the mathematical model described in the previous sections needs to be manipulated into state space form. Combining the above equations and assuming that only n terms are used in the modal approximation of Equation (5), the equations of motion of the slewing active structure can be written in matrix form. This is accomplished by substituting the piezoceramic moment Equations (17) and (18) into Equation (7) and writing the summations as matrices. Next, Equation (13) is substituted into Equation (6) and combined with the above to yield the vector differential equation.

$$M\ddot{q} + D\dot{q} + Kq = B_f u \tag{18}$$

where the vector q is defined by $q^T = [\theta(t)\, q_1(t)\, q_2(t) \ldots q_n(t)]$. The mass, damping and stiffness coefficient matrices are:

$$M = \begin{bmatrix} I_h + I_s & I_1 + I_s\Gamma_1(0) & \cdots & I_n + I_s\Gamma_n(0) \\ I_1 + I_s\Gamma_1(0) & M_1 & & \vdots \\ \vdots & & & \vdots \\ I_n + I_s\Gamma_n(0) & \cdots & & M_n \end{bmatrix} \tag{19}$$

$$D = \begin{bmatrix} b_v & b_v\Gamma_1(0) & \cdots & b_v\Gamma_n(0) \\ b_v\Gamma_1(0) & b_v\Gamma_1(0)^2 & \cdots & b_v\Gamma_1(0)\Gamma_n(0) \\ \vdots & & & \vdots \\ b_v\Gamma_n(0) & b_v\Gamma_n(0)\Gamma_1(0) & \cdots & b_v\Gamma_n(0)^2 \end{bmatrix} \tag{20}$$

$$K = \begin{bmatrix} 0 & & 0_{1n} & \\ & M_1\omega_1^2 & & \vdots \\ 0_{n1} & & & \vdots \\ & \cdots & & M_n\omega_n^2 \end{bmatrix} \tag{21}$$

where $\Gamma_i = \phi_i(0)$, the ith modal participation factor. In addition, M_i is the ith modal mass, ω_i denotes the beam natural frequencies and the ith inertia term is given by

$$I_i = \int_0^L \varrho x \phi_i(x) dx$$

which represents the coupling between the flexible mode and the slewing motion.

The constant b_v is the coefficient of $\dot{\theta}$ in Equation (13). The constant I_s is the servo system inertia defined by the coefficient of the angular acceleration term in Equation (13). The control input vector u is the 2×1 vector $u^T = [e_a, V_p]$ and the control coefficint matrix is

$$B_f^T = \begin{bmatrix} \dfrac{N_g K_t}{R_a} & \dfrac{N_g K_t}{R_a}\Gamma_1 & \cdots & \dfrac{N_g K_t}{R_a}\Gamma_n \\ 0 & \mu[\phi_1'(L_1) - \phi_1'(L_2)] & \cdots & \mu[\phi_n'(L_1) - \phi_n'(L_2)] \end{bmatrix} \tag{22}$$

for a single segment piezoceramic actuator.

Active control is performed by using state feedback and solving a standard linear quadratic regulator (LQR) control law design. The system of Equation (18) is first put into state space form by defining the state vector x as

$$x = \begin{bmatrix} q \\ \dot{q} \end{bmatrix} \tag{23}$$

and the corresponding state matrix

$$A = \begin{bmatrix} 0 & I \\ -M^{-1}K & -M^{-1}C \end{bmatrix} \tag{24}$$

where 0 denotes the matrix of zeros and I denotes the identity matrix of appropriate dimension. With this change of coordinates, Equation (18) becomes

$$\dot{x} = Ax + Bu \tag{25}$$

with output measurements defined by

$$y = Cx \tag{26}$$

Here the matrix of constants C specifies the relationship between the coordinates of the vector x and the measurements. State feedback control is implemented by specifying the relation

$$u = -K_f x \tag{27}$$

In the simulation presented here K_f is chosen to reflect full state feedback. In experimental work this matrix would reflect the placement of piezofilm and/or strain gauges. The LQR control algorithm then calculates the value of the gain matrix K_f such the cost functional

$$J = \int_0^\infty (x^T Q x + u^T R u) dt \tag{28}$$

is minimized. The matrices Q and R are symmetric positive definite weighting matrices which are chosen to produce acceptable response. In the case presented here the matrix Q was chosen to be

$$Q = \text{diag}\,[8\ 3\ 1\ 1\ 8\ 3\ 1\ 1] \tag{29}$$

which places emphasis on minimizing the angular displacement (and velocity) and the first modal displacement (and velocity). The control law determined from this weighting attempts to drive the angular position and beam displacement to zero. The weighting matrix R is chosen to have two different values to generate a control law for vibration suppression both with and without the use of the piezoceramic actuator. For the case with the added piezo actuator, the matrix R is chosen to be

$$R_1 = \text{diag}\,[1.0 \quad 1 \times 10^{-4}] \tag{30}$$

This choice penalizes the use of the motor voltage in favor of the piezoelectric actuator voltage. For the case without piezo actuator control, the weighting matrix R is chosen to be

$$R_2 = \text{diag}\,[1.0 \quad 1 \times 10^{6}] \tag{31}$$

A comparison of the results of using the piezoceramic actuator versus using only the motor torque for vibration suppression is illustrated in Figures 5–8. In each case the control or response without the advantage of the piezoceramic is given by the dashed line and those with the use of the active beam are given by the solid line. Figure 5 illustrates that the voltage supplied to the armature of the motor is reduced by 33% (from -3 volts to -2 volts) when slewing is performed on an active beam versus a passive beam. Figure 6 plots the angular position in each case. Figure 7 clearly illustrates that the maximum tip deflection (overshoot) is reduced by almost 50% by using the piezoceramic actuator. Figure 8 illustrates the control voltage applied to the piezoceramic.

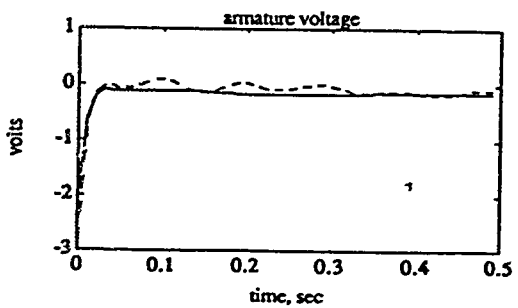

Figure 5. Voltage applied to the armature of the motor for each of the two control laws.

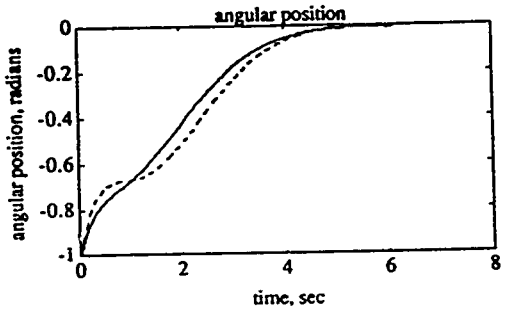

Figure 6. Angular position versus time for each of the two control laws.

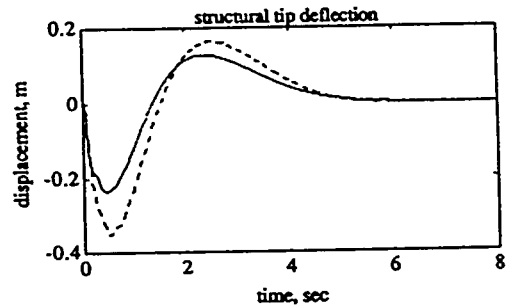

Figure 7. The deflection of the tip of the beam versus time for each of the two control laws.

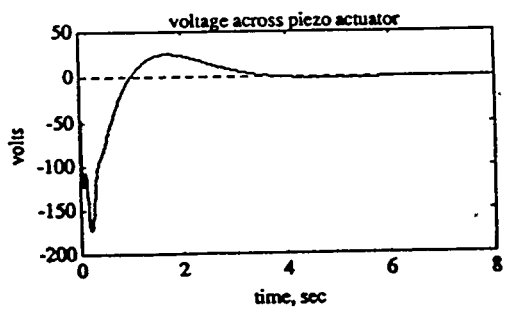

Figure 8. The voltage applied to the piezoceramic versus time for each of the two control laws.

CLOSING REMARKS

This paper examines slewing control by introducing the concept of using an active structure to improve performance. Slewing an active structure, as opposed to slewing a passive structure, offers the advantage of reducing the peak voltage demands on the slewing motor hence increasing reliability and potentially saving weight (a smaller motor could be used). In addition, the active structure approach promises to substantially reduce maximum tip deflection of the structure.

ACKNOWLEDGEMENT

The authors gratefully acknowledge the support of the Air Force Office of Scientific Research (contract number F49620-88-C0018).

REFERENCES

1. Burke, S. B. and J. E. Hubbard. 1987. "Active Vibration Control of a Simply Supported Beam Using a Spatially Distributed Actuator," *IEEE Control Systems Magazine*, Vol. 7, No. 4.
2. Cannon, H. C., Jr. and E. Schmitz. 1984. "Initial Experiments on the End-Point Control of a Flexible One-Link Robot," *International Journal of Robotics Research*, 3(3):62–75.
3. Crawley, E. F. and E. H. Anderson. 1990. "Detailed Models of Piezoceramic Actuation of Beams," *Journal of Intelligent Material Systems and Structures*, 1:4–25. Also AIAA paper number 89-1388 CP in the *Proceedings of 1989 AIAA Structure Dynamic and Material Conference*, pp. 2000–2010.
4. Fanson, J. L. and T. K. Caughey. 1987. "Positive Position Feedback Control for Large Space Structures," AIAA Paper No. 87-0902.
5. Garcia, E. 1989. "On the Modeling and Control of Slewing Flexible Structures," Ph.D. Thesis, Department of Mechanical and Aerospace Engineering, State University of New York at Buffalo.
6. Garcia, E. and D. J. Inman. 1990. "Modeling Actuator–Structure Interaction in the Slewing of Flexible Structures," *Proceedings of the American Controls Conference*, San Diego, California, May 23–25, pp. 1962–1967.
7. Hastings, G. G. and W. J. Book. 1987. "A Linear Dynamic Model for Flexible Robotic Manipulators," *IEEE Control Systems Magazine*, pp. 61–64.
8. Juang, J. N., L. G. Horta and H. Robertshaw. 1986. "A Slewing Control Experiment for Flexible Structures," *AIAA Journal of Guidance, Control and Dynamics*, 9(5):599–607.
9. Meirovitch, L. 1980. *Computational Methods in Structural Dynamics*, The Netherlands: Sijthoff and Noordhoff.
10. Park, Y.-P., S.-H. Kim, Y.-K. Ha and H.-S. Park. 1989. "Analysis and Test on the Digital Optimal Control of a Flexible Rotor Arm Vibration," *Proceeding of the 7th International Modal Analysis Conference*, pp. 1489–1495.
11. Randáll, D. S. and C. G. O'Neill. 1981. "Axial-Mode Piezoelectrically-Driven Beam Deflectors," *SPIE Vol. 299 Advances in Laser Scanning Technology*.
12. Wada, B. K., 1989. *Adaptive Structures*, Book No. AD-Vol. 5, ASME, New York, N.Y.
13. Yurkovich, S. and A. Tzes. 1990. "Experiments in Identification and Control of Flexible-Link Manipulators," *IEEE Control Systems Magazine*, Vol. 10, No. 2.

On the Nature of the Interaction Between Structures and Proof-Mass Actuators

David C. Zimmerman*
University of Florida, Gainesville, Florida
[illegible]†
Brown [illegible] Providence, Rhode Island

This paper presents an analysis of the interaction between a structure, an actuator used to control the vibration of the structure, and the control law to be implemented. The actuator used is a proof-mass actuator with experimentally verified dynamics capable of being used in a space structure configuration. A local rate-feedback control law is used. The control of two different structures is presented. The first structure is a cantilevered beam constructed of a quasi-isotropic composite material that is controlled by a single actuator forming the experimental component of the investigation. The second structure is a finite-element model of a truss system controlled by a single actuator. Models of both structures predict the presence of potential instabilities in system performance if proper consideration is not given to interactions between the control law, the structure, and the actuator.

I. Introduction

THE control of large flexible space structures by a small number of control devices acting at a few points along the structure has sparked intensive research over the last ten years.[1-3] A majority of the work in this area has neglected the effects of actuator dynamics in modeling the closed-loop system. Recently, concern has developed over the effects of actuator dynamics in the design of control laws for flexible structures.[4-6] The emphasis of this paper is to examine the effects that both actuator dynamics and control forces have on the performance of the actuator/structure system. Both experimental and numerical results are presented.

The control device used in this work is a proof-mass actuator (PMA) developed for the Structural Dynamics Branch of the NASA Langley Research Center by researchers at the University of Virginia[7,8] and the State University of New York at Buffalo.[9,10] This actuator has been extensively tested[10] and is capable of generating arbitrary control forces. The onboard microcontroller is capable of implementing dedicated control laws or can serve as a local controller in a hierarchical control architecture. The actuator characteristics are described in Sec. II.

The first structure used in this study is a simple cantilevered beam constructed of a quasi-isotropic composite material being considered for use in flexible space structure construction.[11] The material has unusual damping properties[12] but is strong and lightweight. A simple experiment using the PMA and the composite beam provide a preliminary look at control/structure interaction phenomena. The actuator composite beam system and corresponding experiment and analysis is discussed in detail in Sec. III.

The numerical study consists of using a reduced [illegible] finite-element model of the proposed Control of Flexible Structures (COFS) I flight article.[4] The control devices mounted on the COFS I flight article are fundamentally the same as the PMA described in Sec. II. The configuration used in the study is the COFS I flight article controlled in one plane of vibration using a rate-feedback control law. This model is described in Sec. IV and analyzed for different actuator configurations in Sec. V.

II. Actuator Dynamics

The actuation device chosen for this study is the NASA/UVA/UB proof-mass actuator.[9] The actuator system is composed of a movable proof-mass, a fixed coil, two colocated sensors, a digital microcontroller, and a power amplifier as described in detail in Refs. 9 and 10. All of the actuator components are mounted as a single unit with power lines being the only external connection required by the actuator system to operate. The PMA is a reaction-type force actuator in that it creates a force by reacting against an inertial mass. Figure 1 shows an experimentally verified model of the PMA attached to a single-degree-of-freedom structural model. The dynamics of the PMA can be modeled as a single-degree-of-freedom oscillator with the addition of a force generator acting between the proof-mass and the structure. The equations of motion for this model are given as

$$\begin{bmatrix} M_s & 0 \\ 0 & m_p \end{bmatrix}\begin{bmatrix} \ddot{x}_1 \\ \ddot{x}_2 \end{bmatrix}+\begin{bmatrix} c_s+c_p & -c_p \\ -c_p & c_p \end{bmatrix}\begin{bmatrix} \dot{x}_1 \\ \dot{x}_2 \end{bmatrix} +\begin{bmatrix} K_s+k_p & -k_p \\ -k_p & k_p \end{bmatrix}\begin{bmatrix} x_1 \\ x_2 \end{bmatrix}=\begin{bmatrix} -f_g \\ f_g \end{bmatrix} \tag{1}$$

Here M_s is the equivalent lumped mass of the structure and the parasitic mass of the actuator (PMA system mass minus the proof mass). The structure is also assumed to have viscous damping coefficient C_s and stiffness K_s. The mass of the proof mass is denoted by m_p. The inherent electronic damping of the PMA system due to the back-emf in the fixed coil is denoted [illegible]. The electronic stiffness force required to keep the proof [illegible] in its housing is denoted by k_p. This centering force is [illegible] in laboratory experiments to overcome the component of gravity that would cause the proof mass to slide to one end and impact the outer case. Additionally, it will be

Received March 16, 1988; revision received Sept [illegible]

*Assistant Professor, Department of [illegible] Mechanics, and Engineering Science. Member AIAA.
†Professor, Division of Applied Mechanics. Member AIAA. Mechanical and Aerospace Engineering, State University of New York, Buffalo, New York. Member AIAA.

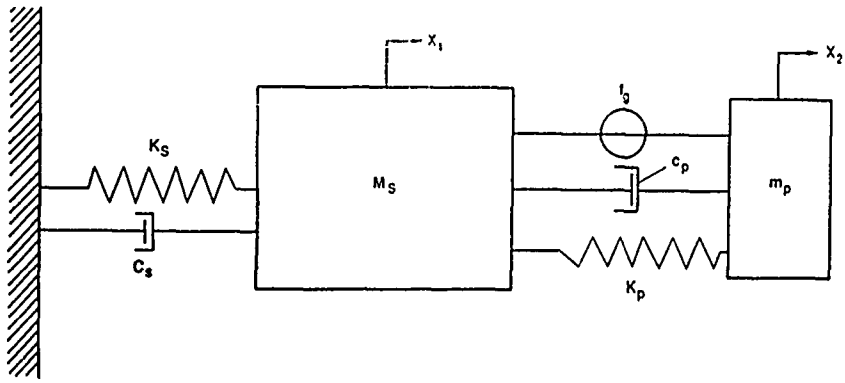

Fig. 1 Dynamic model of proof-mass actuator.

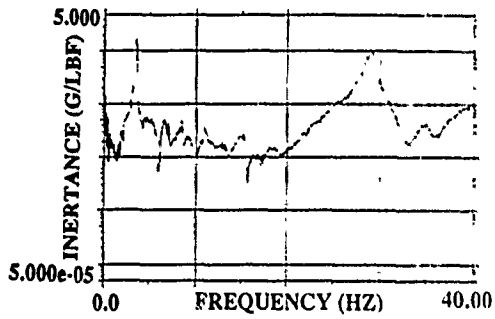

Fig. 2 Open-loop inertance frequency response function.

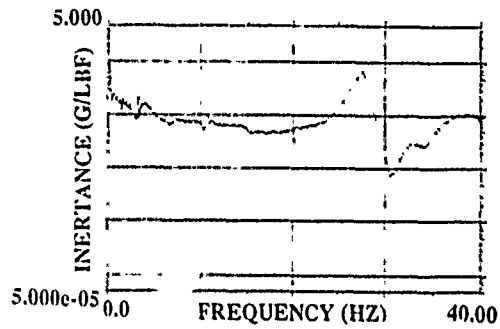

Fig. 3 Closed-loop inertance frequency response function.

shown in Sec. III that the centering force is required for the closed-loop system to be asymptotically stable. The coordinate x_1 denotes the displacement of the structure, while x_2 denotes the displacement of the proof mass. The overdots represent time derivatives. The addition of the desired control law is modeled as f_g, a force generator that applies equal but opposite forces onto the structure and the proof mass.

To determine the inherent dynamic properties of the PMA system, the actuator was attached to a nonmoving structure (M_s locked in Fig. 1). The frequency response function of the total force applied to the structure (the reactions of the spring, damper, and force generator) to the voltage command to the force generator was measured experimentally. Let $F(s)$ and $V(s)$ denote the Laplace transform of the total applied force and the voltage command to the force generator, respectively. The experimentally[9] verified transfer function for the PMA system is

$$\frac{F(s)}{V(s)} = \frac{G_1 G_2 m_p s^2}{m_p s^2 + G_1 G_2 c_p s + G_1 G_2 k_p} = G_1 G_2 \frac{s^2}{s^2 + 2\zeta_p \omega_p + \omega_p^2}$$

$$\omega_p^2 = \frac{G_1 G_2 k_p}{m_p}, \qquad 2\zeta_p \omega_p = \frac{G_1 G_2 c_p}{m_p} \tag{2}$$

Here, $G_1(N/A)$ is the electromagnetic gain of the PMA's coil, and $G_2(A/V)$ is the power amplifier gain. The inherent dynamics of the PMA are seen to be that of a high-pass filter whose characteristics are shaped by the spring and damper rates. The simplest way to characterize the dynamics of the actuator is by its break frequency ω_p, which indicates the frequency at which the Bode magnitude plot of the PMA breaks flat from a 40 dB/decade rise, and the phase plot goes through 90 deg. The break frequency corresponds roughly to the natural frequency of the actuator.

The transfer function relating the total applied force $F(s)$ and the output of the force generator $f_g(s)$ can be obtained from Eqs. (2) by considering a free-body diagram of mass m_p in Fig. 1 (again with M_s locked) and is given by

$$\frac{f_g(s)}{F(s)} = 1 - \frac{2\zeta_p \omega_p s + \omega_p^2}{s^2} \tag{3}$$

Equation (3) reveals that as $s \to \infty$, the total force applied to the structure is equal to the output of the force generator. Physically, this corresponds to the fact that both the displacement and velocity of the proof mass tend to zero as the frequency content of the force generator command signal tends to infinity.

III. Composite Beam System

An experimental test of the PMA's ability to control vibration using a rate-feedback control law was performed using a test structure made of a quasi-isotropic composite material[11] configured as a cantilevered beam. The PMA system was attached at the tip (free end). In addition to the two sensors contained within the PMA system, an independent accelerometer was mounted at the tip to monitor the vibrations of the beam. The rate-feedback control law was implemented by digitally integrating the accelerometer signal contained within the PMA system and multiplying by an appropriate gain. In this experiment, the electronic centering force gain k_p was selected such that the break frequency of the actuator was slightly lower than the fundamental mode of vibration of the cantilevered beam. A detailed description of the experimental setup, control law implementation, and experimental methods is provided in Ref. 10.

The modal properties of the uncontrolled and controlled structure were determined using both time and frequency domain identification techniques. The uncontrolled, or open-loop, system consists of the cantilevered beam with the parasitic mass of the actuator. The measured inertance (acceleration/force) frequency response function is shown in Fig. 2. Using the circle-fit identification technique,[13] the natural frequencies were determined to be 3.49 and 29 Hz, with

damping ratios of 0.2 and 1.0%, respectively. These values were also confirmed by using the eigensystem realization algorithm[14] (ERA) time domain modal identification technique.

The closed-loop system consists of the open-loop system with the proof mass added and the control law turned on. Although difficult to see from the measured inertance frequency response function of the closed-loop system in Fig. 3, an additional natural frequency appears. These three frequencies and corresponding damping ratios were again identified using the circle-fit method and verified using ERA. The closed-loop system exhibits natural frequencies at 3.19, 4.03, and 28 Hz, with damping ratios of 0.2, 9.4, and 1.9%. The appearance of a third mode of vibration is due to the PMA dynamics, and is referred to as the actuator-dominated mode. The actuator-dominated mode is the sharp narrow peak at 3.19 Hz in Fig. 3. The first structural mode is shifted up to 4.03 Hz, in accordance with the first monotonicity principle,[15] and is heavily damped by the control law.

The effect of the control system on the structure's response is best examined in the time domain. Figure 4 illustrates the open-loop time response of the accelerometer located at the tip of the beam. Examination of the response indicates that the open-loop system is very lightly damped, illustrating substantial oscillation even after 16 s have elapsed. The closed-loop system response illustrated in Fig. 5, subject to an equivalent impact, shows a substantial increase in damping, essentially reducing the structural vibration to small levels in less than 2 s. However, Fig. 5 also illustrates that a very small amplitude and lightly damped oscillation occurs at 3.19 Hz, which is the actuator-dominated mode. This oscillation represents a degradation of the closed-loop system performance because of the interaction between the structure, the control law, and the actuator dynamics.

To gain a further understanding of the structure/actuator dynamics in conjunction with the rate-feedback control law, consider a two-mode model of the controlled structure consisting of the actuator-dominated mode (3.19 Hz) and the first structural dominated mode (4.03 Hz). The second structural dominated mode (28 Hz) is not included in this model because its contribution to the total time response of Figs. 4 and 5 is minimal. The equations of motion are then given by Eq. (1), with f_g being the rate-feedback control law, $f_g = -d\dot{x}_1$. Substitution of the control law into Eq. (1) and moving the control term to the left side of the equation yields a closed-loop damping matrix of

$$\begin{bmatrix} C_s + c_p - d & -c_p \\ -c_p + d & c_p \end{bmatrix} \tag{4}$$

The homogeneous equation for the closed-loop system is no longer symmetric and positive semidefinite, indicating the possibility of an unstable response.[16] The Routh stability criteria can be utilized to determine the stable and unstable regions in the parameter space. The characteristic equation for the system is given as

$$\lambda^4 + (C_s/M_s + c_p/M_s + c_p/m_p - d/M_s)\lambda^3 + (K_s/M_s + k_p/M_s + k_p/m_p + C_s c_p/(M_s m_p))\lambda^2 + (K_s c_p/(M_s m_p) + C_s k_p/(M_s m_p))\lambda + K_s k_p/(M_s m_p) = 0 \tag{5}$$

With the aid of MACSYMA,[17] the inequality relations for the rate-feedback gain d in terms of the actuator and structural properties for a stable closed-loop system are given as

$$d < C_s + c_p + M_s c_p/m_p \tag{6a}$$

$$d < [m_p^2(K_s(C_s + c_p) + k_p(C_s + c_p) + m_p(2M_s c_p k_p + C_s c_p^2 - C_s^2 c_p) + M_s(C_s c_p^2 + M_s c_p k_p)]/[m_p^2(K_s + k_p) + m_p(M_s k_p - C_s c_p)] \tag{6b}$$

$$d \le -C_s^2 c_p[1/(2K_s m_p) + 1/(2k_p m_p)] + (1/2)(C_s + c_p - K_s c_p/k_p + M_s c_p/m_p - M_s C_s k_p/K_s m_p - C_s k_p/K_s \pm \{4[(K_s(C_s m_p c_p k_p)^2 + C_s K_s^2 m_p^2 c_p^3 k_p)(M_s + m_p) + M_s C_s K_s m_p^2 c_p k_p^3(M_s + 2m_p) + K_s^3 m_p^4 c_p k_p(C_s + c_p) + C_s K_s m_p^3 c_p k_p(m_p + C_s K_s c_p) + C_s K_s m_p^3 k_p(C_s^2 k_p + C_s m_p k_p - 2M_s K_s c_p k_p)] + [(K_s m_p c_p k_p - C_s m_p k_p^2)(M_s + m_p) + C_s K_s m_p(m_p k_p - c_p^2) - c_p m_p(C_s^2 k_p + K_s^2 m_p)]^2\}^{(1/2)}/(2K_s m_p^2 k_p) \tag{6c}$$

Additionally, inspection of the last term of the characteristic equation reveals that the electronic centering force k_p is a requirement for the closed-loop system to be asymptotically stable. If no centering force is provided, the last term in Eq. (5) is zero and, thus, the system would exhibit an uncontrollable rigid-body mode. This can also be seen by examining the stiffness matrix of Eq. (1) for the case of $k_p = 0$. The existence of this rigid-body mode is independent of the choice of control law implemented by the actuator.

The physical parameters of the two-mode model described by Eq. (1) were determined by independent tests of the actuator[10] and the beam.[12,18] The constants associated with the beam dynamics M_s, C_s, and K_s were determined to be 1.1537 kg, 0.2 N-s/m, and 554.75 N/m, respectively. In determining these constants, it was assumed that the structure behaved as an ideal cantilevered beam. The constants associated with the actuator dynamics m_p and c_p (converted to mechanical units) were determined to be 0.232 kg and 0.76 N-s/m, respectively. In the control experiment, the value of k_p converted to mechanical units was 108.27 N/m. Substituting these values into Eq. (6), it is found that Eq. (6c) is the active

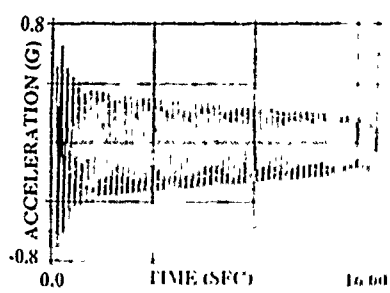

Fig. 4 Open-loop free decay tip acceleration

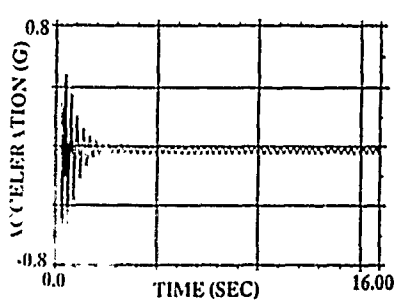

Fig. 5 Closed-loop free decay tip acceleration.

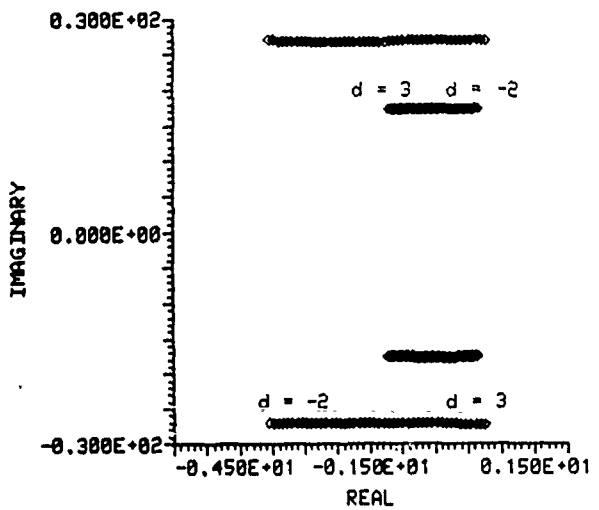

Fig. 6 System root locus.

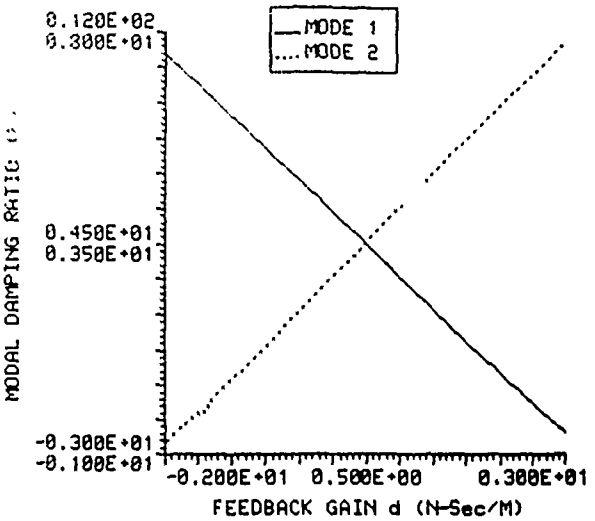

Fig. 7 Modal damping ratio vs feedback gain d.

constraint, and the rate-feedback d for a stable control system must satisfy the inequality

$$-1.55 \le d \le 2.145 \qquad \text{N-s/m} \tag{7}$$

In the active control experiment, the gain d implemented by the 8751 control program was $d = -1.2$ N-s/m, whereas the gain required to match the model damping ratios experimentally identified and those predicted by Eq. (1) is $d = -1.4$ N-s/m. This difference can be accounted for by the relative error in the identified structural parameters. In either case, the rate-feedback gain used in the experiment is relatively close to the unstable region.

The effect of the rate-feedback gain on the closed-loop poles can be demonstrated by plotting the root locus of the system transfer function. With x_1 defined to be the output and f_g the input, the root locus as a function of the rate-feedback gain d (expressed in mechanical units) is shown in Fig. 6. The root-locus plot provides information beyond that provided by Eqs. (6) for a given set of physical parameters. Specifically, Fig. 6 reveals that it is the first mode of vibration that goes unstable when the gain d is less than -1.55, and that the second mode of vibration goes unstable when the gain d exceeds 2.145. However, inspection of the root-locus plot does not directly reveal the relationship between the gain d and the modal damping ratios of the controlled structure.

A plot of the modal damping ratios vs the gain d is shown in Fig. 7. Like the root-locus plot, Fig. 7 reveals which mode goes unstable when the gain violates the Routh stability criteria. It also reveals more clearly and quantifiably that changing the gain to increase the damping in one of the modes results in a decrease in damping of the other mode. This high (in magnitude) gain instability provides an explanation of the low frequency, low amplitude, lightly damped response found in the previously described experiment, as evidenced in Fig. 5. As the magnitude of the rate-feedback gain is increased, the damping ratio of the structure-dominated mode is increased. At the same time, the damping ratio of the actuator-dominated mode decreases. Apparently the system is adding damping to one mode at the expense of the electronic damping in the actuator mode. Eventually, the gain is increased to the point where the actuator-dominated mode damping becomes negative, driving the closed-loop system unstable. The time response shown in Fig. 5 was for the closed-loop system operating at a value of gain just below that at which the system goes unstable. A classical control design would see this as a system with poor gain margin. In this region, the damping ratio is very small causing the first-mode vibration to persist for a long period of time.

IV. Structural Model

In order to investigate more thoroughly the high gain instability suggested by the simple beam experiment and analysis described in Sec. III in a large space structure application, a simplified numerical model of the COFS I truss flight article was constructed. This three-mode model consists of a two-mode approximation of the COFS I structure with an additional degree of freedom for the linear DC motor (LDCM)[4] control actuator. The three-mode model allows for an investigation into the effect of placing the break frequency of the actuator below, in between, and above the modes of vibration of the uncontrolled structure.

The LDCM developed for the COFS flight article has the same dynamic characteristics as the PMA discussed in Sec. II.[4] Therefore, Eq. (2) is also the transfer function for the LDCM control actuators. A continuum beam model[4] of the truss developed for control law design studies was used. The equivalent beam characteristics are given as length 60.693 m, mass per unit length 4.461 kg/m, and flexural rigidity 28.63×10^6 N-m^2. The continuum model was then approximated using a statically reduced two-element finite-element model. Nodes zero, one, and two were located at the base, mid-point, and tip of the beam, respectively, as shown in Fig. 8. This physical modeling approach was used as an alternate approach to the more standard modal model because the interaction of the actuator and structural dynamics become more apparent. A lumped mass (100 kg) was added at the tip of the beam. The open-loop natural frequencies for this approximate model are calculated to be 1.429 and 10.39 rad/s. The equations of motion of the controlled system are given as

$$\begin{bmatrix} 140.8 & 0 & 0 \\ 0 & 170.4 & 0 \\ 0 & 0 & m_p \end{bmatrix} \begin{bmatrix} \ddot{x}_1 \\ \ddot{x}_2 \\ \ddot{x}_3 \end{bmatrix} + \begin{bmatrix} 0 & 0 & 0 \\ 0 & c_p & -c_p \\ 0 & -c_p & c_p \end{bmatrix} \begin{bmatrix} \dot{x}_1 \\ \dot{x}_2 \\ \dot{x}_3 \end{bmatrix}$$

$$+ \begin{bmatrix} 14045 & -4395 & 0 \\ -4395 & 1752 + k_p & -k_p \\ 0 & -k_p & k_p \end{bmatrix} \begin{bmatrix} x_1 \\ x_2 \\ x_3 \end{bmatrix} = \begin{bmatrix} 0 \\ f_g \\ -f_g \end{bmatrix} \tag{8}$$

where x_1 and x_2 are the displacements of the two finite-element model nodes of the truss at the midpoint and tip, and x_3 is the displacement of the proof mass.

V. Actuator Limitation

In this section several cases of actuator design are considered to point out control system design limitations and to investigate the nature of the interaction between the control

law, the actuator dynamics, and the structural dynamics. The criteria used to explain the nature of this interaction is to examine the modal damping ratios of the closed-loop system as a function of the rate-feedback gain d.

First, consider the common case of control system design without considering the actuator dynamics. Figure 9 illustrates that increasing the control gain d substantially increases the damping ratio of mode 1. In addition, the second-mode damping ratio is also increased, but to a much lesser extent, due to placement of the control actuator near the node of the second mode. This naive modeling approach seems to indicate that a reasonable design exists for reducing vibration levels in the first mode. The danger of this modeling approach is illustrated in the following.

Next, consider the addition of the actuator dynamics to the previous case. The break frequency ω_p is chosen to be less than the first structural mode [$\omega_p = 0.5 < 1.43 = \omega_1$ (rad/s)]. In this case the closed-loop equations become

$$\begin{bmatrix} 140.8 & 0 & 0 \\ 0 & 170.4 & 0 \\ 0 & 0 & 22 \end{bmatrix} \begin{bmatrix} \ddot{x}_1 \\ \ddot{x}_2 \\ \ddot{x}_3 \end{bmatrix} + \begin{bmatrix} 0 & 0 & 0 \\ 0 & 1.1+d & -1.1 \\ 0 & -1.1-d & 1.1 \end{bmatrix} \begin{bmatrix} \dot{x}_1 \\ \dot{x}_2 \\ \dot{x}_3 \end{bmatrix}$$

$$+ \begin{bmatrix} 14045 & -4395 & 0 \\ -4395 & 1757.5 & -5.5 \\ 0 & -5.5 & 5.5 \end{bmatrix} \begin{bmatrix} x_1 \\ x_2 \\ x_3 \end{bmatrix} = \begin{bmatrix} 0 \\ 0 \\ 0 \end{bmatrix} \quad (9)$$

where $c_p = 1.1$ (N-s/m) results from assuming that the actuator back-emf damping is 5%. The mass m_p used in Eq. (9) is consistent with the moving mass of the pair of LDCM tip actuators mounted in one plane on the COFS flight hardware. The 5% modal damping ratio of the inherent actuator dynamics is representative of measurements of various PMA's built.

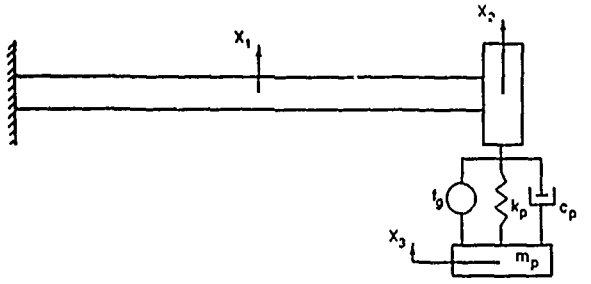

Fig. 8 Equivalent continuum beam and actuator configuration.

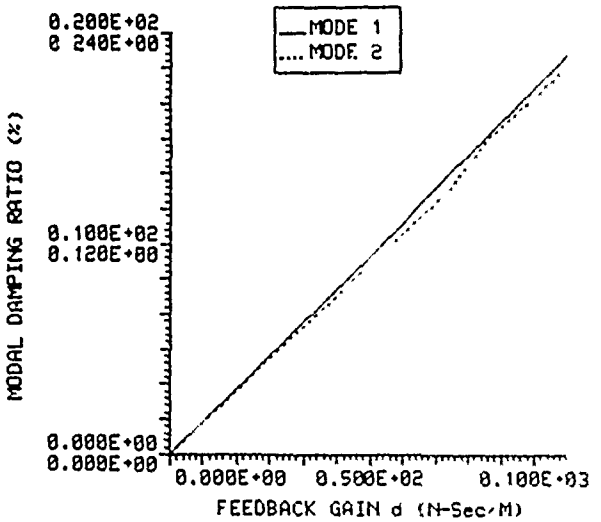

Fig. 9 Damping vs gain—actuator dynamics ignored.

The undamped ($c_p = d = 0$) eigenvalues and eigenvectors are

$$\omega_1 = 0.496 \text{ rad/s}, \quad \underline{u}_1 = [0.0051 \quad 0.163 \quad 1.0]^T$$

$$\omega_2 = 1.44 \text{ rad/s}, \quad \underline{u}_2 = [0.3196 \quad -1.0 \quad -0.1369]^T$$

$$\omega_3 = 10.39 \text{ rad/s}, \quad \underline{u}_3 = [1.0 \quad -0.2640 \quad 0.006]^T \quad (10)$$

The first mode of vibration is termed actuator-dominated because the third coordinate, which corresponds to the actuator displacement, illustrated the largest amplitude, whereas the other two coordinates are relatively small. By this criteria, modes 2 and 3 are structure-dominated, but both have some actuator influence.

The modal damping ratios for this case are plotted vs the gain in Fig. 10. Note that, again, the first structure-dominated mode (mode 2) shows an increase in damping ratio, from almost zero for the open-loop system, to as much as 20% for the high-gain closed-loop case. Again, the other structure-dominated mode increases in damping as well. However, note that the damping ratio of the actuator-dominated mode (mode 1) decreases with increasing gain. In fact, there is some value of the gain at which the modal damping ratio becomes negative, driving the closed-loop system unstable. This again represents a high-gain limitation on the local rate-feedback control law, the actuator, and the structure.

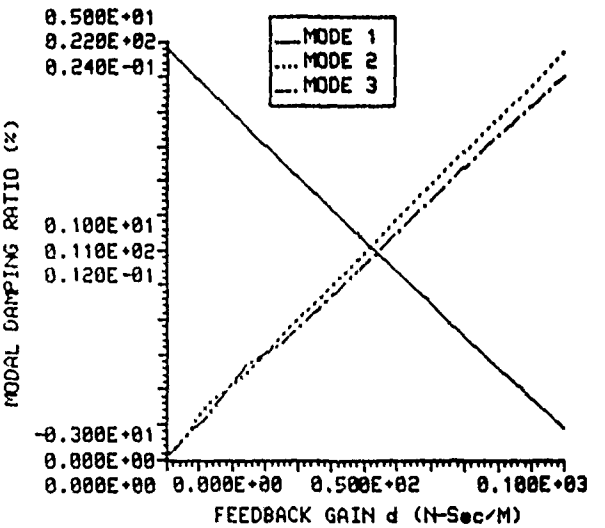

Fig. 10 Damping vs gain, $\omega_p < \omega_1$.

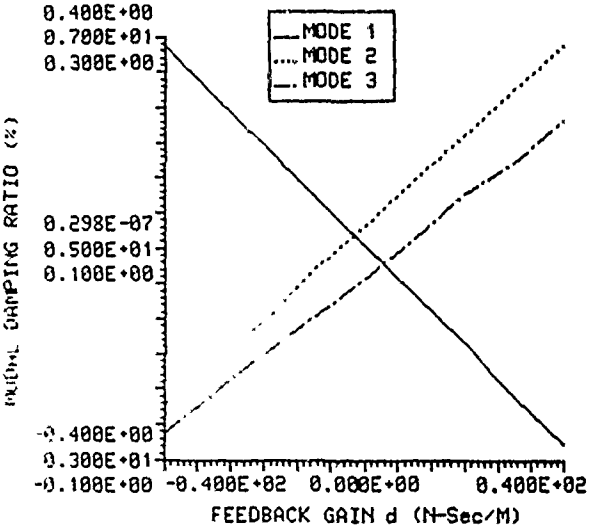

Fig. 11 Damping vs gain, $\omega_1 < \omega_p < \omega_2$.

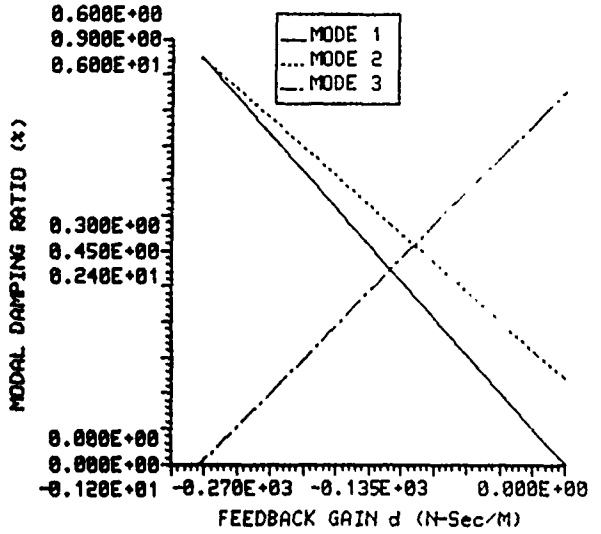

Fig. 12 Damping vs gain, $\omega_p > \omega_2$.

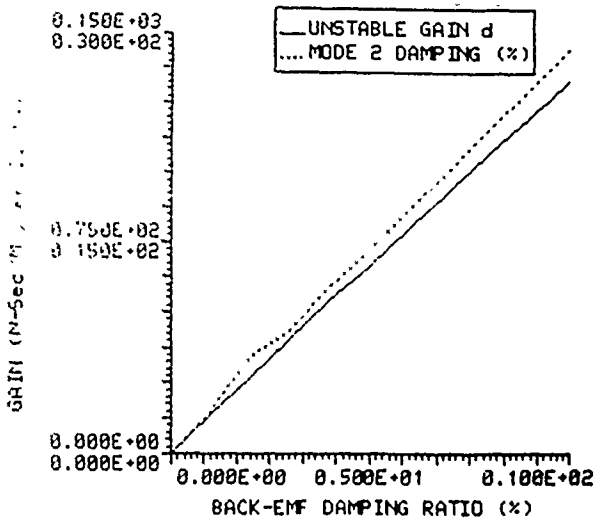

Fig. 13 Modal stability design chart.

Next, consider the case that the break frequency is chosen to fall in between the two structural frequencies. Specifically, consider $\omega_1 = 1.35 < \omega_p = 6 < \omega_2 = 10.41$. An eigenvector analysis of this system reveals that mode 1 is dominated by both the structure and the actuator, mode 2 is actuator dominated, and mode 3 is structure dominated. The modal damping ratios of each mode are plotted vs the actuator gain in Fig. 11. Note that in this case, one of the damping ratios is negative for almost any nonzero value of the gain that achieves reasonable structural damping. Hence, the closed-loop system is almost always unstable, and selecting the break frequency of the actuator to lie between two structural modes is not feasible (without further compensation). This is due to the phase characteristics of the PMA. For the rate-feedback control law, the voltage command to and force output of the force generator will have a frequency content equal to the damped natural frequencies of the closed-loop system. For a stable closed-loop system, the sign of the rate-feedback gain is chosen such that the force component at each individual frequency opposes the corresponding modal velocity of the structure. At frequencies well below the break frequency of the actuator, there is an 180-deg phase difference between the voltage command and the actual applied force, whereas at frequencies well above the break frequency, there is no phase difference. Therefore, when the break frequency of the actuator is chosen to lie in between two of the structural modes and the voltage command corresponds to a physical velocity (not a known sum of individual modal velocities), the individual applied force components on one side of the break frequency will oppose the corresponding modal velocities, thereby removing energy from these modes. However, because of the 180-deg phase difference, the individual applied force components on the other side of the break frequency will aid the modal velocities, thereby adding energy to these modes. If the energy dissipated by the inherent modal damping of these modes is not greater than the energy added by the applied force components, the closed-loop system will become unstable.

Some researchers[19] have suggested that placing the break frequency of the actuator above the highest frequency of interest is a feasible method of reducing the effects of actuator dynamics on control design. Several problems arise in the control structure configuration examined here. First, because the magnitude of the actuator force output breaks down at 40 dB/s below the break frequency, the output force level would be severely limited at low frequencies, typically where the highest levels of control force are required. Secondly, if the structure is very flexible, the model approaches a partial differential equation model with an infinite number of frequencies, as pointed out in Ref. 20. Hence, there is always some structural frequency larger than the break frequency, and the unstable closed-loop situation of Fig. 11 results. In addition, the high-gain instability problem of the previous case is still present. In practical terms, although a structure does not exhibit the infinite number of frequencies the partial differential equation would predict, the question of how one would pick the highest structural frequency that can be excited is not yet answered.

With $\omega_p > \omega_2$, eigenvector analysis reveals that the actuator effect is strongly present in each mode with the third mode being clearly actuator dominated. Figure 12 illustrates the modal damping ratio vs gain plots for each of the modes. Note that increasing the feedback gain increases the modal damping, but to a much smaller extent than for the case with the break frequency below the first structural frequency indicated in Fig. 10. In fact, for the case considered, the highest achievable closed-loop damping ratio is less than 1%. This happens because the actuator is force-output limited in this condition, as described in the previous paragraph. Again, the system goes unstable at higher values of the gain. At least for the system configuration presented here, placing the actuator break frequency above the highest structural frequency offers no apparent advantage.

Returning to the case with the break frequency chosen to be smaller than the lowest structural natural frequency, the high-gain limitation can be represented in terms of the modal design chart of Fig. 13. This is also used to illustrate the importance of back-emf damping in actuator design. The solid line of Fig. 13 divides the plot into stable and unstable regions. For a given back-emf actuator damping ratio (defined by ζ_p), the solid line yields the largest feedback gain before the system becomes unstable. This curve represents the system's high-gain limit. The dashed line indicates the maximum achievable damping ratio for the second mode (which is the first structural mode) before the high-gain instability occurs.

VI. Summary

The interaction between a structure, an actuator used to control the structure, and the control law used to drive the system has been examined for two different systems. The first system considered consisted of a simple cantilevered beam controlled using a rate-feedback control law implemented by a proof-mass actuator. The second system consisted of controlling the vibrations of the COFS I flight article using a rate-feedback control law implemented by a Linear DC

Motor. A simplified model of the COFS I structure was used so that the control/structure interaction phenomena were more clearly revealed. In the past, the simple rate-feedback control law has been viewed as being a stable control law, because it is equivalent to an increase in the passive damping level of the structure. However, when proof-mass actuator dynamics are included, it was shown that a high-gain instability prevents arbitrarily high levels of damping from being added to the system by active control. This high-gain instability was investigated using Rouths' stability criteria in a general sense and through root-locus and modal damping plots for specific cases.

With added damping to the first (lowest) structural mode as a design criteria, it was shown that the break frequency of the actuator should be designed below the first natural frequency of the structure for best performance. In addition, it was shown that the closed-loop system exhibits a high-gain limitation, and that this limitation is determined by the amount of back-emf damping available. It was also shown that as the high-gain limit of a given structure/actuator/control law configuration is approached, system performance degrades substantially.

Acknowledgments

This work was supported in part by NASA Grants NGT 33183801 and NAG-1985 through the Structural Dynamic Branch of NASA Langley Research Center, Air Force Office of Scientific Research Grants 85-0220 and F49620-86-6-0111 through the Mathematics and Information Sciences Directory, and National Science Foundation Grant MSM 8351807. The instrumentation was provided by Equipment Grant AFOSR 850119. The composite beam and the proof-mass actuator were provided by the Structural Dynamics Branch of NASA Langley Research Center through the efforts of R. Miserentino and G. C. Horner.

References

[1]Juang, J.-H. and Longman, R. W. (eds.), "Special Issue on Structural Modeling and System Identification of Flexible Space Structures," *Journal of the Astronautical Sciences*, Vol. 33, No. 1, Jan.-March, 1985.

[2]Meirovitch, L. (ed.), *Proceedings of the Sixth VPI&SU AIAA Symposium on the Dynamics and Control of Large Structures*, Virginia Polytechnic Inst. and State Univ., Blacksburg, VA, June-July 1987; also see proceedings of preceding years, 1977, 1979, 1981, 1985.

[3]Balas, M. J., "Trends in Large Space Structure Control Theory: Fondest Hopes, Wildest Dreams," *IEEE Transactions on Automatic Controls*, Vol. AC-27, No. 3, June 1982, pp. 522-535.

[4]Wright, R. L. (ed.), *Proceedings of the 1st NASA/DOD Control Structures Interaction Technology Conference*, Norfolk, VA, NASA CP-2447, Pts. 1 and 2, Nov. 1986.

[5]Swanson, A. D. (ed.), NASA/DOD Control/Structures Interaction Technology—1987, Colorado Springs, CO, AFWAL-TR-88-3052, Nov. 1987.

[6]Caughey, T. K. and Goh, C. J., "Vibration Suppression in Large Space Structures," *Proceedings of the Workshop on Applications of Distributed System Theory to the Control of Large Space Structures*, Jet Propulsion Lab., Pasadena, CA, Pub. 83-46, 1983, pp. 119-142.

[7]Pilkey, W. D. and Haviland, J. K., "Large Space Structure Damping Design—Final Report," Univ. of Virginia, Charlottesville, VA, 1983.

[8]Haviland, J. K., Lim, T. M., Pilkey, W. D., and Politansky, H., "The Control of Linear Dampers for Large Space Structures," *Proceedings of the 1987 AIAA Guidance and Control Conference*, AIAA, New York, Aug. 1987, pp. 106-116.

[9]Zimmerman, D. C., "Dynamic Characterization and Microprocessor Control of the NASA/UVA Proof-Mass Actuator," M.S. Thesis, Dept. of Mechanical and Aerospace Engineering, State Univ. of New York at Buffalo, Buffalo, NY, June 1984.

[10]Zimmerman, D. C., Horner, G. C., and Inman, D. J., "Microprocessor Controlled Force Actuator," *Journal of Guidance, Control, and Dynamics*, Vol. 11, No. 3, May-June 1988, pp. 230-236.

[11]Wilson, M. L. and Miserertino, R., "Pertrusion Process Development for Long Space Boom Models," *Proceedings of the 41st Annual Conference of the Society of Plastics Industry*, institute paper 60, Jan. 1986.

[12]Banks, H. T., Cudney, H. H., Inman, D. J., and Wang, Y., "Parameter Identification Techniques for the Estimation of Damping in Flexible Structure Experiments," *Proceedings of the 26th IEEE Conference on Decision and Control*, Research Studies Press, Letchworth, England, UK, Dec. 1987.

[13]Ewins, D. J., *Modal Testing: Theory and Experiment*, Research Studies Press, 1986.

[14]Juang, J.-N. and Pappa, R. S., "An Eigensystem Realization Algorithm for Modal Parameter Identification and Model Reduction," *Journal of Guidance, Control, and Dynamics*, Vol. 8, Sept.-Oct. 1984, pp. 620-627.

[15]Weinberger, H. F., "Variational Methods for Eigenvalue Approximation," *Regional Conference Series in Applied Mathematics*, Society of Industrial and Applied Mechanics, Philadelphia, PA, March 1974, pp. 58-62.

[16]Inman, D. J., "Dynamics of Asymmetric Nonconservative Systems," *Journal of Applied Mechanics*, Vol. 50, No. 1, 1983, pp. 199-203.

[17]Bogen, R., *MACSYMA Reference Manual*, Version 10, Mathlab Group, Massachusetts Inst. of Technology, Cambridge, MA, 1983.

[18]Zimmerman, D. C. and Cudney, H. H., "Practical Implementation Issues for Active Control of Large Flexible Structures," *ASME Journal of Vibration, Acoustics, Stress, and Reliability in Design*, Vol. 111, No. 3, July 1989, pp. 283-289.

[19]Balas, M. J., "Observer Stabilization of Singularly Perturbed Systems," *Journal of Guidance and Control*, Vol. 1, Jan.-Feb. 1978, pp. 93-95.

[20]Goh, C. J. and Caughey, T. K., "On the Stability Problem Caused by Finite Actuator Dynamics in the Colocated Control of Large Space Structures," *International Journal of Control*, Vol. 41, No. 3, March 1985, pp. 787-802.

Matching Finite Element Models to Modal Data

C. Minas
Graduate Research Assistant.

D. J. Inman
Professor.

Mechanical and Aerospace Engineering Department,
State University of New York at Buffalo,
Buffalo, NY 14260

A technique is proposed which systematically adjusts a finite element model of a structure to produce an updated model in agreement with measured modal results. The approach suggested here is to consider the desired perturbations in stiffness and damping matrices as gain matrices in a feedback control algorithm designed to perform eigenstructure assignment. The improved stiffness and damping matrices combined with the analytical mass matrix, more closely predict the modal test results. The technique is applicable to undamped, proportionally damped, as well as nonproportionally damped models. The proposed method assumes that the analytical mass, damping and stiffness matrices are known and that vibration test data is available in the form of natural frequencies, damping ratios, and mode shapes.

Introduction

The method proposed here addresses the problem of comparing an analytical model of a given structure with the experimentally measured vibration response of the same structure in the form of modal data. The analytical finite element model is generally of larger order than the experimentally determined model and the two seldom yield the same natural frequencies, damping ratios and mode shapes. Previous work, see Berman and Nagy (1983), Heylen (1982), Kammer (1987) and Fuh et al (1984) for instance, have suggested adjusting the finite element model in the hope of producing a modified model, more in agreement with the measured response.

The modal data collected in a vibration test can easily be cast into eigenvalue and eigenvector information, if one assumes that the structure under test can be successfully modeled by a linear lumped parameter multiple-degree-of-freedom system. The problem of matching finite element models with test data can be restated as follows. Given a dynamical system, and its finite element model, find correction matrices for the stiffness matrix and damping matrix such that the corrected system has the measured eigenvalues and eigenvectors. If one identifies the measured eigenstructure (i.e., modal data) with the desired eigenstructure, this is exactly the statement of the eigenstructure assignment problem, using velocity and position feedback common in control theory.

The method proposed here, capitalizes on these similarities and uses an eigenstructure assignment algorithm from control theory to calculate corrections in the finite element model (Andry et al, 1982-3, Srinathkumar, 1978). The result is a corrected finite element model which agrees with experimental data. Note that in this proposed method, active control is not performed, only an algorithm from control theory is used.

The technique of using an eigenstructure assignment methodology with measured modal data as the desired eigenstructure works equally well for both real mode shapes and complex mode shapes. This well known and established control theory method is used and adopted to physical coordinates rendering these procedures compatible with experimental measurements. Several examples are presented to explain and clarify the procedure.

The proposed technique is applicable where a finite element model of an existing structure is available in the form of mass, damping and stiffness matrices. The finite element model can be undamped, proportionally damped, as well as nonproportionally damped. In addition, modal testing results for the same structure consisting of a set of eigenvalues and eigenvectors is assumed to be available. The eigenvalues and eigenvectors can be real as well as complex. As in most test situations, it is assumed that the number of measured modes is smaller than the number of analytical modes and that they are not necessarily of the same order.

Analytical Model

The dynamic structures under consideration are assumed to be successfully modeled by a linear damped multiple-degree-of-freedom system. The free vibration of the model is described by the differential equation of the form

$$M\ddot{\mathbf{q}}(t)+\mathrm{D}\dot{\mathbf{q}}(t)+K\mathbf{q}(t)=\mathbf{0}$$

where, M is the mass matrix and D and K are the damping and stiffness matrix respectively. The mass and stiffness matrices are assumed to be symmetric, positive definite matrices and the damping matrix is assumed to be symmetric, positive semi-definite (Shames, 1985, Stasa, 1985). The analytical model is obtained by finite element structural analysis. As a result, the damping matrix is proportional to the mass and stiffness matrices, that is

$$D=\alpha M+\beta K$$

where, α and β are constants. This proportionally damped model usually has complex eigenvalues and real eigenvectors. The complex eigenvalues of the system are in complex conjugate pairs, since the matrices, M, D and K consist of real constant parameters. The eigenvalues and eigenvectors of the

Contributed by the Technical Committee on Vibration and Sound for Publication in the JOURNAL OF VIBRATION AND ACOUSTICS Manuscript received July 1988.

analytical model are referred to as the *open-loop* eigenvalues (λ_i^*) and eigenvectors ($\mathbf{v}_i^*$) of the system.

Experimental Model

The experimentally obtained modal data can easily be cast into a set of natural frequencies (ω_i), damping ratios (ζ_i) and mode shapes by using modal parameter estimation methods, such as circle-fit (Ewins, 1986), polyreference method and eigensystem realization algorithm (Allemang and Brown, 1987). These quantities can be further transformed into a set of eigenvalues (λ_i) and associated eigenvectors ($\mathbf{z}_i$). Note that the eigensystem realization algorithm yields the eigenvalues and eigenvectors directly (Juang and Pappa, 1985). The eigenvalues are given by the following equation:

$$\lambda_i = -\zeta_i\omega_i \pm j\omega_{d_i}$$

where,

$$\omega_{d_i} = \omega_i\sqrt{1-\zeta_i^2}$$

for the underdamped case. The eigenvalues and eigenvectors in general, can be real or complex. In the case where some of the eigenvalues and eigenvectors are complex, they will be in complex conjugate pairs for the model to be real.

Model Correction

The proposed technique uses an eigenstructure assignment algorithm to obtain correction matrices for the damping and stiffness matrices. Those matrices are considered as gain matrices in a feedback control algorithm. The first step in the theoretical formulation of the proposed technique, is to consider a multiple-degree-of-freedom vibrating system of order n, subject to feedback control of the form:

$$M\ddot{\mathbf{q}}(t) + D\dot{\mathbf{q}}(t) + K\mathbf{q}(t) = B_0\mathbf{u}(t) \tag{1}$$

The output or measurement vector $\mathbf{y}(t)$ is given by

$$\mathbf{y}(t) = C_0\mathbf{q}(t) + C_1\dot{\mathbf{q}}(t) \tag{2}$$

where C_0 and C_1 are the position and velocity measurement matrices, respectively. Here $\mathbf{q}$ is a real valued vector of dimension $n\times 1$, $\mathbf{u}$ is a real valued vector of dimension m, and $\mathbf{y}$ is a real valued vector of dimension r.

The control vector $\mathbf{u}(t)$ is given by:

$$\mathbf{u}(t) = F\mathbf{y}(t) \tag{3}$$

The quantities M, D, K, C_0, C_1 and $\mathbf{q}$ are rearranged such that the first m coordinates of $\mathbf{x}(t)$ correspond to the measured coordinates, that is

$$\mathbf{x}(t) = T\mathbf{q}(t) \tag{4}$$

where T is an $n\times n$ transformation matrix. Note that it is important here for the finite element analyst and the test engineer to use compatible coordinate systems. This means that accelerometers should be placed at positions on the structure corresponding to nodes of the finite element model. Since the finite element and the modal tests are often performed by different people, (in some cases, by different departments) it is important to ensure that the test data used in this procedure is consistent with the finite element code which is being verified. Note that the number of nodes of the finite element model can and will be, much larger than the number of accelerometers used in the modal test.

Substitution of (2), (3) and (4) in (1) yields:

$$MT^{-1}\ddot{\mathbf{x}}(t) + DT^{-1}\dot{\mathbf{x}}(t) + KT^{-1}\mathbf{x}(t) = B_0FC_0T^{-1}\mathbf{x}(t) + B_0FC_1T^{-1}\dot{\mathbf{x}}(t) \tag{5}$$

Let,

$$M_1 = MT^{-1} \quad D_1 = MT^{-1} \quad K_1 = KT^{-1}$$
$$C_0^* = C_0T^{-1} \quad C_1^* = C_1T^{-1} \tag{6}$$

Substitution of (6) into (5) yields:

$$M_1\ddot{\mathbf{x}}(t) + D_1\dot{\mathbf{x}}(t) + K_1\mathbf{x}(t) = B_0FC_0^*\mathbf{x}(t) + B_0FC_1^*\dot{\mathbf{x}}(t) \tag{7}$$

where M_1, D_1, and K_1 are generally asymmetric $n\times n$ matrices. The *closed-loop* system described by (7) has $2n$ eigenvalues and $2n$ ($n\times 1$) eigenvectors. Given $\{\lambda_i\}$, $i = 1,2,\ldots,r$ as the desired eigenvalues, and $\mathbf{v}_i$ the eigenvec-

Nomenclature

B_0 = full rank constant coefficient feedback matrix
B = modified constant coefficient feedback matrix
C_0 = position measurement matrix
C_1 = velocity measurement matrix
C_0^* = transformed position measurement matrix
C_1^* = transformed velocity measurement matrix
D = system damping (symmetric positive definite)
D_1 = transformed damping matrix
F = output feedback gain matrix
G_i = partition of $\mathbf{R}_i$
I_n = nxn identity matrix
J = objective function
K = system stiffness matrix (symmetric positive definite)
K_1 = transformed stiffness matrix
m = number of independent inputs (actuators)
M = system mass matrix (symmetric positive definite)
M_1 = transformed mass matrix
n = number of degrees of freedom
p = number of measured modes
$\mathbf{q}(t)$ = displacement vector
Q_i = partition of $\mathbf{R}_i$
r = number of independent outputs (sensors)
$\mathbf{R}_i$ = subspace of ith eigenvector
T = transformation matrix
$\mathbf{u}(t)$ = control vector
$\mathbf{v}_i^*$ = *open-loop* system ith eigenvector
$\mathbf{v}_i$ = *closed-loop* system ith eigenvector
W = system eigenvector matrix
$\mathbf{x}(t)$ = transformed displacement vector
$\mathbf{y}(t)$ = output vector
$\mathbf{z}_i$ = ith measured eigenvector
δ_{iD} = measure of changes of damping matrix, $i = 1, 2$
δ_{iK} = measure of changes of stiffness matrix, $i = 1, 2$
δD = damping matrix of changes
δK = stiffness matrix of changes
λ_i^* = *open-loop* system ith eigenvalue
λ_i = *closed-loop* system ith eigenvalue
Λ = eigenvalue matrix
ζ_i = measured damping ratio
ω_i = measured undamped frequency
ω_{d_i} = measured damped frequency

Superscripts

T = matrix transpose
$\cdot$ = time derivative

tors corresponding to λ_i, then the eigenvector equation of the *closed-loop* system is given by:

$$(I_n\lambda_i^2 + M_1^{-1}D_1\lambda_i + M_1^{-1}K_1)\mathbf{v}_i = (M_1^{-1}B_0FC_1^*\lambda_i + M_1^{-1}B_0FC_0^*)\mathbf{v}_i \quad (8)$$

After simple matrix manipulation, this becomes:

$$\mathbf{v}_i = (I_n\lambda_i^2 + M_1^{-1}D_1\lambda_i + M_1^{-1}K_1)^{-1}M_1^{-1}B_0F(C_1^*\lambda_i + C_0^*)\mathbf{v}_i \quad (9)$$

Here it is assumed that none of the assigned eigenvalues λ_i, match the system *open-loop* eigenvalues λ_i^*, therefore, the inverse of $(I_n\lambda_i^2 + M_1^{-1}D_1\lambda_i + M_1^{-1}K_1)$ exists.

Next define the mx1 vector $\mathbf{m}_i$, as

$$m_i = F(C_1^*\lambda_i + C_0^*)\mathbf{v}_i \quad (10)$$

Then (9) becomes

$$\mathbf{v}_i = (I_n\lambda_i^2 + M_1^{-1}D_1\lambda_i + M_1^{-1}K_1)^{-1}M_1^{-1}B_0\mathbf{m}_i \quad (11)$$

The implication of (11) is of great importance (Srinathkumar, 1978, Andry et al, 1983). It states that the *closed-loop* eigenvector $\mathbf{v}_i$ which is associated with the *closed-loop* eigenvalue λ_i must lie in the subspace spanned by the columns of the matrix

$$R_i = (I_n\lambda_i^2 + M_1^{-1}D_1\lambda_i + M_1^{-1}K_1)^{-1}M_1^{-1}B_0F(C_1^*\lambda_i + C_0^*) \quad (12)$$

This means that there is a constraint on the eigenvector and not just any complete eigenvector can be assigned to a given structure. The dimension of this subspace is m, the number of independent control-inputs to the system. The orientation of this subspace depends upon the parameters in M, D, K, T and the desired eigenvalue λ_i. Therefore M, D and K must be a "good" representation of the structure for this subspace to be physically meaningful.

Srinathkumar's (1978) work has very important implications for this approach. It implies the following theorem which uniquely determines the feedback gain matrix F.

Eigenstructure Assignment Theorem. Given a controllable and observable dynamical system (see Chen, 1984, or Inman, 1989, for definition), the elements of the feedback gain matrix F, can be specified such that max (m, r) *closed-loop* eigenvalues can be assigned, max (m, r) eigenvectors can be partially assigned, and min (m, r) entries in each eigenvector can be partially assigned.

According to this eigenstructure assignment theorem we can only assign (m, r) eigenvalues and min (m, r) entries in each eigenvector. If $m = r$, that is the number of sensors is equal to the number of actuators then, m eigenvalues can be assigned and m eigenvectors can be partially assigned and m entries in each eigenvector can be arbitrarily assigned. If the eigenvectors are of dimension $m \times 1$, then the eigenvectors can be fully assigned. The measured eigenvectors are assumed to be of dimension $p \times 1$, where p is the number of the measured modes. The choice of the number of actuators is up to the user in this case as no physical device need be present in this application. Therefore if p is set equal to m, then all the experimental modal parameters can be fully assigned. Let the experimental eigenvalues be $\{\lambda_i\}$, $i = 1,2, \ldots, m$ and the experimental eigenvectors $\{\mathbf{z}_i\}, i = 1,2, \ldots, m$. The assigned eigenvectors are of dimension $n \times 1$ and are given by:

$$\mathbf{v}_i = \begin{bmatrix} \mathbf{z}_i \\ \mathbf{d}_i \end{bmatrix} \quad (13)$$

where $\mathbf{d}_i$ is an $(n\text{-}m) \times 1$ vector of unspecified components.

Next the vector $\mathbf{d}_i$ is chosen such that (12) is satisfied, that is $\mathbf{v}_i$ lies in the subspace spanned by the columns of the matrix R_i. Then, R_i can be partitioned into G_i and Q_i

$$R_i = \begin{bmatrix} G_i \\ Q_i \end{bmatrix} \quad (14)$$

where G_i is an $m \times m$ square matrix and Q_i is an $(n\text{-}m) \times m$ matrix. The matrices G_i and Q_i can be further partitioned into column vectors as follows:

$$G_i = [\mathbf{g}_1 : \mathbf{g}_2 : \mathbf{g}_3 : \ldots : \mathbf{g}_m]$$
$$Q_i = [\mathbf{q}_1 : \mathbf{q}_2 : \mathbf{q}_3 : \ldots : \mathbf{q}_m] \quad (15)$$

Note that the elements of R_i, Q_i and G_i are complex in the case of complex experimental eigenvalues and eigenvectors. Here it is assumed that G_i is nonsingular, so that the elements of $\mathbf{z}_i$ can be expressed as a linear combination of $\mathbf{g}_1$, $\mathbf{g}_2$, $\mathbf{g}_3$, . . . , $\mathbf{g}_m$ that is

$$\mathbf{z}_i = a_1\mathbf{g}_1 + a_2\mathbf{g}_2 + a_3\mathbf{g}_3 + \ldots + a_m\mathbf{g}_m \quad (16)$$

where the elements a_i are constant expansion coefficients. This last expression can be written in matrix notation as

$$\mathbf{z}_i = G_i\mathbf{a} \quad (17)$$

where the vector $\mathbf{a}$ is given by

$$\mathbf{a} = [a_1, a_2, a_3, \ldots, a_m] \quad (18)$$

Similarly, the vector $\mathbf{d}_i$ is unspecified and forced to satisfy:

$$\mathbf{d}_i = Q_i\mathbf{a} \quad (19)$$

If equation (17) is multiplied by G_i^{-1}, the vector $\mathbf{a}$ is calculated to be:

$$\mathbf{a} = G_i^{-1}\mathbf{z}_i \quad (20)$$

Substitution into (19) then yields

$$\mathbf{d}_i = Q_iG_i^{-1}\mathbf{z}_i \quad (21)$$

Thus, the ith assigned eigenvector is given by

$$\mathbf{v}_i = \begin{bmatrix} \mathbf{z}_i \\ Q_iG_i^{-1}\mathbf{z}_i \end{bmatrix} \quad (22)$$

Equation (22) is a physically meaningful relationship between the unmeasured elements of $\mathbf{v}_i$ and those elements which are measured. However, this relationship is true only when the analytical model is a "good" representation of the structure. The assigned eigenvalues can be arbitrary, but the assigned eigenvectors must lie in a certain subspace. Furthermore, the orientation of this subspace depends on the analytical mass, damping and stiffness matrices. This is equivalent to the equation derived by Berman (1983) relating the measured and unmeasured components of an eigenvector.

Next the procedure for calculation of the feedback gain matrix is presented.

Calculation of Feedback Gain Matrix. Equation (8) holds for all m *closed-loop* eigenvalue/eigenvector pairs. In the compact form of matrix notation, the m equations represented by (8) become

$$W\Lambda^2 = -M_1^{-1}D_1W\Lambda - M_1^{-1}K_1W + BFC_1^*W\Lambda + BFC_0^*W \quad (23)$$

where,

$$W = [\mathbf{v}_1 : \mathbf{v}_2 : \mathbf{v}_3 : \ldots\ldots \mathbf{v}_m] \quad (24)$$

$$\Lambda = \text{diag}(\lambda_1, \lambda_2, \lambda_3, \ldots\ldots, \lambda_m) \quad (25)$$

$$B = M_1^{-1}B_0 \quad (26)$$

Solving (23) for the matrix F yields

$$F = (B^TB)^{-1}B^T[W\Lambda^2 + M_1^{-1}D_1W\Lambda + M_1^{-1}K_1W][C_1^*W\Lambda + C_0^*W]^{-1} \quad (27)$$

From a mathematical view, $[C_1^*W\Lambda + C_0^*W]^{-1}$ will exist as long as the only point of intersection of the nullspace of the output matrix $[C_1 : C_0]$, and the space spanned by the columns of the matrix of the desired eigenvectors $\mathbf{W}$, is the origin.

The new damping and stiffness matrices can be calculated as:

$$D^* = D - B_0 F C_1$$
$$K^* = K - B_0 F C_0 \tag{28}$$

It is noted that the new damping and stiffness matrices are not symmetric because the matrices B_0FC_0 and B_0FC_1 are generally not symmetric. This problem is overcome by optimizing an appropriate objective function.

It is also noted that the original FEM will in general not produce a model with complex modes. This is true because the standard choice for a damping matrix in FEM is to assume it to be a linear combination of the mass and stiffness matrices (i.e., proportional damping). The new damping and stiffness matrix given in equation (28) will in general not be proportional. Hence the adjusted FEM will yield complex modes, which is what is observed in most structural tests.

Choice of Objective Function. As is noted in the previous section, the elements of C_0 and C_1, that is the position and velocity measurement matrices respectively, cannot be determined analytically if symmetry of the new model is required.

In general, the asymmetric part of a square matrix A, see Inman (1989) for instance, is given by,

$$A_{as} = .5(A - A^T) \tag{29}$$

If A is symmetric, the matrix A_{as} must be a matrix with zero entries. Next define A_1, A_2, A_3, A_4 to be the following matrices:

$$A_1 = B_0FC_1 \quad A_2 = B_0FC_0$$
$$A_3 = A_1 - A_1^T \quad A_4 = A_2 - A_2^T \tag{30}$$

An objective function J, is set to be the sum of the squares of the elements of A_3 and A_4. The objective function J is minimized over the elements of the measurement matrices C_0 and C_1. If the final value of J is zero then that the elements of A_3 and A_4 are zero, which implies that matrices A_1 and A_2 are symmetric. Therefore the necessary condition for symmetry of the new model

$$B_0FC_1 = C_1^T F^T B_0^T$$
$$B_0FC_0 = C_0^T F^T B_0^T \tag{31}$$

is satisfied.

To express matrices A_3 and A_4 and finally J, in terms of C_0 and C_1, the expression for B_0F from equation (23) can be used to yield:

$$B_0F = M_1[W\Lambda^2 + M_1^{-1}D_1W\Lambda + M_1^{-1}K_1W][C_1^*W\Lambda + C_0^*W]^{-1} \tag{32}$$

Then, by transposing (32), the matrix $F^TB_0^T$ is calculated to be

$$F^TB_0^T = [C_1^*W\Lambda + C_0^*W]^{-T}[W\Lambda^2 + M_1^{-1}D_1W\Lambda + M_1^{-1}K_1W]^TM_1^T \tag{33}$$

Finally this results in the objective function J, in terms of only known quantities and in terms of the independent variable vector that contains the elements of C_0 and C_1:

$$J = \|M_1[W\Lambda^2 + M_1^{-1}D_1W\Lambda + M_1^{-1}K_1W][C_1^*W\Lambda + C_0^*W]^{-1}C_0 - [C_1^*W\Lambda + C_0^*W]^{-T}[W\Lambda^2 + M_1^{-1}D_1W\Lambda + M_1^{-1}K_1W]^TM_1^TC_0\|^2 + \|M_1[W\Lambda^2 + M_1^{-1}D_1W\Lambda + M_1^{-1}K_1W][C_1^*W\Lambda + C_0^*W]^{-1}C_1 - [C_1^*W\Lambda + C_0^*W]^{-T}[W\Lambda^2 + M_1^{-1}D_1W\Lambda + M_1^{-1}K_1W]^TM_1^TC_1\|^2 \tag{34}$$

An unconstrained optimization algorithm was used to minimize the above objective function. Since the gradient vector and the Hessian matrix of J are not trivial and have to be calculated numerically, a canned subroutine from IMSL Math Library was used (IMSL 10, CONDIR). The optimization routine uses the conjugate directions technique to minimize the objective function. A subroutine that provides the function to be minimized in terms of the independent variable vector is necessary.

Iterative Procedure. After the optimization procedure is applied, J is not always exactly zero which implies that the new damping and stiffness matrices are not perfectly symmetric. It is important to realize that the improved damping and stiffness matrices must be symmetric. Therefore only the symmetric parts of D^* and K^* are taken into consideration in the calculations. However, by throwing away the asymmetric part of D^* and K^*, the new model does not have the exact assigned (measured) eigenvalues and eigenvectors. An iterative procedure is then applied to the updated model until the elements of the gain feedback matrix F are negligibly small, yielding an almost symmetric system. During the iterative procedure the eigenvalues and eigenvectors are repeatedly assigned to the updated model, throwing away the asymmetric part of the new damping and stiffness matrices at each step. After every iteration the model is updated and checked for convergence of the eigenvalues and eigenvectors of the updated model to the assigned data.

Summary of Adopted Procedure. The application of the method is straightforward and is performed in 7 steps, listed here and illustrated in Fig. 1.

(1) Choose B_0
(2) Choose initial values for the elements of C_0 and C_1
(3) Use the optimization algorithm to minimize J. Get F and new C_0, C_1

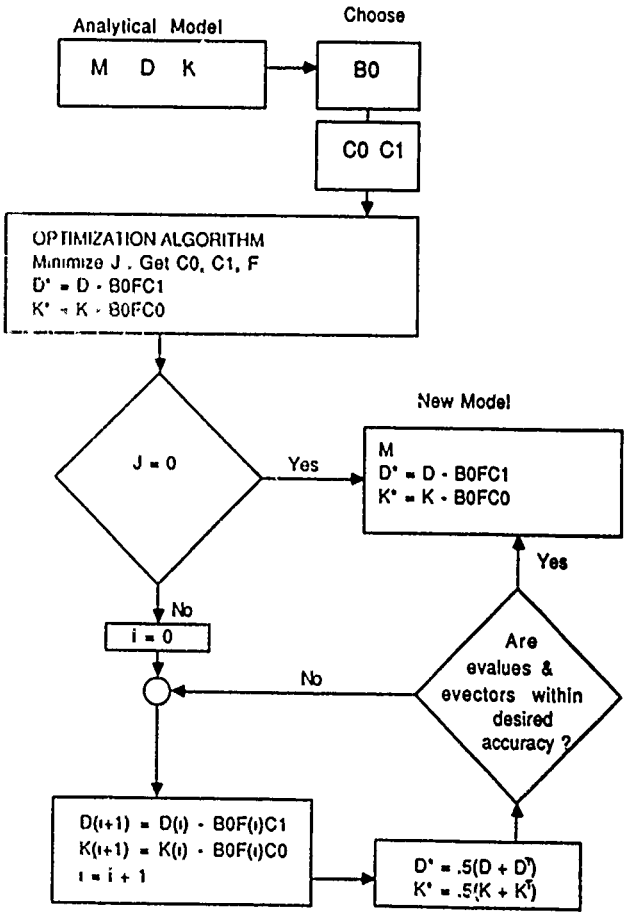

Fig. 1 Flowchart of adopted procedure

$$D^* = D - B_0 F C_1$$
$$K^* = K - B_0 F C_0$$

(4) If J is not exactly zero, D^* and K^* are not symmetric

Set $D^* = .5\,(D^* + D^{*T})$
$K^* = .5\,(K^* + K^{*T})$

(5) The new model M, D^*, K^* does not have the exact assigned eigenvalues and eigenvectors.

(6) Iterate procedure, that is,

$$D^{(i+1)} = D^{(i)} - B_0 F^{(i)} C_1$$
$$D^{(i+1)} = .5(D^{(i+1)} + D^{(i+1)T})$$
$$K^{(i+1)} = K^{(i)} - B_0 F^{(i)} C_0$$
$$K^{(i+1)} = .5(K^{(i+1)} + K^{(i+1)T})$$

until desired accuracy in eigenvalues/eigenvectors is achieved.

(7) The improved model M, D, K results.

A flowchart of the method is presented in Fig. 1.

Measures of Changes. The evaluation of changes in the damping and stiffness matrices is necessary if one is to pass judgement on the acceptability of the improved model. No single measure of these changes can be completely meaningful. Therefore, two separate parameters were calculated to assist in this evaluation. The first, δ_1, is the mean square of the element changes divided by the mean square of the elements of the original matrix. Thus δ_1 for the damping and stiffness matrices are defined as:

$$\delta_{1D} = \frac{\sum_{i=1}^{n}\sum_{j=1}^{n} \delta D_{ij}^2}{\sum_{i=1}^{n}\sum_{j=1}^{n} D_{ij}^2} \qquad \delta_{1K} = \frac{\sum_{i=1}^{n}\sum_{j=1}^{n} \delta K_{ij}^2}{\sum_{i=1}^{n}\sum_{j=1}^{n} K_{ij}^2} \tag{35}$$

where δD, δK are defined as the matrices of changes of the damping and stiffness matrices, respectively, that is:

$$\delta D = D^* - D \qquad \delta K = K^* - K \tag{36}$$

This measure makes no recognition of the relative changes of the elements. In a sense, the diagonal elements may be considered to be indicators of the magnitude of the data in the corresponding rows and columns. Thus, the second measure of changes was calculated, which is simply the mean square of the relative changes in the diagonal elements. Thus, δ_2 is defined as:

$$\delta_{2D} = \frac{\sum_{i=1}^{n} \delta D_{ii}^2}{\sum_{i=1}^{n} D_{ii}^2} \qquad \delta_{2K} = \frac{\sum_{i=1}^{n} \delta K_{ii}^2}{\sum_{i=1}^{n} K_{ii}^2} \tag{37}$$

The above procedure is illustrated in the examples that follow. The measure of changes in the damping and stiffness matrices are also shown.

Examples

In this section two examples are shown to illustrate the proposed method. The examples are fictitious and do not correspond to real experiments or structures. However, they do simulate the standard case for real structures in the sense that the FEM is larger than the "measured" modal model. The first example illustrates an eight-degree-of-freedom, nonproportionally damped model which is assigned three real eigenvalues and three (3 × 1) eigenvectors. This simulates three sets of measured mode shapes, natural frequencies and damping ratios. The second example is a four-degree-of-freedom, nonproportionally damped model which is assigned two measured complex eigenvalues and two measured complex eigenvectors. The complex eigenvalues and eigenvectors are in complex conjugate pairs. This is necessary if the entries of the mass, damping and stiffness matrices are required to be real numbers.

Example 1

In this example an eight-degree-of-freedom, nonproportionally damped model is assumed. It is also assumed that measured model data in the form of three real eigenvalues (i.e., an overdamped response so that the three measured damping ratios are greater than one) and three (3×1) mode shapes is available.

Analytical Model. The model is given by equation (1) with the following banded coefficient matrices:

$M = \text{diag}\{3.0, 0.5, 0.4, 1.0, 1.0, 1.5, 1.0, 0.5\}$

$$D = \begin{bmatrix} 2.5 & .0 & -2.5 & .0 & .0 & .0 & .0 & .0 \\ & 2.5 & .0 & -2.5 & .0 & .0 & .0 & .0 \\ & & 2.5 & .0 & .0 & .0 & .0 & .0 \\ & & & 2.5 & .0 & .0 & .0 & .0 \\ & & & & 2.5 & -2.5 & .0 & .0 \\ & \text{symmetric} & & & & 10.5 & -4.0 & -4.0 \\ & & & & & & 4.0 & .0 \\ & & & & & & & 4.0 \end{bmatrix}$$

$$K = \begin{bmatrix} 8.0 & -1.0 & -1.0 & .0 & .0 & .0 & .0 & .0 \\ & 2.0 & .0 & -1.0 & .0 & .0 & .0 & .0 \\ & & 4.0 & .0 & -3.0 & .0 & .0 & .0 \\ & & & 4.0 & .0 & -3.0 & .0 & .0 \\ & & & & 4.0 & -1.0 & .0 & .0 \\ & \text{symmetric} & & & & 8.0 & -2.0 & -2.0 \\ & & & & & & 2.0 & .0 \\ & & & & & & & 2.0 \end{bmatrix}$$

$$B_0 = \begin{bmatrix} 1 & 0 & 0 \\ 0 & 0 & 0 \\ 0 & 0 & 0 \\ 0 & 1 & 0 \\ 0 & 0 & 0 \\ 0 & 0 & 0 \\ 0 & 0 & 0 \\ 0 & 0 & 1 \end{bmatrix}$$

The sixteen eigenvalues of the *open-loop* (FEM) system are calculated and presented below for comparison:

$$\{\lambda_j^*, j = 1,16\} = \{-6.7072, -5.4904, -0.7160, -8.8625 \pm 3.2731i, -1.6916 \pm 1.7638i, -0.0462 \pm 1.8055i, 0.2242 \pm 1.6361i, -0.0645 \pm 0.4199i - 0.4843 \pm 0.0078i\}$$

Measured Results. Next, it is assumed that the measured results are available in the form of eigenvalues and associated eigenvectors, that is:

Eigenvalues:

$$\{\lambda_1, \lambda_2, \lambda_3\} = \{-7.0000, -5.0000, -0.7500\}$$

Associated Eigenvectors:

$$z_1 = \begin{bmatrix} .0100 \\ 1.0000 \\ -.0500 \end{bmatrix} \quad z_2 = \begin{bmatrix} -.2000 \\ .0500 \\ 1.0000 \end{bmatrix} \quad z_3 = \begin{bmatrix} .2500 \\ 1.0000 \\ -.0050 \end{bmatrix}$$

These eigenvalues and eigenvectors are then assigned to the above model using the proposed method to produce the following correction factors. Note that only the first three elements of each eigenvector are available. This simulates the situation in most structural test, that only partial mode shapes can be determined and only a few of the eigenvalues can be measured.

1(a) Results from Optimization Procedure

The resulting measurement matrices C_0 and C_1 become

$$C_0 = \begin{bmatrix} -7.77 & 8.62 & 9.99 & 9.31 & \cdot & \cdot & 16.21 & 49.03 \\ 32.26 & -10.94 & -0.78 & 13.96 & -5.51 & \cdot & 2.76 & -17.54 \\ -291.65 & 76.99 & 102.36 & -54.17 & 11.4\cdot & \cdot & 14.64 & 280.54 \end{bmatrix}$$

$$C_1 = 10^3 \begin{bmatrix} .0105 & -.0447 & -.0480 & .0243 & -0.398 & .1165 & .0103 & -.0918 \\ -.0078 & .0498 & .0569 & -.0272 & .0637 & .1610 & .0601 & .0190 \\ .1783 & -4.167 & -.4749 & .2714 & -3.143 & 1.0394 & .1723 & -.8831 \end{bmatrix}$$

The modal parameters of the new system, that are of interest, are the following set of eigenvalues and eigenvectors, that is

Eigenvalues:

$$\{\lambda_1, \lambda_2, \lambda_3\} = \{-7.0654, -5.4857, -0.6864\}$$

Associated Eigenvectors:

$$\mathbf{v}_1 = \begin{bmatrix} -.0309 \\ 1.0000 \\ .1954 \\ \text{xxxx} \\ \text{xxxx} \\ \text{xxxx} \\ \text{xxxx} \\ \text{xxxx} \end{bmatrix} \quad \mathbf{v}_2 = \begin{bmatrix} -.1562 \\ -.1445 \\ 1.0000 \\ \text{xxxx} \\ \text{xxxx} \\ \text{xxxx} \\ \text{xxxx} \\ \text{xxxx} \end{bmatrix} \quad \mathbf{v}_3 = \begin{bmatrix} .1260 \\ 1.0000 \\ -.2517 \\ \text{xxxx} \\ \text{xxxx} \\ \text{xxxx} \\ \text{xxxx} \\ \text{xxxx} \end{bmatrix}$$

The new adjusted model is described by the original mass matrix and the damping and stiffness matrices that follow, that is:

$$D^* = \begin{bmatrix} 2.872 & .082 & -2.478 & .424 & .155 & -.355 & .220 & .139 \\ & 2.500 & .0 & -2.553 & .0 & .0 & .0 & -.034 \\ & & 2.500 & -.183 & .0 & .0 & .0 & -.004 \\ & & & 2.952 & .029 & -.001 & .182 & .0 \\ & & & & 2.500 & 2.500 & .0 & .232 \\ & & \text{symmetric} & & & 10.500 & -4.000 & -2.334 \\ & & & & & & 4.000 & -1.028 \\ & & & & & & & 1.666 \end{bmatrix}$$

and

$$K^* = \begin{bmatrix} 6.952 & -1.025 & -.988 & -1.382 & \cdot & .165 & .365 & -.301 \\ & 2.000 & .0 & .1.002 & \cdot & .0 & .0 & -.012 \\ & & 4.000 & .028 & \cdot & .0 & .0 & .146 \\ & & & 2.673 & \cdot & 2.852 & .615 & -.537 \\ & & & & & 1.000 & 0 & -.044 \\ & & \text{symmetric} & & & & .000 & -2.070 \\ & & & & & & 000 & -.156 \\ & & & & & & & 2.897 \end{bmatrix}$$

1(b) Results After Iterative Procedure

After 47 iterations the modal parameters of the new system, that are of interest, (i.e., those corresponding to the measured data set) is the following set of eigenvalues and eigenvectors:

$$\{\lambda_1, \lambda_2, \lambda_3\} = \{-7.0000, -5.0000, -0.7500\}$$

Associated Eigenvectors:

$$\mathbf{v}_1 = \begin{bmatrix} .0100 \\ 1.0000 \\ .0500 \\ \text{xxxx} \\ \text{xxxx} \\ \text{xxxx} \\ \text{xxxx} \\ \text{xxxx} \end{bmatrix} \quad \mathbf{v}_2 = \begin{bmatrix} -.2000 \\ .0500 \\ 1.0000 \\ \text{xxxx} \\ \text{xxxx} \\ \text{xxxx} \\ \text{xxxx} \\ \text{xxxx} \end{bmatrix} \quad \mathbf{v}_3 = \begin{bmatrix} .2500 \\ 1.0000 \\ -.0050 \\ \text{xxxx} \\ \text{xxxx} \\ \text{xxxx} \\ \text{xxxx} \\ \text{xxxx} \end{bmatrix}$$

changes of the damping and stiffness matrices are calculated and shown in Table 1. Next, this procedure is iterated to improve the corrected model.

ed by the original mass matrices that follow.

$$D^* = \begin{bmatrix} 3.410 & -.942 & \cdot & \cdot & .501 & 1.110 & .297 & 2.151 \\ & 2.500 & \cdot & \cdot & 1.024 & 0 & .0 & -1.606 \\ & & 2.500 & \cdot & .077 & .0 & .0 & 1.066 \\ & & & \cdot & .097 & 2.579 & .056 & -2.079 \\ & & & & 2.654 & 3.255 & .077 & 1.572 \\ & & \text{symmetric} & & & 10.500 & -4.000 & -2.163 \\ & & & & & & 4.000 & .043 \\ & & & & & & & 5.152 \end{bmatrix}$$

and

$$K^* = \begin{bmatrix} 7.490 & -2.050 & -9.11 & -3.462 & -.778 & .165 & -.559 & 1.442 \\ & 2.000 & .0 & -1.500 & -1.024 & .0 & .0 & -1.584 \\ & & 4.000 & .098 & -2.923 & .0 & .0 & 1.217 \\ & & & 2.673 & -.518 & -2.852 & .117 & -.537 \\ & & & & 1.952 & -1.000 & -1.024 & -1.616 \\ & & \text{symmetric} & & & 8.000 & -2.000 & -2.070 \\ & & & & & & 2.000 & -1.727 \\ & & & & & & & 2.897 \end{bmatrix}$$

Table 1 Measures of changes

Example/case	δ_{1D}	δ_{1K}	δ_{2D}	δ_{2K}
	%	%	%	%
1a	5.28	3.08	3.34	1.95
1b	20.61	21 03	1.37	3 73
2a	0.80	10.83	1.19	6 03
2b	0.80	10.86	1.18	6 [illegible]

The measures of changes of the damping and [illegible] matrices are calculated and the results are shown in Table [illegible]. Note that the eigenvalues and eigenvectors of the [illegible] model are much closer to the simulated measured data [illegible] the result obtained by just using equations (28) without [illegible] tion. In either case, the modal information of the [illegible] model is much closer to the measured data than the original model.

Example 2

In the last example, a four [illegible] tionally damped system is used [illegible] to be two complex eigenvalues [illegible] with damping ratios less than unity) and [illegible] eigenvectors (complex mode shapes). This example [illegible] because most structures are underdamped and exhibit [illegible] plex, or moving, mode shapes. Consider the model given [illegible] equation (1) with the following, coefficient matrices

$$M = \text{diag}[2.0, 3.0, 4.0, 2.0]$$

$$D = \begin{bmatrix} 6 & -2 & -4 & 0 \\ -2 & 2 & 0 & 0 \\ -4 & 0 & 6 & -2 \\ 0 & 0 & -2 & 2 \end{bmatrix} \quad K = \begin{bmatrix} 4 & -1 & 2 & 0 \\ -1 & 2 & -1 & 0 \\ -2 & -1 & 5 & -2 \\ 0 & 0 & -2 & 2 \end{bmatrix}$$

$$B = \begin{bmatrix} 1 & 0 \\ 0 & 0 \\ 0 & 0 \\ 0 & 1 \end{bmatrix}$$

The eight eigenvalues of the *open-loop* (FEM) system are calculated and presented below for comparison:

$$\{\lambda_j^*, j = 1,8\} = \{-3.2813, -0.7269, -0.7681$$
$$\pm 1.0158i, -0.0126 \pm 0.2749i, -0.2986 \pm 0.7[illegible]i\}$$

Measured Results. Next, it is assumed that the [illegible] results, are available in the form of eigenvalues and eigenvectors, that is:

Eigenvalues:

$$\{\lambda_1, \lambda_2\} = \{-1.0000 + 1.0000i, \quad 1.0000 \quad 1.00[illegible]$$

Associated Eigenvectors:

$$z_1 = \begin{bmatrix} 1.0000 \\ \\ -1.0000\text{-}0.0500i \end{bmatrix} \quad z_2 = \begin{bmatrix} 1.0000 \\ \\ 1.0000 \quad 0.0500i \end{bmatrix}$$

These eigenvalues and eigenvectors are then assigned to the above model using the proposed method to produce the following correction factors.

2(a) Results from Optimization Procedure

The resulting measurement matrices C_0 and C

$$C_0 = \begin{bmatrix} 27.4251 & -4.1599 & 0.2934 & 16[illegible] \\ 79.0766 & -0.8280 & 0.106[illegible] & [illegible] \end{bmatrix}$$

$$C_1 = \begin{bmatrix} 23.1963 & 11.8602 & [illegible] & [illegible] \\ -10.7962 & 1.2258 & [illegible] & [illegible] \end{bmatrix}$$

The modal parameters of the new system, corresponding to the measured data, are the following set of eigenvalues and eigenvectors, that is:

Eigenvalues:

$$\{\lambda_1, \lambda_2\} = \{-1.0000 + 0.9999i, -1.0000 - 0.9999i\}$$

Associated Eigenvectors:

$$v_1 \begin{bmatrix} 1.0000 \\ 0.9908 \quad 0.0868i \\ \text{xxxx} \\ \text{xxxx} \end{bmatrix} \quad v_2 = \begin{bmatrix} 1.0000 \\ -0.9908 + 0.0868i \\ \text{xxxx} \\ \text{xxxx} \end{bmatrix}$$

The new model is described by the original mass matrix and the damping and stiffness matrices that follow, that is:

$$\begin{bmatrix} 5.8095 & 2.0246 & -3.9628 & -.1777 \\ 2.0246 & 2.0000 & .0000 & .0174 \\ 3.9628 & .0000 & 6.0000 & -2.0287 \\ [illegible] & .0174 & -2.0287 & 2.9560 \end{bmatrix}$$

$$\begin{bmatrix} 4.4298 & -.9928 & -2.0011 & 1.5036 \\ .0[illegible] & 2.0000 & -1.0000 & -.0098 \\ -2.0011 & -1.0000 & 5.0000 & -2.0009 \\ 1.5036 & -.0098 & -2.0009 & 3.6639 \end{bmatrix}$$

The measures of changes of the damping and stiffness matrices are calculated and the results are presented in Table 1. Next, this procedure is iterated to improve the corrected model.

2(b) Results After Iterative Procedure

After ten iterations the modal parameters of the new system corresponding to the measured data are the following set of eigenvalues and eigenvectors:

Eigenvalues:

$$\{\lambda_1, \lambda_2\} = \{-1.0000 + 1.000i, -1.0000 - 1.0000i\}$$

Associated Eigenvectors:

$$v_1 = \begin{bmatrix} 1.0000 \\ -1.0000\text{-}0.0500i \\ \text{xxxx} \\ \text{xxxx} \end{bmatrix} \quad v_2 = \begin{bmatrix} 1.0000 \\ -1.0000 + 0.0500i \\ \text{xxxx} \\ \text{xxxx} \end{bmatrix}$$

[illegible]nal improved model is described by the original mass [illegible] and the damping and stiffness matrices that follow,

$$\begin{bmatrix} [illegible] & 2.0246 & -3.9582 & -.1991 \\ 2.0[illegible] & 2.0000 & .0126 & .0013 \\ 3.9582 & 0126 & 6.0034 & -2.0312 \\ [illegible] & .1991 & -.0013 & -2.0312 & 2.9528 \end{bmatrix}$$

and

$$K = \begin{bmatrix} 4.4391 & -1.0016 & -1.9994 & 1.5048 \\ 1.0016 & 1.9679 & -1.0037 & -.0114 \\ -1.9994 & -1.0037 & 5.0000 & -2.0009 \\ 1.5048 & -.0114 & -2.0009 & 3.6639 \end{bmatrix}$$

The measures of changes of the damping and stiffness matrices are calculated and the results are presented in Table 1. Again, the procedure for concerning an analytical model using measured modal data and an eigenstructure assignment procedure produced an improved model with modal data matching experimental observation.

[illegible]ssion of Results

[illegible] the above examples, the proposed tech-

nique successfully assigned a complete set of the experimentally obtained (simulated in this case) eigenvalues and eigenvectors. This provides a systematic method for updating analytical models by experimentally observed data. The proposed method is limited to updating or improving the stiffness matrix and the damping matrix. Some FEM practitioners believe that the mass matrix is actually a larger source of error in modeling and hence should also be changed. The current method does not allow the mass matrix to be changed but it is believed that the feedback algorithm used here could be altered to accommodate mass changes and represent future research. The proposed method does, however, address the important issue of constructing a damping matrix for the FEM which yields complex mode shapes (Inman and Jha, 1986). This represents an important improvement on standard FEM practice as the standard FEM damping matrix is proportional (yielding real mode shapes) and most measured data contains complex mode shapes. In the case where the mode shapes are not available, other pole placement techniques (Inman, 1989, Chen, 1984, Kimura, 1975, Davison, 1970, 1973, 1975) can be used for eigenvalue assignment and model improvement.

The procedure described here produces asymmetric positive definite stiffness and positive semi-definite damping matrices to adjust to an existing FEM. It does not, however, guarantee that the resulting modified stiffness and damping matrices have the same physical significance they had from the original modeling. The procedure only guarantees that the improved model yields the natural frequencies, damping ratios and mode shapes obtained from an experimental modal analysis of the modeled structures.

For a gyroscopic system described by:

$$A_1\ddot{\mathbf{q}}(t)+A_2\dot{\mathbf{q}}(t)+A_3\mathbf{q}(t)=B_0\mathbf{u}(t)$$

where A_1, A_2, and A_3 are real, asymmetric matrices, the proposed technique is a one iteration method. The optimization algorithm is skipped, since symmetry of the improved model is not required.

The proposed method does not use the orthogonality relations for normal modes (Berman, 1983, Heylen, 1986). Therefore, it can be applied to undamped, proportionally damped, as well as non-proportionally damped models.

A disadvantage of the proposed technique is the fact that additional coupling is introduced in the damping and stiffness matrices. This problem can be avoided by optimizing the objective function, using a constrained optimization algorithm and setting as constraints the coupling terms that are originally zero. This will potentially lead to a more accurate result and improvement of the model.

It should also be noted that if the experimental analysis and the finite element model [illegible] the same or very close, then the inverse [illegible] not exist. This problem is avoided by not [illegible] measured eigenvalues that are already in agreement with the analytical model (FEM). Note that the number of measured eigenvalues and eigenvectors assigned by the above process is arbitrary and up to the user. Therefore, modal data with low confidence factor need not be assigned. Likewise, measured modal data that matches the analytical data also need not be assigned. Those familiar with pole placement and eigenstructure assignment methods will recognize the possibility that the analytical eigenvalues (that matched the experimental ones) left unassigned will probably move. In that event the procedure is repeated until all those measured modes assigned high confidence are assigned to the finite element model. An introduction to using feedback control in vibration and measurement problems can be found in Inman (1989).

As a final remark, it was shown that the eigenstructure assignment method can be used to link analysis with experiment in a systematic way. Previously, the modal testing [illegible] more ad hoc and less systematic [illegible] analytical and experimental models. It [illegible] to stress that many structures and machines exhibit complex mode shapes. However, the common approach to modeling damping in finite element procedures is to assume that the damping is proportional leading to real mode shapes. The proposed approach at correcting the analytical model forces the corrected model to have complex modes as measured.

The following list summarizes this paper.

(1) A technique is developed which assigns measured modal information to a given finite element model of an existing structure by using eigenstructure assignment methods common in control theory.

(2) The approach taken is to consider the desired perturbations in stiffness and damping matrices as gain matrices in feedback control algorithms.

(3) The perturbation matrices obtained by the eigenstructure assignment technique are not necessarily symmetric. This can be overcome by using an optimization algorithm which uses the elements of the position and velocity gain matrices such that the symmetry of the new model is preserved.

(4) An iterative procedure is then applied to the improved model to ensure that the assigned modal test results are correctly assigned. Convergence of the iterative procedure is not always guaranteed.

(5) The developed technique is applicable to undamped, proportionally damped, as well as non-proportionally damped models.

(6) Further improvement of the algorithm and optimization of the objective function under coupling constraints will lead to more accurate and physically meaningful results.

Acknowledgment

This research was supported in part under grants number AFOSR-F49620-86-C-0011, AFOSR-85-0220 and NSF-MSM-8351807. The author gratefully acknowledges the helpful and constructive comments of the reviewers.

References

[illegible] and Brown, D. L., 1987, "Modal Analysis: Twenty Years [illegible] Measurement and Vibration, January, pp. 10-16.

[illegible], 1982, "Modal Control for a [illegible] Systems," *Proceedings of the* [illegible] Florida, November, pp.

[illegible], 1983, "Eigenstructure [illegible] *Transactions on Aerospace and Electronic Systems*, pp. 711-729.

[illegible], "Improvement of a Large Analytical [illegible] Vol. [illegible] pp. 1168-173

[illegible] *Theory and Design*, CBS College [illegible] Chapter 7, pp. 324-384.

[illegible], 1970, "On Pole Assignment in Linear Systems with Incomplete Feedback," *IEEE Transactions on Automatic Control*, AC-15, [illegible]

Davison, E. J. and Chow, S. G., 1973, "An Algorithm for the Assignment of Closed-Loop Poles Systems Using Output Feedback in Large Linear Multivariable Systems," *IEEE Transactions on Automatic Control*, AC-18, 1, [illegible]

Davison, E. J., and Wang, S. H., 1975, "On Pole Assignment in Linear Multivariable Systems Using Output Feedback," *IEEE Transactions on Automatic Control*, AC-20, 4, pp. 516-518.

Ewins, D. J., 1986, *Modal Testing: Theory and Practice*, Research Studies Press Ltd., England.

Fuh, J., Chen, S., and Berman, A., 1984, "System Identification of Analytical Models of Damped Structures," AIAA Structures, SDM Conference, Paper 84-0926, Palm Springs, California, May, pp. 112-116.

[illegible], W., 1982, "Optimization of Model Matrices By Means of Experimentally Obtained Dynamic Data," *Proceedings of the 1st International* [illegible] *Conference*, Orlando, Florida, November, pp. 32-38.

Inman, D. J., 1989, *Vibration with Control, Measurement and Stability*, Prentice-Hall, Inc., Englewood Cliffs, NJ.

Inman, D. J., and Jha, S. K., 1986, "Identification of a Damping Matrix for Tires," *Proceedings of the 4th International Modal Analysis Conference*, February, Vol. II, pp. 1078-1080.

Juang, J. N., and Pappa, R. S., 1985, "An Eigensystem Realization Algorithm (ERA) for Modal Parameter Identification and Model Reduction," *AIAA Journal of Guidance, Control and Dynamics*, Vol. 8, 5, Sept.-Oct., pp. 620-627.

Kammer, D. C., 1987, "An Optimum Approximation for Residual Stiffness in Linear System Identification," AIAA, SDM Conference, Paper 87-0911, pp. 277-287.

Kimura, H., 1975, "Pole Assignment by Gain Output Feedback," *IEEE Transactions on Automatic Control*, AC-20, 4, pp. 509-516.

Minas, C., and Inman, D. J., 1988, "Correcting Finite Element Models with Measured Modal Results using Eigenstructure Assignment Methods," *Proceedings of the 6th International Modal Analysis Conference*, Orlando, Florida, February, pp. 583-587.

Shames, I. H., and Dym, C. L., 1985, *Energy and Finite Element Methods in Structural Mechanics*, Hemisphere Publishing Corp., Chapter 16, pp. 643-657.

Srinathkumar, S., 1978, "Eigenvalue/Eigenvector Assignment using Output Feedback," *IEEE Transactions on Automatic Control*, AC-23, 1, pp. 79-81.

Stasa, F. L., 1985, *Applied Finite Element Analysis for Engineers*, CBS Publishing, Chapter, 10, pp. 577-618.

MODELING OF A SLEWING MOTOR-BEAM SYSTEM

Jy-Jen Sah
Graduate Student

and

Roger W. Mayne
Professor

Department of Mechanical and Aerospace Engineering

State University of New York at Buffalo

Buffalo, NY 14260

ABSTRACT

A model for slewing motor-beam systems is described in this paper based on a finite element beam representation modified to include a dynamic model of a DC motor as the actuator. The system model is in state equation form and by including the effect of actuator-load interaction, can closely represent the physical system. The beam model is placed in moving coordinates to eliminate the rigid body mode and is connected to the motor drive by a clamped boundary condition in its local coordinates. The overall response of the system shows that the effective beam boundary conditions in a global sense depend on the motor parameters and can vary from pinned-free to clamped-free. The overall system damping also depends on various motor-beam interaction. Several examples are presented to illustrate the varying nature of the system modes and to show that with proper selection of motor parameters, damping of the first few system modes may be increased by motor-beam interaction.

INTRODUCTION

Slewing structures are used in a wide variety of industrial applications and in space structures. Due to the angular motion involved, the dynamic behavior is more complicated than that of similar translational systems and, for a flexible structure attached to an actuator, it is important to take actuator-structure interaction into consideration when constructing the mathematical model. This model, either continuous or discrete, may then closely represent the actual physical system. However, if the interaction is not considered, the dynamic response of the mathematical model may be biased, and will be accurate only when actuator interaction is negligible or weak.

The most popular approach in slewing structure modeling is the modal model approach (Juang, 1986, Hasting, 1987, Fukuda, 1985, Cannon, 1984). With this approach, the eigenstructure of the structural system must be obtained prior to considering actuator interaction. Certain difficulties may arise with this approach. First, for complex structures, for instance a three dimensional truss, the analytical eigenvalues and eigenvectors are almost impossible to obtain. Thus, a discrete method such as the finite element method is more appropriate to determine the mode shapes and natural frequencies of the system. Second, the eigenstructure of a flexible structure is obtained for given boundary conditions. With the structure attached to an actuator, the boundary conditions become unclear. Some researchers have noted the typical clamped boundary condition at the base of the slewing structure and have assumed clamped-free modes for the analysis. However, unless the actuator is powerful enough to dominate the slewing motion with negligible beam interaction, this assumption is not generally appropriate. An improved modal model considering the modal participation factor for the actuating torque has been proposed by Garcia (1989). This representation can include part of the actuator-structure interaction, but still is restricted to very basic flexible structures, for example, a simple beam.

Slewing structure modeling by the finite element method (FEM), utilizes a physical coordinate system throughout the modeling process (Bayo, 1987, Usoro, 1986). However, FEM is not naturally capable of modeling generalized active elements and the mutual interactions between active and passive system elements. Rigid body motions also complicate FEM modeling and require special considerations. In this paper, a modified FEM model is suggested for a DC motor-simple beam system. This idea can be extended to any type of structure, as long as it can be expressed in an FEM model, and any actuator that can be expressed in state equation format. The coupling of the two sub-systems is considered when the mathematical model for the overall system is constructed. This approach has the following advantages, (a) it stays in physical coordinates, (b) it can be applied to any structure and actuator, (c) it implicitly matches the boundary conditions of the structure to the actuator, (d) the effects of actuator-load interactions are included and (e) the mathematical model is in a simple state equation format. Since the system is represented in state equation form (first order differential equations) which are expanded from the FEM model (second order differential equations) combined with the actuator representation, the matrix size necessary to describe the system is approximately doubled. This may not be a severe problem for many applications.

Numerical results using a DC motor and a simple beam with different gear ratios are presented in the discussion below. The transient response of this system is studied to understand the role that interaction plays in the overall system character. Eigenanalysis of various motor-beam slewing systems has been performed and results are presented here which show system characteristics bounded by clamped-free and pinned-free beam behavior. Results for transient response and eigenvalue analysis of

the motor-beam system also show that damping can be provided by natural interaction of the structure and actuator without relying on structural damping.

MATHEMATICAL MODEL

Consider a flexible beam driven by a DC motor through a gear set with speed ratio r as shown in Figure 1.

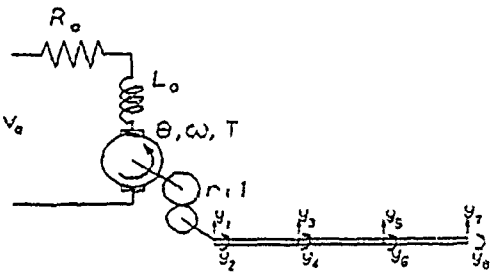

Figure 1
Motor-Beam System Schematic Diagram

Two coordinate systems are used in the model. The first is the coordinate system for the DC motor, which is an angular coordinate system. The second is the beam's nodal coordinates which are defined with respect to the rigid body motion of the beam and are aligned with the motor's angular coordinate. The coordinate system describing the motion of the motor and beam is shown in Figure 2.

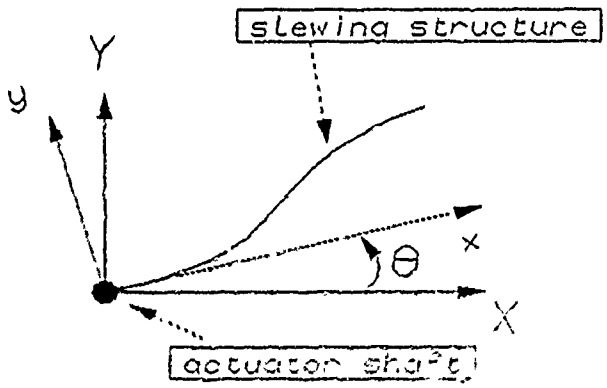

Figure 2
Coordinates Used in the Motor-Beam System

By defining the coordinate system as described in Figure 2, the rigid body motion of the beam is extracted. The boundary conditions of the beam in its local coordinate system can be legitimately specified as "clamped" on the motor shaft. It should be noted that the "clamped-free" boundary condition is viewed from the local coordinates, i.e., if a camera is mounted rigidly on the motor shaft and pointed toward the beam tip, clamped-free motion will be observed. However, in a global sense, the beam does not have clamped-free mode shapes.

A DC motor is an electro-mechanical device that can be expressed by a linearized state equation set including its electrical and mechanical components as (Kuo, 1987)

$$L_a \frac{di}{dt} = V - iR_a - K_b\omega \qquad (1)$$

$$J_m \frac{d\omega}{dt} = K_m i - b_m\omega - T(t) \qquad (2)$$

where L_a and R_a are the electrical inductance and resistance

K_b is the back EMF coefficient

K_m is the torque constant

J_m and B_m are the inertia and friction of the rotor

$T(t)$ is the reaction torque or load due to the vibration of the beam

Assuming that there is no structural damping, the FEM representation for the beam with n elements is described in Figure 3 and the governing equations are

$$M\ddot{Y} + KY = F \qquad (3)$$

where M and K are (2n+2)x(2n+2) inertia and stiffness matrices, and the excitation vector F is (2n+2)x1. The forcing functions can be split into two parts. The first part is due to the angular acceleration of the motor and the inertia of the beam, and may be called an implicit forcing function. Other externally applied forces and torques not related to the motor would be explicit forcing functions but are not specifically considered in this discussion.

The boundary conditions of the beam in beam's local coordinates are

$$y(t,0) = y_x(t,0) = 0$$

or, in the FEM representation,

$$y_1(t) = y_2(t) = 0 \qquad (4)$$

Because of the boundary conditions, we can reduce the size of the model by partitioning the M and K matrices as

$$M = \begin{bmatrix} M_{r1} & M_{r2} \\ M_{s1} & M_{s2} \end{bmatrix} \qquad K = \begin{bmatrix} K_{r1} & K_{r2} \\ K_{s1} & K_{s2} \end{bmatrix} \qquad (5)$$

where M_{r1} and K_{r1} are 2x2 matrices while M_{s2} and K_{s2} are 2nx2n matrices. Y is also partitioned as $Y = [Y_r^T \quad Y_s^T]^T$ where $Y_r = [y_1 \quad y_2]^T$ and $Y_s = [y_3 \quad y_4 \cdots y_{2n+2}]^T_{2n\times 1}$. Since Y_r is defined by the boundary conditions (4), only Y_s is unknown and the dynamic equations for the beam reduce to

$$M_{s2}\ddot{Y}_s + K_{s2}Y_s = F_s \qquad (6)$$

where F_s is the corresponding sub-vector of F.

The reaction force R_f and torque R_t on node 1 are obtained by solving

$$\begin{bmatrix} R_f \\ R_t \end{bmatrix} = M_{r2}\ddot{Y}_s + K_{r2}Y_s \qquad (7)$$

Since just slewing motion is considered, only the torque will react with the motor and

$$R_t = M_r\ddot{Y}_s + K_rY_s \qquad (8)$$

where M_r and K_r are sub-matrices of M_{r2} and K_{r2} corresponding to R_t. The effective torque transmitted to the motor through the gears

$$T(t) = r \cdot R_t(t) \qquad (9)$$

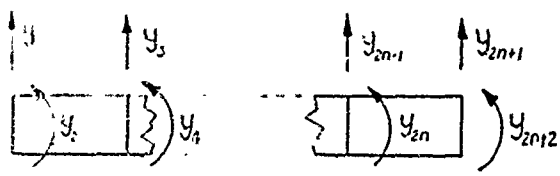

Figure 3
Coordinate Sysyem for Finite Element Beam Model

Substituting (9) into (2) yields

$$J_m \frac{d\omega}{dt} = K_m i - B_m \omega - r(M_r \ddot{Y}_s + K_r Y_s) \tag{10}$$

Also, rearranging (6) results in

$$\ddot{Y}_s = M_{22}^{-1} F_s - M_{22}^{-1} K_{s2} Y_s \tag{11}$$

It was assumed that only the implicit forcing function due to angular acceleration exists in this system, and such forcing functions are proportional to the angular acceleration of the motor. Thus the implicit force $F_s = -r\hat{F}_s \cdot \frac{d\omega}{dt}$ where $\hat{F}_s$ depends only on beam dimensions and material properties. This can be obtained directly from the beam description without any knowledge of the DC motor. Combining (10) and (11) yields

$$\frac{d\omega}{dt} = \frac{K_m}{J_c} i - \frac{B_m}{J_c}\omega - \frac{r}{J_c}(-M_r M_{22}^{-1} K_{s2} + K_r) Y_s \tag{12}$$

where $J_c = J_m - r^2 M_r M_{22}^{-1} \hat{F}_s$.

Defining the state variables for the beam as $X_1 = Y_s$ and $X_2 = \dot{X}_1 = \dot{Y}_s$, and substituting these definitions and (12) into (11), the derivative equation (11) becomes

$$\dot{X}_2 = -M_{22}^{-1}\hat{F}_s \frac{rK_m}{J_c} i + M_{22}^{-1}\hat{F}_s \frac{rB_m}{J_c}\omega \tag{13}$$

$$+\left[-M_{22}^{-1}K_{s2} + \frac{r^2}{J_c} M_{22}^{-1}\hat{F}_s(-M_r M_{22}^{-1} K_{s2} + K_r)\right] X_1$$

Combining (1), (12) and (13) along with $\dot{X}_1 = X_2$, we can represent the system in the state equation format

$$\dot{X} = AX + BU \tag{14}$$

where

$$X = [\omega \quad i \quad X_1^t \quad X_2^t]^t$$

$$U = v_a$$

$$A = \begin{bmatrix} -\frac{B_m}{J_c} & \frac{K_m}{J_c} & -\frac{r}{J_c}(-M_r M_{22}^{-1} K_{s2} + K_r) & 0 \\ -\frac{K_b}{L_a} & -\frac{R_a}{L_a} & 0 & 0 \\ 0 & 0 & 0 & I \\ M_{22}^{-1}\hat{F}_s \frac{rB_m}{J_c} & -M_{22}^{-1}\hat{F}_s \frac{rK_m}{J_c} & -M_{22}^{-1}K_{s2} + \frac{r^2}{J_c} M_{22}^{-1}\hat{F}_s(-M_r M_{22}^{-1} K_{s2} + K_r) & 0 \end{bmatrix} \tag{15}$$

and

$$B = \begin{bmatrix} 0 \\ \frac{1}{L_a} \\ 0 \\ 0 \end{bmatrix} \tag{16}$$

The above equations represent the dynamic characteristics of an interacting slewing motor-beam system. In systems containing different type of actuators or more complex structures, a similar approach may be applied to the model. The beam and motor parameters are scattered through matrix A, these terms represent the interactions between the motor and beam. Several transient and frequency response results for a motor-beam system with different gear ratios are presented below. These examples show that the interaction between the motor and beam changes the boundary conditions of the beam and affects damping of the overall system

NUMERICAL RESULTS

Numerical evaluations of a motor-beam system can be carried out by integrating (14) numerically for transient response, or by finding the eigenvalues of A in (15) for frequency analysis. In this section, an open-loop system with an Electro-Craft E586 DC servo motor and an aluminum beam is considered. Their specifications are listed in Table 1 and Table 2.

K_m	5.5158×10^{-2} N•M/A
K_g	5.8 V/krpm
R_a	1.1 Ω
J_m	3.889×10^{-5} Kg•M^2
L_m	2.3 mH
B_m	7.071×10^{-4} N•M/krpm

Table 1
Motor Parameters

Length	0.9144 M
Width	3.81×10^{-2}
Thickness	1.5875×10^{-3}M
Density	2700 Kg/M^3
Elastic Modulus	7.2568×10^{10} N/M^2

Table 2
Beam Parameters

The DC motor and the aluminum beam are connected through a set of gears, and the system is assumed to have zero initial conditions. A unit step voltage drives the DC motor for $t \geq 0$. Two state variables are monitored, angular velocity of the motor and tip displacement of the beam with respect to the rigid body motion. Figures 4(a) and (b) show the response of the system for unity gear ratio. Figure 4(a) shows the plot of motor angular velocity vs. time. Apparently at t = 5s the system has not reached steady state velocity. The oscillations on the curve indicate that the vibration of the beam is interacting with the motor. Also, from Figure 4(b), there are signs that the motor has influence on the beam. First, the tip displacement of the beam is negative for the time period shown. This results because the motor is accelerating and the inertia of the beam produces an overall beam deflection during the acceleration. The second observation is that even without structural damping in the FEM representation, damping occurs in the motor-beam system since the peak-to-peak amplitude of tip displacement is decaying. This suggests that the structure can gain damping through the structure-actuator interaction.

In order to further explore the interactions between the motor and the beam, different gear ratios are considered for the system. In Figure 4, with a gear ratio equal to unity the motor provides only modest torque to drive the beam, thus the response is slow. With a decreased gear ratio, driving torque for the slewing beam is increased by $1/r$ and this increases the dynamic response speed. Figures 5 and 6 present the transient response of the system with r=0.1 and r=0.01 respectively subject to the same unit step input. In Figure 5(a), it can be seen that the speed of response has been increased significantly, with settling time[1] $t \approx 0.5$s. The influence of the vibration of the beam can still be seen in the transient for $t <$ 1.5s. Figure 5(b) shows the tip displacement of the beam. Noticeable differences between r=1 and r=0.1 can be observed. The maximum tip displacement for r=0.1 in Figure 5(b) is larger than that of r=1 because the starting torque is 10 times larger. The first system mode in the r=0.1 case possesses more damping than the r=1 case, as the peak-to-peak amplitude decays faster. This also yields a faster settling time for the tip motion with r=0.1. Also, the system's natural frequencies are different for the two gear ratios, this can be further considered by looking at the eigenvalues of each system.

1 settling time defined here is ±5% of steady state value

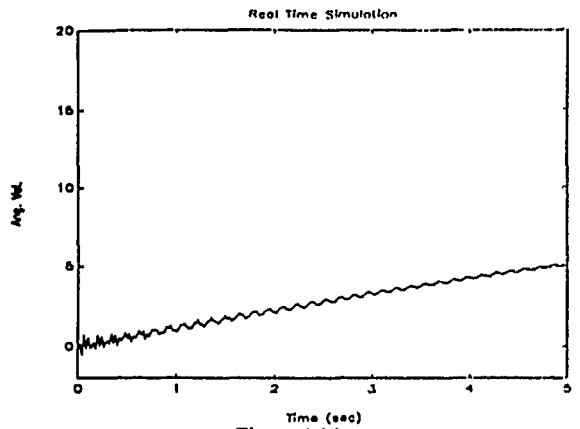

Figure 4 (a)
Motor Angular Velocity (rad/sec) for gear ratio r=1

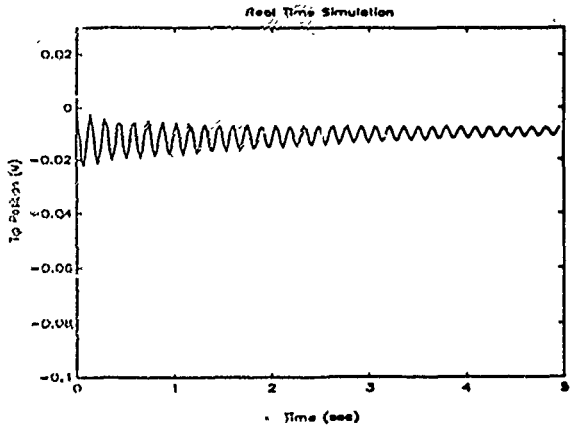

Figure 4 (b)
Beam tip displacement with respect to rigid body motion in (M) for gear ratio r=1

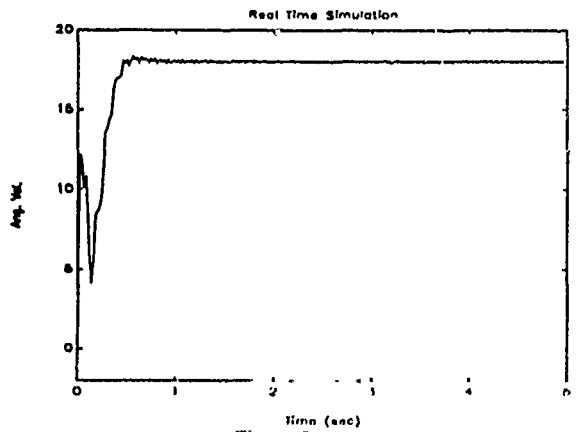

Figure 5 (a)
Motor Angular Velocity (rad/sec) for gear ratio r=0.1

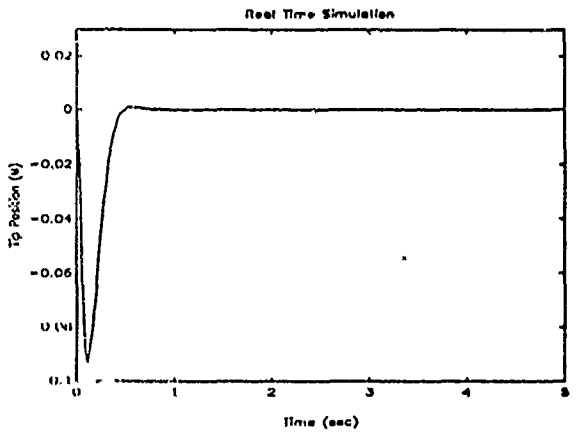

Figure 5 (b)
Beam tip displacement with respect to rigid body motion in (M) for gear ratio r=0.1

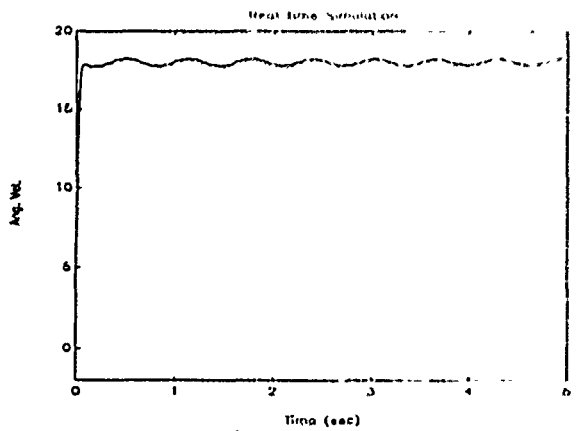

Figure 6 (a)
Motor Angular Velocity (rad/sec) for gear ratio r=0.01

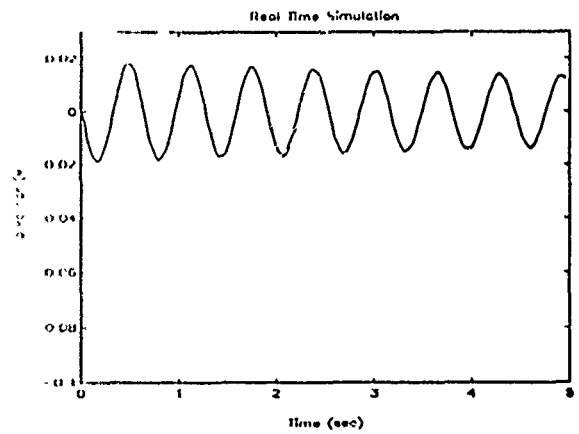

Figure 6 (b)
Beam tip displacement with respect to rigid body motion in (M) for gear ratio r=0.01

In the two previous examples, it can be seen that a gear ratio reduction can yield a faster, better-damped dynamic system. In Figure 6, the same motor and beam are considered with the further gear ratio reduction to r=0.01, which again intensifies the driving torque as it reduces the driving speed. The angular velocity in Figure 6(a) shows that the settling time has been further reduced, however, the first system mode is no longer well damped and the system is not in steady state at the end of the simulation. The motor response is generally complete before $t \approx 0.5$s but oscillations in the shaft speed persist because of the continuning beam vibration. In Figure 6(b), it is clear that the initial acceleration of the motor initiates the beam vibration. Due to the low gear ratio the starting angular acceleration of the beam is lower and this reduces the magnitude of the tip displacement. The beam vibration is only lightly damped and causes the motor angular velocity to oscillate slightly about its steady-state. This system has the potential for a fast transient response but has light damping because of limited motor-beam interaction.

The fact that different gear ratios on the same motor/beam system will yield different dynamic behavior can also be seen in the frequency domain. Eigenvalues, natural frequencies and damping ratios are listed in Table 3 for the various gear ratios.

i^{th} mode	λ_i	ω_i (Hz)	ξ_i (%)
1	$-0.3320 \pm 43.0297\,i$	6.8486	0.771
2	$-1.2615 \pm 135.8777\,i$	21.6265	0.928
3	$-3.2642 \pm 271.6337\,i$	43.2349	1.202

Table 3 (a)
Eigenvalues, Natural Frequencies and Damping Ratios for r=1

i^{th} mode	λ_i	ω_i (Hz)	ξ_i (%)
1	$-9.7357 \pm 6.8014\,i$	1.8902	81.977
2	$-5.9619 \pm 65.9479\,i$	10.5387	9.004
3	$-1.3345 \pm 179.3217\,i$	28.5407	0.744

Table 3 (b)
Eigenvalues, Natural Frequencies and Damping Ratios for r=0.1

i^{th} mode	λ_i	ω_i (Hz)	ξ_i (%)
1	$-0.0703 \pm 9.9318\,i$	1.5807	0.708
2	$-0.0485 \pm 62.4264\,i$	9.9355	0.078
3	$-0.0129 \pm 176.3269\,i$	28.0633	0.007

Table 3 (c)
Eigenvalues, Natural Frequencies and Damping Ratios for r=0.01

It can be seen that the variation in gear ratio changes the eigenstructures of the system. To explain this effect, the boundary conditions of the beam should be considered. Pinned-free and clamped-free natural frequencies of the beam are shown in Table 4.

With high gear ratio, the motor can give little torque to drive the beam, however, the vibration of the beam can turn the motor shaft easily. This situation is very similar to the boundary condition of a pinned-free beam. On the other hand, when the gear ratio is low, the motor is dominating the slewing motion while the beam's

i^{th} mode	Clamped-Free Natural Frequency (Hz)	Pinned-Free Natural Frequency (Hz)
1	1.5756	6.8934
2	9.8477	22.3811
3	27.6182	46.5526

Table 4
Natural Frequencies of Clamped-Free and Pinned-Free Beam

vibration hardly influences the transient of the motor. This situation is similar to the clamped-free boundary condition. Comparing Table 3 and Table 4, it can be found that the system's natural frequencies lie between the pinned-free and clamped-free natural frequencies of the beam, depending on the gear ratios, as shown in Table 5

Mode	Clamped-Free	r=0.01	r=0.1	r=1	Pinned-Free
1	1.5756	1.5807	1.8902	6.8486	6.8934
2	9.8477	9.9355	10.5387	21.6265	22.3811
3	27.6182	28.0633	28.5407	43.2349	46.5526

Table 5
Comparisons of Natural Frequencies Between Different Boundary Conditions

From the examples above, depending upon the motor parameters, a particular beam can gain various amounts of damping from motor-beam interaction in open loop. By tuning the gear ratio alone in the above system, the first mode damping ratio reaches a value of 81.977% at r=0.10 (Table-3b). Best damping effect may possibly achieved with a more careful selection of r. If further damping is required, full tuning of the motor parameters and gear ratio may approach critical damping of the first mode. When a closed-loop controller is to be designed, various feedback signals and feedbackgains may be considered for the control loop. If all the states are not available for feedback, full eigenstructure assignment becomes impossible. Controlling such a system with available output feedback may depend heavily on the open-loop characteristics of the system. A well designed open-loop system, in such situation, can help provide inherent damping and improve the closed-loop system performance.

CONCLUSIONS

This model, in general, demonstrates a precise model for a motor-beam system and considers the interactions between the actuator and load. It can be treated as a foundation for designing closed-loop systems based on traditional control strategies, optimal control or design optimization. Furthermore, many structures with interacting actuator dynamics can be modeled by a similar approach. In this study both the motor and the beam are modeled as linear systems, the coupled system is also linear, as matrix A is a matrix of constants. When modeling non-linear systems, the above procedures are still valid with the exception that the coupled system should be expressed in the form of $\dot{X} = f(x,u,t)$. As with all non-linear models, frequency domain studies can not be performed in general, but the transient responses can still be obtained by integrating the non-linear state equations. Explicit forcing functions, which are externally applied, can be added to the model by including appropriate terms in the B matrix if the applied forces/moments do not have dynamic interactions with the system. Otherwise, each external actuator needs to be considered separately.

As presented above, appropriate design of the motor may change the eigenstructure of the system, and may enhance damping of the system through motor-beam interactions. When a more stable open-loop system is desired, analysis and perhaps optimization

of actuator-load interactions should be considered to select the most suitable motor to drive the beam including dynamic interaction as well as power and torque requirements. The boundary conditions of the beam also change for the slewing systems as the motor or gear ratio is changed. This suggests that in many situations the assumption of clamped-free boundary conditions may be questionable.

REFERENCES

Juang,J.N., L.G. Horta, H.H. Robertshaw, 1986,"A Slewing Control Experiment for Flexible Structures" J. of Guidance, Vol.9, No.5.

Hasting, G.G., W.J. Book, 1987,"A Linear Dynamic Model for Flexible Robotic Manipulators" IEEE Control Systems Magazine, Feb.

Fukuda, T "Flexible Control of Elastic Robotic Arms, 1985, " J. of Robotic Systems Vol.2, No.1.

Cannon, R.H.,Jr., E. Schmitz, 1984, "Initial Experiments on the End-Point Control of a Flexible One-Link Robot" Int'l Journal of Robotics Research, Vol.3, No.3.

Garcia, E., 1989, "On the Modeling and Control of Slewing Flexible Structures" Ph.D. Dissertation, SUNY at Buffalo.

Bayo, E., 1987, "A Finite Element Approach to Control the End-Point Motion of a Single-Link Flexible Robot" J. of Robotic System, Vol.4, No.1.

Usoro, P.B., R.Nadira, S.S. Mahil, 1986, "A Finite Element/Lagrange Approach to Modeling Lightweight Flexible Manipulators" J. of Dynamic Systems, Measurement and Control, Vol.108, No.3.

Kuo, B.C., 1987, Automatic Control Systems, Fifth Edition, Prentice Hall.

Shames, I.H., C.L. Dym, 1985, Energy and Finite Element Methods in Structural Mechanics, McGraw Hill

Enhanced Realization/Identification of Physical Modes

By Michael J. Roemer,[1] Member, ASCE, and D. Joseph Mook[2]

Abstract: Physical structures are often sufficiently complicated to preclude constructing an accurate mathematical model of the system dynamics from simple analysis using the laws of physics. Consequently, determination of an accurate model requires utilization of (generally noisy) output measurements from dynamic tests. In this paper, we present a robust method for constructing accurate, structural-dynamic models from discrete time-domain measurements. The method processes the measurements in order to determine the number of modes present, the damping and frequency of each mode, and the mode shape. The structure may be highly damped. Although the mode-shape identification is more sensitive to measurement noise than the order, frequency, and damping identification, the method is considerably less sensitive to noise than other leading methods. Accurate detection of the modal parameters and mode shapes is demonstrated for modes with damping ratios exceeding 15%.

Introduction

The enduring problem of accurately identifying the mode shapes of structures and/or systems using (noisy) output measurements is of significant importance in several aspects of mechanical and aerospace engineering. For example, the structural community has expended considerable effort attempting to correctly identify modal properties of flexible structures (Hendricks 1984; Ibrahim and Mikulcik 1977; Rajaram and Junkins 1985; Chen 1983). However, mode-shape identification methods are very sensitive to measurement noise, and lose accuracy in high measurement noise circumstances. Addressing this problem, the paper develops an algorithm that aids in accurately identifying mode shapes of a structure from output measurements. The algorithm combines a recently developed identification/realization technique with a method of model-error reduction to successfully identify mode shapes even with high noise levels in the measurements. Note, modal properties refers to: (1) Natural frequencies and damping ratios; and (2) mode shapes.

Recently, the eigensystem realization algorithm (ERA) was developed by Juang and Pappa (Juang and Pappa 1985; Pappa and Juang 1985). The algorithm was developed for the realization and identification of minimum-order structural dynamic models. The ERA technique is based on the singular value decomposition of a generalized Hankel matrix, composed of discrete, time-domain measurements. In theory, the order of the realized model is determined from the number of nonzero singular values computed from the Hankel matrix decomposition. However, due to the real world presence of noise in the output measurements, the decomposition produces nonzero singular values that should, in theory, be zero. Consequently, the user must choose a cutoff magnitude of singular values, below which the singular values are assumed to be due to noise and not due to extra order in the model. In a paper extending their original work, Juang and Pappa (1986) study the effects of singular value truncation. Their results show that the choice of singular value cutoff affects the number of modes retained in the realization and the accuracy of the modal properties identified. Choosing a low cutoff produces a model that includes more modes than the true number, and results in reduced accuracy of the identified modal properties. Conversely, choosing a high cutoff results in a lower order model (some real modes are truncated), but more accurately identifies the modal properties of the retained modes. Therefore, the difficult choice of an appropriate cutoff magnitude, when a high degree of noise is present, is of great importance for accurate mode shape identification.

The ERA technique is capable of accurately identifying modal properties for cases involving perfect or low-noise measurements. The procedure of singular value decomposition, as opposed to transfer function analysis, has the benefit of good numerical stability (Klema and Laub 1980), and the ERA is accurate and simple to implement. However, difficulties may arise when high noise levels are present in the output measurements.

Reducing the noise sensitivity of the eigensystem realization algorithm was investigated by Roemer and Mook (1989a), whose results were based on the simulation of a structure with a three-mode truth. Given a highly noisy measurement set (20% deviation from the truth), their combined ERA/MME algorithm demonstrated significant improvements in the identification of the structure's natural frequencies as well as model order determination. However, they did not attempt to derive any results for improving upon the identification of the physical mode shapes of the structure. Damping was also excluded from their simulated structure.

In this paper, we develop an algorithm, via noise reduction in the measurements, that is less sensitive to measurement noise and can identify mode shapes accurately. Also, the algorithm demonstrates the ability to identify mode shapes of structures including significant damping. The combined results reveal that mode-shape identification is much more dependent on measurement noise than identification of natural frequencies, yet may still be significantly enhanced by combining the ERA and MME procedures.

Eigensystem Realization Algorithm

The basic development of the state-space realization concept is attributed to Ho and Kalman (1965), who introduced the principle of minimum-order realization. The Eigensystem Realization Algorithm (ERA) utilizes singular value decomposition to develop a method of minimum-order realization. The ERA algorithm has been successfully applied to realization/identification of several structures from experimental data (Pappa and Juang 1985). We now give a summary of the algorithm.

Consider the discrete-time linear time-invariant dynamic equation

$$\mathbf{x}(k+1) = \mathbf{A}\mathbf{x}(k) + \mathbf{B}\mathbf{u}(k) \quad \ldots\ldots (1)$$

$$\mathbf{y}(k) = \mathbf{C}\mathbf{x}(k) \quad \ldots\ldots (2)$$

[1]Grad. Res. Asst., Dept. of Mech. and Aerospace Engrg., State Univ. of New York at Buffalo, Buffalo, NY 14260.
[2]Asst. Prof., Dept. of Mech. and Aerospace Engrg., State Univ. of New York at Buffalo, Buffalo, NY.

Note. Discussion open until September 1, 1990. To extend the closing date one month, a written request must be filed with the ASCE Manager of Journals. The manuscript for this paper was submitted for review and possible publication on July 10, 1989. This paper is part of the *Journal of Aerospace Engineering*, Vol. 3, No. 2, April, 1990. ©ASCE, ISSN 0893-1321/90/0002-0122/$1.00 + $.15 per page. Paper No. 24566.

where $\mathbf{x}$ is the $n \times 1$ state vector, $\mathbf{u}$ is the $p \times 1$ input vector, $\mathbf{y}$ is the $q \times 1$ output vector; and $\mathbf{A}$, $\mathbf{B}$, and $\mathbf{C}$ are $n \times n$, $n \times p$, and $q \times n$ constant matrices, respectively. Two special solutions for Eqs. 1 and 2 are given by Markov parameters as the impulse response,

$$\mathbf{Y}(k) = \mathbf{C}\mathbf{A}^{k-1}\mathbf{B} \quad \text{(3)}$$

and the initial state response,

$$\mathbf{Y}(k) = \mathbf{C}\mathbf{A}^{k}[\mathbf{x}_1(0)\ \mathbf{x}_2(0) \ldots \mathbf{x}_i(0) \ldots \mathbf{x}_p(0)] \quad \text{(4)}$$

where $\mathbf{x}_i(0)$ represents the ith set of initial conditions. The ERA begins by forming the $r \times s$ block matrix

$$\mathbf{H}(k-1) = \begin{pmatrix} \mathbf{Y}(k) & \mathbf{Y}(k+m_1) & \cdots & \mathbf{Y}(k+m_{s-1}) \\ \mathbf{Y}(k+l_1) & \mathbf{Y}(k+l_1+m_1) & \cdots & \mathbf{Y}(k+l_1+m_{s-1}) \\ \vdots & \vdots & \ddots & \vdots \\ \mathbf{Y}(k+l_{r-1}) & \mathbf{Y}(k+l_{r-1}+m_1) & \cdots & \mathbf{Y}(k+l_{r-1}+m_{s-1}) \end{pmatrix} \quad \text{(5)}$$

where r and s are arbitrary integers satisfying the inequalities $rq \geq n$, $sp \geq n$, and l_i ($i = 1, 2, \ldots, r-1$) and m_j ($j = 1, 2, \ldots, s-1$) are arbitrary integers. For the initial-state response measurements, $\mathbf{H}(k-1)$ is replaced by $\mathbf{H}(k)$. From Eqs. 3–5 it can be shown that

$$\mathbf{H}(k) = \mathbf{V}_r\mathbf{A}^k\mathbf{W}_s \quad \text{(6)}$$

where

$$\mathbf{V}_r = \begin{pmatrix} \mathbf{C} \\ \mathbf{C}\mathbf{A}^{l_1} \\ \vdots \\ \mathbf{C}\mathbf{A}^{l_{r-1}} \end{pmatrix}$$

$$\mathbf{W}_s = \begin{pmatrix} \mathbf{B} \\ \mathbf{A}^{m_1}\mathbf{B} \\ \vdots \\ \mathbf{A}^{m_{s-1}}\mathbf{B} \end{pmatrix}^T$$

$\mathbf{V}_r$ and $\mathbf{W}_s$ are generalized observability and controllability matrices. The ERA is derived by using singular value decomposition for $\mathbf{H}(0)$, defined by

$$\mathbf{H}(0) = \mathbf{P}\mathbf{D}\mathbf{Q}^T \quad \text{(7)}$$

where $\mathbf{P}$ and $\mathbf{Q}$ are $rq \times n$ and $sp \times n$ isometric matrices, respectively, and $\mathbf{D}$ is a diagonal matrix, for which diagonal elements are the positive singular values. The rank n of $\mathbf{H}(0)$ is determined by testing the singular values for zero, i.e., by choosing the cutoff magnitude below which the singular values are assumed to represent noise and not modes. The reduced-order realization of dimension n can be constructed by forming

$$\mathbf{A}^k = \mathbf{D}_n^{-1/2}\mathbf{P}_n^T\mathbf{H}(k)\mathbf{Q}_n\mathbf{D}_n^{-1/2} \quad \text{(8)}$$

$$\mathbf{B} = \mathbf{D}_n^{1/2}\mathbf{Q}_n^T\mathbf{E}_p \quad \text{(9)}$$

$$\mathbf{C} = \mathbf{E}_q^T\mathbf{P}_n\mathbf{D}_n^{1/2} \quad \text{(10)}$$

where $\mathbf{P}_n$ and $\mathbf{Q}_n$ are formed from the first n columns of $\mathbf{P}$ and $\mathbf{Q}$, $\mathbf{D}_n$ is an $n \times n$ left upper block matrix, $\mathbf{E}_p^T$ is $[\mathbf{I}_p, \mathbf{0}]$, and $\mathbf{E}_q^T$ is $[\mathbf{I}_q, \mathbf{0}]$, where $\mathbf{I}_p$ and $\mathbf{I}_q$ are identity matrices of order p and q, respectively, and $\mathbf{0}$ is the zero matrix of appropriate dimensions.

Finally, from the eigensolution of the realized state-space matrix $\mathbf{A}^k$, the modal damping ratios and damped natural frequencies are calculated from the real and imaginary parts of the eigenvalues, after transformation from the z to s plane using the relationship

$$s = \frac{\ln(z) \pm i2k\pi}{(\Delta\tau)}; \qquad i = \sqrt{-1}$$

where z = eigenvalues of $\mathbf{A}^k$. The mode shapes are then calculated using the matrix

$$\mathbf{E}_q^T\mathbf{P}_n\mathbf{D}_n^{1/2}\Psi$$

where Ψ = eigenvector matrix of $\mathbf{A}^k$.

Minimum Model Error Estimation

The idea of filtering noise from measurement data is certainly not unique. Various versions of Kalman filters and other similar algorithms have been extensively studied and implemented (Gelb 1974; Lewis 1986). A major problem with utilizing traditional filter algorithms is that they require accuracy in the assumed model for the measured signal. In the case of structural realization/identification, the object of the work is to obtain this model. Therefore, while it is possible that judicious use of a filter-smoother algorithm may benefit the ERA, we have not pursued this approach because of the theoretical modeling difficulties just mentioned.

Recently, a new approach for performing optimal state estimation in the presence of significant model error has been developed (Mook and Junkins 1988). The new technique, called minimum model error (MME) estimation, does not assume that the model error is a white noise of known covariance, as do the filters. Instead, the model error is assumed to be an unknown quantity and is estimated as part of the solution. The theoretical advantages of this assumption are significant for the present problem, since the model is unknown a priori. In several previous studies, the MME has been shown to produce state estimates of high accuracy for problems involving both significant model error and significant measurement error (Mook and Lin 1987; Mook 1988; Junkins and Mook 1985). A brief derivation of the minimum model error estimation technique follows.

Given a system with state vector dynamics modeled by the (linear or nonlinear) system of equations,

$$\dot{\mathbf{x}} = \mathbf{f}[\mathbf{x}(t), \mathbf{u}(t), t] \quad \text{(11)}$$

where $\mathbf{x} = n \times 1$ state vector; $\mathbf{f} = n \times 1$ vector of model equations; $\mathbf{u} = p \times 1$ vector of forcing terms, and given a set of discrete measurements modeled by the (linear or nonlinear) system of equations,

$$\bar{\mathbf{y}}(t_j) = \mathbf{g}_j[\mathbf{x}(t_j), t_j] + \mathbf{v}_j, \qquad j = 1, \ldots, m \quad \text{(12)}$$

where $\bar{\mathbf{y}}(t_j) \equiv r \times 1$ measurement set at t_j; $\mathbf{g} = r \times 1$ measurement model

equations; $\mathbf{m} \equiv$ total number of measurement sets; $\mathbf{v}_j \equiv r \times 1$ measurement error vector; and where $\mathbf{v}_j$ represents a zero-mean, Gaussian random sequence of known covariance $\mathbf{R}_j$, determine the optimal estimate for $\mathbf{x}(t)$ [denoted by $\hat{\mathbf{x}}(t)$], during some specified time interval $t_0 \leq t \leq t_f$.

In the MME, the optimal state trajectory estimate is determined on the basis of the assumption that the measurement-minus-estimate error covariance matrix must match the measurement-minus-truth error covariance matrix. This condition is referred to as the "covariance constraint." The covariance constraint is defined mathematically by requiring the following approximation to be satisfied:

$$(\{\tilde{\mathbf{y}}(t_j) - \mathbf{g}[\hat{\mathbf{x}}(t_j), t_j]\}\{\tilde{\mathbf{y}}(t_j) - \mathbf{g}[\hat{\mathbf{x}}(t_j), t_j]\}^T) \approx \mathbf{R}_j \quad \ldots\ldots (13)$$

Thus, the *estimated measurements* $\mathbf{g}[\hat{\mathbf{x}}(t_j), t_j]$ are required to fit the *actual measurements* $\tilde{\mathbf{y}}(t_j)$ with approximately the same error covariance as the actual measurements fit the truth. Otherwise, the estimate cannot be correct.

The estimated measurement set at time t_j is based on the current state estimate, $\hat{\mathbf{x}}(t_j)$. The between-measurement state estimate is based on integration of the system dynamic model. Thus, if the system dynamic model contains errors, the integration does not yield the correct state estimate, and the residuals between the estimated and the actual measurements are too large. However, due to the noise in the measurements, it is not appropriate to force the model to predict the measurements exactly. Instead, the measurement-minus-estimate residuals should have the same covariance as the measurement noise. This condition is enforced by the covariance constraint.

When the covariance constraint has been satisfied, the state estimate is considered to have been optimized. If errors are present in the state dynamic equations, satisfaction of the covariance constraint generally requires that these errors be corrected when the model is integrated between measurements. The MME method may be used to produce these model error corrections.

Model error is represented by adding a to-be-determined unmodeled disturbance vector $\mathbf{d}(t)$ to the right-hand sides of the original state model equations, Eq. 11, to produce the modified state-governing equations,

$$\dot{\mathbf{x}} = \mathbf{f}[\mathbf{x}(t), \mathbf{u}(t), t] + \mathbf{d}(t) \quad \ldots\ldots (14)$$

Next, the following cost functional is minimized with respect to $\mathbf{d}(t)$:

$$J = \sum_{j=1}^{m} (\{\tilde{\mathbf{y}}(t_j) - \mathbf{g}[\hat{\mathbf{x}}(t_j), t_j]\}' \mathbf{R}_j^{-1} \{\tilde{\mathbf{y}}(t_j) - \mathbf{g}[\hat{\mathbf{x}}(t_j), t_j]\}) + \int_{t_0}^{t_f} \mathbf{d}(\tau)' \mathbf{W} \mathbf{d}(\tau) d\tau \quad \ldots\ldots (15)$$

where $\mathbf{W} \equiv k \times k$ weight matrix to be determined.

The functional J in Eq. 15 is the sum of two penalty terms. The first is a weighted sum of discrete terms, which penalize the deviation of the predicted measurements (based upon the estimated states) from the actual measurements. Minimization of this summation term tends to drive the state estimates toward values that when substituted into the measurement model, predict the actual measurements. The weighting $\mathbf{R}_j^{-1}$ on each of these penalty terms is the inverse of the associated measurement error covariance; thus, accurate measurements (small $\mathbf{R}_j$) are weighted more heavily than the inaccurate measurements (large $\mathbf{R}_j$). The second term in J is an integral term, which reflects the assumption that the amount of unmodeled effect to be

added should be minimized. However, the unmodeled effect must be sufficient to cause the estimate to satisfy the covariance constraint. The proper balance between the two competing effects depends on the choice of $\mathbf{W}$. The weight matrix, $\mathbf{W}$, is determined such that the covariance constraint is satisfied.

An algorithm for the minimization of J in Eq. 15 follows directly from a modification of the so-called Pontryagin's necessary conditions. For a given $\mathbf{W}$, the minimization of J in Eq. 15 with respect to $\mathbf{d}(t)$ leads to the two-point boundary value problem, (TPBVP) summarized as:

$$\dot{\boldsymbol{\lambda}} = -\left(\frac{\partial \mathbf{f}}{\partial \mathbf{x}}\right)^T \boldsymbol{\lambda} \quad \ldots\ldots (16)$$

$$\mathbf{d} = -\frac{1}{2} \mathbf{W}^{-1} \left[\frac{\partial \mathbf{f}}{\partial \mathbf{u}}\right]^T \boldsymbol{\lambda} \quad \ldots\ldots (17)$$

$$\mathbf{x}(t_0) = \text{specified}, \qquad \text{or } \boldsymbol{\lambda}(t_0^-) = \mathbf{0} \quad \ldots\ldots (18)$$

$$\boldsymbol{\lambda}(t_j^+) = \boldsymbol{\lambda}(t_j^-) + 2\mathbf{H}_j^T \mathbf{R}_j^{-1} [\tilde{\mathbf{y}}(t_j) - \mathbf{g}(\hat{\mathbf{x}}(t_j), t_j)] \quad \ldots\ldots (19)$$

$$\mathbf{x}(t_f) = \text{specified}, \qquad \text{or } \boldsymbol{\lambda}(t_f^+) = 0 \quad \ldots\ldots (20)$$

where

$$\mathbf{H} \equiv \left.\frac{\partial \mathbf{g}}{\partial \mathbf{x}}\right|_{\hat{\mathbf{x}}(t_j), t_j}$$

If the assumed model in the MME algorithm is linear, then a multiple shooting technique may be used to solve the two-point boundary value problem described by Eqs. 14–20. This technique converts the TPBVP into a set of linear algebraic equations, which may be solved using any linear-equation solver (Roemer and Mook 1989b). In the present case, the model produced by the ERA and used for input to the MME is always linear, so the MME solution is obtained from linear algebraic equations.

Mode Shape Identification Algorithm

The enhanced (i.e., higher accuracy in the presence of noise) mode-shape identification algorithm for robust system realization/identification can be summarized in the following steps.

1. Apply the ERA procedure to the measurements in the usual manner to produce a minimum-order realization model with mode shapes.
2. Input the realized model and the measurements into the MME algorithm to produce optimal state estimates.
3. Sample the MME-produced state estimates at discrete-time intervals to create simulated measurements of higher accuracy than the original measurements.
4. Apply ERA to the simulated measurements in order to realize/identify the new mode shapes.
5. Examine the newly calculated mode shapes for some convergence criteria, and repeat the procedure if necessary.

Example Simulations

The following examples contrast the mode-shape identification abilities of the proposed algorithm versus ERA by itself. Consider the axial vibrations

of a cantilever beam. Rather than solving the continuous differential eigenvalue problem (Meirovitch 1975), the approach taken here is to discretize the cantilever beam into a four-degree-of-freedom system, consisting of four masses with idealized springs and dampers between each mass. The governing equations of the discrete system are transformed into the state-space form that follows, and the proper constants for each mass, spring, and damper are substituted.

$$\begin{pmatrix} \dot{\mathbf{x}}(t) \\ \cdots \\ \ddot{\mathbf{x}}(t) \end{pmatrix} = \begin{pmatrix} 0 & \vdots & I \\ \cdots & \cdots & \cdots \\ \mathbf{M}^{-1}\mathbf{K} & \vdots & \mathbf{M}^{-1}\mathbf{C} \end{pmatrix} \begin{pmatrix} \mathbf{x}(t) \\ \cdots \\ \dot{\mathbf{x}}(t) \end{pmatrix}$$

For the first example, $\mathbf{C} = \mathbf{0}$ with $\mathbf{M}$ and $\mathbf{K}$ equal to:

$$\mathbf{M} = \begin{pmatrix} 1 & 0 & 0 & 0 \\ 0 & 1 & 0 & 0 \\ 0 & 0 & 1 & 0 \\ 0 & 0 & 0 & 1 \end{pmatrix}; \quad \mathbf{K} = \begin{pmatrix} 10 & -5 & 0 & 0 \\ -5 & 10 & -5 & 0 \\ 0 & -5 & 10 & -5 \\ 0 & 0 & -5 & 10 \end{pmatrix}$$

For the second example, $\mathbf{M}$ and $\mathbf{K}$ stay the same but,

$$\mathbf{C} = \begin{pmatrix} 0.3 & 0 & 0 & 0 \\ 0 & 0.3 & 0 & 0 \\ 0 & 0 & 0.3 & 0 \\ 0 & 0 & 0 & 0.3 \end{pmatrix}$$

Utilizing the matrix exponential, the exact time-domain solution of each example is calculated. The exact mode shapes, natural frequencies, and damping ratios are then calculated by ERA using the exact time-domain solution as input measurements.

For the first example, no damping was included in the system's model ($\mathbf{C} = 0$). Assuming only positional measurements are available, the exact solution as given by ERA is indicated in Tables 1 and 2. The solution consists of the singular values (revealing the number of modes identified), the eigenvalues (indicating each mode's natural frequency and damping ratio), and the mode shapes. It should be noted that each mode identified is normally associated with a pair of singular values. However, for simplicity each pair of singular values is averaged together so that the number of nonzero averaged singular values equals the number of modes identified.

With the exact solution known, a Guassian-distributed white noise approximately 5–10% of the size of the signal amplitude is added to the perfect measurements to investigate the performance of each algorithm. The results of the stand alone eigensystem realization algorithm processing the noisy measurements are also displayed in Tables 1 and 2. Examining the singular values, one would conclude that only three modes were identified, and the remaining nonzero singular values represented noise in the measurements. Directly related to this, a pair of eigenvalues and the corresponding mode shape were completely unidentifiable. Therefore, due to measurement uncertainty, the ERA algorithm only identified three of the four participating modes. Moreover, the identification of the eigenvalues and mode shapes are very poor.

In the second example, the system's model includes proportional damping

TABLE 1. Solution Comparisons for Example 1

Exact solution (1)	ERA alone (2)	ERA/MME (3)
	(*a*) Singular values	
17.706	17.692	17.654
10.192	10.282	10.159
3.215	3.132	3.204
0.269	0.398	0.301
0	0.306	0.089
0	0.278	0.080
0	0.256	0.071
0	0.240	0.064
	(*b*) Eigenvalues	
$0 \pm 4.253i$	$-0.075 \pm 4.042i$	$-0.045 \pm 4.343i$
$0 \pm 3.618i$	$-33.86 \pm 0.000i$	$-0.194 \pm 3.798i$
$0 \pm 2.629i$	$-0.020 \pm 2.654i$	$-0.029 \pm 2.634i$
$0 \pm 1.382i$	$-0.017 \pm 1.384i$	$-0.013 \pm 1.393i$

TABLE 2. Mode-Shape Comparison for Example 1

Exact solution (1)	ERA alone (2)	ERA/MME (3)
	(*a*) Mode 1	
0.3717	0.4012	0.3705
0.6015	0.5743	0.6098
0.6015	0.5912	0.6005
0.3717	0.3992	0.3891
	(*b*) Mode 2	
−0.6015	−0.5945	−0.5685
−0.3717	−0.3622	−0.3810
0.3717	0.4039	0.3711
0.6015	0.6069	0.6395
	(*c*) Mode 3	
0.6015	0.2087	0.5645
0.3717	0.2532	0.4193
0.3717	0.1717	0.3486
0.6015	0.3515	0.6312
	(*d*) Mode 4	
0.37	−0.0751	−0.3223
0.6015	0.4508	0.6001
−0.6015	−0.7844	−0.7101
0.3717	0.6279	0.4541

TABLE 3. Solution Comparisons for Example 2

Exact solution (1)	ERA alone (2)	ERA/MME (3)
	(*a*) Singular Values	
13.298	13.132	13.219
7 023	6.931	7.668
2.374	2.332	2.235
0.197	0.326	0.232
0	0.289	0.089
0	0.262	0.090
0	0.250	0.077
0	0.239	0.069
	(*b*) Eigenvalues	
$0.150 \pm 4.250i$	$-0.464 \pm 4.039i$	$-0.299 \pm 4.324i$
$0.150 \pm 3.615i$	$-15.93 \pm 0.000i$	$-0.281 \pm 3.795i$
$0.150 \pm 2.624i$	$-0.171 \pm 2.663i$	$-0.176 \pm 2.636i$
$0.150 \pm 1.374i$	$-0.176 \pm 1.372i$	$-0.161 \pm 1.387i$

TABLE 4. Mode-Shape Comparison for Example 2

Exact solution (1)	ERA alone (2)	ERA/MME (3)
	(*a*) Mode 1	
0.3717	0.4048	0.3901
0.6015	0.5613	0.5843
0.6015	0.5971	0.5944
0.3717	0.4067	0.3965
	(*b*) Mode 2	
−0.6015	−0.5982	−0.6165
−0.3717	−0.3470	−0.3767
0.3717	0.4052	0.3825
0.6015	0.6154	0.5983
	(*c*) Mode 3	
0.6015	0.5294	0.4645
−0.3717	0.5839	−0.2193
−0.3717	0.5217	−0.4486
0.6015	−0.1205	0.7312
	(*d*) Mode 4	
−0.3717	-0.0482	−0.3165
0.6015	0.4502	0.6341
−0.6015	−0.7690	−0.5622
0.3717	0.6332	0.4541

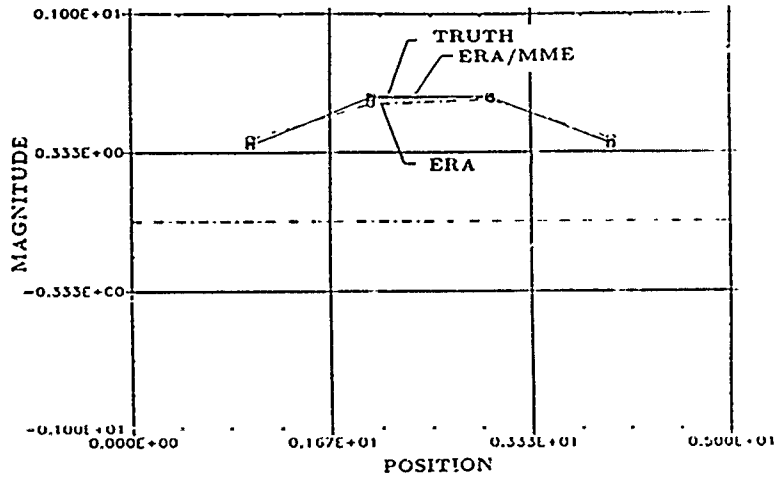

FIG. 1. Mode Shape No. 1 (No Damping)

exceeding a 15% damping ratio. The results were calculated in the same fashion as the previous example. The results are given in Tables 3 and 4. Again, by examination of the singular values, it is obviously that only three modes were identified by ERA and the remaining nonzero singular values represented noise in the measurements. Also, the same pair of eigenvalues and the corresponding mode shape were not identified. Therefore, due to the combination of measurement uncertainty and structural damping, the ERA algorithm only identified three modes.

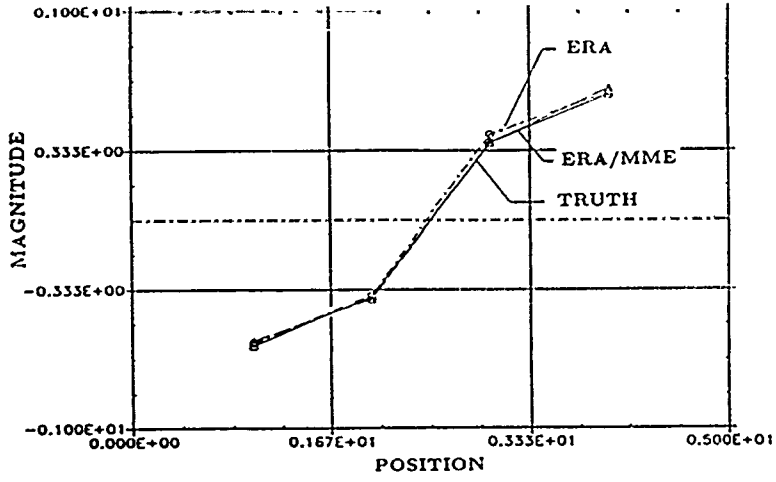

FIG. 2. Mode Shape No. 2 (No Damping)

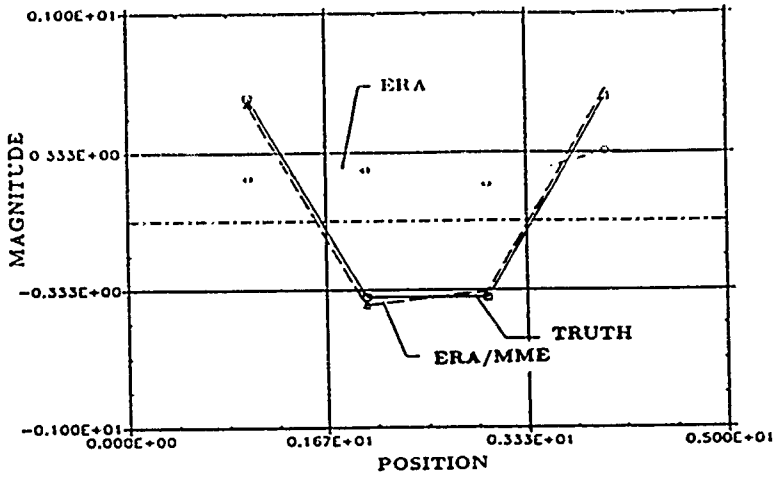

FIG. 3. Mode Shape No. 3 (No Damping)

Note: The final tabulated results for both algorithms given in Tables 1–4 are an average of 10 individual results provided by 10 different seeds of a random number generator. This truncated use of a Monte Carlo analysis produced convergence upon the true mode shapes, otherwise not obtained for individual cases. Therefore, in analyzing real world problems, taking many different sets of measurements and averaging the results should produce more reliable results.

Table 2 gives the results of the enhanced mode-shape identification al-

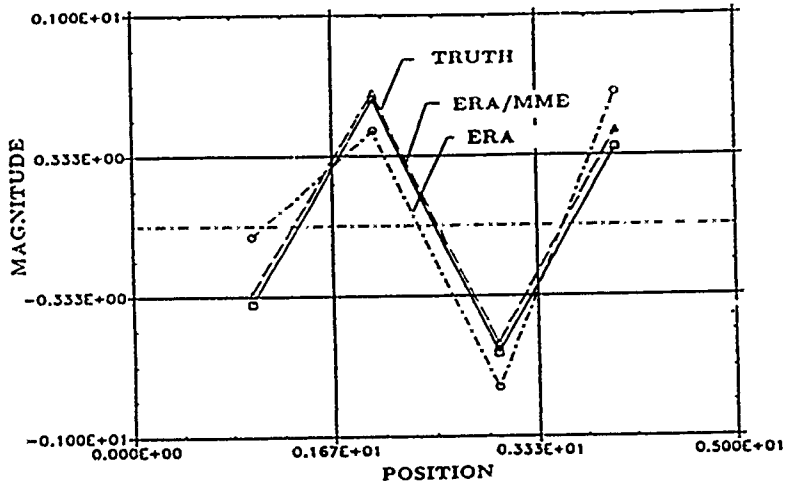

FIG. 4. Mode Shape No. 4 (No Damping)

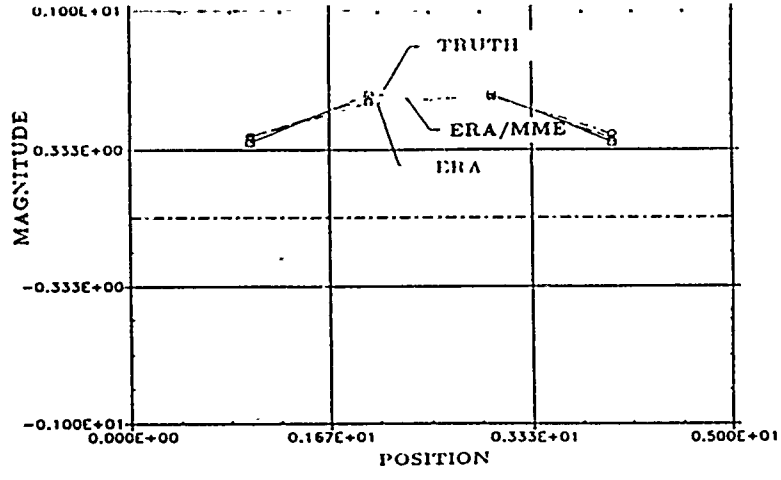

FIG. 5. Mode Shape No. 1 (with Damping)

gorithm proposed in this paper. For this particular example, only two cycles of the procedure summarized were needed for convergence. Examining the singular values, one would conclude that four modes were identified by the enhanced algorithm, and the remaining singular values represented noise. Notice, the mode not identified by the stand-alone ERA is accurately recovered by the combined algorithm. Also, the other three mode shapes are more precisely identified. The improved accuracy of the eigenvalues is also apparent. For this example, the true mode shapes and those identified by

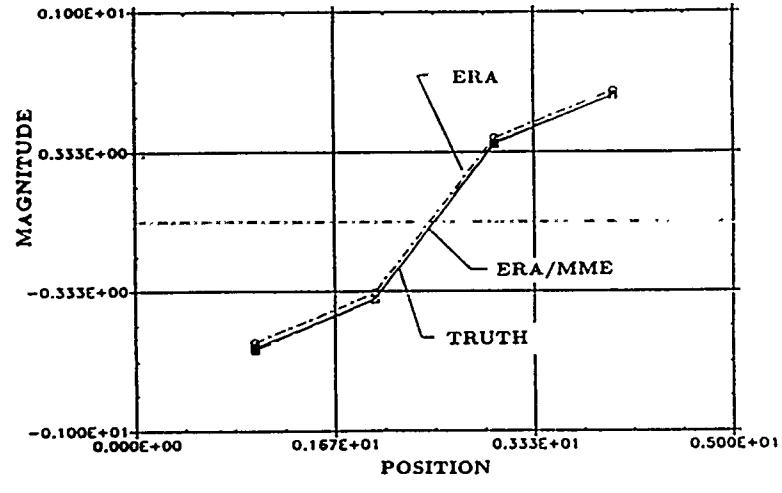

FIG. 6. Mode Shape No. 2 (with Damping)

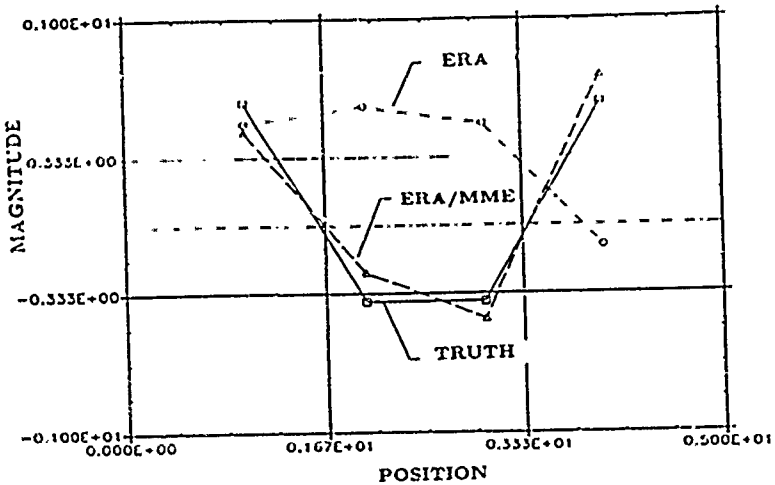

FIG. 7. Mode Shape No. 3 (with Damping)

ERA alone (measurements), and the enhanced algorithm (estimate) are illustrated in Figs. 1–4.

Tables 3 and 4 show the results of the enhanced mode-shape identification algorithm for the second example including damping. Similar to the first example, only two cycles of the algorithm's summarized steps were necessary for convergence. The singular values reveal that four modes were identified by the proposed algorithm, as opposed to the three modes identified by ERA. The mode not identified by the stand-alone ERA was again

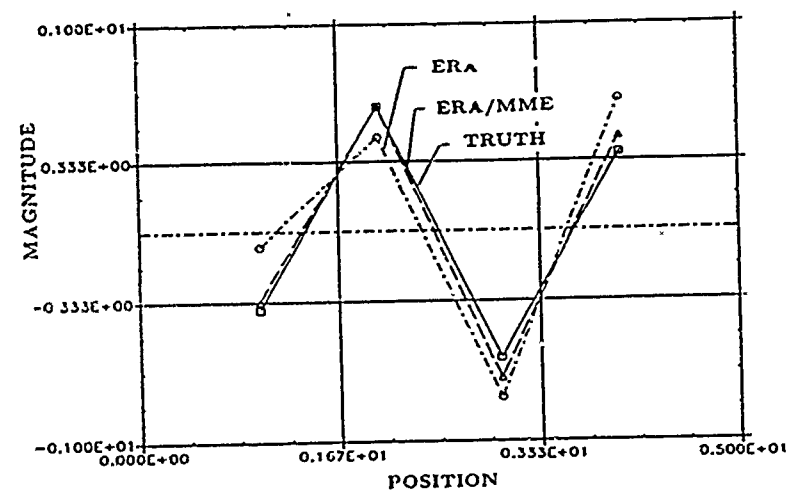

FIG. 8. Mode Shape No. 4 (with Damping)

accurately identified by the combined algorithm. The illustrations of the mode shapes identified by both algorithms are given in Figs. 5–8. The presence of damping in the structure did affect the mode-shape identification, however, an accurate recovery of all four mode shapes was still obtained.

Conclusions

The successful results from the proposed algorithm convey significant improvements when identifying mode shapes in structures with corrupted output measurements. For instance, when the example structures were subjected to a 5–10% noise level, one mode shape was completely unidentifiable using the eigensystem realization algorithm alone (with and without damping). However, when the enhanced mode-shape identification algorithm was tested under the same circumstances, all four mode shapes could be identified accurately (with and without damping). These results are consistent with the singular values calculated from the realized state matrix. The cutoff point (indicating the number of modes identified) for the singular values of Tables 1 and 3 (ERA) was clearly three, while the cutoff for the enhanced ERA/MME algorithm was clearly four.

Also, for noise levels of less than 3% of the signal amplitude both algorithms could identify all four mode shapes, while for noise levels exceeding 15% different combinations of identified modes were observed. However, in all cases the enhanced mode-shape identification algorithm gave improved results. These results confirm the robust nature of the enhanced mode-shape identification algorithm and demonstate structural realization/identification of mode shapes in the presence of high measurement noise.

Acknowledgments

This work was partially supported by the Air Force Office of Scientific Research (Anthony Amos, contract monitor) and NASA Langley Research Center (Jer-Nan Juang, contract monitor). This support is gratefully acknowledged.

Appendix I. References

Chen, J. C., et al. (1983). "Direct structural parameter identification by modal test results." *24th Structures, Structural Dynamics, and Materials Conference*, Pt. 2.

Applied Optimal Estimation. (1974). A. Gelb, ed., MIT Press, Cambridge, Mass.

Hendricks, S. L., et al. (1984). "Identification of mass, damping, and stiffness matrices for large linear vibratory systems." *J. Guid. Control Dyn.*, American Institute of Aeronautics and Astronautics, 7(2), 244–245, Mar.–Apr.

Ho, B. L., and Kalman, R. E. (1965). "Effective construction of linear state-variable models from input/output data." *3rd Annual Allerton Conference on Circuit and System Theory*, 449–459.

Ibrahim, S. R., and Mikulcik, E. C. (1977). "A method for the direct identification of vibration parameters from the free response." *Shock Vib. Bull.*, 47(4), 183–198, Sep.

Juang, J.-N., and Pappa, R. S. (1985). "An eigensystem realization algorithm (ERA) for modal parameter identification and model reduction." *J. Guid. Control Dyn.*, American Institute of Aeronautics and Astronautics, 8(5), 620–627, Sep.–Oct.

Juang, J.-N., and Pappa, R. S. (1986). "Effects of noise on modal parameters identified by the eigensystem realization algorithm." *J. Guid. Control Dyn.*, American

Institute of Aeronautics and Astronautics, 9(3), 294–303, May–Jun.
Junkins, J. L., and Mook, D. J. (1985). "Enhanced spacecraft attitude estimation." *Final Report, Contract No. N60921-83-G-9-A165*, Naval Surface Weapons Center, Dahlgren, Va.
Klema, V. C., and Laub, A. J. (1980). "The singular value decomposition: Its computation and some applications." *Trans. on Automatic Control*, Institute of Electrical and Electronic Engineers, AC-25(2), 164–176, Apr.
Lewis, F. L. (1986). *Optimal estimation*. Wiley Interscience Publications, New York, N.Y.
Meirovitch, L. (1975). *Elements of vibration analysis*. McGraw-Hill, Inc., New York, N.Y.
Mook, D. J., and Junkins, J. L. (1988). "Minimum model error estimation for poorly modeled dynamic systems." *J. Guid. Control Dyn.*, American Institute of Aeronautics and Astronautics, 11(4), 367–375, May–Jun.
Mook, D. J., and Lin, J.-C. (1987). "Minimum model error estimation of modal truncation errors." *Proc., of the 1987 Spring Meeting*, the Society for Experimental Mechanics, Houston, Tex., Jun.
Mook, D. J. (1989). "Estimation and identification of nonlinear dynamic systems." *AIAA J.*, 27(7), 968–974, Jul.
Pappa, R. S., and Juang, J.-N. (1985). "Galileo spacecraft modal identification using an eigensystem realization algorithm." *J. Astronaut. Sci.*, 33, 15–33, Jan.–Mar.
Rajaram, S., and Junkins, J. L. (1985). "Identification of Vibrating Flexible Structures." *J. Guid. Control Dyn.*, 8(4), 463–470, Jul.–Aug.
Roemer, M. J., and Mook, D. J. (1989a). "Robust identification of damped structures." *Damping 1989 Conf. Proc.*, Feb.
Roemer, M. J., and Mook, D. J. (1989b). "An enhanced mode shape identification algorithm." *Proc., 30th Structures, Structural Dynamics and Materials Conf.*, Apr.

Appendix II. Notation

The following symbols are used in this paper:

- $\mathbf{A}$ = dynamic state-space matrix;
- $\mathbf{B}$ = input matrix;
- $\mathbf{C}$ = output matrix;
- $\mathbf{D}$ = singular values diagonal matrix;
- $\mathbf{d}(t)$ = unknown model error;
- $\mathbf{f}$ = model equations vector;
- $\mathbf{g}$ = measurement model equations;
- $\mathbf{H}$ = Hankel matrix;
- $\mathbf{J}$ = cost functional;
- $\mathbf{K}$ = stiffness matrix;
- $\mathbf{M}$ = mass matrix;
- $\mathbf{P}$ = isometric matrix from singular value decomposition (SVD);
- $\mathbf{Q}$ = isometric matrix from SVD;
- $\mathbf{R}_j$ = measurement noise covariance;
- $\mathbf{u}$ = dynamic input vector;
- $\mathbf{V}_r$ = observability matrix;
- $\mathbf{v}_j$ = measurement error vector;
- $\mathbf{W}$ = weighting matrix;
- $\mathbf{W}_c$ = controllability matrix;
- $\mathbf{x}$ = state vector;
- $\mathbf{y}$ = output vector;
- $\hat{\mathbf{Y}}$ = output measurements;
- $\tilde{\mathbf{y}}$ = measurement set; and
- $\boldsymbol{\lambda}$ = co-state vector.

DSC-Vol. 20

ADVANCES IN DYNAMICS AND CONTROL OF FLEXIBLE SPACECRAFT AND SPACE-BASED MANIPULATIONS

PRESENTED AT
THE WINTER ANNUAL MEETING OF
THE AMERICAN SOCIETY OF MECHANICAL ENGINEERS
DALLAS, TEXAS
NOVEMBER 25–30, 1990

SPONSORED BY
THE DYNAMIC SYSTEMS AND CONTROL DIVISION, ASME

EDITED BY
SURESH M. JOSHI
NASA-LANGLEY RESEARCH CENTER

THOMAS E. ALBERTS
OLD DOMINION UNIVERSITY

YOGENDRA P. KAKAD
UNIVERSITY OF NORTH CAROLINA

THE AMERICAN SOCIETY OF MECHANICAL ENGINEERS
345 East 47th Street ☐☐ United Engineering Center ☐☐ New York, N.Y. 10017

CONTROL FORMULATIONS FOR VIBRATION SUPPRESSION OF AN ACTIVE STRUCTURE IN SLEWING MOTIONS

Ephrahim Garcia and Daniel J. Inman
Mechanical Systems Laboratory
Department of Mechanical and Aerospace Engineering
State University of New York at Buffalo
Buffalo, New York

ABSTRACT

The slewing control of a flexible structure is considered by examining the equations of motion of an integrated control/structure system containing both the actuator and structure dynamics. The system under consideration is a slewing flexible structure, a thin aluminum beam, torque driven by an armature controlled DC electric motor and actuated by a piece-wise distributed piezoceramic actuator. An improvement in performance is gained by a) including the effects of the motor-actuator and beam dynamic interaction and b) using a piezoelectric device, layered on the structure, for direct vibration suppression of the structural dynamics. Various control laws are considered for the vibration suppression control problem. These include a standard linear quadratic regulator controller and an output feedback control scheme. A comparison is made between the performance of the output feedback control scheme and the full state feedback controller.

NOMENCLATURE

A	- state space system matrix
B	- state space control matrix
B_f	- control matrix in physical coordinates
b_v	- equivalent viscous damping
c_v	- viscous damping in the motor (bearing friction)
C	- state space output matrix
e_a	- voltage applied across the armature circuit
D	- damping matrix
E	- elastic modulus
EI	- flexural rigidity
I	- cross sectional moment of inertia
I_b	- rotatory inertia of the beam about the slewing axis
I_m	- motor inertia
I_{nxn}	- n by n identity matrix
I_s	- effective motor inertia
K	- stiffness matrix
K_b	- back electro-motor force (emf) constant
K_p	- position feedback gain
K_t	- motor torque constant
L	- beam length
M	- inertia matrix
N_g	- gear ratio
q_i	- ith modal coordinate
q	- displacement vector
R_a	- armature resistance
t_b	- beam thickness
x	- system state vector
$y(x,t)$	- deflection of the beam wrt x
y	- measurement vector
$\phi_i(x)$	- i^{th} eigenfunction
Γ_i	- modal participation factor of the ith mode
μ	- piezo layer constant
θ	- angular position of the rigid body motion
θ_m	- angular position of the motor
ρ	- mass density per unit length
τ	- torque applied to beam
$(\cdot)^t$	- matrix transpose
$(\cdot)'$	- differentiation wrt x

INTRODUCTION

It has been shown by Garcia (1989) that the dynamic interaction between the slewing actuator, the DC motor, and the flexible structure can lead to improved vibration suppression. Traditionally, the slewing control of a flexible single link structure has been a single actuator problem. This problem has been studied both by researchers in the control of large flexible space structures, Juang et al. (1986), and by researchers in the robotics community, Cannon and Schmitz (1984), Hastings and Book (1987), and by Yurkovich and Tzes (1990).

Recently, Park et al. (1990) proposed the use of a "voice-coil" actuator in addition to the slewing motor. This actuator was rigidly attached to the slewing hub and actuated the beam near the clamped end. This approach achieved improved structural dynamic performance and reduced peak motor voltages, but at the cost of adding the mass of the coil actuator and its supporting mechanical interface to the slewing payload. Garcia and Inman (1990b) showed that similar increases in performance can be achieved by slewing an

active structure rather than a passive structure. This structure consists of a beam layered with piece-wise distributed, or segmented, piezoceramic crystal. The active beam being considered here is similar to those considered earlier by Fanson and Caughey (1987) and Burke and Hubbard (1987). They considered a cantilevered flexible beam controlled by a collocated pair of piezoelectric actuators and strain sensors coupled with a positive position feedback control law.

A study is performed which examines various control law formulations; in particular, an output feedback control formulation is compared to a linear quadratic regulator (LQR), as discussed by Kirk (1970) and Sage and White (1977). The goal here is to design an output feedback control strategy that performs nearly and well as a full state feedback controller. The application of an output feedback controller reduces the number of feedback paths in the control loop, which is essential to experimental implementation of the control law. More importantly, an output feedback [illegible] generates a feedback matrix that is based on [illegible] information rather than relying on the actual [illegible] model.

SYSTEM DYNAMICS

The schematic of Figure 1 is an edge view of a thin beam slewing in the horizontal plane such that gravity does not play a significant role in the dynamics. The driving torque, τ, is applied at the slewing axis.

The motion of the structure is assumed to have a modal expansion given by

$$y(x,t) = \sum_{i=1}^{n} \phi_i(x)\, q_i(t) \tag{1}$$

where n is the number of modes used in the solution, $\phi_i(x)$ is the ith mode of vibration and $q_i(t)$ is the modal amplitude. A detailed schematic of a experimental piezo-actuated structure is presented in Figure 2.

Garcia and Inman (1990b) derived the equations of motion for a piezo-actuated beam in slewing motions. This analysis revealed that the equation for the rigid body motion of the system is given by

$$I_b\ddot{\theta} + \sum_{i=1}^{n}\left[\int_0^L \rho x \phi_i\, dx\right] q_i = \tau \tag{2}$$

The flexible motion of the structure is governed by the following set of n equations of motion

$$\left[\int_0^L \rho x \phi_i\, dx\right]\ddot{\theta} + \left[\sum_{j=1}^{n}\int_0^L \rho \phi_i \phi_j\, dx\right]\ddot{q}_i +$$

$$\left[\sum_{j=1}^{n}\int_0^L EI\phi_i''\phi_j''\, dx\right] q_i = \phi_i'(0)\,\tau + \int_0^L \frac{\partial^2}{\partial x^2}(\mathcal{M}(x,t)\Lambda(x))\phi_i(x)\, dx \tag{3}$$

where n refers to the number of modes assumed in the solution. The actuator dynamics - that is, the interaction of motor and beam - is included in this model. This interaction takes into account the rotation of the structure due to flexure brought about by the applied torque in the Hamiltonian's expression for the nonconservative work (Garcia and Inman, 1990a). This interaction appears in Equation (3) as the direct transmission of applied torque to the mode through its modal participation factor. Garcia and Inman (1990b) calculated the moment generated by adding piecewise distributed piezo actuators. The distributed moment term on the right hand side of Equation (3) can be rewritten as,

$$\int_0^L \frac{\partial^2}{\partial x^2}(\mathcal{M}(x,t)\Lambda(x))\,\phi_i(x)\, dx = \mu\, V_p(t)\,[\,\phi_i'(L_1) - \phi_i'(L_2)] \tag{4}$$

The moment distribution, $\mathcal{M}(x,t)$, can be calculated by the product of a constant, μ, and the voltage applied across the segment, $V_p(t)$. The constant μ, is a function of the geometry and properties of the actuator. This analysis follows that of Fanson and Caughey and Burke and Hubbard (1987). A more detailed analysis of the [illegible] of layered piezo actuation of a structure was given by [illegible] and Anderson (1990). Finally, the equations of motion [illegible] slewing structure are assembled in a lumped mass formulation as

[illegible] (5)

The displacement vector $q(t)$ is defined by $q(t)^T = [0(t)\ q_1(t)$ [illegible]. The mass, damping and stiffness coefficient [illegible]

$$M = \begin{bmatrix} I_b+I_s & I_1+I_s\Gamma_1(0) & \cdots & I_n+I_s\Gamma_n(0) \\ I_1+I_s\Gamma_1(0) & M_1 & & \vdots \\ \vdots & & & \vdots \\ I_n+I_s\Gamma_n(0) & \cdots & & M_n \end{bmatrix} \tag{6}$$

$$D = \begin{bmatrix} b_v & b_v\Gamma_1(0) & \cdots & b_v\Gamma_n(0) \\ b_v\Gamma_1(0) & b_v\Gamma_1(0)^2 & \cdots & b_v\Gamma_1(0)\Gamma_n(0) \\ \vdots & & & \vdots \\ b_v\Gamma_n(0) & b_v\Gamma_n(0)\Gamma_1(0) & \cdots & b_v\Gamma_n(0)^2 \end{bmatrix} \tag{7}$$

$$K = \begin{bmatrix} 0 & 0_{1xn} \\ & M_1\omega_1^2 \quad \cdots \quad 0 \\ 0_{nx1} & \vdots \qquad\qquad \vdots \\ & 0 \quad \cdots \quad M_n\omega_n^2 \end{bmatrix} \tag{8}$$

[illegible] $\Gamma_i(0) = \phi_i'(0)$; this is the ith torsional modal participation [illegible] for the beam. The coefficient b_v is an equivalent viscous [illegible] term which is a combination of the viscous damping in the [illegible] and the back emf of the motor, K_b. The term I_s is equal [illegible] reflective inertia of the motor acting through the gear ratio, [illegible] The ith inertia term is given by

$$I_i = \int_0^L \rho x \phi_i(x) dx \tag{9}$$

which represents couples the flexible motion of the structure with the rigid body slewing motion. The control input vector $u(t)$ is the 2 x 1 vector $u^T(t) = [e_a(t), V_p(t)]$ and the control coefficient matrix is

$$B = \begin{bmatrix} \frac{N_g K_t}{R_a} & \frac{N_g K_t}{R_a}\Gamma_1(0) & \cdots & \frac{N_g K_t}{R_a}\Gamma_n(0) \\ 0 & \mu[\phi_1'(L_1)-\phi_1'(L_2)] & \cdots & \mu[\phi_n'(L_1)-\phi_n'(L_2)] \end{bmatrix} \tag{10}$$

[illegible] segment piezoceramic actuator. The system of equation [illegible] into state space form by defining the state vector x as

$$x = \begin{bmatrix} q \\ \dot{q} \end{bmatrix} \tag{11}$$

and the corresponding state matrix

$$A = \begin{bmatrix} 0 & I \\ -M^{-1}K & -M^{-1}D \end{bmatrix} \tag{12}$$

where 0 denotes the matrix of zeros and I denotes the identity matrix of appropriate dimension. With this change of coordinates, Equation (5) becomes

$$\dot{x} = Ax + Bu \tag{13}$$

with output measurements defined by

$$y = Cx \tag{14}$$

Here the matrix of constants C specifies the relation between the measurements and the state vector x(t).

VIBRATION SUPPRESSION CONTROL

Presented will be an LQR controller design where the focus of the design will be for the vibration suppression of the structure. While the solutions to such problems are analytically convenient, full state feedback controllers are not easily implemented in actual hardware without the aid of an on-line full state estimator. Since estimators only approximate plant behavior, the prediction of system performance requires that estimator dynamics be included in the overall system models. Although this type of controller is a standard formulation in control technology, experimentally implementing these controllers is not always trivial in the laboratory. Therefore, an investigation into an output feedback control formulation is pursued. An output feedback control strategy reduces the number of feedback paths and allows these gains to be functions of the instrument measurements. This generates a lower order controller which is simpler to implement in actual hardware, and arguably more reliable than a more complex full state feedback controller. A comparison of the performance of these controllers is given.

An Output Feedback Control Formulation

Some early formulations for LQ type optimal output feedback were made by Levine and Athans (1970) and Kosut (1970). These algorithms do not guarantee stability, and were found to yield unsatisfactory results for high order systems. A more recent algorithm was derived by Moerder and Calise (1985). This approach yielded a stable algorithm for finding optimal output feedback solution by adding to the cost functional a penalty on the feedback gains. Sah (1990) considered a simplified approach for a single actuator slewing problem which comprised of a least squares solution between an LQR controller and an output feedback controller. This approach is presented here as follows. Let u^* be the solution to the infinite time, linear quadratic regulator (LQR) problem, such that

$$u^*(t) = -K^*x^*(t) \tag{15}$$

where K^* is the optimal feedback gain matrix, and $x^*(t)$ is the optimal state vector. The LQR control algorithm then calculates the value of the gain matrix K^* such that the cost functional

$$J = \int_0^\infty (x^TQx + u^TRu)dt \tag{16}$$

is minimized. The matrices Q and R are chosen to provide a desired and system performance. Now let u_o be a controller which is a function of the measurements of the system, i.e.,

$$u_o = K_o y^*(t) \tag{17}$$

Now define the function

$$\phi = [u_o(t)-u^*(t)]^T[u_o(t)-u^*(t)] \tag{18}$$

and minimize ϕ with respect to the gain matrix, K_o.

Substituting for u_o, setting $\frac{\partial \phi}{\partial K_o} = 0$, and solving for K_o, the following expression is obtained.

$$K_o = [y^*(t)^Ty^*(t)]^{-1}y^*(t)^Tu^*(t) \tag{19}$$

This obtains a least squares approximation for the solution of the output feedback gain matrix, K_o.

Control and Simulations of an Active Beam

The example given here is of an experimental slewing beam, as depicted in Figure 2. This structure is currently housed in the Mechanical System Laboratory at the State University of New York at Buffalo. The aluminum beam is 0.8 m long, 0.81 mm thick, and 1.27 cm wide. The actuators of the structure consists of two pairs of lead zirconate piezoceramic layers (Piezo Electric Products, Inc. G-1195), and a Electro-Craft 586 DC electric motor. The moment distribution generated for each pair of the piezo actuators is

$$\mathcal{M}(x,t) = 4.345\text{x}10^{-5}\ V_p \ \text{Nm/volt} \tag{20}$$

A more complete description of this system was given by Inman et al. (1990).

The measurements assumed to be available for this slewing control simulation are strain and angular position transducers. The angular position and angular velocity signals are easily measured for a system utilizing optical encoders, or potentiometers, for position and a tachometer for velocity sensing. With respect to the system of equation (5), the angular position signal is the sum of the undeflected beam position, θ, and the deflection due to the structural rotation at the slewing axis, i.e.,

$$\tilde{\theta}(t) = \theta(t) + \sum_{i=1}^{n} \phi_i'(0)\, q_i(t) \tag{21}$$

where the angular velocity is simply the time rate of change of Equation (21). The strain of a beam sensed at position L_s is given by

$$\frac{\partial^2 y(L_s,t)}{\partial x^2} = \frac{t_b}{2} \sum_{i=1}^{n} \frac{\partial^2 \phi_i(L_s)}{\partial x^2} q_i(t) \tag{22}$$

as presented by Juang et al. (1986). Piezoelectric polymer sensors yield a time rate of strain for a given system so that it will be assumed that such a signal could be included in our control formulation.

The quadratic regulator penalty function was determined by choosing the weighting matrices as

$$Q = \text{DIAG}[\ 10.0,\ 4.0,\ 1.0,\ 10.0,\ 4.0,\ 1.0] \tag{23a}$$
$$R = \text{DIAG}[\ 1.0,\ 0.01] \tag{23b}$$

This yielded a satisfactory response for the structure in terms of the peak current requirements of the motor, the structural tip deflection, angular position response and the voltage requirements of the piezo actuators. The response of the system to the LQR controller is given by the solid line in Figures 3-5, while the dashed lines represent the response of the system to the output feedback controller. The structural displacement response of Figure 3 appears slightly smoother than in the LQR. This is due in part to the insensitivity of the output feedback controller to the higher modes of vibration, as shown in Figure 5. Figure 4, shows the total angular deflection of the system during the slewing maneuver.

The performance, as defined by the cost functional Equations (16) and (23), is J=10.987 for the standard LQR formulation. The cost for the output feedback controller scheme is J=11.074, and is higher as one might expect. Overall the performance of the output feedback controller closely resembled the performance of the LQR.

CLOSING REMARKS

An investigation has been performed into the use of an output feedback control scheme applied to an active structure. This controller scheme has been found to yield satisfactory results that perform nearly as well as a full state feedback, LQR, controller. The output feedback controller reduces the number of feedback paths, and hence, the complexity of the controller. More importantly, it utilizes sensor measurements rather than relying on state information which may not always be available.

REFERENCES

Burke S. B., and Hubbard J. E.,1987, "Active Vibration Control of a Simply Supported Beam Using a Spatially Distributed Actuator," *IEEE Control Systems Magazine*, Vol . 7 No. 4 .

Cannon, H.C. Jr. and Schmitz, E., 1984,"Initial Experiments on the End-Point Control of a Flexible One-Link Robot," *International Journal of Robotics Research*, Vol. 3, No. 3, pp. 62-75.

Crawley, E.F. and Anderson, E.H., 1990, "Detailed Models of Piezoceramic Actuation of Beams," *Journal of Intelligent Material Systems and Structures*, Vol. 1, pp. 4-25. Also AIAA paper number 89-1388 CP in the *Proceedings of 1989 AIAA Structures Dynamic and Materials Conference*, pp. 2000-2010.

Fanson J. L. and Caughey T.K., 1987, "Positive Position Feedback Control for Large Space Structures," AIAA Paper No. 87-0902.

Garcia, E., 1989, "On the Modeling and Control of Slewing Flexible Structures," Ph. D. Thesis, Department of Mechanical and Aerospace Engineering, State University of New York at Buffalo, Buffalo, New York.

Garcia, E., and Inman, D.J., 1990a, "Modeling Actuator-Structure Interaction in the Slewing of Flexible Structures," *Proceedings of the American Controls Conference*, San Diego, California, May 23-25.

Garcia, E., and Inman, D.J., 1990b, "Advantages of Slewing an Active Structure," *Journal of Intelligent Material Systems and Structures*, to appear in 1990.

Hastings, G.G. and Book, W.J., 1987, "A Linear Dynamic Model for Flexible Robotic Manipulators," *IEEE Control Systems Magazine*, pp. 61-64, February.

Inman, D.J., Garcia, E., Pokines, B, "Issues in Slewing an Active Structure," *U.S.-Japan Workshop on Smart/Intelligent Structures and Systems*, Honolulu, Hawaii, March, 1990.

Juang, J.-N., Horta, L.G. and Robertshaw, H.H., 1986, "A Slewing Control Experiment for Flexible Structures," *AIAA Journal of Guidance, Control and Dynamics*, Vol. 9, No. 5, pp. 599-607.

Kirk, D.E., 1970,*Optimal Control Theory an Introduction*, Prentice-Hall, Inc., Englewood Cliffs, New Jersey.

Kosut, R.L., 1970, "Suboptimal Control of Linear Time-Invariant Systems Subject to Control Structure Constraints," *IEEE Transactions on Automatic Controls*, vol. AC-15, No. 5, October

Levine, W.S., and Athans, M., 1970, "On the Determination of the Optimal Feedback Gains for Linear Multivariable Systems," *IEEE Transactions on Automatic Control*, vol. AC-15, pp. 44-48, February.

Park, Y.-P., Kim, S.-H., Ha, Y.-K., Park, H.-S., 1989, "Analysis and Test on the Digital Optimal Control of a Flexible Rotor Arm Vibration," *Proceeding of the 7th International Modal Analysis Conference*, pp. 1489-1495.

Randall, D. S., and O'Neil, C. G., 1981, "Axial-mode Piezoelectrically-Driven Beam Deflectors" SPIE Vol. 299 Advances In Laser Scanning Technology.

Sage, A.P., and White, C.C., 1977, "Optimum System Control," 2nd edition, Prentice-Hall, Englewood Cliffs, New Jersey.

Sah, J.-J., 1990, "On the Interaction Between an Actuator and a Slewing Structure," Ph.D. Thesis, State University of New York at Buffalo, Buffalo, New York.

Yurkovich, S. and Tzes, A., 1990, "Experiments in Identification and Control of Flexible-Link Manipulators," *IEEE Control Systems Magazine*, Vol. 10, No. 2.

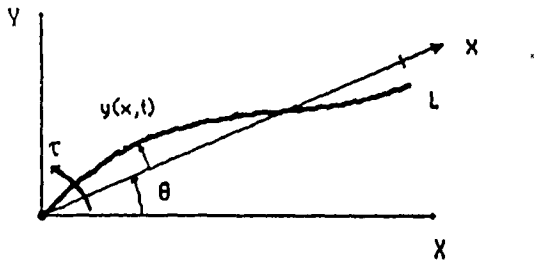

Figure 1. Flexible beam in slewing motions.

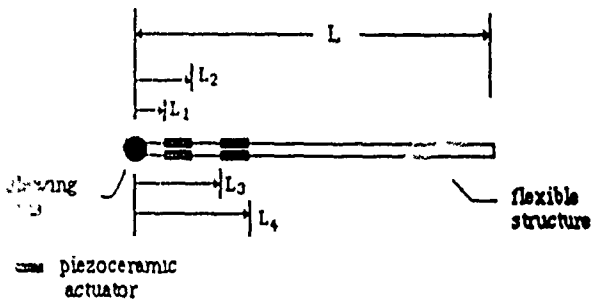

Figure 2. Schematic of the slewing beam showing the location of embedded piezoceramic actuators.

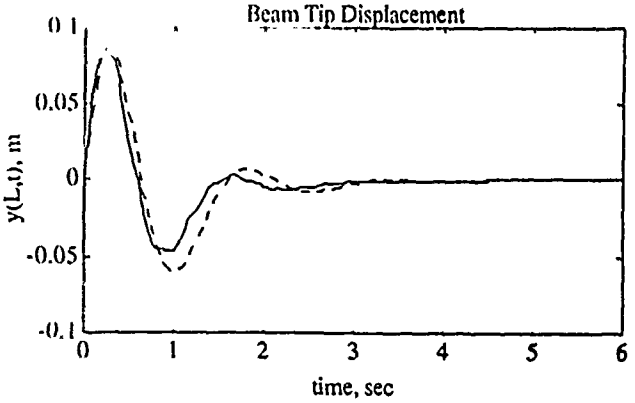

Figure 3 Structural tip deflection during for an initial displacement error.

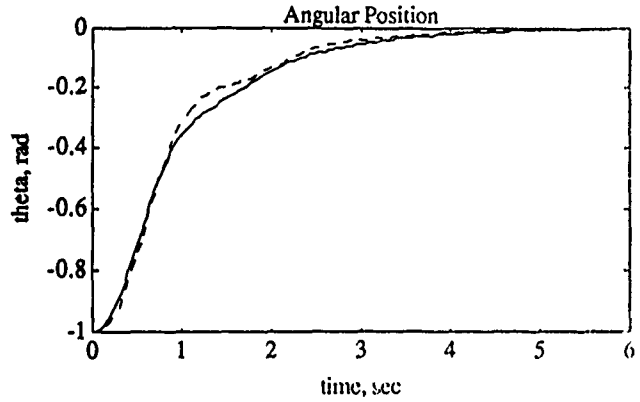

Figure 4. Angular position response for an initial displacement error.

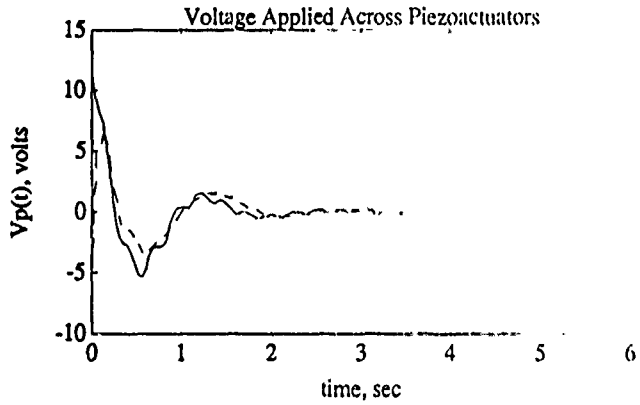

Figure 5. Voltage applied to the piezo segments for an initial displacement error.